TOLERANCE ANALYSIS OF COMPLIANT METAL PLATE ASSEMBLIES CONSIDERING WELDING DISTORTION

by

Hyun Chung

A dissertation submitted in partial fulfillment
of the requirements for the degree of
Doctor of Philosophy
(Naval Architecture and Marine Engineering)
in The University of Michigan
2006

Doctoral Committee:

Associate Professor Dale G. Karr, Co-Chair
Adjunct Professor Thomas Lamb, Co-Chair
Professor Jun Ni
Professor Michael G. Parsons
Assistant Research Scientist, Mark H. Spicknall

To my family, for their invaluable love,
support and encouragement

ACKNOWLEDGMENTS

I would like to express my sincere appreciation for my Co-Chairperson, Professor Thomas Lamb, for his advice, continuous support and allowing me the opportunity to work with him. His remarkable work experiences and keen philosophical insights on the ship production field were the reason why I came to Ann Arbor to pursue a doctoral degree at the University of Michigan. His words of encouragement, quiet urgings and careful reading of all of my writing will never be forgotten.

I would like to thank my other Co-Chairperson, Professor Dale G. Karr, for his helpful suggestions and comments throughout the course of this research, especially during the final stages. His guidance and careful reviews have been essential to the successful completion of this dissertation. I am also very grateful for having an exceptional doctoral committee and wish to thank Professor Michael G. Parsons, Professor Jun Ni, and Mark H. Spicknall for their continual support and encouragement. Professor Parsons' epigram on the Ph.D. works, "expanding the whole body of human knowledge", became an important milestone and enlightened me to the world of research. Mark Spicknall's research actually "introduced" me to the field of dimensional control management, and it finally became the topic of my dissertation. Also it was a great pleasure to learn and catch the dimensional control research trends in the automotive industry from the publications of Professor Jun Ni and the members of his research center.

My family have all been encouraging even though they often would scratch their heads at one of my incoherent ramblings on the research. My wife Kyung-A bore witness and affirmed as a representative of my whole family in Korea through the completion of a long journey. Her presence helped me to make the transition from where I came to where I am. Our son Joshua Jiwon has cheered me along the way--refreshing me with his smiles whenever I struggled with the unexplainable results. My parents in Korea were a constant source of support. My mother has supported me down to the loving tears she shed at the news that I have passed the final oral defense. They gave me the courage to risk being my creative self wherever that may lead me, especially to this doctoral degree.

Finally, I extend many thanks to my colleagues and friends, especially Dr. Jongho Nam, Dr. Jaehoon Han, Dr. Sangbum Hong, Dr. Kunho Kim, Bonhyung Koo and Jaehong Lee, who made my days at the University of Michigan an unforgettable experience. I would like to thank Ramesh Kumar for sharing his experiences in the dimensional control management.

TABLE OF CONTENTS

LIST OF TABLES

Table

LIST OF FIGURES

Figure

ABSTRACT

The ship block construction process mostly consists of cutting, welding and assembling of steel plates and sections. Even though the plates are relatively thick, the weight and the large size make them behave similar to compliant sheet metal during the block construction processes. Heat flux welding, the major joining process in block erection, causes distortions as well as residual stresses in assemblies due to its highly non-uniform heat flux over very short periods of time, which often results in the degradation of the dimensional quality of the blocks. Compared to the ship's total dimension (on the order of a hundred meters) the required accuracy between the interface of adjacent blocks (on the order of millimeters) is about one in one hundred thousand. Block joint alignment thus requires relatively very high accuracy. Misalignment and nonconformance between the building blocks being erected will adversely impact the total productivity of shipyard significantly by consuming one of the most critical resources in the shipyard.

Distortion caused by the welding process is heavily dependent on the plate's boundary conditions such as clamping of the plates being welded and the sequence of assembly can change these boundary conditions. Also, the plate part variations can be varied through the assembly sequences due to its compliancy. The assembly sequence when designed adequately can positively affect the distortions and deformations during the assembly process without costly mitigation processes.

The concept investigated in this research involves the combining of tolerance analysis/synthesis and finite element analysis, to develop compliant assembly models of ship block construction. The ultimate goal of this research is to investigate the factors that control the deformation of non-nominal plate assemblies after being welded and reduce construction time and cost.

In this dissertation, both tolerance analysis and welding distortion simulation are vigorously investigated to develop a new method for tolerance analysis method for ship block joining. The mechanistic variation simulation, which statistically combines the sensitivity matrix with root sum square method to determine mean and standard deviation without Monte-Carlo simulation, are used for the tolerance analysis and equivalent loading method based on the inherent strain. The method combines B-Spline finite element analysis with empirical data to determine welding distortion without computationally intensive three dimensional nonlinear finite element analysis. A Modified Method of Influential Coefficients is developed for tolerance optimization of ship block erection considering welding distortion. For validation purposes, an example of ship block which consists of two base plates, four stiffeners, and one web frame is tested by the Modified Method of Influential Coefficients and the results compare favorably with that of Monte-Carlo Simulation.

Keywords: Block Assembly, Assembly Sequence, Tolerance, Welding Distortion, Variational Simulation, Inherent Strain, Equivalent Loading Method, Method of Influencial Coefficient, B-Spline Finite Element Method

CHAPTER I

INTRODUCTION

1.1 Motivation

The concept investigated in this research involves the combining of tolerance analysis and finite element analysis, to develop compliant assembly models of ship block construction. The ultimate goal of this research is to investigate the factors that control the deformation of non-nominal plate assemblies after being welded.

Typically, the number of commercial ships produced from one design is at most three to five; i.e., ships are built-to-order products. Therefore, during the block construction process, an intermediate product that does not meet tolerance requirements is not scrapped, but reworked. At the final construction stage, a ship is built by erecting and joining blocks or grand blocks in the dry dock, which is one of the most constrained resources in a shipyard. Compared to its total dimension (on the order of hundred meters) the required accuracy between the interfaces of adjacent blocks (on the order of millimeters) is about one in one hundred thousand. Thus it requires relatively very high accuracy. Misalignment and nonconformance between the building blocks being erected will adversely impact the total productivity of shipyard significantly by consuming the most critical resource in the shipyard much more than the case of well-aligned and conformed blocks.

The ship block construction process mostly consists of cutting, welding and assembling of steel plates. Even though the plates are relatively thick compared to that of the automotive industry, the weight and the large size of the plates make them behave somewhat like compliant sheet metal during the material handling process. In addition, the major joining process in block construction, heat flux welding, causes distortions as well as residual stresses in assemblies due to its high intensity heat flux that actually melts the steel locally over very short periods of time.

Due to these characteristics of the ship block construction processes, many shipbuilders have tried to minimize the welding distortions during block assembly processes in order to achieve higher productivity as well as higher product quality. They have developed several mitigation techniques such as preheating, pre-stretching, tempering, etc. The idea of these mitigation techniques comes from the fact that the distortion is heavily dependent on the mechanical and thermal boundary conditions such as clamping of the plates being welded and the non-uniformity of high temperature distributions during the welding process. Since the sequence of assembly can change these boundary conditions, the proper assembly sequence can positively affect the distortions and deformations during assembly process without costly mitigation processes. [Liu 1995, Roh and Shin 1999].

In addition, variation simulation analysis has been gradually adopted in the automotive industry to predict the variation of the assembled product and identify the major component tolerances and associated process-related dimensional variations that can contribute to non-conformance of the final product. They have been successfully applied to sheet metal assembly cases when welding distortions are negligible.

The goal of this research is to investigate the factors that control the deformation and final dimensional quality of ship block assembly with non-nominal plates. In order to

achieve the goal, welding distortion prediction methods and variational simulation methods are vigorously investigated and a new composite method based on two existing methods, equivalent loading based on inherent strain and method of influential coefficients, is developed. Also, a B-Spline plate finite element is developed for applications in which the slopes and curvatures of final product are important.

1.2 Overview of Related Research

In the strict sense 'assembly planning' can be defined as 'an act of preparing detailed instructions for the assembly of a product' [Parkinson 1985]. In this context, an assembly model in this dissertation is defined as a systematic and generic way of performing assembly planning with consideration of variations, including welding distortions, to achieve an optimal plate assembly outcome.

Since assembly planning and assembly modeling must consider a variety of aspects that affect the production system, this research covers several different but closely related research fields. This literature review surveys the most important areas that are indispensable to understand assembly modeling with tolerance considerations, which are Tolerance Analysis, Tolerance Synthesis, Finite Element Analysis, and Manufacturing Systems Modeling.

1.2.1 Tolerance Analysis

Assembly planning has significant importance for production systems that build complex products such as ships, aircraft and automobiles. These products are produced mainly by assembly through sequential and interdependent steps. Due to these sequential

and dependent characteristics, part variations or intermediate product variations may be cumulative so that very small amounts of variations in intermediate products can result in considerable dimensional errors in the final product. This in turn significantly influences the quality of a product as well as productivity [Chirillo et al. 1982 and 1985].

The study of this aggregate behavior of given individual variations is referred to as tolerance analysis, while the process of allocating tolerances to each intermediate product is tolerance synthesis or tolerance allocation [Lee and Woo 1990]. Among many methods in tolerance analysis, variation simulation analysis has been gradually adopted in the early design stage to predict the variation of the assembled product and identify the major component tolerances that can contribute to non-conformance of the final product [Liu and Hu 1995].

1.2.1.1 Tolerance Analysis and Variational Simulation

Tolerance analysis is the process of estimating the accumulation of the design tolerances on component dimensions and features to ensure that parts can be assembled during production. Tolerance is defined as the permissible variations of a dimension in engineering design. Since tolerance typically only defines the upper and lower limits on dimensions, a dimension can occur anywhere in the range, and thus, the notion of random variables arises with a probabilistic treatment [Henzold 1995].

Tolerance synthesis or allocation is the reverse process of tolerance analysis by which a rational assignment of tolerances to each intermediate product is made during the design phase so that the final product can satisfy the desired tolerance criteria. Tolerance of a part can be represented loosely speaking as a vector since a part may have multiple tolerances on its dimensions. Usually it is necessary to find the tolerance of a part, i.e., a

tolerance vector,υ , where the υ_i component represents the tolerance at i -th source of variation.

$$\upsilon = f(\upsilon_1, \upsilon_2, \cdots, \upsilon_N) \tag{1.1}$$

In special cases, the function f is a linear function. Typically, during the tolerance analysis, systems of nonlinear equations must be solved. However, because the variations in manufacturing processes are relatively small compared to the part dimensions, the above equations can usually be linearized [Gao 1993]. A comprehensive review of dimensioning, tolerancing, the analysis processes may be found in Roy et al. (1991) and Chase and Parkinson (1991).

Currently, the primary methods available for the analysis of assembly variation are worst case, statistical analysis and Monte Carlo simulation. The worst case method was the first approach used for the stack-up in one-dimensional assemblies. It evaluates the assembly under the assumption that all parts are at their extreme values. However, the probability of every part in an assembly having the worst case dimensions at the same time is very low. Hence, this technique generally overestimates assembly variation and requires very tight tolerances for the product to meet the design specification [Chase and Parkinson 1991].

In statistical analysis, the variation of parts are specified as random variables that follow certain statistical distributions and then the corresponding assembly dimension can be calculated according to the tolerance chain of the assembly. A subcase of statistical analysis is the Root Sum Square (RSS) Method. It is based on the assumption that the variance of the dependent variable can be expressed as a first order Taylor's series expansion of independent variables. Also, it is common practice to take the part variation as a normal distribution with mean value at the tolerance midpoint [DeVor et al 1992].

This RSS method yields a more realistic estimate and looser part tolerances than the worst case method [Chase and Parkinson 1991, Lee and Woo 1990].

However, both the worst case and statistical methods are difficult to apply to complex two-dimensional and three-dimensional assemblies because in both cases, it is very difficult to represent the tolerances of each part. Monte-Carlo simulation can be applied to more complex assemblies. This is a widely adopted method that evaluates individual assemblies using a random number generator to select values for each instance of each manufactured dimension, based on the type of statistical distribution assigned by the designer or determined from the production data. By simulating a large number of assemblies, the output can be represented as a statistical distribution [Craig 1989].

1.2.1.2 Tolerance Analysis of Compliant Assemblies

All the above methods are based on the rigid-body assumption and do not consider the non-rigid behavior of compliant parts. Gordis and Flannelly (1994) examined stresses arising from bolt hole tolerances. They showed how the variation in a simple assembly may be mapped into the frequency domain and solved as transient dynamic finite element problem. Also Fang and Liou (1994) applied system dynamics to assembly variation by analyzing a low velocity dynamic assembly of components. This was accomplished by adding springs at the contact points and updating the stiffness matrix at each point in a dynamic solution.

Takezawa (1980) applied linear regression models to real production data for automotive body assemblies in modeling variation stack-ups. He concluded that for compliant sheet metal assemblies, "the conventional addition theorem of variance is no longer valid", because of possible part deformation and springback. In fact, the assembly

process is capable of absorbing variation of the assembled structure provided the process is properly designed. This is clearly a function of part compliance. Furthermore, he noted that "the assembly variance has decreased and is closer to the variance of the stiffer components".

Liu and Hu (1995, 1997a, and 1997b) have advanced the area of tolerancing compliant assemblies. They show that in assemblies of sheet metal on a rigid frame the final tolerances correspond more closely to the tolerance of the rigid frame. Part deformation must be considered to accurately predict the assembly tolerances. They introduce the concept of mechanistic variation simulation to analyze the assembly stack-up of deformable parts. In this concept, Monte Carlo analysis is used to randomly displace nodes in a finite element model and then determine the mean and standard deviation of the assembly.

They expand the concept of mechanistic variation simulation and show how the order of assembly (parallel vs. serial) affects assembly tolerances [Liu et al. 1996]. Finally, they develop the Method of Influence Coefficients [Liu and Hu 1995] as a more efficient method of calculating variations due to compliant assemblies. This method uses a sensitivity matrix obtained from the influence coefficients of the unassembled and assembled parts. These sensitivities are combined statistically using a root sum square to determine the mean and standard deviation. However, they deal only with spot-welded sheet metal assemblies. They do not describe how to combine tolerance stack-ups with compliant assemblies, and they apply their methods only to simple geometries.

Hsieh and Oh (1997) proposed a similar method for the computer simulation of variation in vehicle assembly processes, which combines traditional elastostatic structural analysis with techniques used to evaluate statistics of the system with stochastic parameters. Soman (1996), and Chang and Gossard (1997) proposed similar models for

predicting variations in an assembly consisting of compliant non-ideal parts. Merkley (1996) investigated the covariances among the initial variations and their effects on the final variations of the compliant assemblies. However, those variation models do not include variation associated with tooling, i.e., welding and fixtures. In addition, based on those models, it is hard to generalize some common understanding about the variation propagation in compliant assemblies.

Based on the mechanistic variation simulation model, Hu and Long (1997) proposed a unified variation model for compliant sheet metal assemblies by considering both fixture-induced rigid-body motion and springback deflection. Those studies gave more realistic variation models and offered better understanding about the impacts of the tooling variation.

1.2.1.3 Tolerance Synthesis/Tolerance Design

Tolerance Design is the assignment of tolerance based on process capabilities, cost, performance requirement, etc. This process is also known as tolerance synthesis or tolerance allocation. Tolerance synthesis can be said to be the inverse process of tolerance analysis. Given a specification for a design function, tolerances for independent variables need to be assigned. This is a difficult problem because there is only one assembly tolerance condition and many unknown component tolerances that must be determined.

Initial work in this area was also performed by Greenwood and coworkers. He developed the Uncertain Mean Model, which extends linearized methods to allow for a mean shift or bias in the statistical tolerance data [Chase and Greenwood 1988; Greenwood and Chase 1987; Greenwood and Chase 1988; Greenwood and Chase 1990].

Haugland (1987) and Loosli (1987) also performed research in this area. They applied the method of Lagrange Multipliers and cost versus tolerance functions to allocate the specified assembly tolerance among the component dimensions to achieve the least cost. Their algorithm could also select the most economical process for the task [Chase et al. 1990].

Various models of cost versus tolerance, different search algorithms, and different empirical optimized object functions have been proposed such as linear [Bjorke 1978], reciprocal [Chase and Greenwood 1988, Parkinson 1985], reciprocal powers [Lee and Woo 1990, Chase et al. 1990], exponential [Michael and Siddall 1982] and empirical data based on discrete points [Lee and Woo 1989]. Larsen (1989) developed a hybrid Monte Carlo method that included the Method of System Moments. This method used parametrically defined statistical assembly distributions to rapidly reallocate component tolerances without repeating the Monte Carlo simulation. Andersen (1990) generalized the Lagrange Multiplier method to include multiple loop problems and mixed exponent cost functions. An efficient and robust iteration scheme was devised to find the set of tolerances yielding minimum cost.

1.2.2 Welding Distortion Prediction

Traditional research on welding deformation prediction has focused on the simplified load method, numerical simulation method and three-dimensional finite element analysis. The simplified load method uses empirical equations that have been verified through years of practical implementation in shipyards. It is assumed that the quantity of shrinkage deformation and angular deformation can be calculated by solving equivalent in-plane force and bending moment equations, respectively. The simplified

load method provides very fast and rough estimation on welding distortion, but it is difficult to use for complex geometry. The numerical simulation method [Roh and Shin 1998] assumes inherent strain distributions in plates. Inherent strains are determined as total strain minus elastic strain and by integrating this inherent strain the distortion can be obtained. Since this method uses the assumptions of inherent strain and measured data to predict welding deformation, welding deformation data must be stored systematically to build a database. However, this method also requires a large amount of experimental data to predict welding deformation accurately.

1.2.2.1 Finite Element Analysis(FEA)

Three-dimensional FEA is the most straightforward, but computationally expensive and time-consuming method. It can calculate welding distortions of complex three-dimensional shapes and can predict the deformation accurately. However, it requires relevant modeling of the welding process and defined geometry. Typically, for the prediction of welding distortion, the temperature field and stress and strain field are assumed to be decoupled; i.e., heat input from the torch generates a non-uniform temperature field in plates and this temperature field is calculated by solving heat conduction and convection equation using FEA. Then the thermal stress caused by this temperature field is calculated by FEA [Friedman 1975].

In the 1930s, when the studies on welding distortion began, most research was interested in the welding experiments of individual welded structures. As written in Masubuchi (1980), many researchers performed various experiments and established the empirical formulas to estimate welding distortion. The analytic approaches to the welding deformations based on elasticity began in the 1950s, which contain the inherent strain

theory and the dislocation theory. Watanabe and Satoh (1961) and Fujimoto (1970) considered the initial strain or deformation, which would cause the welding distortion, in the welding structure and calculated the analytic solution based on elasticity. This method is far from the reality of welding deformation of actual welded structures since the initial strains and the welding structures are idealized using simple mathematical models. However, it became a basis of the numerical and the equivalent loading method.

Since some numerical methods such as FDM (Finite Difference Method) and FEM (Finite Element Method) were generalized with development of computer technology in 1960-70 timeframe, many attempts have been made to apply them to the numerical analyses of welding deformations.

The numerical approaches are mainly focused on the simulation of physical behaviors of welding, heat transfer analysis and thermo-elasto-plastic analysis due to welding heat input. In order to get the accurate solution through numerical analysis, two requirements should be satisfied. Firstly, accurate modeling of complicated physical behavior during welding is required considering heat source, temperature-dependent material properties and phase transformation of steel. Secondly, some numerical algorithms which can guarantee high accuracy, reliability and efficiency in computing time and cost is also required since welding causes a concentrated local heating and melting with high singularity. Computationally intensive numerical methods provide some merits, and can analyze several features of welding deformation, stresses, temperature, and phase transformation at a time. But it is not efficient for large scale welded structures such as ship hull blocks. The state of the art of welding deformation analyses using the numerical approaches was reviewed in detail by Tekriwal (1989), Lee (1995) and Artem (2001).

1.2.2.2 Equivalent Loading Method Based on Inherent Strain

In order to analyze welding deformation of large-scale welded structures like ship hull blocks, an equivalent load method based on inherent strain, which can obtain final deformation using only elastic analysis, was suggested by Jang et al. (2002).

In the equivalent load method, the intermediate forming stages of welding deformation during each welding process are abbreviated and only the final deformation is obtained. Equivalent loads are calculated under appropriate assumptions using inherent strains obtained from weld test models and heat transfer analysis. Substituting these loads into the FE model, it is possible to get the final welding deformations through elastic FE analysis of welded structures. Therefore, the equivalent load method is more efficient than thermo-elasto-plastic analysis. However, calculation of equivalent loads should be done in full consideration of mechanical features of welding deformation since the accuracy of solution is greatly dependent on the equivalent load.

According to the calculation method of loads, the equivalent load method is divided into two categories, namely the experiment-based equivalent load method and inherent strain-based equivalent load method.

The experiment-based equivalent load method obtains the forces and moments in reverse, which can give the same results as the measured deflections and shrinkage. Ueda et al. (1985 and 1986a) proposed a method, which can calculate equivalent moments corresponding to angular distortion. He modeled angular distortion by fillet welding as a cantilever beam, which was given by equivalent moments, and induced moment formula, which can give the same angular distortion as the empirical formula of Watanabe and Satoh (1961).

In order to obtain longitudinal shrinkage, transversal shrinkage, and the angular distortion of butt and fillet welding, Nomoto et al. (1997) modeled the welding area as

springs, which had extensional and rotational stiffness. In order to obtain equivalent loads for angular distortion and longitudinal bending deformations, Kim et al. (1996) performed experiments, and put the results into equivalent moment formulae proposed by Ueda et al. (1986b). Thus, because of the accumulation of various deformations according to the assembling sequences like ship hull blocks, the calculation of equivalent loads becomes difficult. Traditional methods calculate equivalent loads of all assembly sequences from experimental results of simple members. They are inappropriate to apply to changes of shapes and boundary conditions according to progress of block assembling.

The equivalent load method based on inherent strain obtains the strains distributed near the welding area and calculates equivalent loads by integrating inherent strains on the welding cross section. In order to obtain the inherent strain distribution near the heating line by line heating, Jang et al. (1995 and 1997) performed a thermo-elasto-plastic analysis of circular disk spring model, and assumed the inherent strain region as elliptical. Jang also applied the inherent strain approaches to the line heating problems [Jang et al. 2002 and 2003]. In a study to apply to the deformation of welded structures, Seo and Jang (1997, 1999) calculated inherent strain through thermo-elasto-plastic analysis of one-dimensional bar-spring model. Their studies introduced the concept of the degree of restraints. It denotes the degree of restraint of an adjacent area, which restrains expansion or shrinkage of the welding area. It also reflects dimensions of members, materials, structure shapes, and boundary conditions. Seo and Jang (1997) and Jang et al. (2004) performed an additional elastic analysis to consider the effect of the block assembly process for the degree of restraints. As a result, the theoretical background was prepared, which can consider the effects of changes in boundary conditions and structural shapes on the calculation of inherent strain. On-the-other-hand, assumptions on the shape

and area of inherent strain region, and on the value of inherent strains, needs further improvements for precise analysis for various welding conditions.

Murakawa et al. (1996) used a simplified analysis model to obtain the inherent strain. They represented the inherent strain as a function of the highest temperature and degree of restraint. However, this method has limitations in applying it to complicated structures. Jang and Seo (1995) suggested an efficient method to determine the inherent strain region and expressed the inherent strains as a function of the mechanical melting temperature [Ueda and Ma 1995] and the degree of restraint. Seo and Jang (1999) calculated the deformation of large structure using the unit loading method to obtain the degree of restraint.

1.2.3 Previous Research on Tolerance and Accuracy in the Shipbuilding Industry

Research work on tolerance analysis or tolerance synthesis are rare in the U.S. shipbuilding industry. Chirillo et al. (1982 and 1985) performed research on the basic idea of accuracy control in the ship construction process. Storch (1985) further expands his statistical accuracy control research into several case studies on accuracy control in U.S. shipyards. However this work focused on introducing the concepts of statistical quality and accuracy control into the shipbuilding industry. He further investigated the variation problem in hull construction and proposed rework level simulation to predict rework requirement levels in hull block construction by statistical tolerance analysis [Storch and Giesy 1988]. Their work focused on statistical accuracy control and did not consider welding distortion and compliancy at the same time. Since the welding distortion is the major source of dimensional inaccuracy, Chris and Randy (1997) performed basic research on the control of the welding distortion in think ship panels.

Spicknall and Kumar (2002 and 2003) investigated the dimensional management systems applicable to ship block construction stages and developed a dimensional variation simulation and analysis tool. They included weld shrinkage by considering in-plane shrinkage and its variation in the heat-affected zones of fillet welds. However their approach was based on rigid body assumptions so that it is very hard to model the springback effects of the final assemblies.

In Japan and Korea, prediction of welding deformation has been widely researched for the purpose of accuracy control in ship production process. Nomoto and Aoyama performed basic studies on accuracy management systems based on estimating welding deformations [Aoyama et al. 1997 and Nomoto et al. 1997]. Okumoto and Matsuzaki (1997) proposed a new approach to accurate production of hull structure by predicting the welding deformation. Ueda and colleagues (1975, 1985, 1986a, 1986b, 1989, 1991, and 1995) had performed various research on precise prediction on welding deformation. In addition to prediction of welding deformation, production of curved shell plates by line heating also have been widely researched in Japan and Korea.

Roh and Shin (1998) showed that the assembly sequence affects the final deformation shape of the hull block by numerical simulation considering welding deformation and gravity. However, they only simulated the block assembly but did not consider variations nor provide any systematic approach or methodology to the generate optimal assembly sequences.

1.3 Research Objectives

The goal of this research involves the combining of tolerance analysis and finite element analysis, to develop compliant assembly models of ship block construction. For

this particular model, part variation stack ups and welding distortion of non-nominal parts should be considered. In addition, joining processes like fusion welding typically used in ship block construction, which cause relatively large deformation and residual stresses during the process, must be considered. The combined processes originally suggested by Liu and Hu (1995) are further modified and illustrated in a sketch in Figure 1.1.

Efficient tolerance analysis methodology is essential in efficient tolerance synthesis. In addition, efficient welding distortion prediction is necessary in order to consider the welding distortion in tolerance synthesis. Three-dimensional finite element analysis is a computationally expensive and time consuming process. An alternative is mechanistic variation simulation, which statistically combines the sensitivity matrix with root sum square method to determine means and standard deviations [Liu 1995]. The simulations employ the equivalent loading method based on the inherent strain, which combines finite element analysis with empirical data to determine welding distortion without computationally intensive three-dimensional nonlinear finite element analysis. To fulfill the objective, variational simulation of compliant assemblies and welding distortion are vigorously investigated to develop the Modified Method of Influential Coefficients. In addition a B-Spline plate finite element is developed for applications where the slopes and curvatures of the final product are important.

Finally for validation purposes, variational simulation of the out-of-plane deviation is performed for a ship block which consists of two base plates, four stiffeners, and one web frame, based on the Modified Method of Influentice Coefficients. In the example case, two base plates are butt-welded first, then four equally spaced stiffeners are attached on the welded plate, and the web frame is welded to the plate-stiffener assembly, as shown in Figure 1.2. Figure 1.3 further elaborates the processes with the

examples of ship block assembly. The result is compared to that of Monte Carlo simulation.

1.4 Organization of Dissertation

The presentation of this research is organized as follows. In Chapter II the B-Spline plate finite element is developed and Chapter III includes the characteristics and properties of welding distortion simulation and the formulation of the inherent strain method. Chapter IV provides the method of mechanistic variation model considering welding distortion effects. A small panel assembly example is presented as well. Chapter V presents numerical simulation of butt welding of two plates with initial variation for an example and the assembly case is also examined.

Finally, in Chapter VI, the conclusion and recommendations for future work are presented.

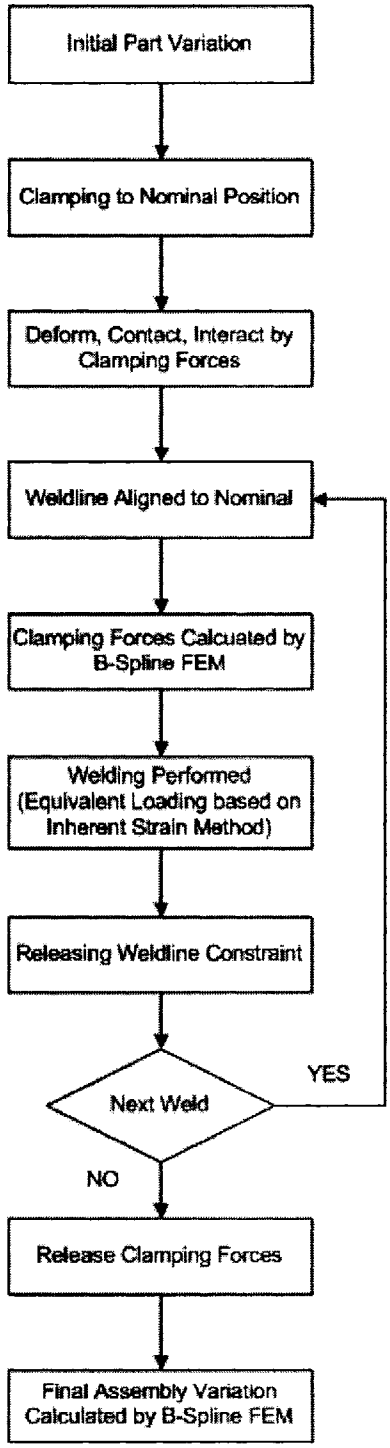

Figure 1. 1: Mechanistic Variation Simulation Process for Compliant Metal Plate Assemblies

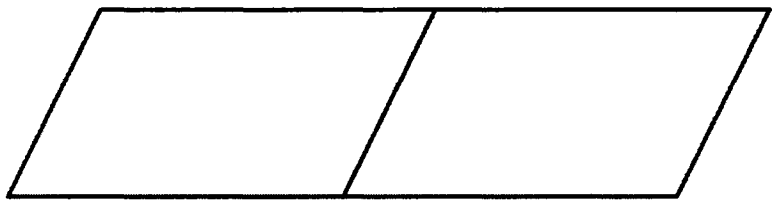

(a) two plates are butt-welded

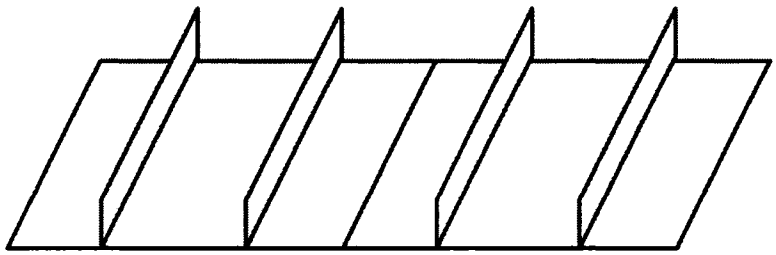

(b) stiffeners are attached and welded

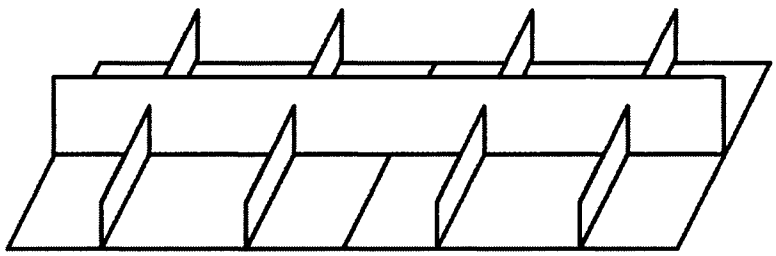

(c) web frame is attached and welded

Figure 1. 2: Assembly Process for Ship Block Example

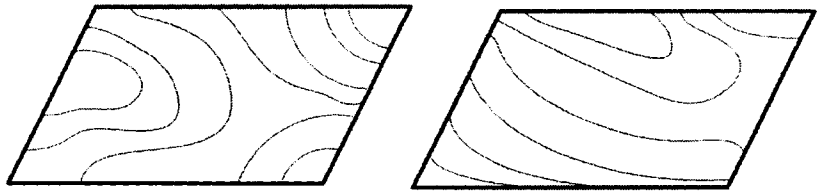

(a) initial part variation in base plates are modeled as B-Spline plate elements

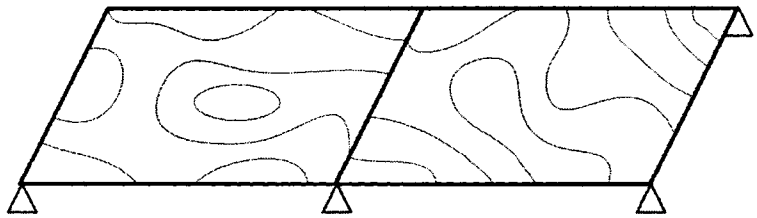

(b) two plates are clamped to their nominal positions

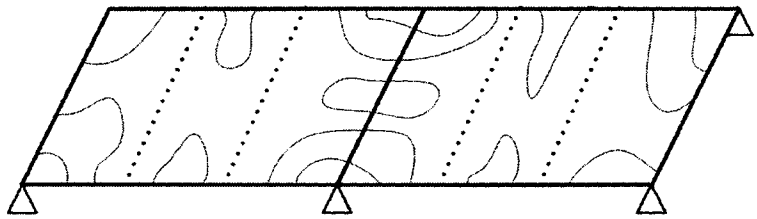

(c) two plates are welded and stiffener weldlines are aligned to nominal positions

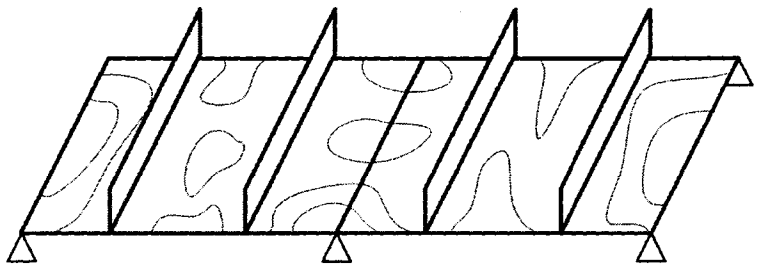

(d) stiffeners are welded and weldline clamping forces are released

Figure 1.3: Mechanistic Variation Simulation Process for Ship Block Example

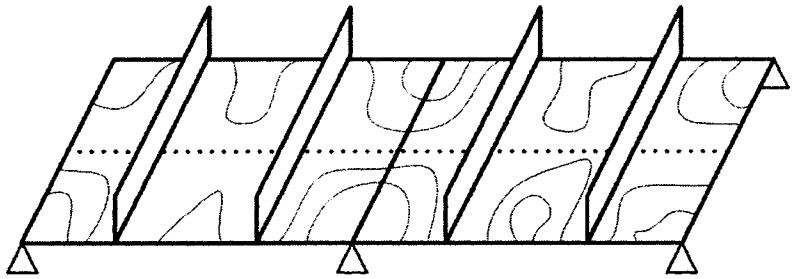

(e) web frame weldline is aligned to its nominal position

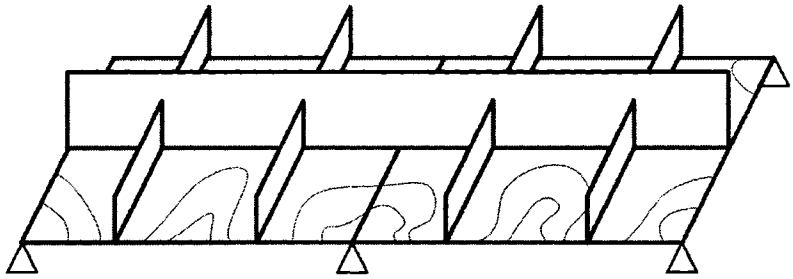

(f) web frame is welded and weldline clamping forces are released

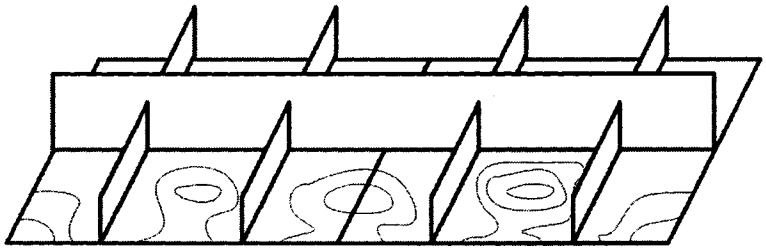

(g) all clamping forces are released and final assembly variations are calculated

Figure 1.3: Mechanistic variation simulation process for ship block example (cont.)

CHAPTER II

RANDOM B-SPLINE CURVES AND SURFACES

Ship structural designs often call for plate elements to be assembled with other plate or stiffener elements. During the manufacturing process, these elements may be clamped to fixtures for fit-up prior to joining. Problems may arise due to the imperfections in the geometry of the assembled elements, which contributes to significant clamping forces required for mating and to distortion and residual stresses after assembly. In order to predict these forces, an adequate description of the plate and stiffener geometry is needed. Generally this data is available only in a statistical sense.

A common and straightforward method is to measure the maximum out-of-plane variation of the plate part. It is simple and easy to apply to shipyard practice. However, it does not account for the point of variation in the part and is not applicable to curved shell parts. Finite element meshing is also used to represent the shape variation of plate parts. This method is to measure the location of every mesh point and compare them point by point with the ideal part geometry. It is relatively simple and robust but cannot effectively express the slope and curvature and their variations in shape in case they are important. In order to consider the slope and curvature of the part, Merkley developed the Random Bézier Curve [Merkley 1998], but it cannot effectively represent the variations of the plate part since it does not support the locality of the shape. B-Spline representation is widely used in geometry representation. However, it is not yet developed to represent statistical shapes such as variations in plate parts. In this chapter, new random B-Spline

curves and surfaces are developed to express plate part shape variation with B-Spline geometry statistically. For the validation purpose, ship structural parts are first established by Cubic B-Spline surface and curve modeling. The geometry is defined by control point coordinates as is common in surface CAD environments. And it is shown that the mean and standard deviation data for the control points defines the mean values and standard deviation for the surfaces [Chung and Karr 2004]. By employing B-Spline finite element analysis, this chapter shows that the control point statistics can be directly related to the forces required to clamp or flatten the plates and stiffeners to prescribed surfaces.

2.1 Statistical Representation of Random Bézier Curve and Surface

A Bézier curve of degree n is defined by:

$$\underline{C}(u) = \sum_{i=0}^{n} B_{i,n}(u)\vec{P}_i, \quad 0 \le u \le 1 \tag{2.1}$$

where $B_{i,n}(u)$ is the i-th Bernstein basis function of degree n, which is defined by:

$$B_{i,n}(u) = \frac{n!}{(n-i)!i!}u^i(1-u)^{n-i} \tag{2.2}$$

and $\vec{P}_i$ are control points, $\vec{P}_i \in R^3$. As parameter u varies from 0 to 1, $\underline{C}(u)$ represents a smooth curve in R^3 space.

For the purpose of part variation representation, an error vector for the i-th control point, $\vec{\varepsilon}_i$, is introduced. The Bézier curve is now represented as

$$\underline{C}(u) = \sum_{i=0}^{n} B_{i,n}(u)(\vec{P}_i + \vec{\varepsilon}_i) = \sum_{i=0}^{n} B_{i,n}(u)\vec{P}_i + \sum_{i=0}^{n} B_{i,n}(u)\vec{\varepsilon}_i$$
$$= \underline{C}_n(u) + \underline{C}_{err}(u) \tag{2.3}$$

where subscript n represents 'nominal' and err 'error'.

Considering the control points, $\vec{P}_i = [X_i, Y_i, Z_i]^T$, as random variables, a family of random curves can be represented by mean value and covariance of the control points. For Cartesian coordinates, the Bézier curve can be decomposed as three independent vector components.

$$\underline{C}(u) = \begin{Bmatrix} x(u) \\ y(u) \\ z(u) \end{Bmatrix} \tag{2.4}$$

Each component of the Bézier curve is described as:

$$x(u) = \sum_{i=0}^{n} B_{i,n}(u) X_i = \vec{B}_n \cdot \vec{P}_X \tag{2.5}$$

where $\vec{B}_n$ represents the vector of Bernstein polynomials of degree n. Similarly, one has:

$$y(u) = \vec{B}_n \cdot \vec{P}_Y$$
$$z(u) = \vec{B}_n \cdot \vec{P}_Z \tag{2.6}$$

The mean values and standard deviations of each of these components are respectively:

$$E[x(u)] = E[\vec{B}_n \cdot \vec{P}_X] = \vec{B}_n \cdot E[\vec{P}_X] = \vec{B}_n \cdot \vec{\mu}_{P_X} = \mu_X(u) \tag{2.7}$$

$$VAR[x(u)] = E[\{x(u) - E[x(u)]^2\}] = E[\{x(u) - E[x(u)]\} \cdot \{x(u) - E[x(u)]\}^T]$$
$$= \overrightarrow{B_n} \cdot E[(\overrightarrow{P_X} - \overrightarrow{\mu_{P_X}}) \cdot (\overrightarrow{P_X} - \overrightarrow{\mu_{P_X}})^T] \cdot \overrightarrow{B_n}^T = \overrightarrow{B_n} \cdot \Sigma_{P_X} \cdot \overrightarrow{B_n}^T = \sigma_{x(u)}{}^2 \tag{2.8}$$

where $\overrightarrow{\mu_{P_X}} = [E[X_0], \quad E[X_1], \quad \cdots \quad E[X_n]]^T$, $\sigma_{x(u)}$ is the standard deviation of x component of the control points, and Σ_{P_X} is defined as covariance matrix of x component of the control points. Similar expressions apply for y and z components.

Each of covariance matrices, Σ_{P_X}, Σ_{P_Y}, and Σ_{P_Z}, is a $n \times n$ matrix that describes the variance of each control point and the associated covariance. While there may be covariance between the control points for a given component direction, there is no covariance between the components. So $x(u)$, $y(u)$, and $z(u)$ are completely independent of each other. Thus the variance statement relating the curve variance to the control point covariance for a random Bézier curve of degree n is:

$$\sigma_{x(u)}{}^2 = \sigma_{y(u)}{}^2 = \sigma_{z(u)}{}^2$$
$$= [B_{o,n}(u) \quad B_{1,n}(u) \quad \cdots \quad B_{o,n}(u)] \cdot \begin{bmatrix} \sigma_{00} & \sigma_{01} & \cdots & \sigma_{0n} \\ \sigma_{01} & \ddots & & \vdots \\ \vdots & & \ddots & \vdots \\ \sigma_{0n} & \sigma_{1n} & \cdots & \sigma_{nn} \end{bmatrix} \begin{Bmatrix} B_{o,n}(u) \\ B_{1,n}(u) \\ \vdots \\ B_{o,n}(u) \end{Bmatrix} \tag{2.9}$$

Material covariance arises from elastic coupling within a compliant assembly. For example as some gaps are closed by joining, the joining not only closes the gap at its location but also decreases the nearby gaps. Geometric covariance describes the correlation of surface errors at adjacent points on a curve or surface. However, if we separate the nominal curve from the error curve, we could ignore the geometric covariance terms in the error curves.

A Bézier surface of degree n is defined by:

$$\underline{S}(u,v)=\sum_{i=0}^{n}\sum_{j=0}^{m}B_{i,n}(u)B_{j,m}(v)\overrightarrow{P_{i,j}} \tag{2.10}$$

where $B_{i,n}(u)$, $B_{j,m}(u)$ are i-th Bernstein basis functions, $0\le u,v\le 1$ and $\overrightarrow{P_{i,j}}$ are the net of control points, $\overrightarrow{P_{i,j}}\in R^3$. Introducing an error vector, $\overrightarrow{\varepsilon_{i,j}}$, to each of the control points, part variation can be represented as 'error' surface.

$$\begin{aligned}\underline{S}(u,v)&=\sum_{i=0}^{n}\sum_{j=0}^{m}B_{i,n}(u)B_{j,m}(v)(\overrightarrow{P_{i,j}}+\overrightarrow{\varepsilon_{i,j}})\\&=\sum_{i=0}^{n}\sum_{j=0}^{m}B_{i,n}(u)B_{j,m}(v)\overrightarrow{P_{i,j}}+\sum_{i=0}^{n}\sum_{j=0}^{m}B_{i,n}(u)B_{j,m}(v)\overrightarrow{\varepsilon_{i,j}}\\&=\underline{S}_n(u,v)+\underline{S}_{err}(u,v)\end{aligned} \tag{2.11}$$

Surface expressions are of the form:

$$\begin{aligned}x(u,v)&=\sum_{i=0}^{n}\sum_{j=0}^{m}B_{i,n}(u)B_{j,m}(v)X_{i,j}\\&=[B_{0,n}\quad B_{1,n}\quad\cdots\quad B_{n,n}]\cdot\begin{bmatrix}X_{00}&X_{01}&\cdots&X_{0m}\\X_{10}&\ddots&&\vdots\\\vdots&&\ddots&\vdots\\X_{n0}&\cdots&\cdots&X_{nm}\end{bmatrix}\begin{Bmatrix}B_{0,m}\\B_{1,m}\\\vdots\\B_{m,m}\end{Bmatrix}\\&=\overrightarrow{B_n}^T[X_{i,j}]_{n\times m}\overrightarrow{B_m}\end{aligned} \tag{2.12}$$

The mean value and variance of the components can be expressed as:

$$\begin{aligned}E[x(u,v)]&=E[\overrightarrow{B_n}^T[X_{i,j}]_{n\times m}\overrightarrow{B_m}]=\overrightarrow{B_n}^T E[\{[X_{i,j}]_{n\times m}\}]\overrightarrow{B_m}\\&=\overrightarrow{B_n}^T\mu_{X_{i,j}}\overrightarrow{B_m}\end{aligned} \tag{2.13}$$

$$\begin{aligned}\sigma_{x(u,v)}{}^2&=VAR[x(u,v)]=E[\{x(u,u)-E[x(u,v)]^2\}]\\&=E[\overrightarrow{B_n}^T([X_{i,j}]-\mu_{X_{i,j}})\overrightarrow{B_m}\cdot\overrightarrow{B_m}^T([X_{i,j}]-\mu_{X_{i,j}})^T\overrightarrow{B_n}\end{aligned} \tag{2.14}$$

The variance can be written as:

$$\begin{aligned}\sigma_{x(u,v)}{}^2 &= \overrightarrow{B_m}\cdot\overrightarrow{B_m}^T\overrightarrow{B_n}^T E[([X_{i,j}]-\mu_{X_{i,j}})([X_{i,j}]-\mu_{X_{i,j}})^T]\overrightarrow{B_n} \\ &= \overrightarrow{B_m}\cdot\overrightarrow{B_m}^T\overrightarrow{B_n}^T\Sigma_{P_X}\overrightarrow{B_n}\end{aligned} \tag{2.15}$$

where $\mu_{X_{i,j}}$ means the mean value of x component of each control points, i.e.,

$$\mu_{X_{i,j}} = \begin{bmatrix} E[X_{00}] & \cdots & E[X_{0m}] \\ \vdots & \ddots & \vdots \\ E[X_{n0}] & \cdots & E[X_{nm}] \end{bmatrix} \tag{2.16}$$

and Σ_{P_X} covariance matrix of X components of the control points net.

Each covariance matrix, Σ_{P_X}, Σ_{P_Y}, and Σ_{P_Z}, is an $(n+1)\times(m+1)$ matrix that describes the variance of each control point and the associated covariance. Therefore the mean value of random Bézier surface can be represented as the nominal value of the control points. In addition, given a distribution of the control points, the statistical distribution of the entire surface can be obtained.

2.2 Statistical Representation of Random B-Spline Curve and Surface

A p-th degree B-Spline curve is defined by:

$$\underline{C}(u) = \sum_{i=0}^{n} N_{i,p}(u)\overrightarrow{P_i}, \quad a \le u \le b \tag{2.17}$$

where $\overrightarrow{P_i}$ are control points, $\overrightarrow{P_i} \in R^3$, and $N_{i,p}(u)$ are p-th degree B-Spline basis functions defined on the nonperiodic (and nonuniform) knot vector:

$$U = \{\underbrace{a, \cdots, a}_{p+1}, u_{p+1}, \cdots, u_{m-p-1}, \underbrace{b, \cdots, b}_{p+1}\} \tag{2.18}$$

and:

$$N_{i,0}(u) = \begin{cases} 1 & \text{if } u_i \le u < u_{i+1} \\ 0 & \text{otherwise} \end{cases}$$
$$N_{i,p}(u) = \frac{u - u_i}{u_{i+p} - u_i} N_{i,p-1}(u) + \frac{u_{i+p+1} - u}{u_{i+p+1} - u_{i+1}} N_{i+1,p-1}(u) \tag{2.19}$$

B-Spline surface is obtained by taking a bi-directional net of control points, two knot vectors, and the products of the univariate B-Spline functions.

$$\underline{S}(u,v) = \sum_{i=0}^{n} \sum_{j=0}^{m} N_{i,p}(u)\ N_{j,q}(v)\ \overrightarrow{P_{i,j}} \tag{2.20}$$

with

$$U = \{\underbrace{a, \cdots, a}_{p+1}, u_{p+1}, \cdots, u_{r-p-1}, \underbrace{b, \cdots, b}_{p+1}\}$$
$$V = \{\underbrace{a', \cdots, a'}_{q+1}, v_{q+1}, \cdots, v_{s-q-1}, \underbrace{b', \cdots, b'}_{q+1}\} \tag{2.21}$$

Since $N_{i,p}(u)$ are piecewise polynomials, a B-Spline curve is a piecewise polynomial curve, which can be expressed as piecewise Bézier curves. If $n = p$ and $U = \{0, \cdots, 0, 1, \cdots, 1\}$, then it is a Bézier curve. For a Bézier curve, it is possible to statistically relate the curve shape with the control points so that B-Spline curve is also statistically related to the control points. A similar argument holds for B-Spline surfaces. Therefore, for B-Spline curve and surface as well, the statistical representations are also piecewise valid as the case of Bézier curve and surface.

2.3 Cubic B-Spline Finite Element Definition

The spline functions are important tools in the analysis of the plates and beams. Among the many spline functions, cubic B-Spline is the most commonly used for plates and shells analysis in case the geometrical shape information such as slope and curvature is important. It is computationally efficient, flexible to model different boundary conditions, and it tends to minimize 'winkles' in the element since it is piecewise continuous so that local shape variation can be modeled without affecting the whole part shape. In this section, cubic B-Spline beam and plate element are developed based on the displacement method [Bathe 1996].

2.3.1 Displacement Discretization

For the general B-Spline curve, positions in the curve should be represented as B-Spline form, such as:

$$P = \underline{C}(u) = \sum_{i=0}^{n} N_{i,p}(u)\vec{P}_i, \quad 0 \le u \le 1 \tag{2.22}$$

in tensor notation:

$$P^i = N_{n,p}(u)P_n^i \tag{2.23}$$

where superscript i represent each component $(i = 1,2,3)$ and the subscript n denotes n-th control points and basis functions. The displacement at any point is a vector and it is approximated by the set of functions of position, called basis functions or shape functions, each multiplied by coefficients.

However, since the generic cubic B-Spline basis function is distributed as Figure 2.1, it is unfavorable to directly apply the functions as the shape function of a finite element model since the magnitudes of basis functions are not uniformly distributed but rather concentrated at the both ends of the curve. It would require special cautions to assemble elements and to apply boundary conditions. To alleviate these problems, a new basis function that requires two additional control points, has been adopted [Leung and Au, 1990], as shown in Figure 2.2. In other words, the displacements are defined by parameters at the knots, some of which are lying outside the curve or surface to be modeled, in order to consider the boundary conditions and assembly of the elements.

2.3.2 Cubic B-Spline Beam Element

A beam element is first divided into m sections of equal length, h. The spline function adopted to represent the displacement, w, is a cubic B-Spline which has equally spaced control points, and is given as:

$$w = \sum_{i=-1}^{m+1} \alpha_i \varphi_i \tag{2.24}$$

where α_i represents the coefficients and φ_i are cubic B-Spline function which has non-zero value over four consecutive sections. φ_i are defined as:

$$\varphi_i(x)=\begin{cases}\dfrac{1}{6h^3}(x-x_{i-2})^3 & x_{i-2}\le x<x_{i-1}\\ \dfrac{1}{6h^3}\{h^3+3h^2(x-x_{i-1})+3h(x-x_{i-1})^2-3(x-x_{i-1})^3\} & x_{i-1}\le x<x_i\\ \dfrac{1}{6h^3}\{h^3+3h^2(x_{i+1}-x)+3h(x_{i+1}-x)^2-3(x_{i+1}-x)^3\} & x_i\le x<x_{i+1}\\ \dfrac{1}{6h^3}(x_{i+2}-x)^3 & x_{i+1}\le x<x_{i+2}\\ 0 & \textit{otherwise}\end{cases} \tag{2.25}$$

φ_i is centered at x_i and is shown in Figure 2.3.

In vector notation, the displacement function for the beam element can be denoted as:

$$\{w\}=[\varphi]\{\alpha\} \tag{2.26}$$

where:

$$[\varphi]=[\varphi_{-1}\quad\varphi_0\quad\varphi_1\quad\cdots\quad\varphi_{m-1}\quad\varphi_m\quad\varphi_{m+1}] \tag{2.27}$$

$$\{\alpha\}=[\alpha_{-1}\quad\alpha_0\quad\alpha_1\quad\cdots\quad\alpha_{m-1}\quad\alpha_m\quad\alpha_{m+1}]^T \tag{2.28}$$

According to the strain-displacement relationship, we could derive:

$$\{\varepsilon\}=\left\{\frac{\partial^2 w}{\partial x^2}\right\}=[\varphi'']\{\alpha\} \tag{2.29}$$

The liner stress-strain relationship for a prismatic beam is:

$$\{\sigma\}=[EI]\{\varepsilon\} \tag{2.30}$$

where EI is the flexural rigidity of the beam. Then the stiffness matrix with respect to the spline parameters, $[K_s]$, can be defined as:

$$[K_s] = \int_{x_0}^{x_m} [\varphi'']^T [EI][\varphi''] dx \tag{2.31}$$

with

$$\{f\} = [K]\{\delta\} \tag{2.32}$$

Let us consider that the displacement and rotations at the ends of the beam element can be expressed in terms of the spline parameters as:

$$\begin{aligned} w_0 &= \frac{1}{6}(\alpha_{-1} + 4\alpha_0 + \alpha_1) \\ \theta_0 &= \frac{1}{2h}(-\alpha_{-1} + \alpha_1) \\ w_m &= \frac{1}{6}(\alpha_{m-1} + 4\alpha_m + \alpha_{m+1}) \\ \theta_m &= \frac{1}{2h}(-\alpha_{m-1} + \alpha_{m+1}) \end{aligned} \tag{2.33}$$

And the displacement vector in physical coordinates are defined as the vector with w_i's and the rotations at both end of the beam, i.e., θ_0 and θ_m.

$$\{\delta\} = [w_0 \quad \theta_0 \quad w_1 \quad \cdots \quad w_{m-1} \quad w_m \quad \theta_m]^T \tag{2.34}$$

Then the transformation matrix $[T]$ is defined as:

$$\{\delta\} = [T]\{\alpha\} \tag{2.35}$$

Finally the stiffness matrix with respect to the physical coordinate is:

$$[K]=[T]^{-T}[K_s][T]^{-1} \tag{2.36}$$

where $[K]$ is $(m+3)\times(m+3)$ square matrix.

2.3.3 Cubic B-Spline Beam Element Example

Let us consider cubic B-Spline beam bending problem with material properties, E and I, and assume that the length of the beam is $4h$ and the spline consists of 4 sections, as shown in Figure 2.4.

The displacement is:

$$w=\sum_{i=-1}^{5}\alpha_i\varphi_i \tag{2.37}$$

And spline parameters and shape fuctions are:

$$\begin{aligned}
[\varphi] &= [\varphi_{-1} \quad \varphi_0 \quad \varphi_1 \quad \varphi_2 \quad \varphi_3 \quad \varphi_4 \quad \varphi_5] \\
\{\alpha\} &= [\alpha_{-1} \quad \alpha_0 \quad \alpha_1 \quad \alpha_2 \quad \alpha_3 \quad \alpha_4 \quad \alpha_5]^T \\
\{\delta\} &= [w_0 \quad \theta_0 \quad w_1 \quad w_2 \quad w_3 \quad w_4 \quad \theta_4]^T
\end{aligned} \tag{2.38}$$

The transformation matrix is derived as:

$$[T]=\begin{bmatrix} \frac{1}{6} & \frac{2}{3} & \frac{1}{6} & 0 & 0 & 0 & 0 \\ -\frac{1}{2h} & 0 & \frac{1}{2h} & 0 & 0 & 0 & 0 \\ 0 & \frac{1}{6} & \frac{2}{3} & \frac{1}{6} & 0 & 0 & 0 \\ 0 & 0 & \frac{1}{6} & \frac{2}{3} & \frac{1}{6} & 0 & 0 \\ 0 & 0 & 0 & \frac{1}{6} & \frac{2}{3} & \frac{1}{6} & 0 \\ 0 & 0 & 0 & 0 & \frac{1}{6} & \frac{2}{3} & \frac{1}{6} \\ 0 & 0 & 0 & 0 & -\frac{1}{2h} & 0 & \frac{1}{2h} \end{bmatrix} \tag{2.39}$$

Assuming that $h=1$, the stiffness matrix is calculated as:

$$[K_s]=\begin{bmatrix} \frac{201}{28} & \frac{123}{28} & -\frac{75}{7} & \frac{9}{2} & -\frac{9}{7} & \frac{9}{28} & -\frac{3}{28} \\ \frac{123}{28} & \frac{97}{28} & -\frac{39}{7} & \frac{3}{2} & -\frac{3}{7} & \frac{3}{28} & -\frac{1}{28} \\ -\frac{75}{7} & -\frac{39}{7} & \frac{132}{7} & -12 & \frac{36}{7} & -\frac{9}{7} & \frac{3}{7} \\ \frac{9}{2} & \frac{3}{2} & -12 & 15 & -12 & \frac{9}{2} & -\frac{3}{2} \\ -\frac{9}{7} & -\frac{3}{7} & \frac{36}{7} & -12 & \frac{132}{7} & -\frac{75}{7} & \frac{39}{7} \\ \frac{9}{28} & \frac{3}{28} & -\frac{9}{7} & \frac{9}{2} & -\frac{75}{7} & \frac{201}{28} & -\frac{123}{28} \\ -\frac{3}{28} & -\frac{1}{28} & \frac{3}{7} & -\frac{3}{2} & \frac{39}{7} & -\frac{123}{28} & \frac{97}{28} \end{bmatrix} \tag{2.40}$$

Figure 2.5 shows the deflection when the beam is simply supported with the concentrated load P in the midspan. As shown in the figure, the deflection exactly

matches that of the exact solution. This is because the polynomial displacement function matches the exact solution from elastic beam bending theory. Figure 2.6 shows the deflection of cubic B-Spline beam when the beam is simply supported and subject to the concentrated moment M at one end. Figure 2.7 represents the deflection of cantilever beam under concentrated load P at the tip.

Let us consider now the clamping force problem. Assuming that the beam is simply supported, the variations are statistically independent, and has the shape variation as:

$$Var_{mean} = \begin{bmatrix} w_0 = 0 & \theta_0 = 0 & w_1 = 0.1 & w_2 = -0.1 & w_3 = 0.1 & w_4 = 0 & \theta_4 = 0 \end{bmatrix}^T$$
$$Var_{stdev} = \begin{bmatrix} 0.01 & 0.01 & 0.01 & 0.01 & 0.01 & 0.01 & 0.01 \end{bmatrix}^T \quad (2.41)$$

where the subscript *mean* and *stdev* represent average and standard deviation of the beam shape, respectively. Then the clamping forces required to straighten the beam can be calculated as:

$$\{f\}_{mean} = EI\begin{bmatrix} -1.65 & -0.75 & 3.6 & -3.9 & 3.6 & -1.65 & 0.75 \end{bmatrix}^T$$
$$\{f\}_{stdev} = EI\begin{bmatrix} 0.1441 & 0.0805 & 0.2596 & 0.2362 & 0.2596 & 0.1441 & 0.0805 \end{bmatrix}^T \quad (2.42)$$

As shown in this example, statistical shape variations in the beam can be directly used to determine the forces required to clamp or flatten the beam to nominal shape.

2.3.4 Cubic B-Spline Plate Element

A rectangular plate element of dimensions $a \times b$ ($0 \le x \le a$ and $0 \le y \le b$) is considered as shown in Figure 2.8. The element is divided into a rectangular grid such that:

$$h_x = a/n, \quad h_y = b/m \tag{2.43}$$

The spline function adopted to represent the displacement, w, can be expressed as:

$$w = \sum_{j=-1}^{m+1} \sum_{i=-1}^{n+1} c_{ij}\, \varphi_i(x) \psi_j(y) = [N]\{\delta_s\} \tag{2.44}$$

where $\varphi_i(x)$ and $\psi_i(y)$ are cubic B-Splines similarly defined in x and y direction as Equation (2.25) for the beam element and $[N]$ is shape function equivalent to $[\varphi]$ in beam element. Similarly, spline functions, spline parameters are defined as:

$$\{\delta_s\} = \left[\{c\}_{-1}^T \quad \{c\}_0^T \quad \{c\}_1^T \quad \cdots \quad \{c\}_{m-1}^T \quad \{c\}_m^T \quad \{c\}_{m+1}^T \right]^T \tag{2.45}$$

$$\{c\}_j = \left[c_{-1,j} \quad c_{0,j} \quad \cdots \quad c_{n+1,j} \right]^T \tag{2.46}$$

$$[\varphi] = [\varphi_{-1} \quad \varphi_0 \quad \cdots \quad \varphi_{n+1}] \tag{2.47}$$

$$[\psi] = [\psi_{-1} \quad \psi_0 \quad \cdots \quad \psi_{m+1}] \tag{2.48}$$

And:

$$[N] = [\psi] \otimes [\varphi] \tag{2.49}$$

where $\otimes$ is the Kronecker product of the matrices. The strain-displacement relationship is obtained from Kirchhoff's theory, which is:

$$\{\varepsilon\} = \begin{Bmatrix} -\dfrac{\partial^2 w}{\partial x^2} \\ -\dfrac{\partial^2 w}{\partial y^2} \\ 2\dfrac{\partial^2 w}{\partial x \partial y} \end{Bmatrix} = \begin{bmatrix} -[\psi] \otimes [\varphi''] \\ -[\psi''] \otimes [\varphi] \\ 2[\psi'] \otimes [\varphi'] \end{bmatrix} \{\delta_s\} = [B]\{\delta_s\} \tag{2.50}$$

And the strain-stress relationship for an isotropic plate can be defined as:

$$\{\delta\} = \frac{Et^3}{12(1-\nu^2)} \begin{bmatrix} 1 & \nu & 0 \\ \nu & 1 & 0 \\ 0 & 0 & \dfrac{(1-\nu)}{2} \end{bmatrix} = [D]\{\varepsilon\} = [D][B]\{\delta_s\} \tag{2.51}$$

where E is Young's modulus, ν Poisson's ratio, and t plate thickness.

The stiffness matrix with respect to the spline parameters can be evaluated by:

$$[K_s] = \int_{y_0}^{y_m} \int_{x_0}^{x_n} [B]^T [D][B] dxdy \tag{2.52}$$

Considering the rectangular knots grid of spacing h_x and h_y along x and y direction, respectively, we get the following relationships for displacement ($w_{i,j}$), rotation about the x-axis ($\theta^x_{i,j}$), rotation about the y-axis ($\theta^y_{i,j}$), and twist ($\theta^{xy}_{i,j}$) expressed in spline parameters:

$$\begin{aligned} w_{i,j} = \frac{1}{36}\{&16c_{i,j} + 4(c_{i,j+1} + c_{i+1,j} + c_{i,j-1} + c_{i-1,j}) \\ &+ (c_{i+1,j+1} + c_{i+1,j-1} + c_{i-1,j-1} + c_{i-1,j+1})\} \end{aligned} \tag{2.53}$$

$$\theta_{i,j}^{x} = \left(\frac{\partial w}{\partial x}\right)_{i,j} = \frac{1}{12h_x}\{4(c_{i+1,j} - c_{i-1,j}) + (c_{i+1,j+1} + c_{i+1,j-1} - c_{i-1,j-1} - c_{i-1,j+1})\} \tag{2.54}$$

$$\theta_{i,j}^{y} = \left(\frac{\partial w}{\partial y}\right)_{i,j} = \frac{1}{12h_y}\{4(c_{i,j+1} - c_{i,j-1}) + (c_{i+1,j+1} - c_{i+1,j-1} - c_{i-1,j-1} + c_{i-1,j+1})\} \tag{2.55}$$

$$\theta_{i,j}^{xy} = \left(\frac{\partial^2 w}{\partial x \partial y}\right)_{i,j} = \frac{1}{4h_x h_y}(c_{i+1,j+1} - c_{i+1,j-1} + c_{i-1,j-1} - c_{i-1,j+1}) \tag{2.56}$$

The displacement vector in physical coordinates are defined as the vector with $w_{i,j}$, $\theta_{i,j}^{x}$, $\theta_{i,j}^{y}$, and $\theta_{i,j}^{xy}$ in appropriate order. As the beam element has the rotations only at the ends of the beam, the grid points on the edge parallel to the y-axis have $\theta_{i,j}^{x}$. Similarly, the grid points on the edge parallel to the x-axis have $\theta_{i,j}^{x}$ and the four corner points have $\theta_{i,j}^{xy}$. Therefore, the displacement vector has the dimension of $(n+3)(m+3)$ as:

$$\{\delta\} = \left[w_{00} \quad \theta_{00}^{x} \quad \theta_{00}^{y} \quad \theta_{00}^{xy} \quad w_{10} \quad \theta_{10}^{y} \quad \cdots \quad \theta_{m,n}^{y} \quad \theta_{m,n}^{xy} \right]^{T} \tag{2.57}$$

Then the transformation matrix is defined as:

$$\{\delta\} = [T]\{\delta_s\} \tag{2.58}$$

Note that $[T]$ is a $(n+3)(m+3)\times(n+3)(m+3)$ square matrix. The transformation matrix can be obtained from Equation (2.53) through (2.56) such that the submatrix of the transformation matrix, $[T_c]_{i,j}$, becomes:

$$\begin{Bmatrix} w_{i,j} \\ \theta^x_{i,j} \\ \theta^y_{i,j} \\ \theta^{xy}_{i,j} \end{Bmatrix} = [T_c]_{i,j} \begin{bmatrix} c_{i-1,j-1} & c_{i,j-1} & c_{i+1,j-1} & c_{i-1,j} & c_{i,j} & c_{i+1,j} & c_{i-1,j+1} & c_{i,j+1} & c_{i+1,j+1} \end{bmatrix}^T \tag{2.59}$$

where

$$[T_c]_{i,j} = \begin{bmatrix} \frac{1}{36} & \frac{4}{36} & \frac{1}{36} & \frac{4}{36} & \frac{16}{36} & \frac{4}{36} & \frac{1}{36} & \frac{4}{36} & \frac{1}{36} \\ -\frac{1}{12h_x} & 0 & \frac{1}{12h_x} & -\frac{4}{12h_x} & 0 & \frac{4}{12h_x} & -\frac{1}{12h_x} & 0 & \frac{1}{12h_x} \\ -\frac{1}{12h_y} & -\frac{4}{12h_y} & -\frac{1}{12h_y} & 0 & 0 & 0 & \frac{1}{12h_y} & \frac{4}{12h_y} & \frac{1}{12h_y} \\ \frac{1}{4h_xh_y} & 0 & -\frac{1}{4h_xh_y} & 0 & 0 & 0 & -\frac{1}{4h_xh_y} & 0 & \frac{1}{4h_xh_y} \end{bmatrix} \tag{2.60}$$

Finally the stiffness matrix with respect to the physical coordinate is:

$$[K] = [T]^{-T} [K_s] [T]^{-1} \tag{2.61}$$

where $[K]$ is $(n+3)(m+3)\times(n+3)(m+3)$ square matrix.

2.3.5 Cubic B-Spline Plate Element Example

Let us consider cubic B-Spline plate with material properties, E and ν, and thickness t. The plate is rectangular and $h_x = h_y = 1$ and the splines consist of 4 sections in x and y direction, respectively. The plate element is shown in Figure 2.9.

The displacement is:

$$w = \sum_{j=-1}^{5} \sum_{i=-1}^{5} c_{ij} \varphi_i(x) \psi_j(y) \tag{2.62}$$

And spline parameters are:

$$\{\delta_s\} = \begin{bmatrix} c_{-1,-1} & c_{0,-1} & \cdots & c_{5,-1} & c_{-1,0} & c_{0,0} & \cdots & c_{4,5} & c_{5,5} \end{bmatrix}^T \tag{2.63}$$

$$[\varphi] = [\varphi_{-1} \quad \varphi_0 \quad \cdots \quad \varphi_5] \tag{2.64}$$

$$[\psi] = [\psi_{-1} \quad \psi_0 \quad \cdots \quad \psi_5] \tag{2.65}$$

The 49×49 stiffness matrix can be evaluated from Equation (2.61). Figure 2.10 shows the deflection when the plate is under concentrated load, P, in the middle and the four edges are fixed. Figure 2.11 is the plate deflection under the same loading condition but the plate is simply supported on all edges. Under distributed load, q, and fixed boundary condition on all edges, the plate deflects as shown in Figure 2.12. In all these cases, the deflections and slopes of the plate are nearly the same as the exact solution obtained by analytical methods [Timoshenko and Goodier 1970].

Let us consider a variation problem. Assuming that two plates with initial variation are to be assembled together as shown in Figure 2.13. For both of the plates, $h_x = h_y = 1\ m$, $E = 2.06 \times 10^{11}\ Pa$, $t = 0.02\ m$, $\nu = 0.29$ and the splines are composed

of 4 sections in x and y directions, respectively. The left hand side plate is assumed to have initial variations only at point A and B, the right hand side plate at point C and D. The edge $\overline{AB}$ and $\overline{CD}$ are to be joined without welding distortion.

Assuming that the joined plates are simply supported only along $\overline{EF}$ and $\overline{GH}$, the variations are statistically independent, and the initial variations (m) are given as:

$$Var_{mean} = \begin{bmatrix} w_A = 0.02 & w_B = 0.01 & w_C = -0.01 & w_D = -0.01 \end{bmatrix}^T$$
$$Var_{stdev} = \begin{bmatrix} 0.01 & 0.01 & 0.01 & 0.01 \end{bmatrix}^T \quad (2.66)$$

Each of the B-Spline plate elements has 49×49 stiffness matrix and the global stiffness matrix for the assembled plates will be 84×84 matrix. The springback displacements are calculated analytically with the global stiffness matrix. Figure 2.14 and Figure 2.15 show the mean and standard deviation of the springback shapes of the assembled plates, respectively. Figure 2.16 and Figure 2.17 show the Monte Carlo Simulation of plate joining with the same initial variations. One thousand random variations were generated with same mean and standard deviations and then the statistics of the springback displacements were collected accordingly. Comparing the cubic B-Spline element results with MCS, the shape and maximum deflections are very similar near the sources of initial variations (A, B, C, and D).

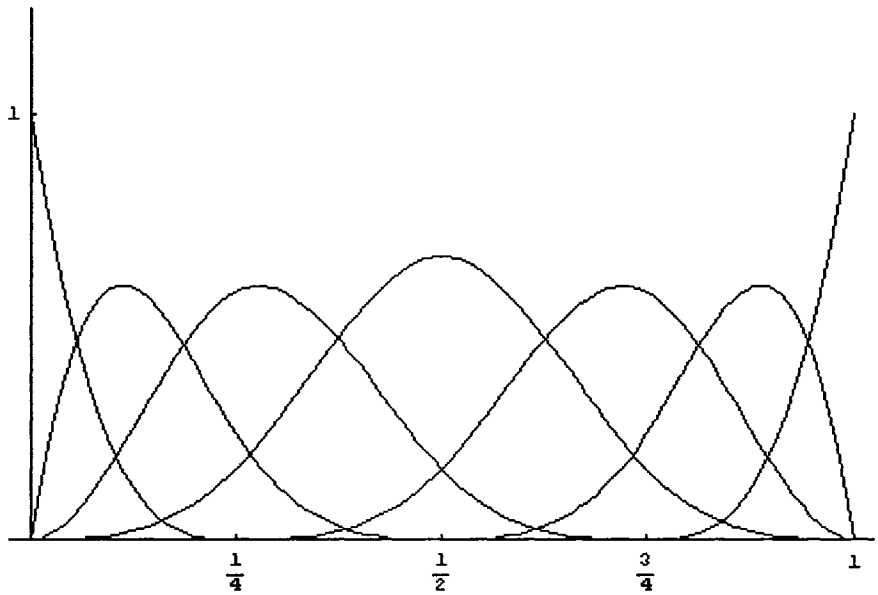

Figure 2. 1: Generic B-Spline Basis Function Distribution

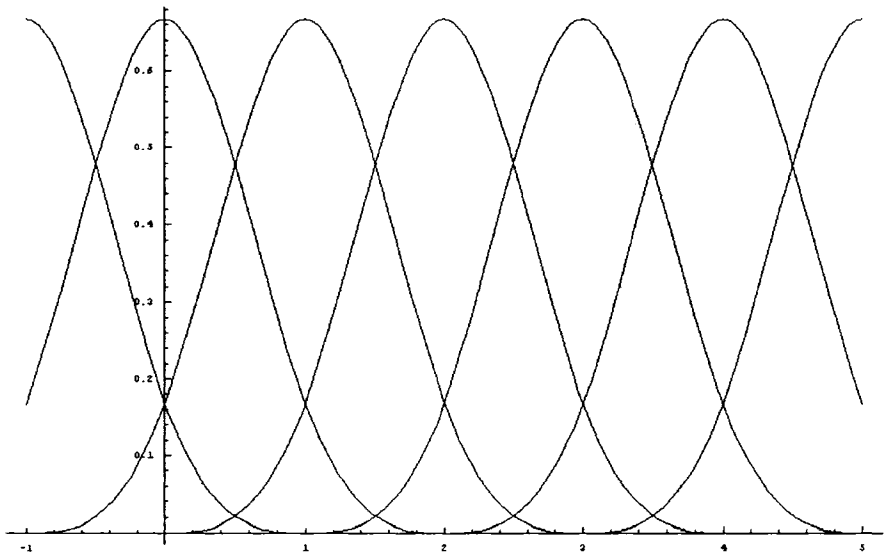

Figure 2. 2: Cubic B-Spline Basis Function Distribution

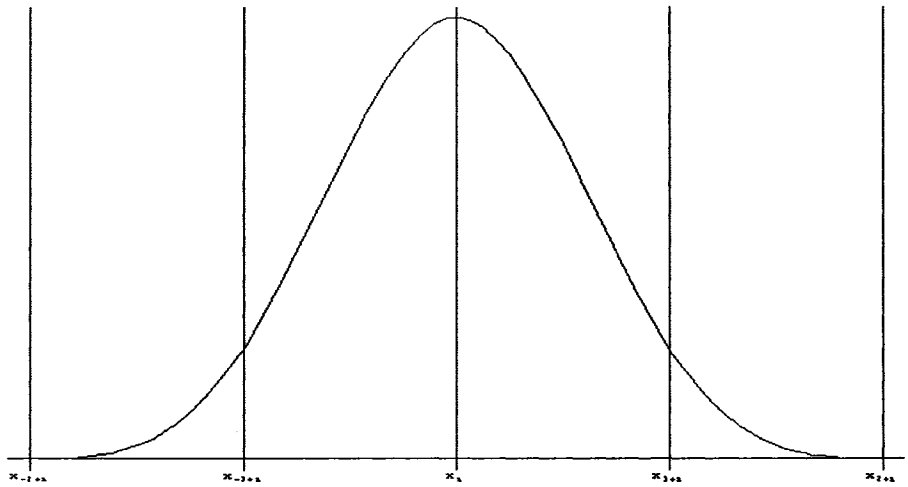

Figure 2. 3: Cubic B-Spline Basis Function

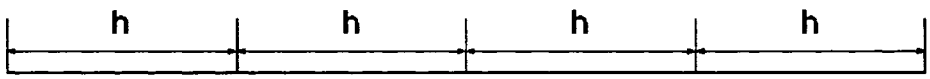

Figure 2. 4: Cubic B-Spline Beam Element Example

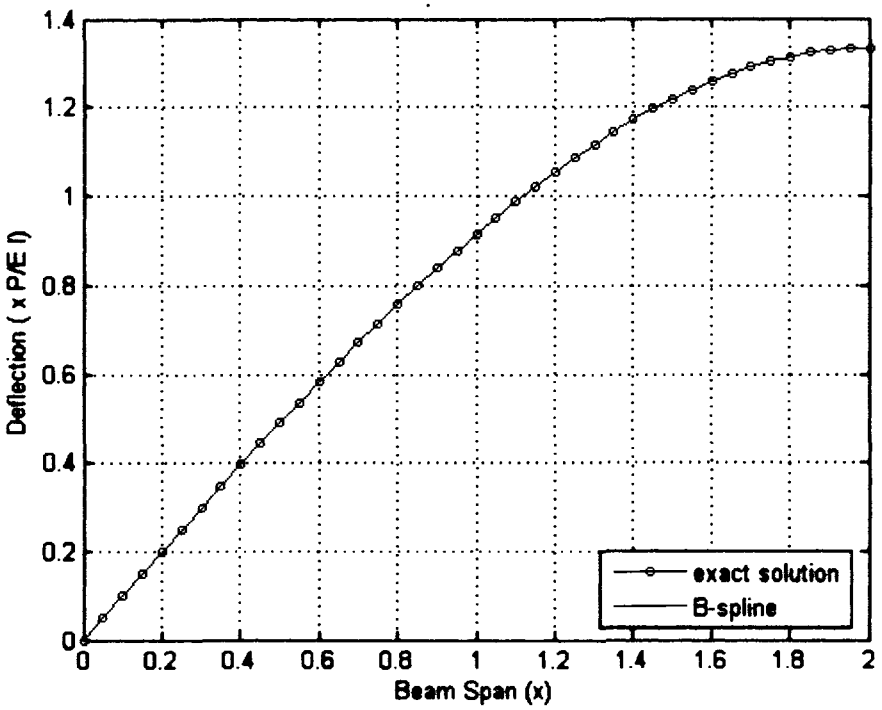

Figure 2. 5: Simply Supported Beam with Concentrated Load in the Midspan

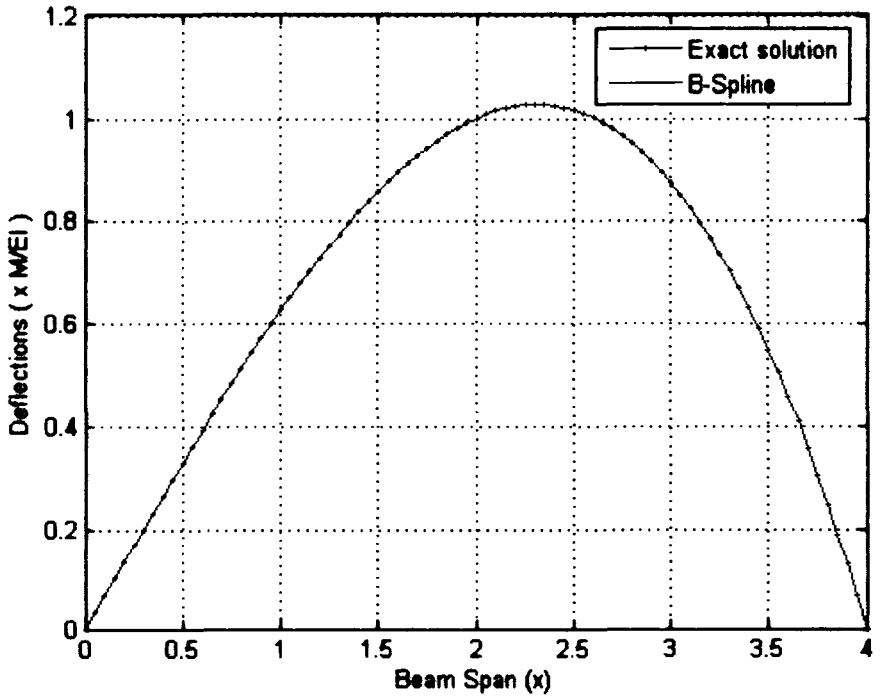

Figure 2. 6: Simply Supported Beam with Concentrated Moment at One End

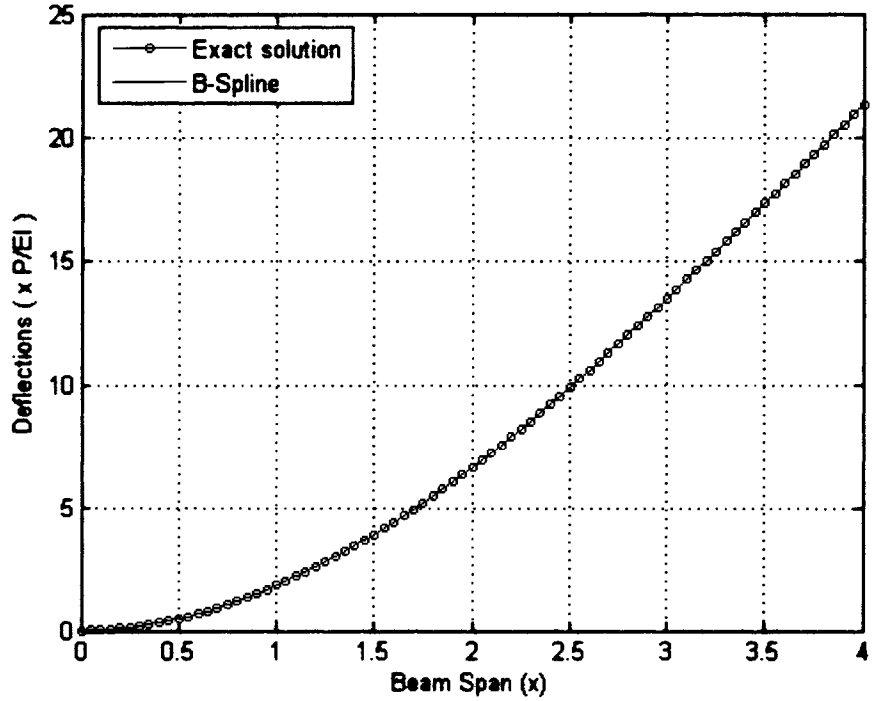

Figure 2. 7: Cantilever Beam with Concentrated Load at the Tip

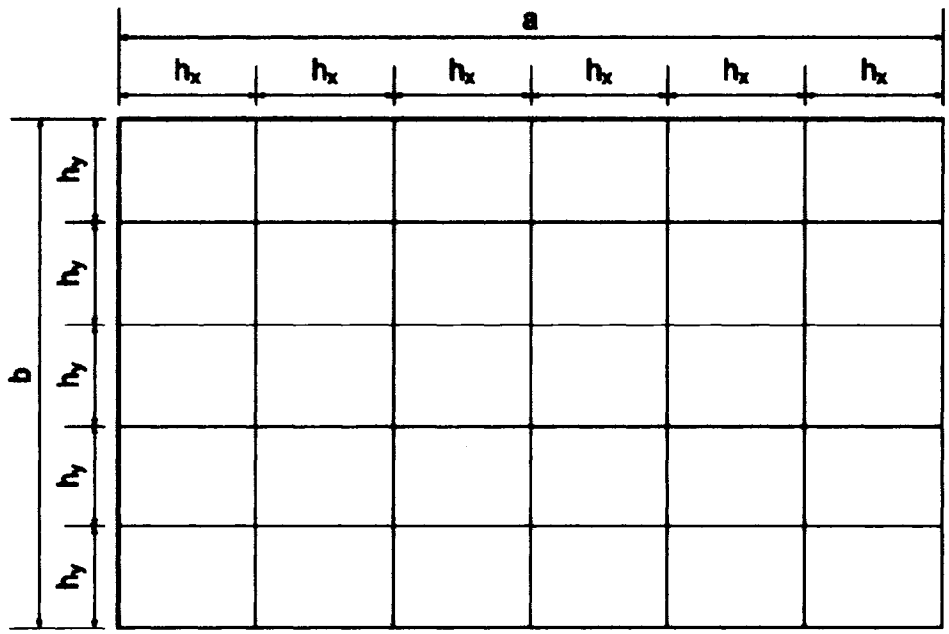

Figure 2. 8: Generic Cubic B-Spline Plate Element

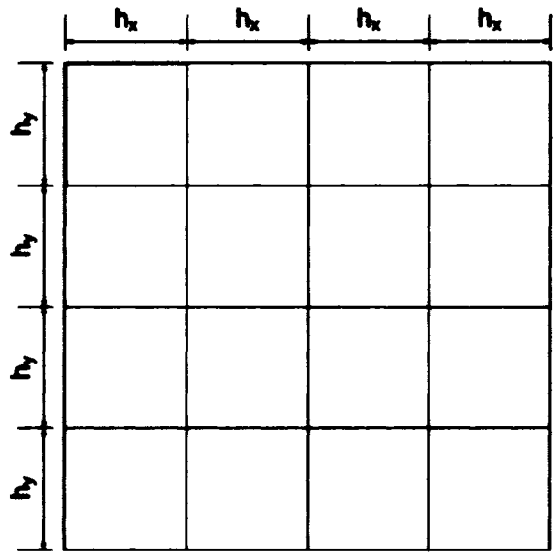

Figure 2. 9: Cubic B-Spline Plate Element Example

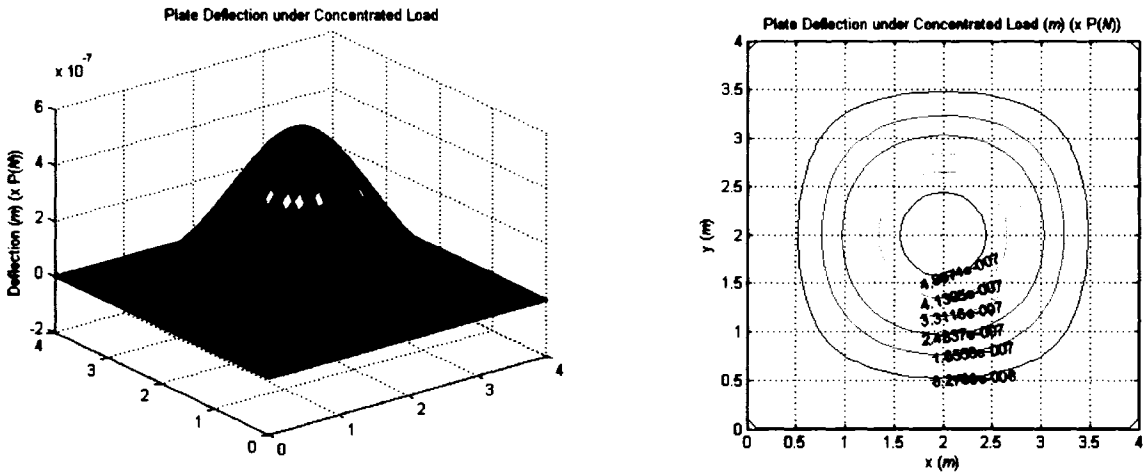

Figure 2. 10: Plate Deflection under Concentrated Load in the Middle (C-C-C-C)

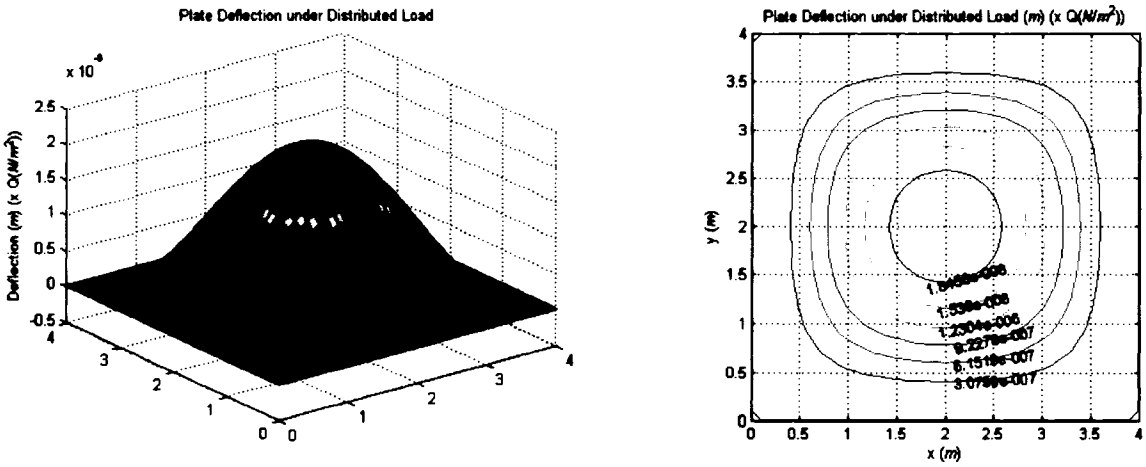

Figure 2. 11: Plate Deflection under Concentrated Load in the Middle (S-S-S-S)

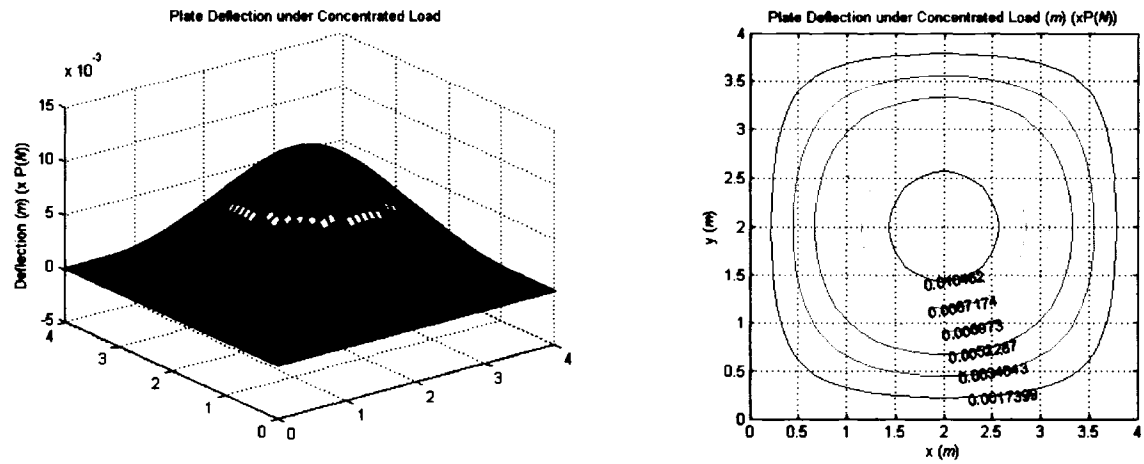

Figure 2. 12: Plate Deflection under Distributed Load (C-C-C-C)

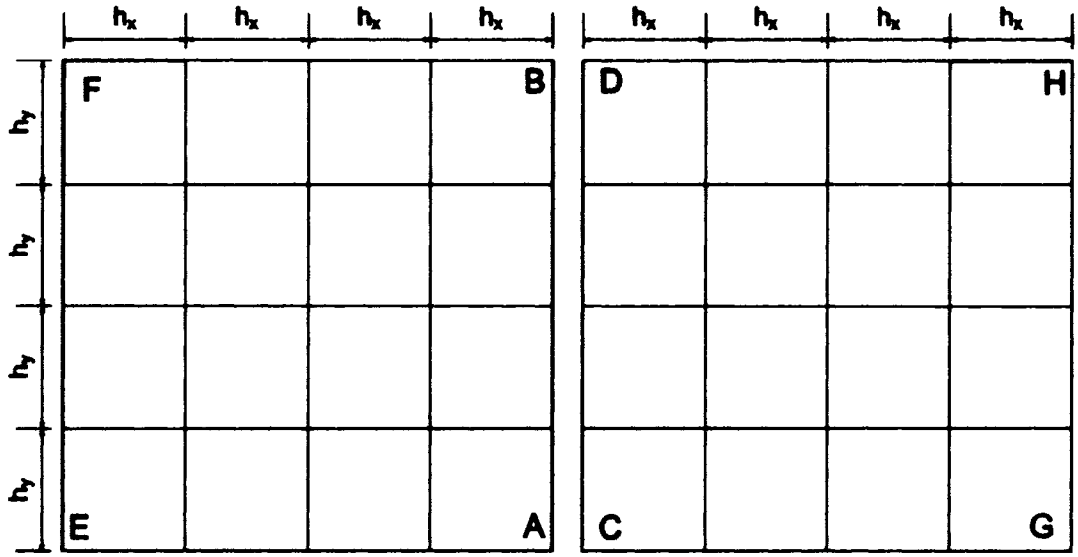

Figure 2. 13: Plate Element Variation Example

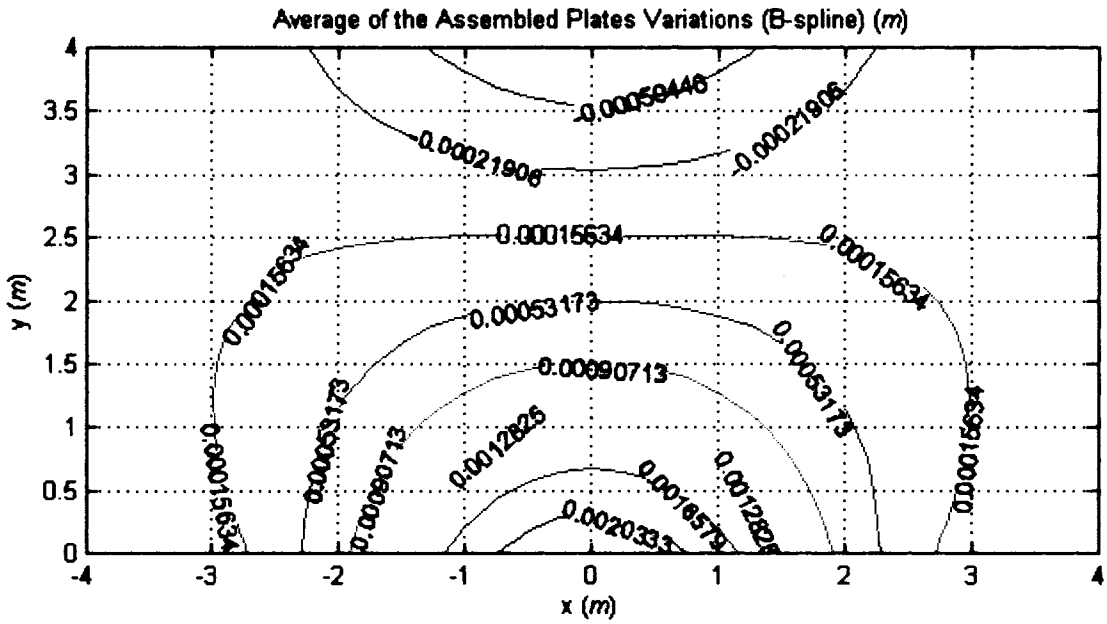

Figure 2. 14: Mean Variation of the Assembled Plates (B-Spline)

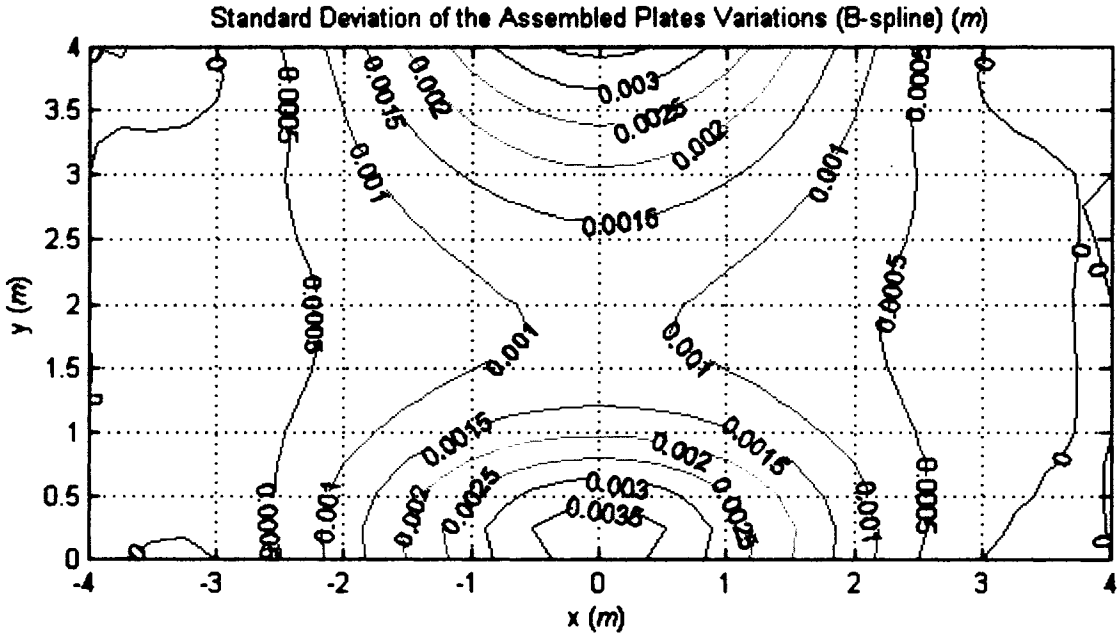

Figure 2. 15: Standard Deviation of the Variation in the Assembled Plates (B-Spline)

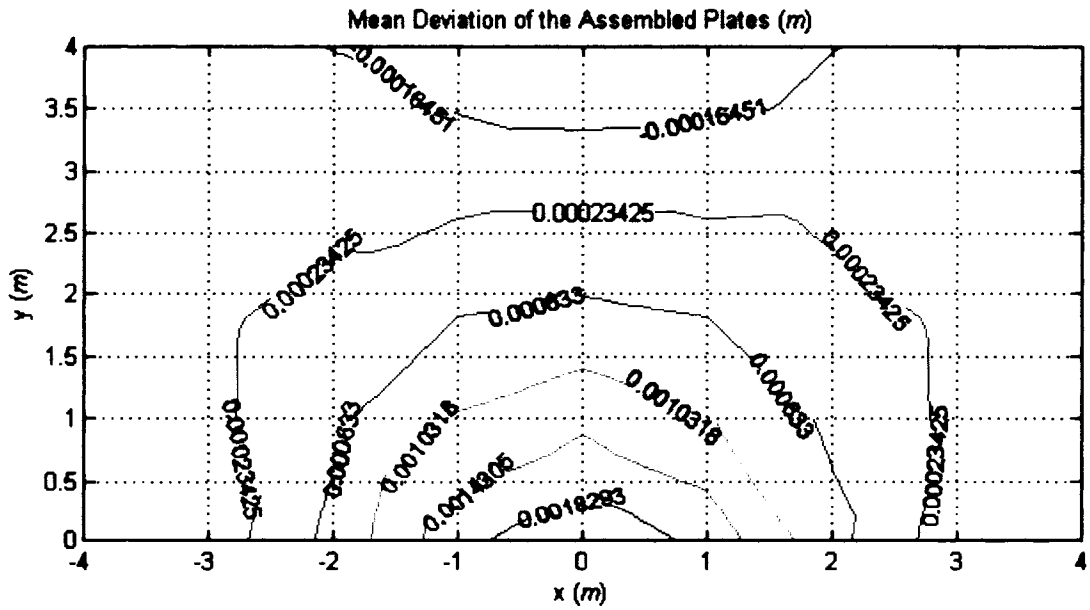

Figure 2. 16: Mean Variation of the Assembled Plates (Monte Carlo Simulation, ANSYS)

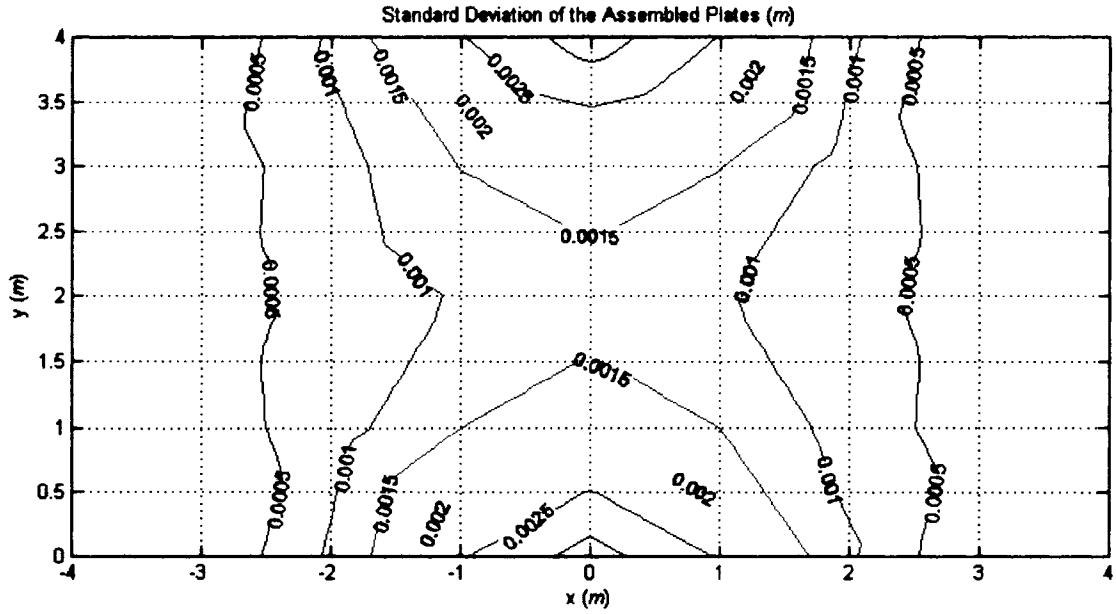

Figure 2. 17: Standard Deviation of the Variation in the Assembled Plates (Monte Carlo Simulation, ANSYS)

CHAPTER III

WELDING DISTORTION SIMULATION

The basic mechanical characteristics of the gas-metal arc welding (GMAW) process, which is very common in shipbuilding, and the concepts of the inherent strain method for welding distortion prediction are presented in this chapter. The mechanical characteristics of welding processes are investigated for the validation purpose of the inherent strain method. The unit load method based on the inherent strain method is also investigated for the purpose of the application of the inherent strain method to the block assembly process.

3.1 Welding Process and Welding Distortion

A series of careful investigations concerning the nature of the welding process in shipbuilding have been conducted so far [Watanabe and Satoh 1961, Fujimoto 1970, Friedman 1975, Masubuchi 1980, Ueda et al. 1986a, ASME 1989, Tekriwal and Mazumder 1991, Brown and Song 1992, Lee 1995, Yuan and Ueda 1996, Mochizuki et al. 1999, Seo and Jang 1999, Jang and Lee 2000, Takeda 2002, Lee 2002, Terasaki and Akiyama 2003]. The welding process causes a highly nonuniform heating of the parts being joined. Areas of the workpiece close to the welding arc are heated to several thousand degrees Celsius depending on the types of welding process, and subsequently cooled down, conducting the heat further to the rest of the body. The local heating and

subsequent cooling induce volumetric changes producing transient and residual stresses and deformation. These volumetric changes, non-uniform temperature distributions, and stresses interact simultaneously during the welding process. Figure 3.1 shows a schematic diagram of these interactions [IIW 1986].

Welding stresses and deformations are closely related phenomena. During heating and cooling, thermal strains occur in the weld and adjacent areas. The strains produced during the heating stage of welding are always accompanied by plastic deformation of the metal. The stresses resulting from these strains produce internal forces that cause a variety of welding distortions.

Residual stresses that develop during the welding process are called internal or locked-in stresses. Internal stresses are those that exist in a material body without external force being applied. By their origin, the welding stresses include thermal stress that are caused by non-uniform temperature distribution, stresses caused by the plastic deformation of the metal, and stresses caused by phase transformation of the material [Karlsson 1992]. Welding deformation can also be temporary or residual. Three fundamental dimensional changes are transverse shrinkage, longitudinal shrinkage, and angular distortion; i.e., rotation around the welded line, which are shown in Figure 3.2. In order to accurately predict welding deformation and residual stress, the microstructural state field should also be considered [Masubuchi 1980]. However, this is out of the scope of this research and many researchers have only considered the temperature fields and stress/deformation fields for predicting welding deformation for practical reasons.

Typically, the prediction of welding distortion is determined in a stepwise fashion. The temperature field and stress and strain field are assumed to be decoupled during each step; i.e., heat input from the torch generates a non-uniform temperature field in plates and this temperature field is calculated by solving heat conduction and

convection equations using FEA. Then the thermal stress caused by this temperature field is calculated by separate FEA.

Let us consider a body to be composed of many equal small cubic elements. The process of heating these elements evenly will lead all the elements to uniformly expand in all spatial directions. Hence, all the elements will have the same size. But, if the heating is nonuniform, then each element tries to expand proportionally to its temperature increase. At the same time, the body is continuous and each element restrains the free expansion of the adjacent elements. As a result stress is built up. In general, the non-uniformity of the temperature distribution during welding process causes a complex three-dimensional stress state.

3.2 Inherent Strain Method

The inherent strain method was developed originally for determination of residual stress within welded structures. Ueda [Ueda et al.1975] proposed a general method for determining six components of residual stress inside the body of interest. His technique for a welded plate is based on a more general "Inherent Strain", which is equivalent to Mura's "Eigenstrain" [Mura 1982]. The assumption is that residual stress is the result of an inelastic strain field that does not satisfy compatibility. This strain field is present because of the mechanical and thermal processes the welded plate has undergone. Ueda refers to this inelastic, non-compatible strain field as "inherent strain".

The dissection method is one of the major methods for the determination of residual stress within a body. In order to determine residual stress within a body, this method dissects the body into small pieces until the residual stress in small pieces are relaxed and measures the residual stresses on the dissected pieces by comparing strains of

the pieces after and prior to sectioning [Rosenthal and Nortom 1945]. This method is very straightforward; however it implies a problem where the residual stress of the body changes during dissection process.

The inherent strain method was developed to overcome this limitation of the dissection method [Ueda et al. 1975]. This method is a half analytic and half experimental, hybrid method. The inherent strain method, first assumes that an arbitrary strain distribution "inherently" exists within the original body and this inherent strain distribution is not affected by any subsequent mechanical or thermal processes, such as sectioning. After the body undergoes processes that result in any deformation (sectioning), the strains and stresses of the deformed body are measured at several points on the body surface. Based on these measured strains and/or stresses the inherent strain distribution, which is assumed to be the linearized relationships between strain and stress within the body, is determined using the finite element method. Once the inherent strain distribution is thus determined, the residual stresses within the body can be calculated using the distribution. However because the inherent strain distribution could be arbitrary, research has been performed to effectively assume the distributions within the body of interest [He et al. 2001a and 2001b].

3.2.1 Definition of Inherent Strain and Inherent Stress

We consider first a body in a hypothetical stress-free and strain-free initial condition. Assembly processes such as bending, rolling, and welding change the internal stress and strain states. Therefore a body with no external forces generally has residual stress and strain locked in. Inherent stress is the stress caused by strains that is generated by assembly forces other than external forces. And inherent strain is defined as the

remaining strain on the small piece after residual stress on the piece is relaxed by cutting from the body which was by some reason under inherent stress. Figure 3.3 clearly explains this concept. The body is assumed to be stress-free and strain-free. The length between the point A and B, dS_0, alters to dS_1 if the body undergoes a certain process that result in residual deformation in the body. If we cut a small piece that contains A' and B', dS_1 may change to dS_2 since the elastic strain of the small piece is released by cutting. Inherent strain in this explanation is defined as:

$$\varepsilon^* = \frac{dS_2 - dS_0}{dS_0} \tag{3.1}$$

3.2.2 Three-bar Example of Inherent Strain Method

The inherent strain can be also defined as total strain minus elastic strain. Let's consider a simple structure that consists of three bars as shown in Figure 3.4. The upper bar is bar number 1, lower left is bar number 2, and lower right is bar number 3 and they all have unit cross section area. For the convenience of explanation, the bars are assumed to have the same length (L) and Young's modulus (E), but different thermal expansion coefficients ($\alpha_i, i = 1,2,3$). The connector among the three bars is assumed to be rigid and constrained against rotation and the only degree of freedom of this structure is the location of this rigid bar. Top and bottom foundations are also assumed to be rigid.

In order to explain the concept of inherent strain method, the residual stresses in each bar after a unit temperature increase are calculated. A unit temperature increase of the structure would result in the shape change of the structure as shown in Figure 3.4 (c) due to different thermal properties. Although it is true that the unit temperature increase

changes the structure from (a) to (c) directly, the problem can be divided into three steps for the purpose of explanation of the inherent strain method.

(1) Stress-free initial condition, as shown in (a)

(2) Stress-free condition following unit temperature increase, as shown in (b)

(3) Final condition in which the compatibility boundary conditions are enforced, following unit temperature increase, as shown in (c).

The inherent strains in each bar can be defined as, inherent strains $\underline{\varepsilon}^* = \{\varepsilon_1^*, \varepsilon_2^*, \varepsilon_3^*\}^T$, elastic strains $\underline{\varepsilon}^e = \{\varepsilon_1^e, \varepsilon_2^e, \varepsilon_3^e\}^T$, and total strains $\underline{\varepsilon} = \{\varepsilon_1, \varepsilon_2, \varepsilon_3\}^T$, respectively. The subscripts identify the bar numbers. According to the concept of the inherent strain, the total strain $\underline{\varepsilon}$ is the sum of elastic strain $\underline{\varepsilon}^e$ and inherent strain $\underline{\varepsilon}^*$. And the inherent strain is defined as the sum of inelastic, non-compatible strains. Therefore:

$$\underline{\varepsilon} = \underline{\varepsilon}^e + \underline{\varepsilon}^* \tag{3.2}$$

And the residual stress is:

$$\underline{\sigma} = E(\underline{\varepsilon} - \underline{\varepsilon}^*) = E\underline{\varepsilon}^e \tag{3.3}$$

Analytically, inherent strains of this example can be calculated since it is a simple thermal expansion problem (the extension of the bars is set to the positive direction). For $\Delta T = 1$,

$$\varepsilon_1^* = \frac{\alpha_1 L}{L} = \alpha_1$$
$$\varepsilon_2^* = \frac{\alpha_2 L}{L} = \alpha_2 \tag{3.4}$$
$$\varepsilon_3^* = \frac{\alpha_3 L}{L} = \alpha_3$$

Therefore:

$$\underline{\varepsilon}^* = \begin{Bmatrix} \alpha_1 \\ \alpha_2 \\ \alpha_3 \end{Bmatrix} \tag{3.5}$$

These inherent strains are shown in Figure 3.4 (b). Once the inherent strains are known, we can solve the residual stresses and strains of the body in final state. The body in the final state must satisfy equilibrium and compatibility conditions.

Applying the equilibrium equation:

$$-\sigma_1 + \sigma_2 + \sigma_3 = 0 \tag{3.6}$$

and compatibility conditions:

$$\varepsilon_2 = \varepsilon_3 = -\varepsilon_1 = \bar{\varepsilon} \tag{3.7}$$

Also the constitutive equation must hold.

$$\underline{\sigma} = E\underline{\varepsilon}^e \tag{3.8}$$

or

$$\sigma_1 = E\varepsilon_1^e,\ \ \sigma_2 = E\varepsilon_2^e,\ \ \sigma_3 = E\varepsilon_3^e \tag{3.9}$$

From the equilibrium equation:

$$-E\varepsilon_1^e + E\varepsilon_2^e + E\varepsilon_3^e = 0 \tag{3.10}$$

Therefore:

$$-\varepsilon_1^e + \varepsilon_2^e + \varepsilon_3^e = 0 \tag{3.11}$$

From the definition of inherent strain, $\varepsilon = \varepsilon^e + \varepsilon^*$, and the elastic strains are:

$$\begin{aligned} \varepsilon_1^e &= -\bar{\varepsilon} - \alpha_1 \\ \varepsilon_2^e &= \bar{\varepsilon} - \alpha_2 \\ \varepsilon_3^e &= \bar{\varepsilon} - \alpha_3 \end{aligned} \tag{3.12}$$

Applying the above results in Equation (3.11):

$$-\varepsilon_1^e + \varepsilon_2^e + \varepsilon_3^e = 0 = 3\bar{\varepsilon} + \alpha_1 - \alpha_2 - \alpha_3 \tag{3.13}$$

Therefore:

$$\bar{\varepsilon} = \frac{-\alpha_1 + \alpha_2 + \alpha_3}{3} \tag{3.14}$$

As a result the total strain is:

$$\underline{\varepsilon} = \begin{Bmatrix} \frac{\alpha_1 - \alpha_2 - \alpha_3}{3} \\ \frac{-\alpha_1 + \alpha_2 + \alpha_3}{3} \\ \frac{-\alpha_1 + \alpha_2 + \alpha_3}{3} \end{Bmatrix} \tag{3.15}$$

The residual stresses in each bar can be calculated as:

$$\underline{\sigma} = E(\underline{\varepsilon} - \underline{\varepsilon}^*) = E(\begin{Bmatrix} \frac{\alpha_1 - \alpha_2 - \alpha_3}{3} \\ \frac{-\alpha_1 + \alpha_2 + \alpha_3}{3} \\ \frac{-\alpha_1 + \alpha_2 + \alpha_3}{3} \end{Bmatrix} - \begin{Bmatrix} \alpha_1 \\ \alpha_2 \\ \alpha_3 \end{Bmatrix}) = E\begin{Bmatrix} \frac{-2\alpha_1 - \alpha_2 - \alpha_3}{3} \\ \frac{-\alpha_1 - 2\alpha_2 + \alpha_3}{3} \\ \frac{-\alpha_1 + \alpha_2 - 2\alpha_3}{3} \end{Bmatrix} \tag{3.16}$$

So far, the three-bar structure example problem has illustrated the use of the inherent strain concept. However, for the most problems, inherent strain distributions cannot be determined as easily as in this example. If it is not viable to analytically determine inherent strain distribution, the distribution may be determined by experimental measurement.

The traditional inherent strain method, as mentioned before, is a partially analytic and partially experimental hybrid method in this context. With some help of domain knowledge, a reasonable inherent strain distribution within the body can be first assumed. Then residual stresses at several points where the measuring is relatively easy are measured. Based on the measured stresses, the assumed inherent strain distribution, which can be represented as a linear system, is determined. Once the distribution is determined, the residual stress distribution can be obtained as shown in the previous example.

3.3 Equivalent Loading Method Based on Inherent Strain Method for Welding Distortion Prediction

In order to predict welding distortion or weld deformation, the use of the inherent strain method by itself is not enough since the inherent strain method is primarily for residual stress prediction within a body of interest. For this purpose, the equivalent loading method, which is based on the concept of inherent strain, was developed by Jang [Jang et al. 2002]. The equivalent loading method based on inherent strain first calculates the inherent strain distributions near the welding area (inherent strain zone) and then obtains equivalent loads by integrating the inherent strains over the inherent strain zone, without any surface stress measurements.

In order to alleviate stress measurements that require dissecting the specimen into numerous cubes, Seo et al. [Seo and Jang 1997 and 1999] suggested a simplified thermo-elasto-plastic model for inherent strain calculation. Their studies introduced the concept of the degree of restraints, which can be further elaborated to account for assembly sequence. It denotes the degree of restraint of adjacent area, which restrains expansion or shrinkage of the welded area. It also reflects dimensions of members, materials, structure shape, and boundary conditions. However, this is not a totally analytical method and is not capable of explaining transient distortion during the welding process. This method also requires experiment data for the calculation of degree of restraints but the number of measurements is only a few and the measurement does not require any sectioning.

3.3.1 Concept of Equivalent Loading Method Based on Inherent Strain Method

From the definition of inherent strain, it is inelastic and non-compatible strain that could account for plastic deformation of the body and it is independent from elastic

strains. The idea of the equivalent loading method is to use these inherent strains to predict the final plastic deformation of the body with the help of elastic finite element analysis. If we already know the inherent strain distribution in the plates to be joined, we could calculate the equivalent loads, i.e., forces and moments relevant to the deformation modes of welded plates, by simply integrating the products of Young's modulus and the inherent strains within the body. Once the equivalent loads are obtained, the final deformation could be calculated by one simple elastic finite element analysis, as shown in Figure 3.5. Among many deformation modes shown in Figure 3.2, longitudinal shrinkage, transverse shrinkage, longitudinal bending, and transverse angular distortion are the major problems in shipbuilding process, for which equivalent loads can account. Now the welding distortion simulation can be reduced to the determination of inherent strain distribution within plates to be welded.

In order to explain the determination of the inherent strain distribution in plates, a one-dimensional schematic bar model is introduced. The model is developed to capture the mechanism of welding deformation as well as the inherent strain calculation. Figure 3.6 shows the model. The only degree of freedom in this model is vertical deformation, i.e., the change of length. The shaded middle bar only undergoes temperature change. K_w is the stiffness of the middle bar and K_S is the stiffness of both of the side bars. The material properties of all the bars are assumed to be the same.

The welding distortion occurs due to highly non-uniform heat applied to joining area. Areas close to the weld arc are heated to several hundred or beyond a thousand degrees Celsius and then cooled down with the heat being propagated to the rest of the body by conduction and to the atmosphere by convection. In the three-bar model, the middle bar represents area close to weld arc and the side bars the areas adjacent to weld area which constrains the thermal expansion of welded area.

The temperature history of stress in the middle bar can be found in Figure 3.7. While temperatures increase, the middle bar tends to expand but it is constrained by side bars so that the middle bar is being compressed. When the temperature exceeds a certain point (T_A), the stress exceeds the yielding stress and plastic deformation occurs. After reaching the maximum temperature (T_B), the middle bar is cooled to the original temperature. During cooling, the middle bar is being stretched. This tension is also due to the restraining side bars. When the stress reaches yield stress (C) again during the cooling, once again plastic deformation occurs.

Relevant thermal strain history of the middle bar is shown in Figure 3.7 (b). It should be noted that depending on the maximum temperature and the material properties as well as the ratio of restraining force of side bars versus thermal expansion forces of middle bar (degree of restraints), the paths could be different. For example, if the maximum temperature of welding process is less than T_A of the material, the final stress as well as plastic strain would be zero. If the maximum temperature is greater than T_A but less than that of point E, the middle bar would yield in compression but not in tension.

In Figure 3.7 (b), $\overline{OD}$ represent the final plastic strain in the middle bar calculated and it is the final inherent strain in the middle bar. It should be noted that the final inherent strain is only dependent on the material properties, the maximum temperature experienced, and the degree of restraints. The equivalent loading method based on inherent strain method assumes that infinitesimal three-bar models are distributed longitudinally (along the weldline) as well as transversally (perpendicular to the weldline) within the plates to be welded. It also assumes that the longitudinal three-bar models are independent from transversal three-bar models [Lee 2002]. Thus the final

inherent strain at a point in plates is only dependent on the material properties, the maximum temperature experienced at the point, and the degree of restraints at the point.

It is notable that the degree of restraints only accounts for the geometry of the plates to be welded among the three elements that determine the inherent strain distribution [Masubuchi and Ich 1970, Park et al. 2002]. Thus we could compile an inherent strain chart that indicates inherent strain values according to the highest temperature and the degree of restraints for a given material prior to the welding distortion analysis. Once the highest temperature values are obtained from simple thermal analysis and the degree of restraints are obtained, we could easily read the inherent strain value from the chart. These steps of equivalent loading methods based on inherent strain method are well illustrated in Figure 3.8.

It is also notable that we could select local inherent strain zone, only where inherent strain occurs, or the area where the maximum temperature does not exceed T_A.

The inherent strain chart, calculated prior to the analysis and stored by degree of restraint and maximum temperature, is used in distortion analysis and help reduce the analysis time.

3.3.2 Definition of Degree of Constraint

To account for the side bars restraining effect, the degree of restraints (DOR) concept is introduced in the equivalent loading method based on the inherent strain method. DOR is defined as:

$$\beta = \frac{K_S}{K_W + K_S} \tag{3.17}$$

where:

K_S : the stiffness of the side bars

K_W : the stiffness of the middle bar

The degree of restraint explains all the other geometrical properties of the welding. The degree of restraint can be different point to point, since the temperature history of the point and the adjacent area cannot be directly explained by the one middle bar that undergoes temperature change and the side bars with constant temperature. However, the collective behavior of these infinitesimal three-bar models in the weld zone shows the welding deformation so that the degree of restraint is also defined collectively by the final distortion shape. The degree of restraint can be determined in two ways. For geometrically simple structure problems such as butt-welding of flat plates or simple fillet welding, it can be determined by a trial-and-error method, comparing the calculated distortion shape with experiment data. Since the degree of restraint is assumed to be the only unknown and distributed uniformly in longitudinal and transverse directions for a simple geometry structure, the degree of restraint could be first guessed and then exactly determined through a few trial-and-error calculations.

For structures with more complex geometry, the unit load method can be employed. In order to calculate the degree of restraints, stiffness of both the weld zone and the adjacent zone must be known. The unit load method is a quantitative approach that calculates the stiffness of the structures through elastic analysis after applying unit loads along the weld zone. Employing this method, we could obtain degree of restraints of complex structures through elastic FEM analysis [Seo and Jang 1997 and 1999].

3.3.3 Three-Bar Model for the Inherent Strain Chart

The three-bar model, as shown in Figure 3.6, is investigated for inherent strain calculation. However for the convenience of calculation, E and A are used instead of stiffnesses K_W and K_S. As mentioned earlier, only the middle bar undergoes temperature increase and decrease, which causes residual plastic strain of the whole structure. According to Figure 3.7 (a), the whole process can be divided into four steps, i.e., elastic state during heating ($\overline{OA}$), plastic state during heating ($\overline{AB}$), elastic state during cooling ($\overline{BC}$), and plastic state during cooling ($\overline{CD}$).

Nomenclature

T:	Temperature ($°C$)
A_m:	Cross sectional area of the center bar
A_s:	Cross sectional area of the side bars
$\alpha(T)$:	Thermal expansion coefficient
$\sigma_Y(T)$:	Yield stress of the bars
$E_m(T)$:	Elastic modulus of the center bar
E_s:	Elastic modulus of the side bars
ε:	Total strain (true atrain a.k.a. logarithmic strain)
ε_m:	Total strain of the center bar
ε_s:	Total strain of the side bars
ε_m^e:	Elastic strain of the center bar
ε_m^p:	Plastic strain of the center bar
ε_m^{th}:	Thermal strain of the center bar
σ_m:	Stress of the center bar
σ_s:	Stress of the side bars

3.3.3.1 Elastic State during Heating ($\overline{OA}$)

During this step, the middle bar undergoes temperature increase until the axial compressive stress exceeds the yielding stress.

Equilibrium requires:

$$\sigma_m A_m + 2\sigma_s A_s = 0 \tag{3.18}$$

The constitutive equations yield:

$$\sigma_s = E_s \varepsilon_s \tag{3.19}$$

$$\sigma_m = E_m(\varepsilon_m - \varepsilon^{th}) = E_m(\varepsilon_m - \int_{T_0}^{T} \alpha(T)dT) \tag{3.20}$$

The compatibility equation is:

$$\varepsilon_m = \varepsilon_s = \varepsilon \tag{3.21}$$

From equilibrium and constitutive equations:

$$E_m(\varepsilon_m - \int_{T_0}^{T} \alpha(T)dT)A_m + 2E_s\varepsilon_s A_s = 0 \tag{3.22}$$

Now applying compatibility condition:

$$(E_m A_m + 2E_s A_s)\varepsilon = A_m E_m \int_{T_0}^{T} \alpha(T)dT \tag{3.23}$$

Therefore, the total strain is:

$$\varepsilon = \frac{E_m(T)A_m \int_{T_0}^{T} \alpha(T)dT}{E_m(T)A_m + 2E_s A_s} \tag{3.24}$$

Once the total strain is determined, the stresses can be calculated from Equation (3.20):

$$\sigma_m = E_m(\varepsilon - \int_{T_0}^{T} \alpha(T)dT) = \frac{-2E_sA_s}{E_m(T)A_m + 2E_sA_s} E_m(T) \int_{T_0}^{T} \alpha(T)dT \tag{3.25}$$

Also, the plastic strain remains zero in this step.

$$\begin{aligned} \varepsilon_m^p &= 0 \\ \varepsilon_m^e &= \varepsilon - \varepsilon^{th} = \varepsilon - \int_{T_0}^{T} \alpha(T)dT \end{aligned} \tag{3.26}$$

3.3.3.2 Plastic State during Heating ($\overline{AB}$)

At a certain temperature (T_A), the internal stress in the middle bar reaches to its yield stress. From then, the stress is given by $-\sigma_Y(T)$. Hence the value of the stress and elastic strain change as the material properties change with temperature increase.

In this step:

$$\sigma_m = -\sigma_Y(T) \tag{3.27}$$

And applying the equilibrium equation yields:

$$\sigma_s = \frac{\sigma_Y(T)A_m}{2A_s} \tag{3.28}$$

The constitutive equation is:

$$\varepsilon_m^{th} = \int_{T_0}^{T} \alpha(T)dT \tag{3.29}$$

and the total strain is:

$$\varepsilon_m = \varepsilon_m^e + \varepsilon_m^p + \varepsilon_m^{th} \tag{3.30}$$

Since the stress state in the bars is determined, the total strain can be derived as:

$$\varepsilon_m = \varepsilon_s = \varepsilon = \frac{\sigma_Y(T)A_m}{2E_sA_s} \tag{3.31}$$

and

$$\varepsilon_m^p = \varepsilon_m - \varepsilon_m^e - \int_{T_0}^{T}\alpha(T)dT = \frac{\sigma_Y(T)A_m}{2E_sA_s} - (-\frac{\sigma_Y(T)}{E_m(T)}) - \int_{T_0}^{T}\alpha(T)dT \tag{3.32}$$

3.3.3.3 Elastic State during Cooling ($\overline{BC}$)

The state of the middle bar returns to the region of elasticity. Thus the strain at the maximum temperature is set as the initial strain.

The thermal constitutive equation remains:

$$\varepsilon_m^{th} = \int_{T_0}^{T}\alpha(T)dT \tag{3.33}$$

Considering the stress and strain at the maximum temperature (point B in Figure 3.7 (a)) as initial stress and strain:

$$\sigma_m = \sigma_m\big|_B - \frac{2E_sE_m(T)A_s}{E_m(T)A_m + 2E_sA_s}(\varepsilon_m^{th} - \varepsilon_m^{th}\big|_B) \tag{3.34}$$

Once the stress in the middle bar is obtained, the stress in side bars can be calculated by applying the equilibrium condition.

$$\sigma_s = \frac{\sigma_m A_m}{-2A_s} \tag{3.35}$$

And from the elastic constitutive equation:

$$\varepsilon_m = \varepsilon_s = \varepsilon = \frac{\sigma_s}{E_s} \tag{3.36}$$

Also, the plastic strain remains the same as the value at point B in traditional plasticity theory. However the value of the plastic strain alters due to temperature dependent material properties during cooling, which explains plastic hardening recovery effect:

$$\varepsilon_m^p = \frac{\sigma_Y(T_B)A_m}{2E_sA_s} + \frac{\sigma_Y(T)}{E_m(T)} - \int_{T_0}^{T_B} \alpha(T)dT \cong \varepsilon_m^p\Big|_B \tag{3.37}$$

Since the bar is now in the elastic state:

$$\varepsilon_m^e = \frac{\sigma_m}{E_m(T)} \tag{3.38}$$

3.3.3.4 Plastic State during Cooling ($\overline{CD}$)

The middle bar suffers the increase of tension induced by the cooling process. At point C the tension reaches the yielding stress. In this step:

$$\sigma_m = \sigma_Y(T) \tag{3.39}$$

From the equilibrium equation:

$$\sigma_s = \frac{\sigma_m A_m}{-2A_s} = \frac{\sigma_Y(T)A_m}{-2A_s} \tag{3.40}$$

Once, the stress in the side bar is obtained, the strain can be calculated from the constitutive equation:

$$\varepsilon_s = \frac{\sigma_s}{E_s} \tag{3.41}$$

By the compatibility condition:

$$\varepsilon_m = \varepsilon_s = \varepsilon = \frac{\sigma_s}{E_s} \tag{3.42}$$

The value of the elastic strain alters due to temperature dependent material properties.

$$\varepsilon_m^e = \varepsilon_m^e\big|_C = \frac{\sigma_Y(T)}{E_m(T)} \tag{3.43}$$

The plastic strain in the middle bar is determined by the constitutive equation.

$$\varepsilon_m^p = \varepsilon_m - \varepsilon_m^e - \varepsilon_m^{th} = \frac{\sigma_Y(T)A_m}{-2A_sE_s} - \frac{\sigma_Y(T)}{E_m(T)} - (\varepsilon_m^{th} - \varepsilon_m^{th}\big|_B) \tag{3.44}$$

3.3.3.5 Degree of Restraints

The definition of degree of restraints:

$$\beta = \frac{K_s}{K_w + K_s}$$

can be rewritten in the three-bar model as:

$$\begin{aligned} K_s &= 2\frac{E_sA_s}{L} \\ K_w &= \frac{E_m(T)A_m}{L} \end{aligned} \tag{3.45}$$

Therefore:

$$\beta = \frac{2E_sA_s}{2E_sA_s + E_m(T)A_m} \tag{3.46}$$

Since the definition of the degree of constraints is about the initial condition and the same material for middle bar and side bars is assumed for welding simulation:

$$\beta = \frac{2A_s}{2A_s + A_m} \tag{3.47}$$

3.3.3.6 Thermal Histories of Stress and Strain

For the validation purpose, analytic calculation results are compared with 3-D FEM analysis (ABAQUS) results, where simple thermal-structural truss elements are used. The thermal histories of stress and strains are calculated and plotted in MATLAB, assuming $\beta = 0.2$, $L = 1\ m$, and equal material properties. Then the thermal histories with various values of β are plotted to investigate the effects of restraints.

Because of the temperature dependent material properties, thermal histories of stress and strains do not always behave as explained in the previous section. Since the value of yielding stress varies rapidly between 600 and 1000 degree Celsius, sometimes the middle bar undergoes elastic state during cooling – plastic state during cooling – elastic state during cooling – plastic state during cooling repeatedly. This phenomenon is taken care of in the MATLAB code. For this reason, the thermal histories with various maximum temperatures (T_{max} =1600, 1200, and 800 $°C$) have been compared with the result of the equivalent ABAQUS results.

In addition to the heating-and-cooling cycle, thermal histories of the cooling cycle only are plotted as well in order to explain the equivalent load in the filler material. These results are also compared with equivalent ABAQUS results. Figures 3.9 through 3.12 show thermal histories of the analytically calculated elastic strain, plastic strain, total strain and stress in the middle bar with various T_{max}, respectively. As shown in the figures, they very closely match Figures 3.13 through 3.16, which are equivalent ABAQUS analysis results, respectively. Strain and stress calculations for the filler material (Figures 3.17 through 3.20) also match equivalent ABAQUS analysis results (Figures 3.21 through 3.24).

As shown in the figures, the middle bar remains in the elastic state until the temperature reaches about 400°C. Until this point, the strain in the middle bar increases

relatively linearly (Figure 3.9 and Figure 3.13) and so does the relevant stress (Figure 3.12 and Figure 3.16), while the plastic strain remains zero (Figure 3.10 and Figure 3.14). It should be noted that the total strain increases in the positive direction during this region (Figure 3.11 and Figure 3.15) but the elastic strain is in the opposite direction since the middle bar is under compression (Figure 3.9 and Figure 3.13).

For the filler material that only undergoes cooling, the thermal histories are quite different. The elastic strains are always positive since they are always under tension (Figure 3.17 and Figure 3.21) and so are the stresses in the middle bar (Figure 3.20 and Figure 3.24). It is notable that the elastic stage is relatively short compared to the plastic stage, which is well shown in Figure 3.18 and Figure 3.24.

The effects of the changes in β are shown in Figures 3.25 through 3.28 and they are compared with ABAQUS simulation results, shown in Figures 3.29 through 3.32, respectively. The patterns of the thermal histories conform to the previous figures (Figures 3.9 through 3.24). However it is clearly shown in the figures that the changes in β affect the slopes of elastic and plastic deformation so that they eventually affect the final inherent strains.

For the filler material, the effects of the changes in β are shown in Figures 3.33 through 3.36 and they are compared with ABAQUS simulation results, shown in Figures 3.37 through 3.40, respectively. Although the elastic region (linear region around 1600°C) is relatively small compared with the plastic region, the slope of elastic strain is affected by the changes in β, as shown in Figure 3.33 and Figure 3.37. As the restraining stiffness increases, the residual plastic strain also increases, as shown in Figure 3.34 and Figure 3.38, so that they eventually affect the final inherent strains.

Validated by the comparison with numerical analysis, the three-bar model analytic calculation is used to generate the inherent strain chart, shown in Figure 3.41 for

base metal and Figure 3.42 for filler material. These results of the analytic calculations are compared with the result of ABAQUS simulation, shown in Figure 3.43 and Figure 3.44, respectively. Figure 3.45 and 3.46 show the butt weld distortion calculated by the equivalent loading method based on the inherent strain method. Figure 3.47 is the result of full 3-D FEM welding distortion simulation. As shown in the figures, the result obtained by the equivalent loading based on the inherent strain method is very similar to that of the full 3-D FEM analysis.

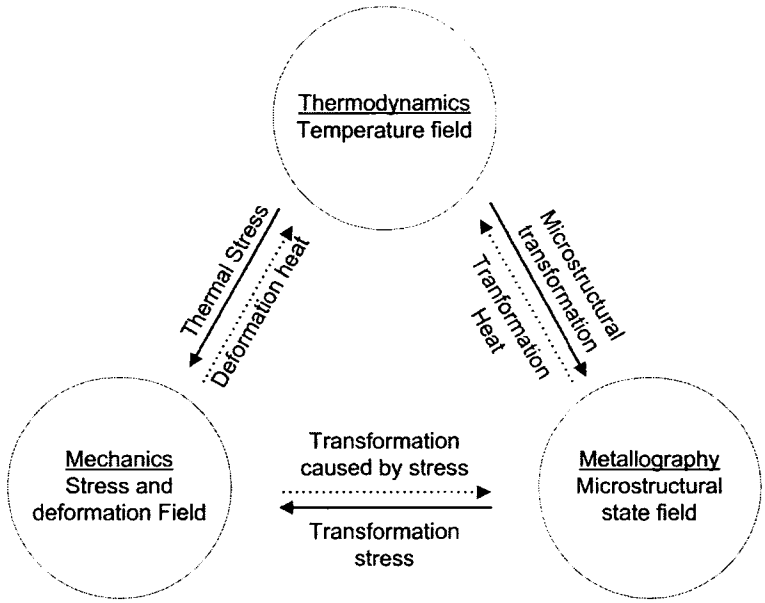

Figure 3. 1: Diagram decoupling and mutual influencing of temperature field, stress and deformation field and microstructural state field.

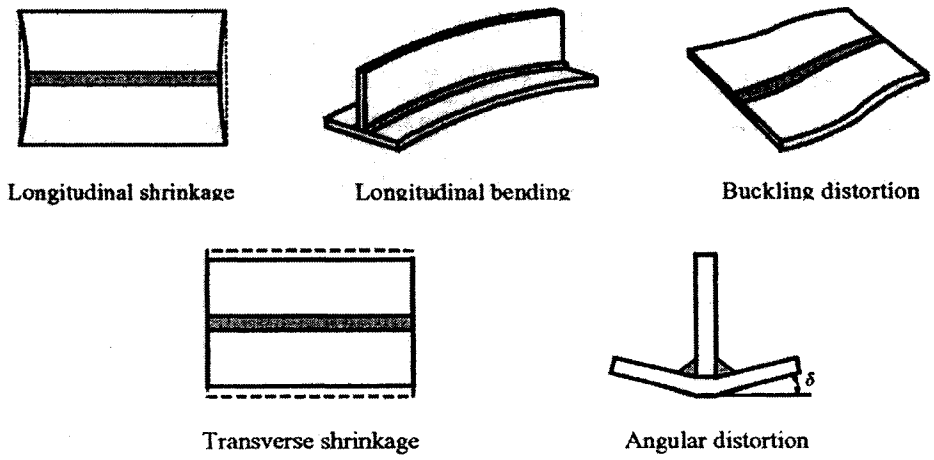

Figure 3. 2: Welding deformation in longitudinal and transverse direction [Lee 2002]

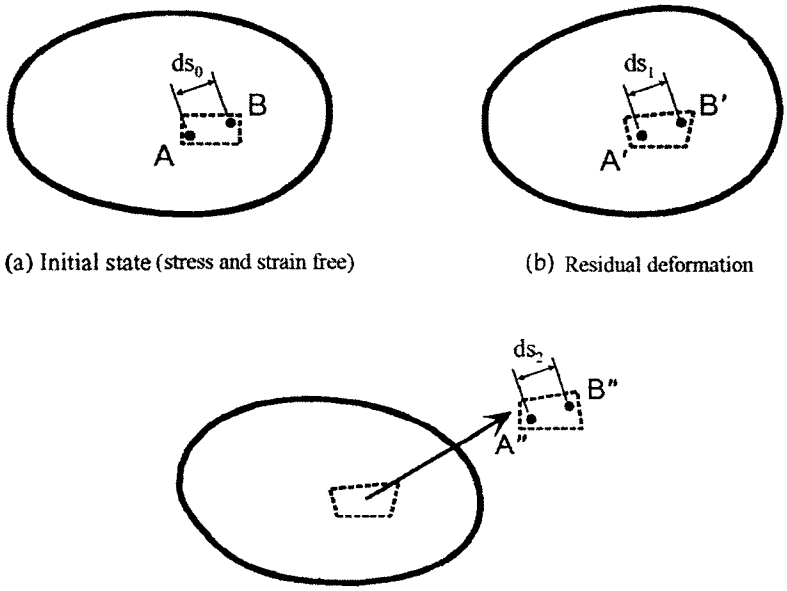

(a) Initial state (stress and strain free)

(b) Residual deformation

(c) Stress-released state by cutting

Figure 3. 3: Definition of Inherent Strain

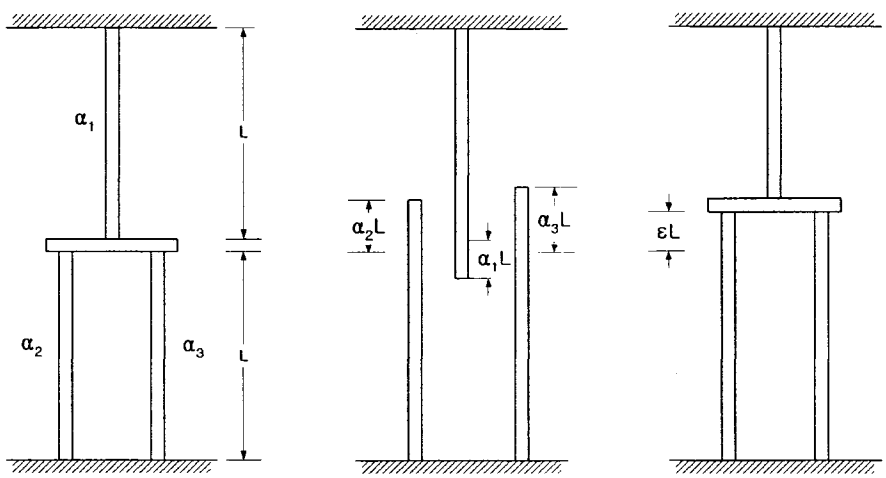

(a) Stress-free initial state

(b) Stress-free condition following unit temperature increase

(c) Compatibility condition enforced following unit temperature increase

Figure 3. 4: Three-bar model of inherent strain method

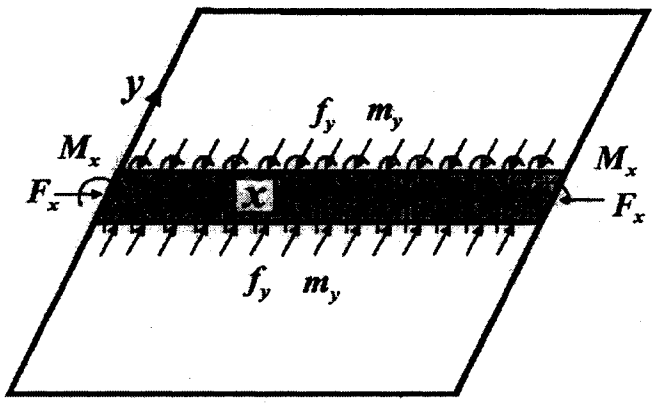

Figure 3. 5: Application of equivalent loads along weld line [Lee 2002]

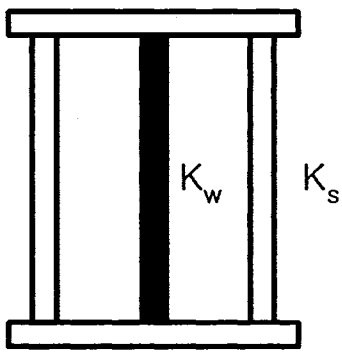

Figure 3. 6: One-dimensional three-bar model for inherent strain calculation

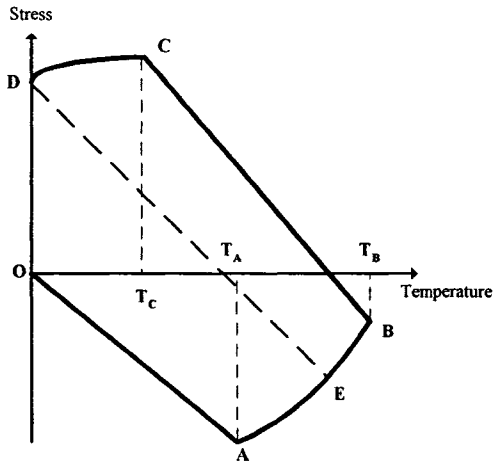

(a) Thermal history of stress in the middle bar

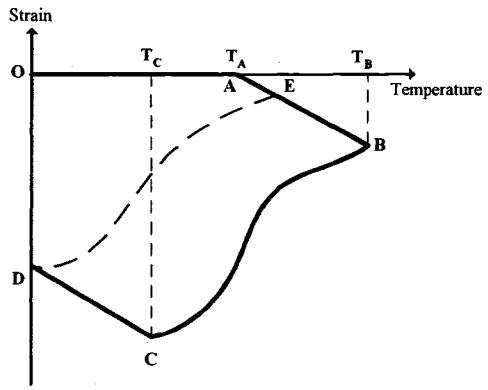

(b) Thermal history of plastic strain in the middle bar

Figure 3. 7: Thermal histories of stress and plastic strain according to maximum temperature

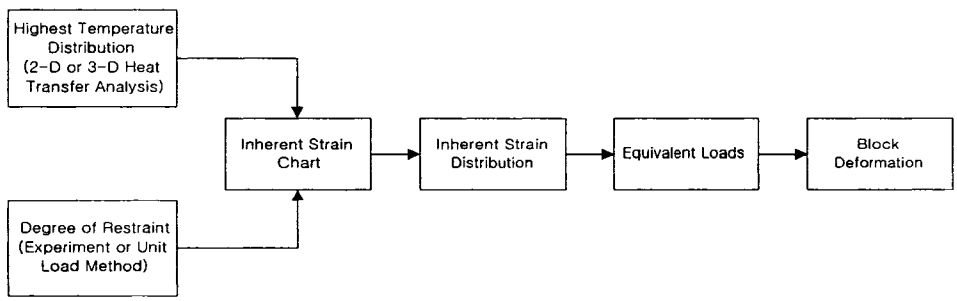

Figure 3. 8: Flow chart for the welding deformation analysis using equivalent load method [Lee 2002]

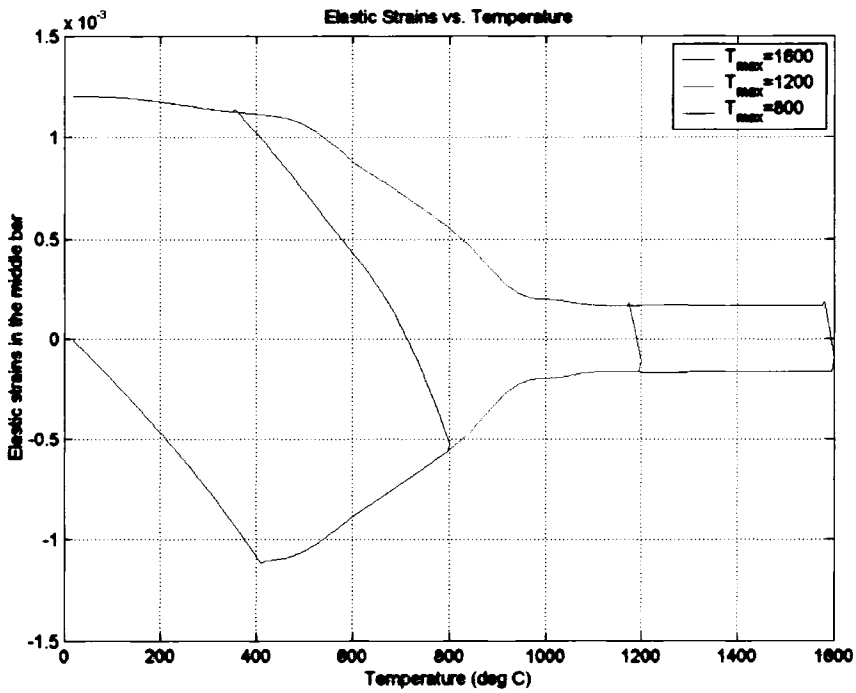

Figure 3. 9: Thermal history of elastic strain in the middle bar with various $T_{\max}$

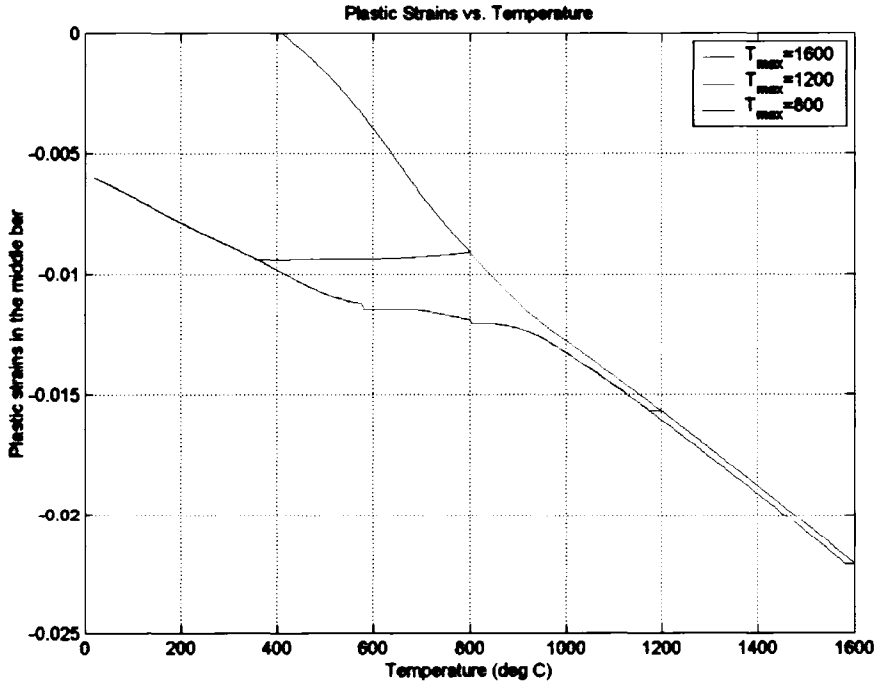

Figure 3. 10: Thermal history of plastic strain in the middle bar with various $T_{\max}$

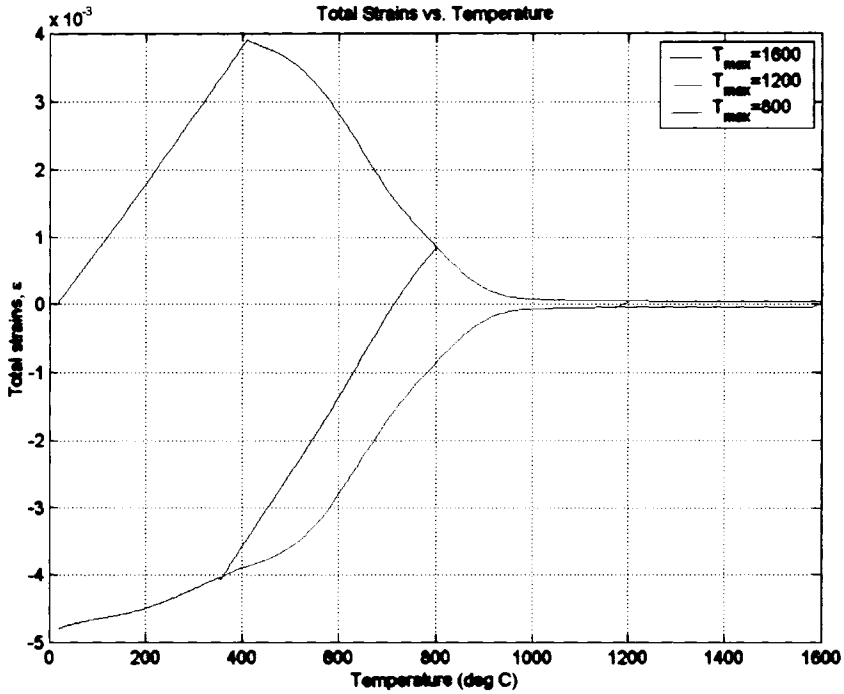

Figure 3. 11: Thermal history of total strain in the middle bar with various $T_{\max}$

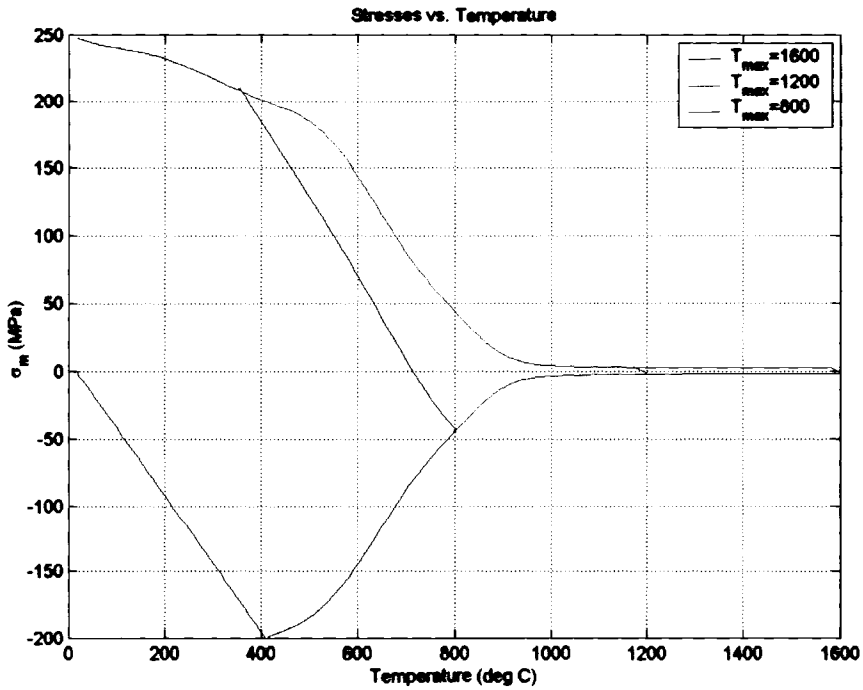

Figure 3. 12: Thermal history of σ_m in the middle bar with various $T_{\max}$

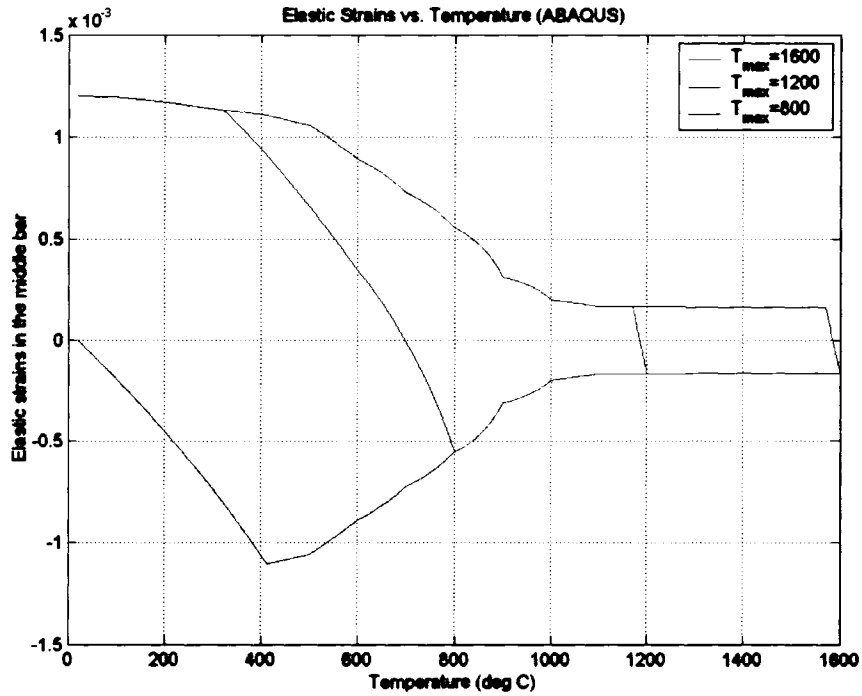

Figure 3. 13: Thermal history of elastic strain with various $T_{\max}$ (ABAQUS)

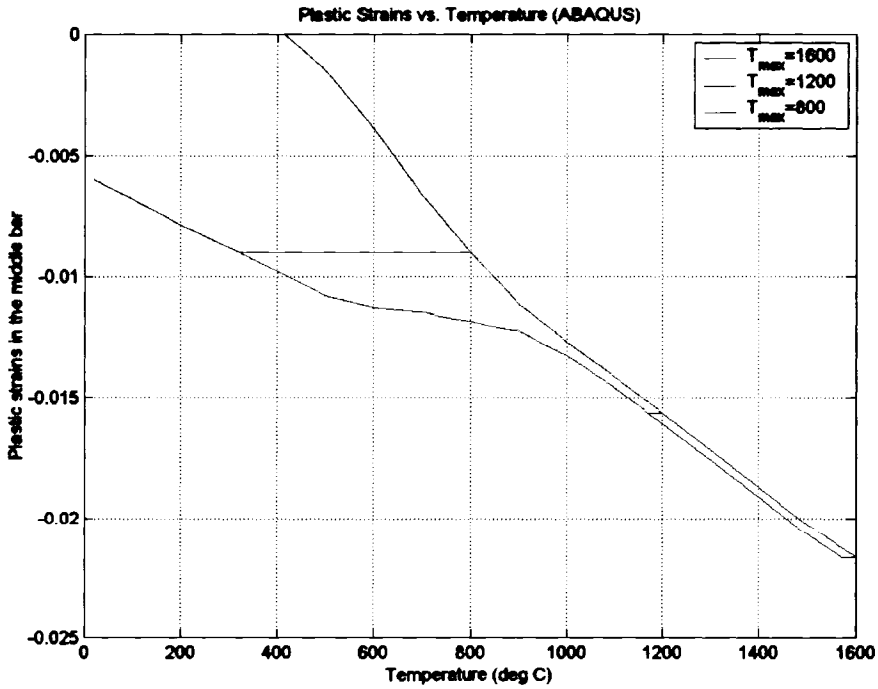

Figure 3. 14: Thermal history of plastic strain with various $T_{\max}$ (ABAQUS)

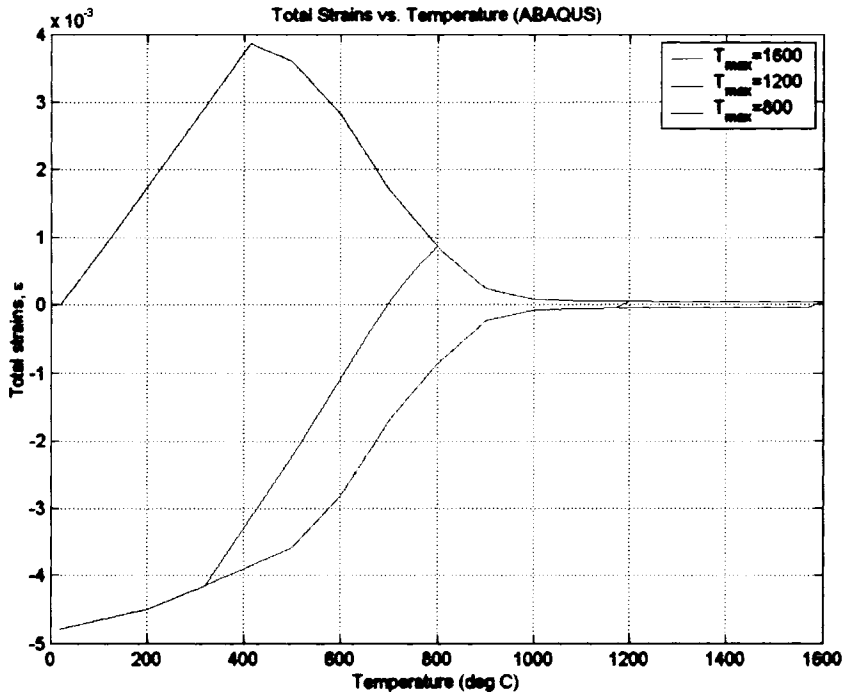

Figure 3. 15: Thermal history of total strain with various $T_{\max}$ (ABAQUS)

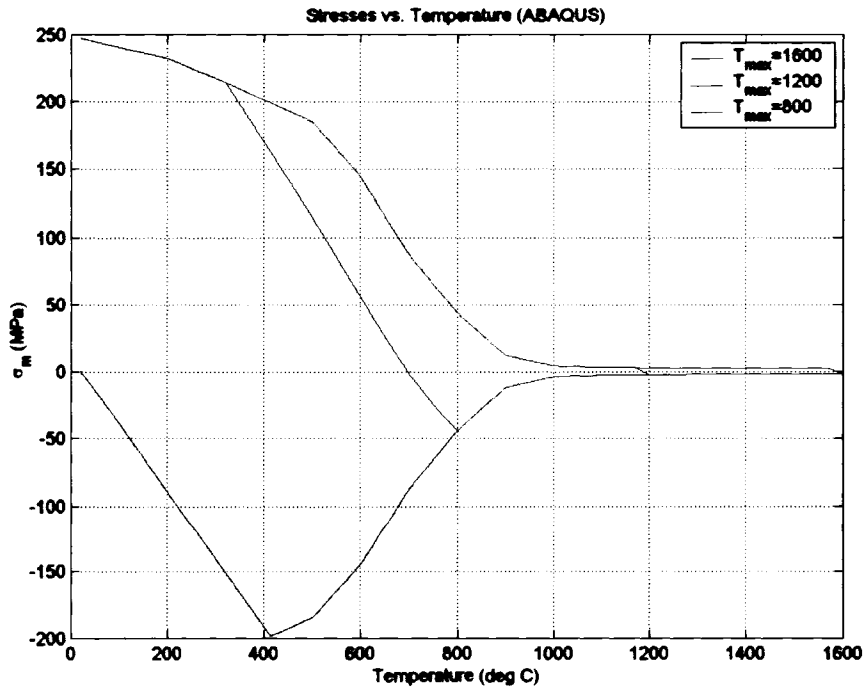

Figure 3. 16: Thermal history of σ_m with various $T_{\max}$ (ABAQUS)

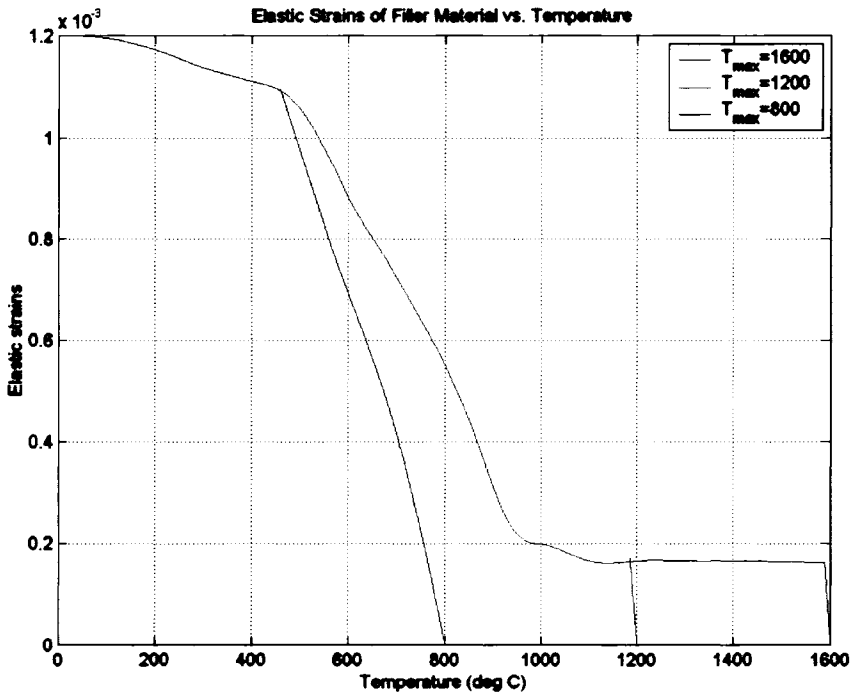

Figure 3. 17: Thermal history of elastic strain in filler material with various $T_{\max}$

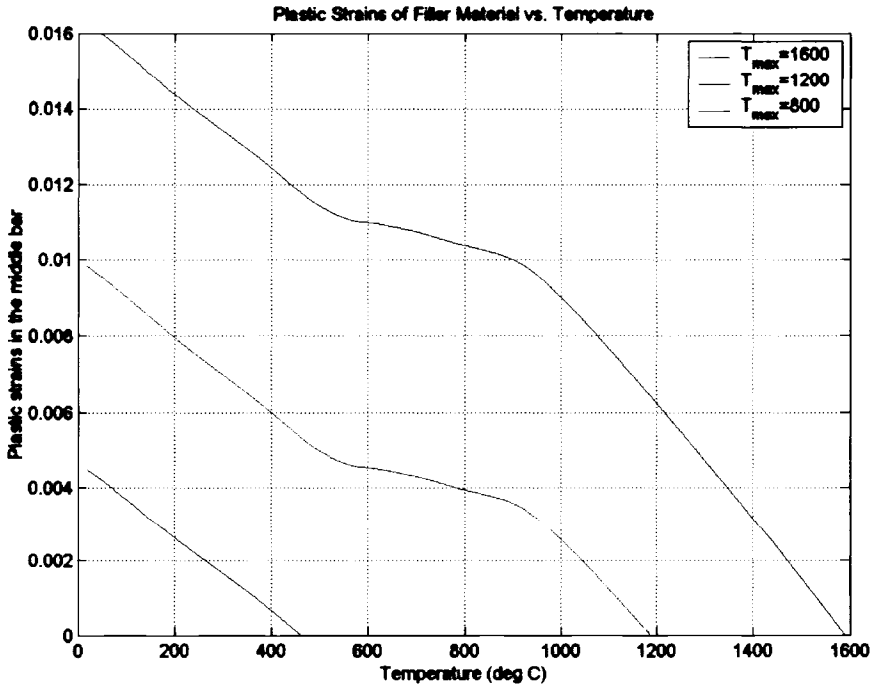

Figure 3. 18: Thermal history of plastic strain in the filler material with various $T_{\max}$

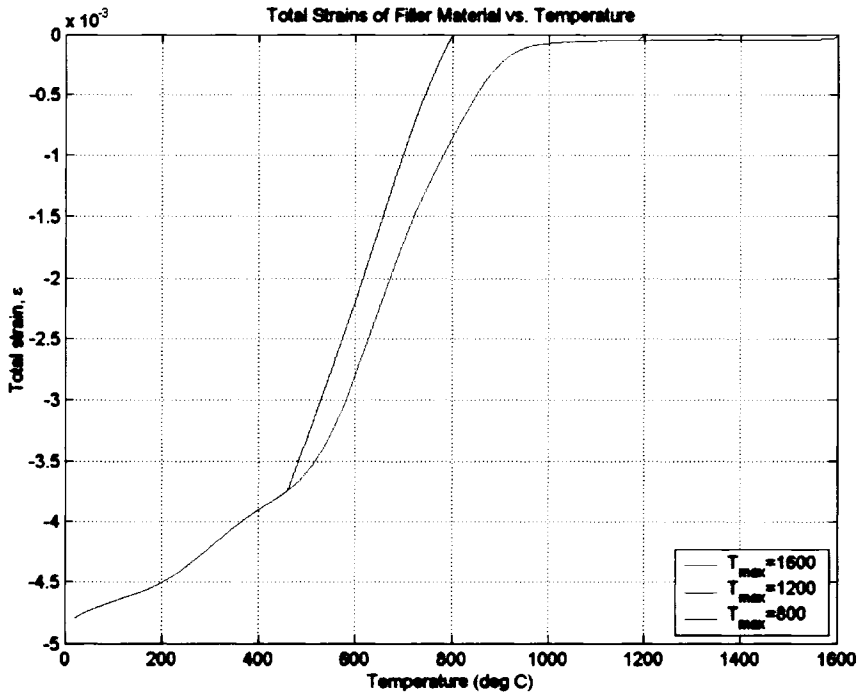

Figure 3. 19: Thermal history of total strain in the filler material with various $T_{\max}$

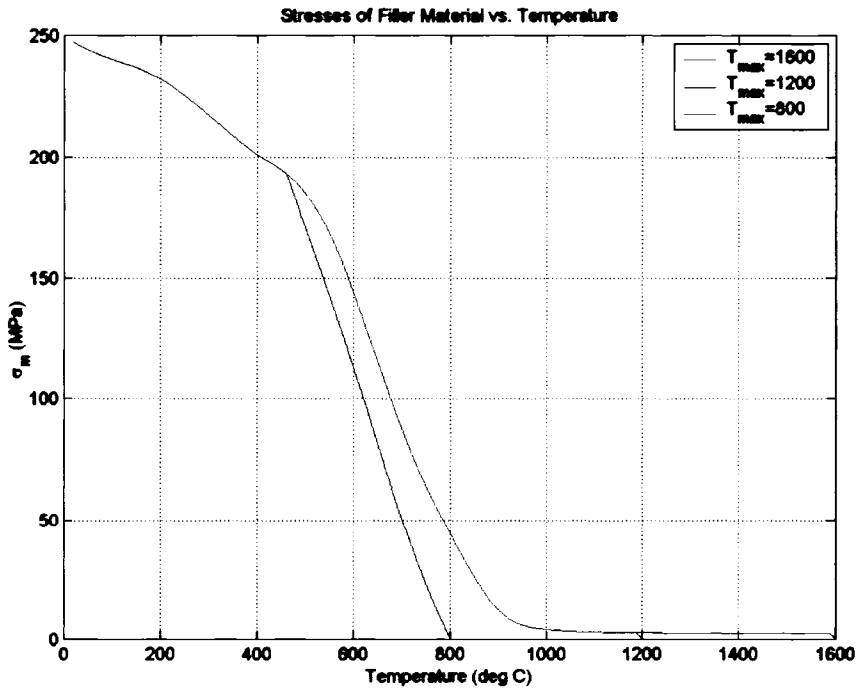

Figure 3. 20: Thermal history of σ_m in the filler material with various $T_{\max}$

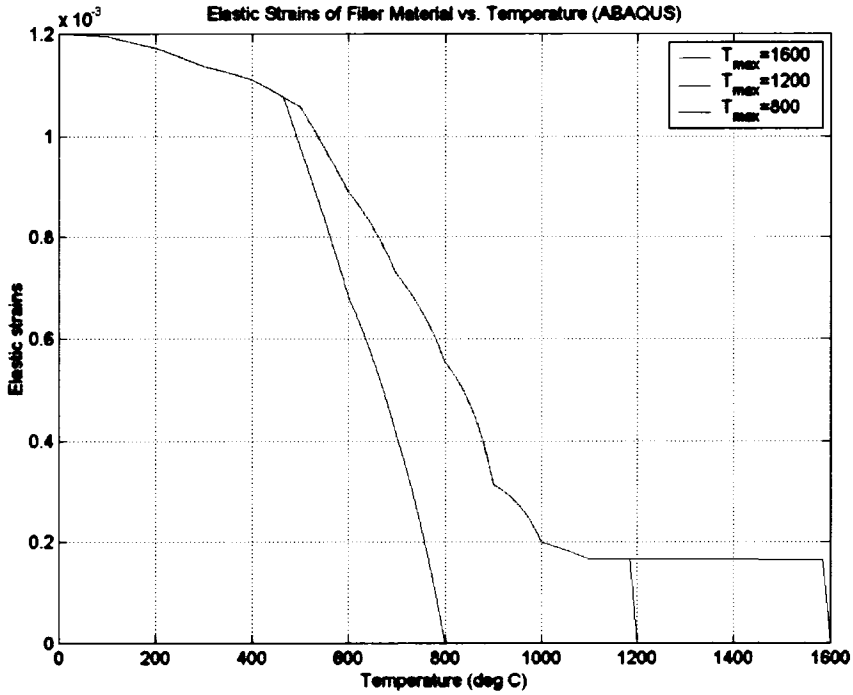

Figure 3. 21: Thermal history of elastic strain in the filler material with various $T_{\max}$ (ABAQUS)

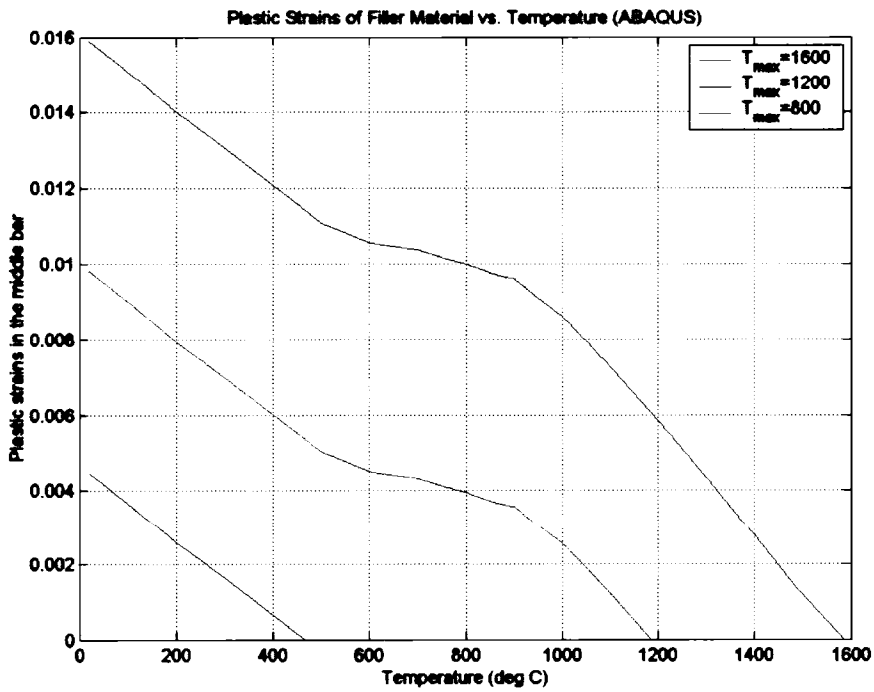

Figure 3. 22: Thermal history of plastic strain in the filler material with various $T_{\max}$ (ABAQUS)

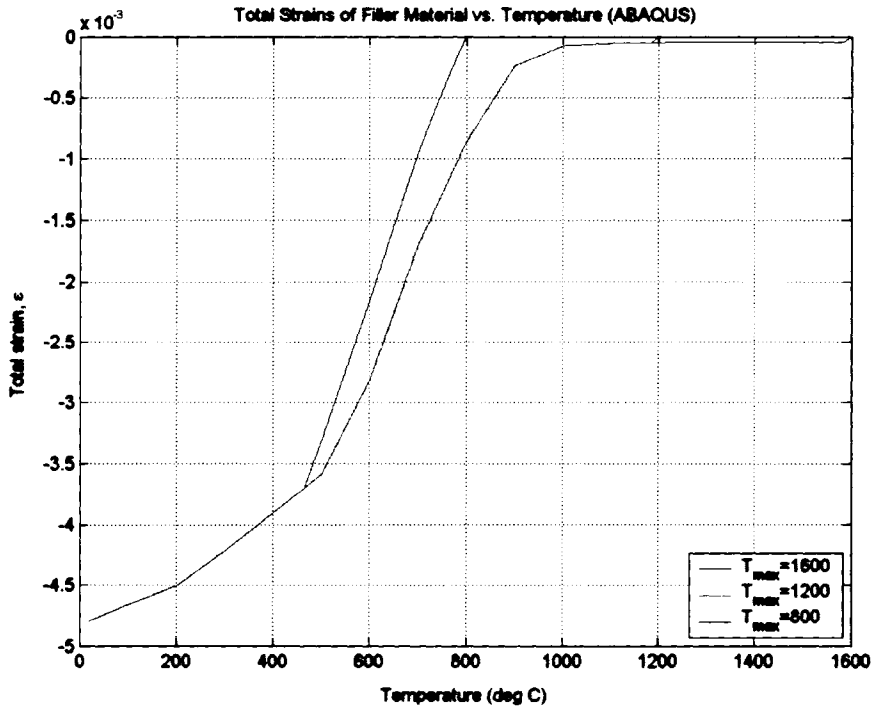

Figure 3. 23: Thermal history of total strain in filler material with various $T_{\max}$ (ABAQUS)

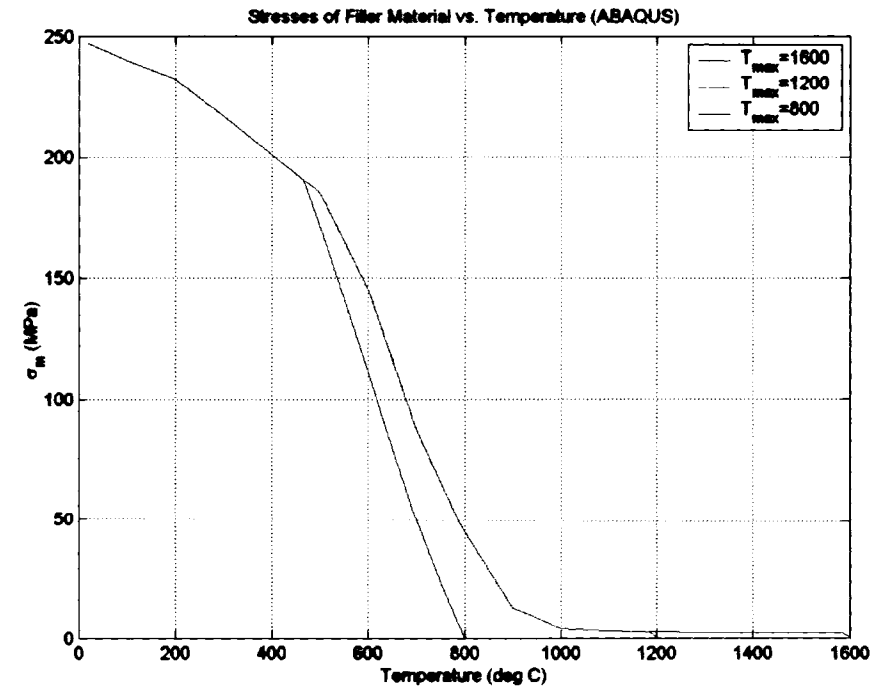

Figure 3. 24: Thermal history of σ_m in filler material with various $T_{\max}$ (ABAQUS)

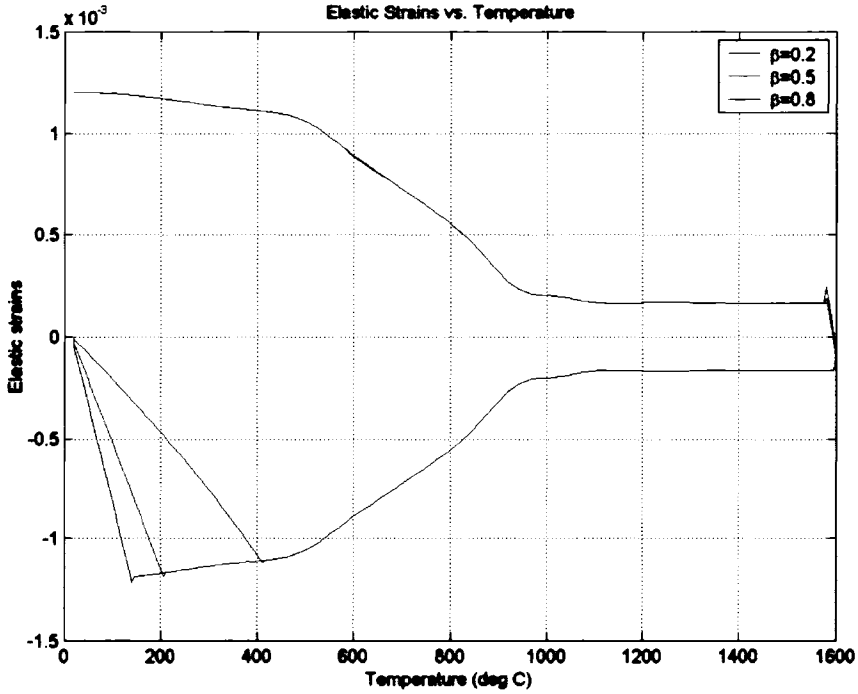

Figure 3. 25: Thermal history of elastic strain in the middle bar with various β

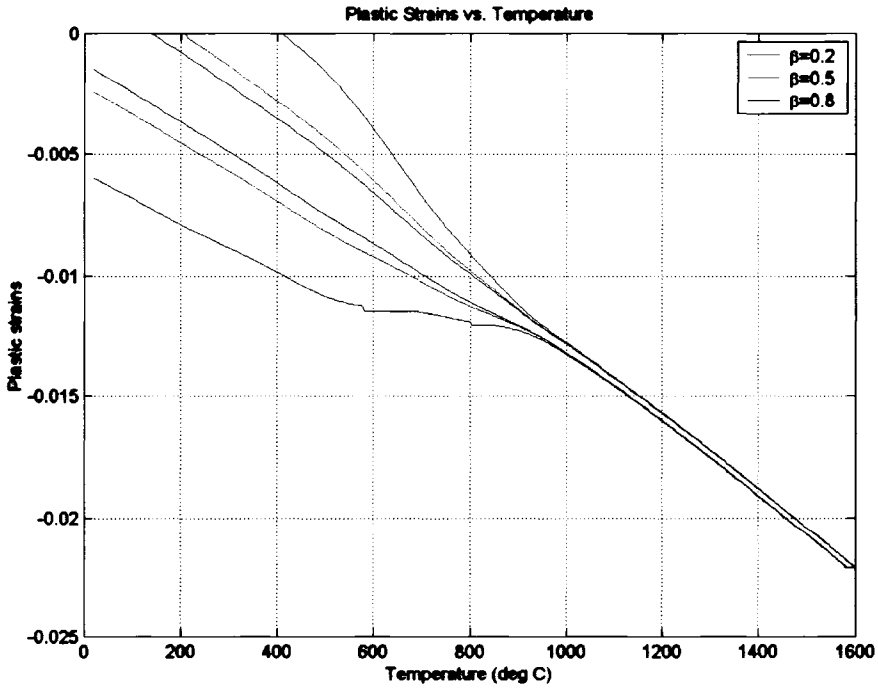

Figure 3. 26: Thermal history of plastic strain in the middle bar with various β

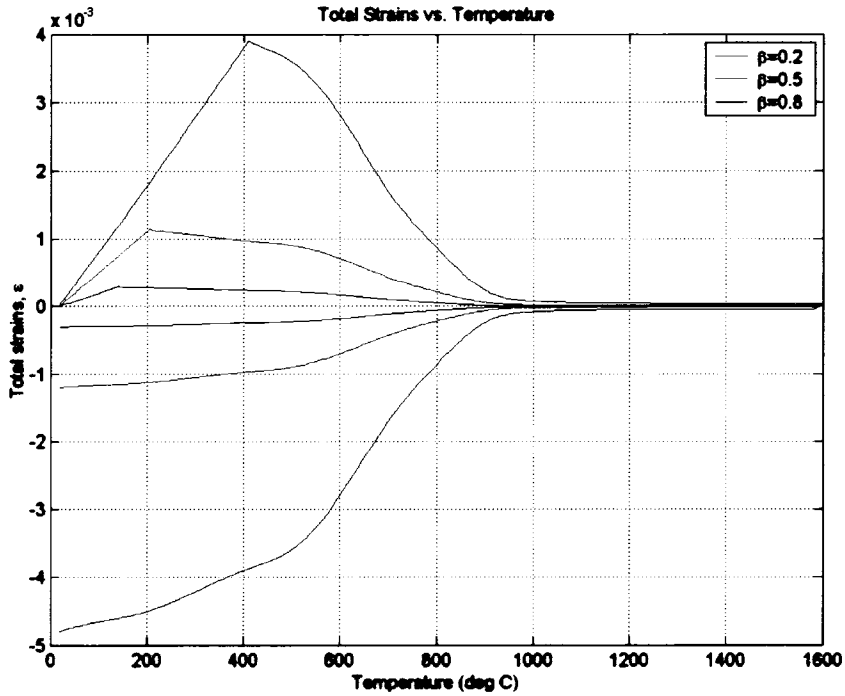

Figure 3. 27: Thermal history of total strain in the middle bar with various β

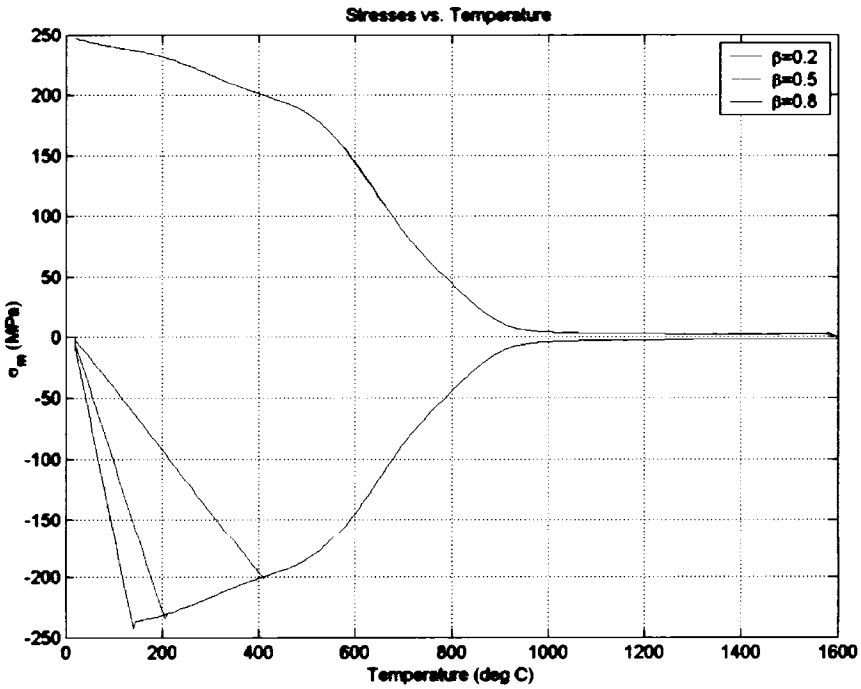

Figure 3. 28: Thermal history of σ_m in the middle bar with various β

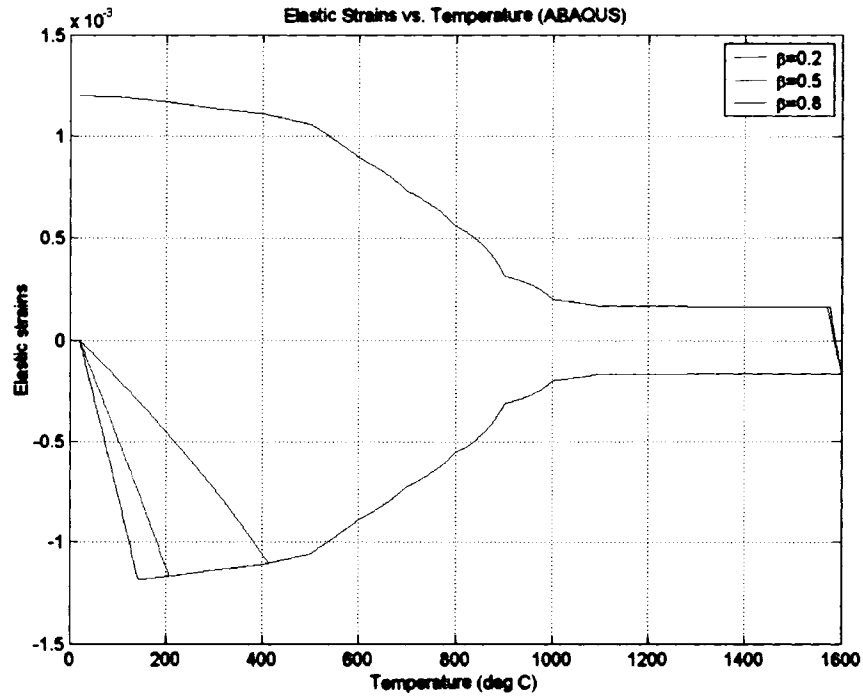

Figure 3. 29: Thermal history of elastic strain in the middle bar with various β (ABAQUS)

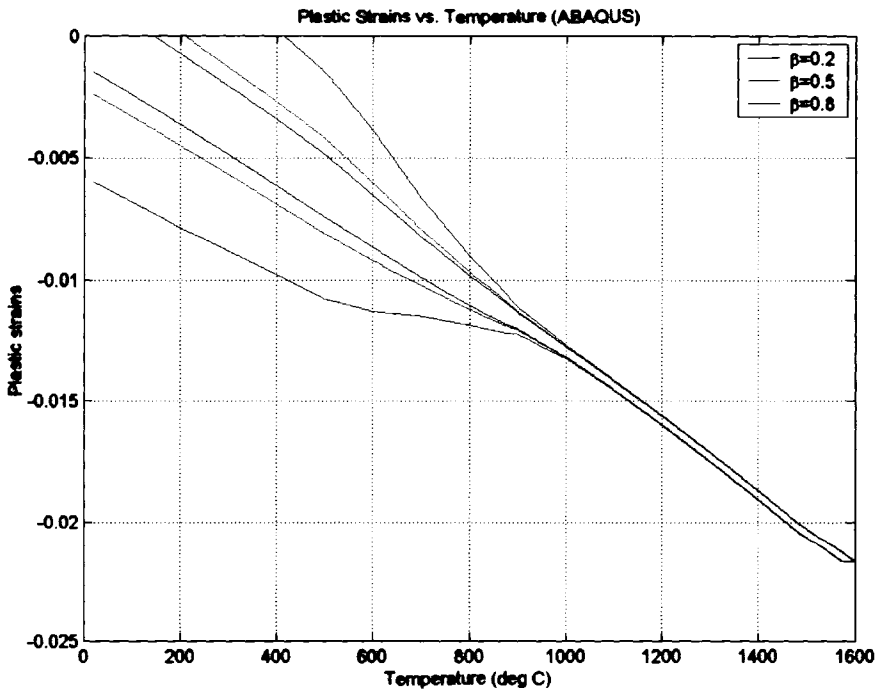

Figure 3. 30: Thermal history of plastic strain in the middle bar with various β (ABAQUS)

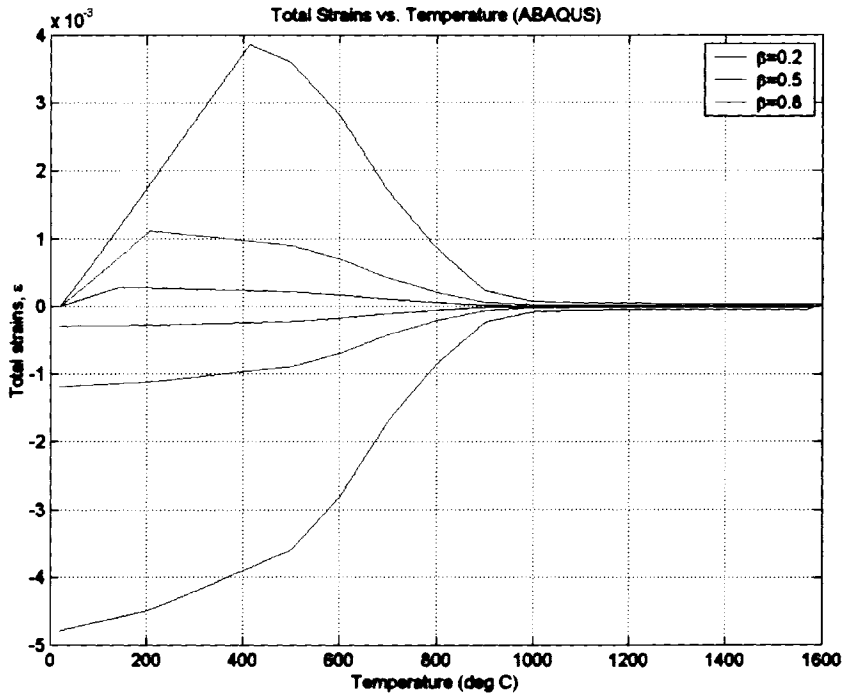

Figure 3. 31: Thermal history of total strain in the middle bar with various β (ABAQUS)

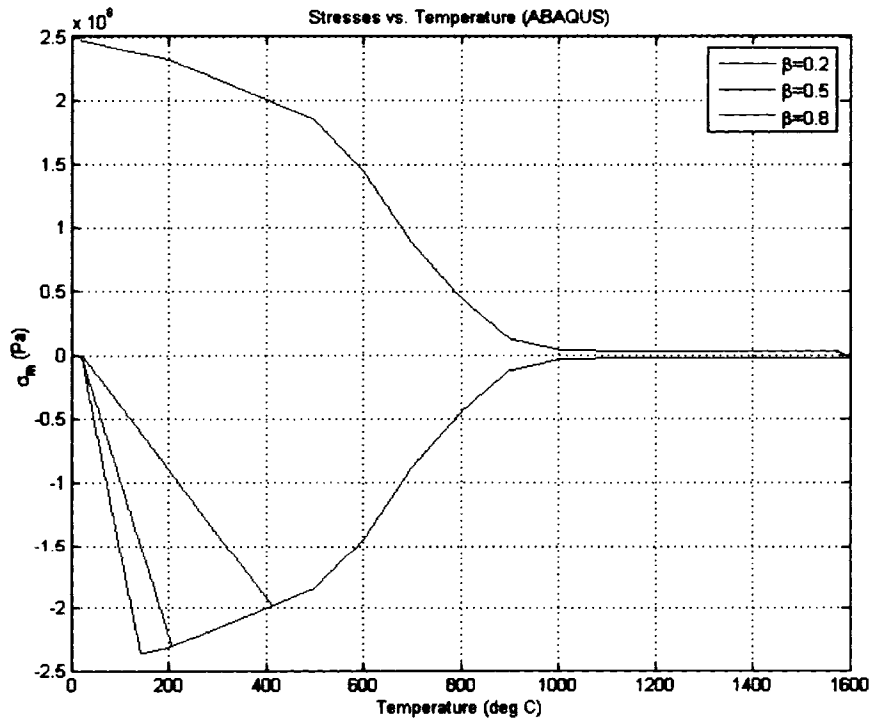

Figure 3. 32: Thermal history of σ_m in the middle bar with various β (ABAQUS)

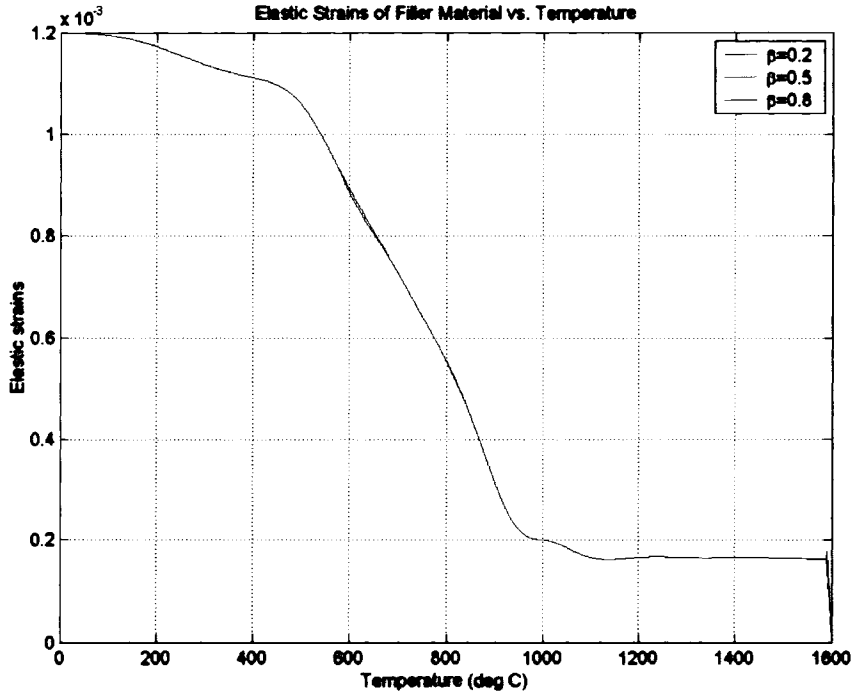

Figure 3. 33: Thermal history of elastic strain in the filler material with various β

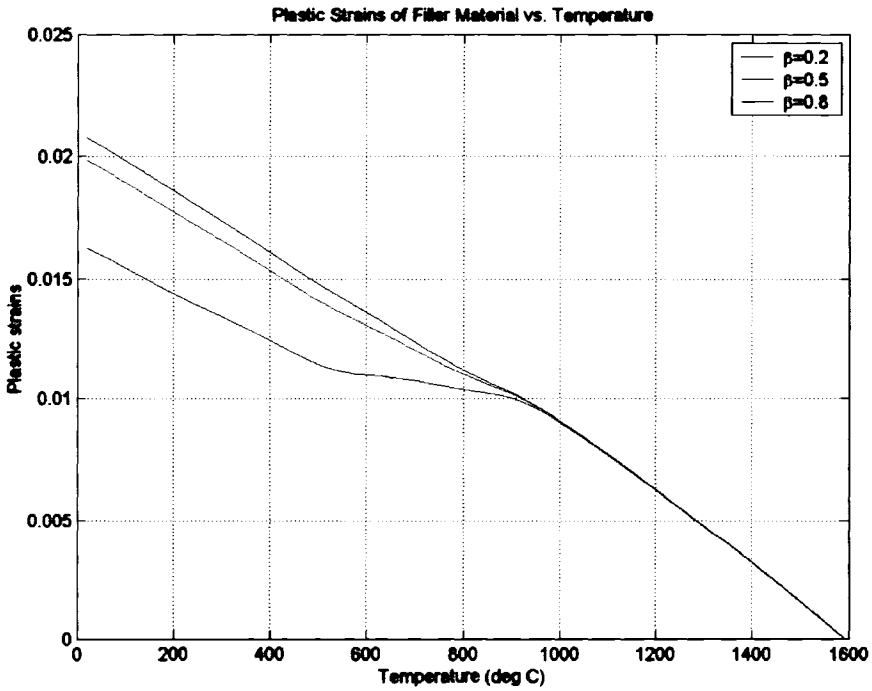

Figure 3. 34: Thermal history of plastic strain in the filler material with various β

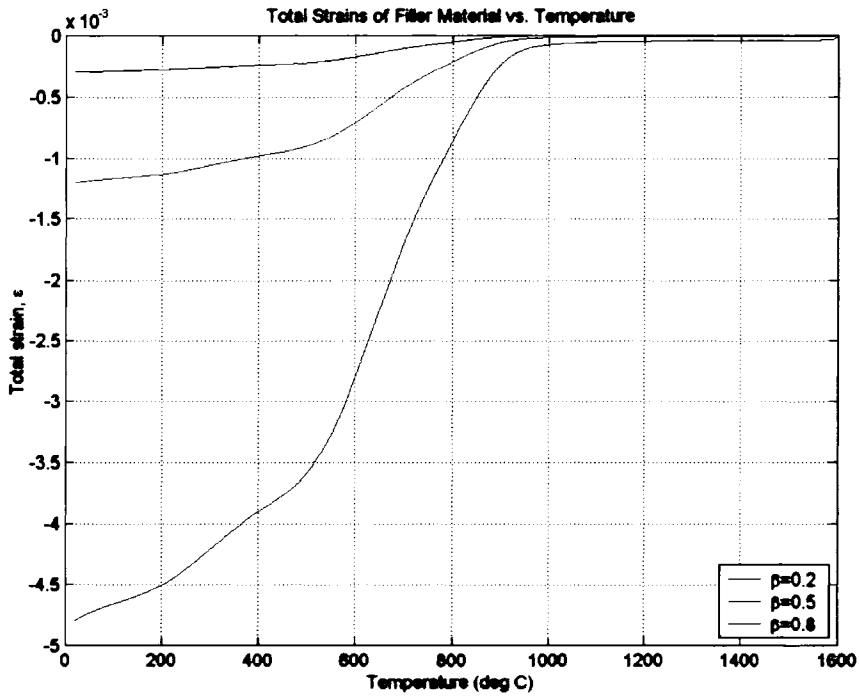

Figure 3. 35: Thermal history of total strain in filler material with various β

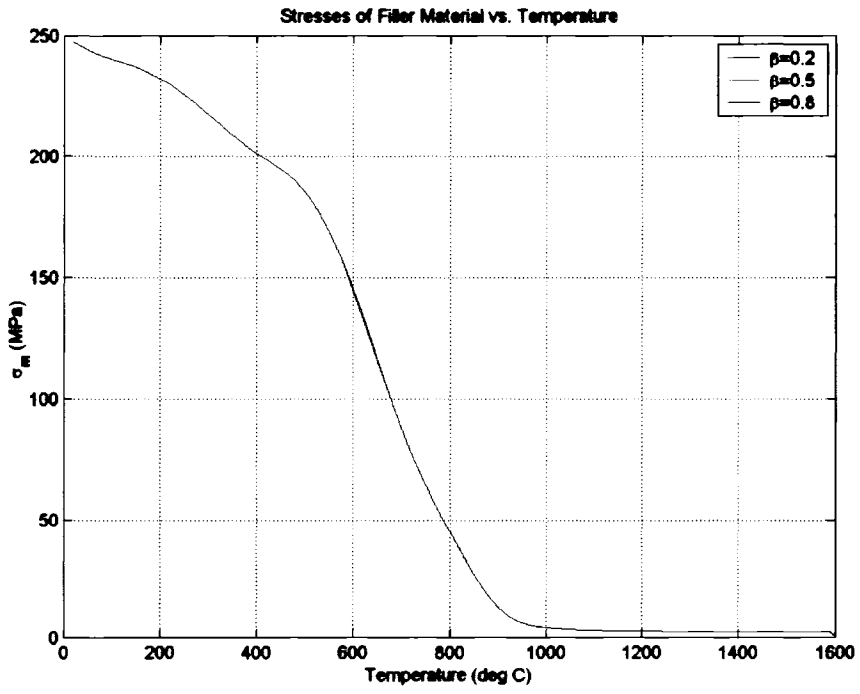

Figure 3. 36: Thermal history of σ_m in the filler material with various β

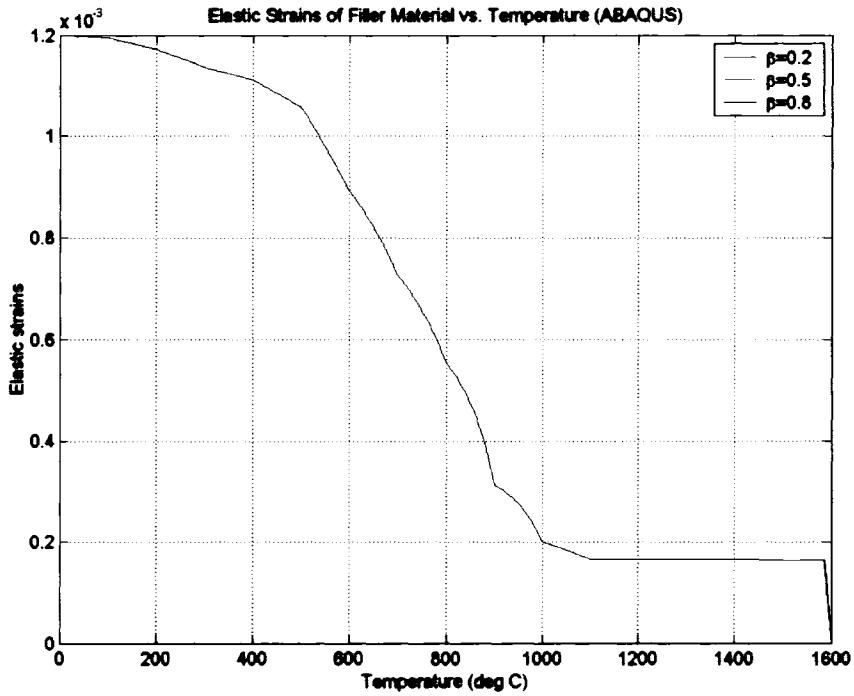

Figure 3. 37: Thermal history of elastic strain in the filler material with various β (ABAQUS)

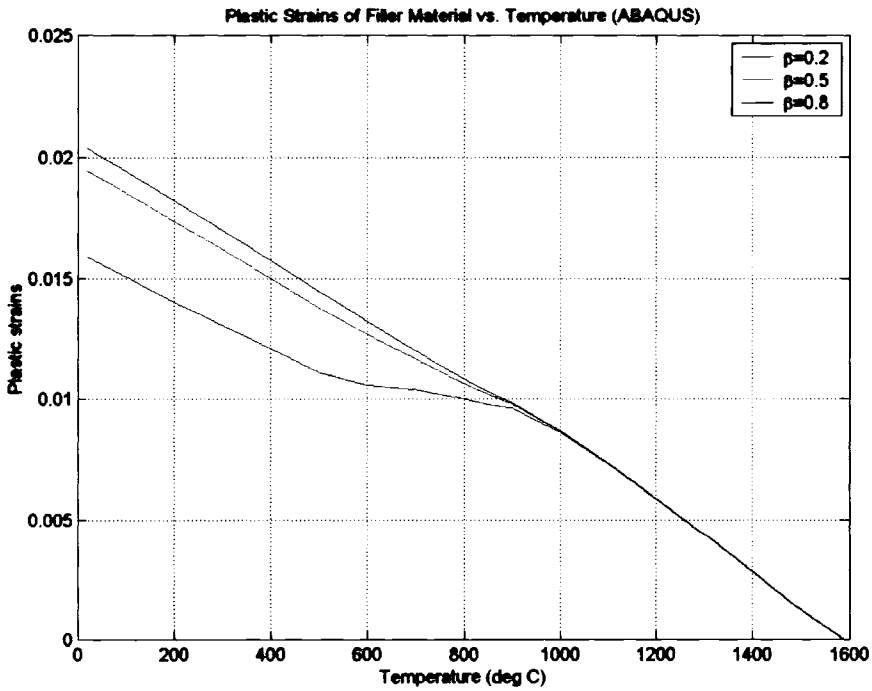

Figure 3. 38: Thermal history of plastic strain in the filler material with various β (ABAUQS)

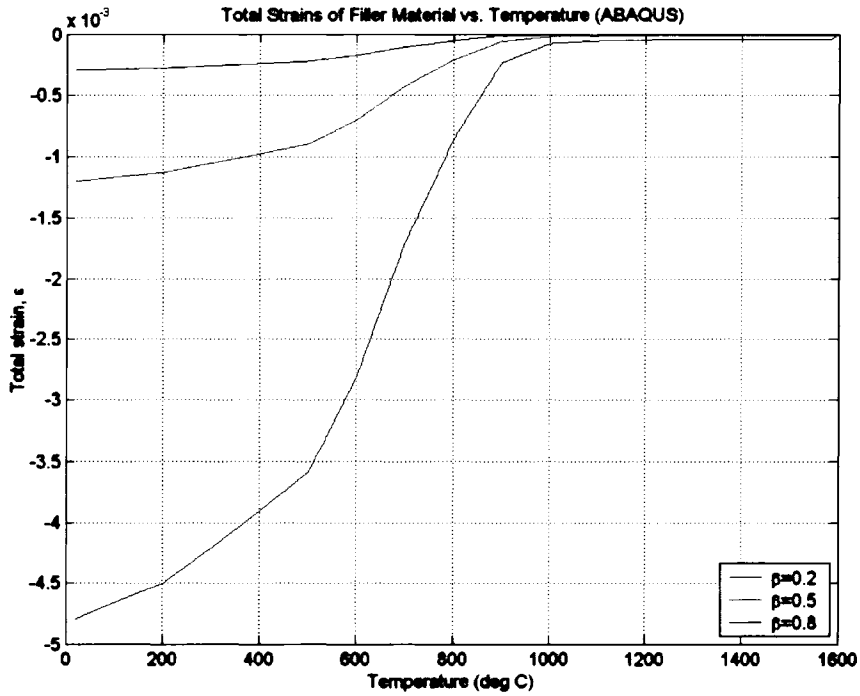

Figure 3. 39: Thermal history of total strain in the filler material with various β (ABAQUS)

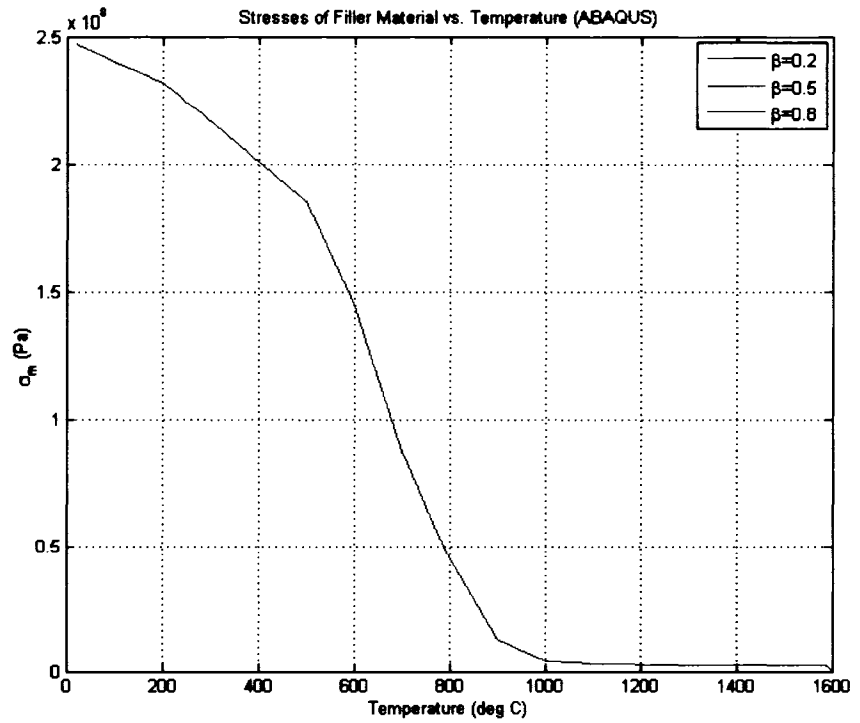

Figure 3. 40: Thermal history of σ_m in the filler material with various β (ABAQUS)

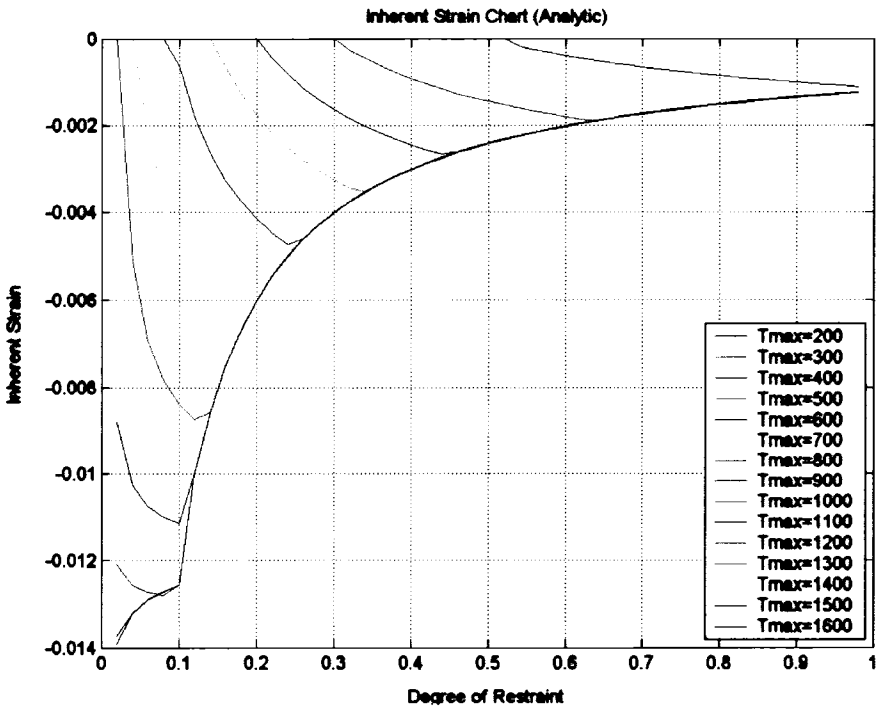

Figure 3. 41: Inherent strain chart

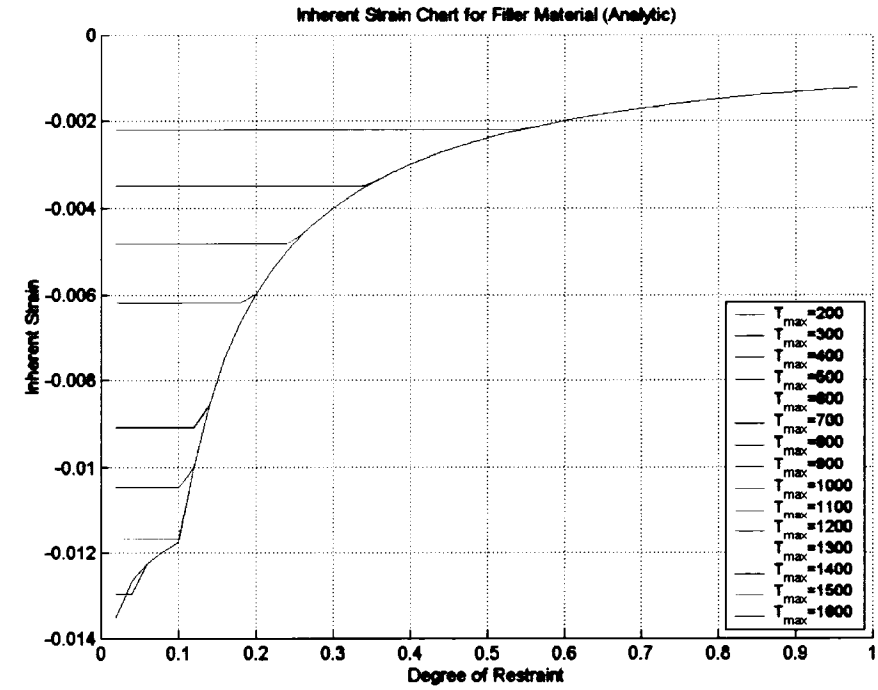

Figure 3. 42: Inherent strain chart for filler material

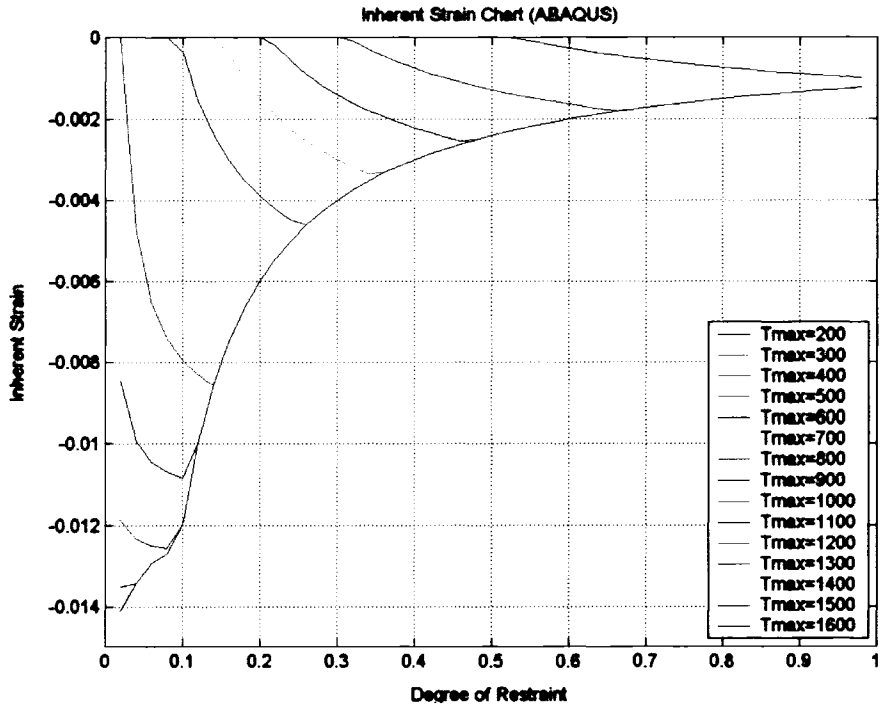

Figure 3. 43: Inherent strain chart (ABAQUS)

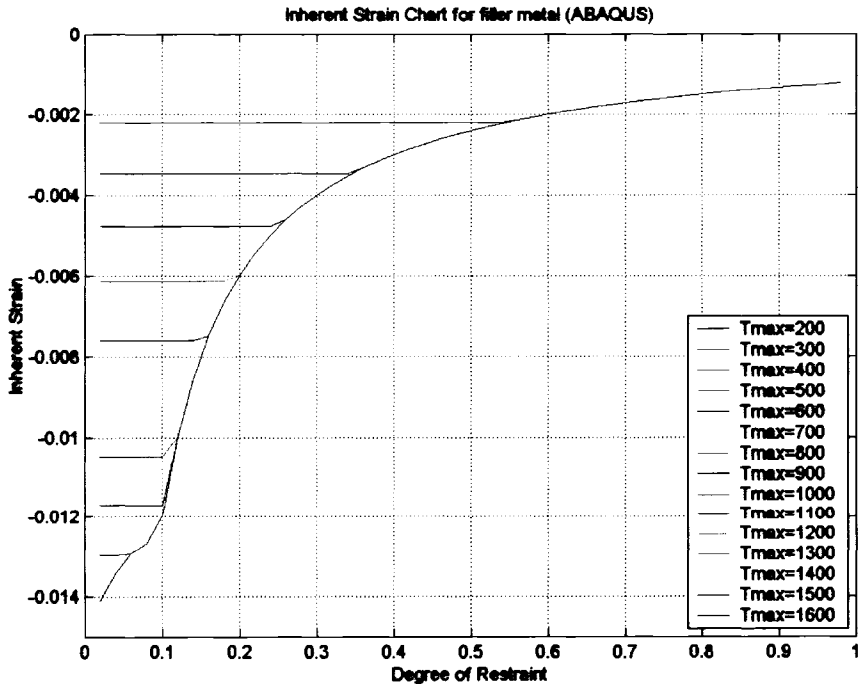

Figure 3. 44: Inherent strain chart for filler material (ABAQUS)

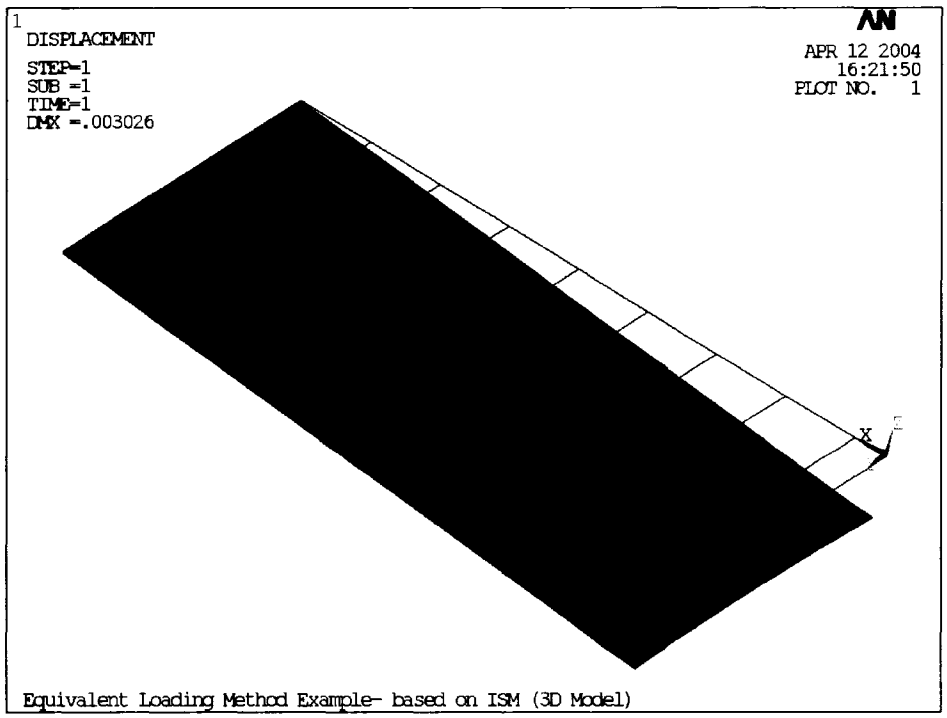

Figure 3. 45: Welding deformation calculated by equivalent loading method

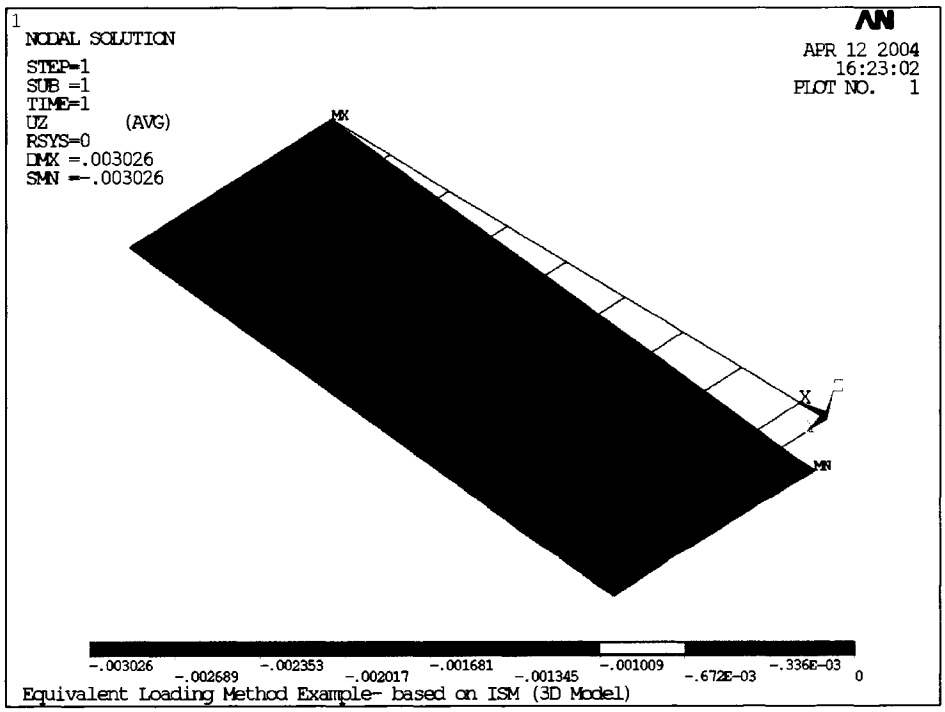

Figure 3. 46: Vertical displacement contour of 10mm plate butt weld (GMAW)

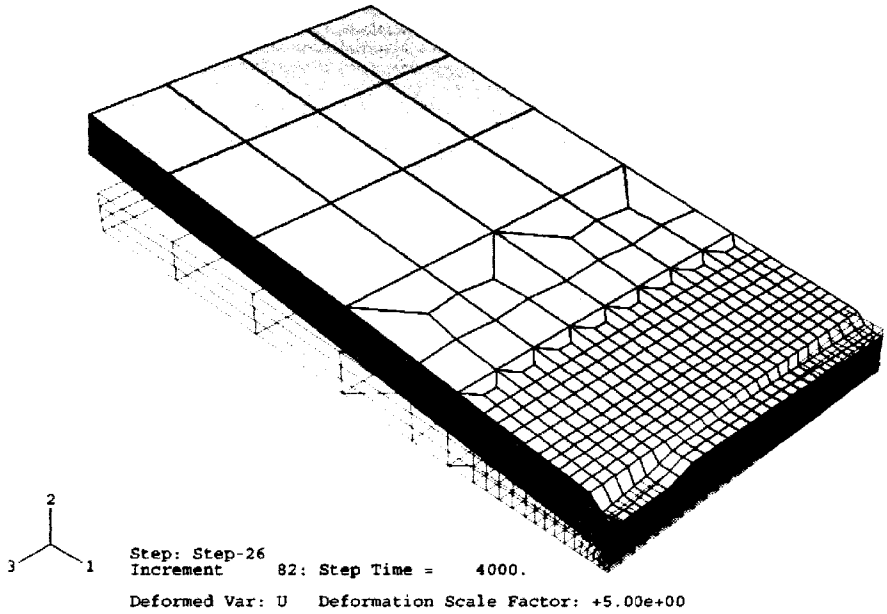

Figure 3. 47: 3D FEM welding distortion simulation - GMAW (ABAQUS)

CHAPTER IV

VARIATION SIMULATION FOR COMPLIANT METAL PLATE ASSEMBLIES

For hull block construction, parts that have variations from previous assembly processes are put together. However, due to their variations, a certain kind of clamping or holding device is required to force them to the nominal or weldable position. This is typically done by use of wedge devices, jacking clamps, strongbacks, and other fixtures. After that, the parts are welded together and the welding distortion affects dimensional quality of the assembly very significantly. Once the welding is done, the fixturing devices are released and the welded structure elastically deforms since the confining forces are removed.

There are several analytical methods to predict the tolerances of compliant steel plates assemblies. However, it is very difficult to apply these methods to complex two-dimensional or three-dimensional problems. For steel plate assemblies with two-dimensional or three-dimensional assemblies, the finite element method (FEM) is used for a general purpose deformation analysis. According to Liu and Hu (1995), there are two feasible approaches. One is Direct Monte-Carlo Simulation and the other is to use the Method of Influence Coefficients.

Direct Monte-Carlo simulation in FEM is straightforward but very time consuming, because hundreds or thousands of FEM runs are required to obtain a realistic assembly variation distribution. Figure 4.1 shows a flow chart for the Monte-Carlo Simulation of compliant steel plate assemblies in order to account for welding distortion

of ship hull block construction. Welding deformation analysis by FEM is added to the conventional variational simulation flow chart. In each run of the flow chart, the FEM must be executed three times. Although the strategy of the Direct Monte-Carlo simulation is easy to understand, it demands even more computation time in addition to the conventional variational simulation since the welding distortion analysis requires relatively smaller mesh grids around the weld area and may necessitate complex thermo-elasto-plastic analysis.

An alternative method, the Method of Influence Coefficients, was developed by Liu and Hu (1995), to improve the computational efficiency, producing improvement by several orders of magnitude. However the Method of Influence Coefficients does not account for any distortions caused during the joining processes.

Thus, a more effective simulation strategy or algorithm needs to be formulated to perform the functions shown in Figure 4.1. In this chapter, a Modified Method of Influence Coefficients is developed based on the Method of Influence Coefficients for the more computationally effective tolerance analysis including welding distortion.

4.1 Method of Influence Coefficients

The key to the Method of Influence Coefficients is to establish a linear relationship between the part variation and the assembly deviations. Liu and Hu showed that this Method of Influence Coefficients gives relatively accurate results compared with Direct Monte-Carlo Simulation, while reducing the computation time by three orders of magnitude [Liu 1995].

The Method of Influence Coefficients can be summarized in the following steps.

Nomenclature

$[K_w]$: welded structure stiffness matrix

$[K_u]$: unwelded structure stiffness matrix

$\{V_u\}$: variation vector

$\{U_w\}$: springback (displacement) vector

$\{F_w\}$: clamping forces of welded structure

$\{F_u\}$: clamping forces of unwelded structure

N : the number of source of variation

M : the number of nodes in FEM model

where the subscript w stands for welded structure and u for the un-welded structure.

1. The right two terms in Equation (4.1) represent the forces required by the clamping device in order to fix non-nominal parts into their nominal position. The left two terms represent the force required by the clamping device after the parts are welded together. Figure 4.2 (a) shows the part variation V_u when the parts are loaded into the holding fixture or jig. Part 1 has an initial variation at the tip of the plate. If more than one source of variation are considered, part variation will be expressed in a form of vector $\{V_u\}$ and this vector representation of part variations is analogous to the displacement representation in FEM. Assuming that the welding process does not produce any welding distortion at all, the clamping forces of the unwelded structure, $\{F_u\}$, and the clamping forces of the welded structure, $\{F_w\}$, are the same. Thus:

$$\{F_w\} = [K_w]\{U_w\} = [K_u]\{V_u\} = \{F_u\} \tag{4.1}$$

2. Since $\{F_w\}$ and $\{F_u\}$ are identical, and if we ignore welding deformation at this point, then $\{U_w\} = [K_w]^{-1}\{F_w\}$ represents springback of the welded structure.

$$\{U_w\} = [K_w]^{-1}[K_u]\{V_u\} = [S_{wu}]\{V_u\} \tag{4.2}$$

3. The $[S_{wu}]$ matrix is the sensitivity matirix [Chase and Parkinson 1991] and represents how sensitive the assembly deviation $\{U_w\}$ is to the part deviation $\{V_u\}$ as shown in Figure 4.2 (d) . Mathematically, the mechanistic variation model is defined as a linear mapping $[S_{uw}]$ between the part deviation $\{V_u\}$ and the assembly deviation $\{U_w\}$, as shown in Equation (4.2). The Method of Influence Coefficients can help construct the sensitivity matrix by the following substeps.

3-1. Unit Force Response: A unit force is applied at the j-th source of variation. The direction of the unit force is the same as the direction of the deviation. FEM can be used to calculate the response under that unit force. The deformations at the N sources of variations are recorded as a column vector. Since the variations are assumed to be relatively small compared to part dimensions, the response of an arbitray force of magnitue of F_j will be:

$$\begin{Bmatrix} c_{1j} \\ \vdots \\ c_{Nj} \end{Bmatrix} F_j \tag{4.3}$$

where c_{ij} represents the displacement response at the i-th source of variation due to unit force applied at the j-th source of variation.

The response of an arbitrary combination of N forces will form a matrix equation as follws:

$$\{V\} = \begin{Bmatrix} V_1 \\ \vdots \\ V_N \end{Bmatrix} = \sum_{j=1}^{N} \begin{Bmatrix} c_{1j} \\ \vdots \\ c_{Nj} \end{Bmatrix} F_j = \begin{bmatrix} c_{11} & \cdots & c_{1N} \\ \vdots & \ddots & \vdots \\ c_{N1} & \cdots & c_{NN} \end{bmatrix} \begin{Bmatrix} F_1 \\ \vdots \\ F_N \end{Bmatrix} = [C]\{F\} \tag{4.4}$$

3-2. Matrix Inversion: The above equation can be inverted numerically. It should be noted that the arbitrary variations $\{V\}$ in the parts now can be translated into the equivalent forces $\{F\}$.

$$\{F\} = [C]^{-1}\{V\} = [K]\{V\} \tag{4.5}$$

3-3. Springback Computation: FEM is used one more time to calculate the springback displacement at any node in any directions for the welded structure or assembly. For the j-th source of variation, the equivalent unit force is applied to the assembly and the response of the assembly at each nodes will be:

$$\begin{Bmatrix} s_{1j} \\ \vdots \\ s_{Mj} \end{Bmatrix} V_j \tag{4.6}$$

where V_j represents the magnitude of the variation at the j-th source of variation.

By summing the responses due to the variations, we can determine the sensitivity matrix $[S_{uw}]$ as follows:

$$\{U_w\} = \begin{Bmatrix} U_1 \\ \vdots \\ U_M \end{Bmatrix} = \sum_{j=1}^{N} \begin{Bmatrix} s_{1j} \\ \vdots \\ s_{Mj} \end{Bmatrix} V_j = \begin{bmatrix} s_{11} & \cdots & s_{1N} \\ \vdots & \ddots & \vdots \\ s_{M1} & \cdots & s_{MN} \end{bmatrix} \begin{Bmatrix} V_1 \\ \vdots \\ V_N \end{Bmatrix} = [S_{uw}]\{V_u\} \tag{4.7}$$

The above equation is the mechanistic variation mode for deformable steel plate assemblies obtained by the Method of Influence Coefficients. The linear relationship is valid as long as the part derivations from the nominal positions are small, and the material properties remain in the linear range. If the variations are statistically independent, the mean deviation vector $\{\mu_a\}$ and the variance vector $\{\sigma_a^2\}$ can be calculated as follows:

$$\{\mu_a\} = [S]\{\mu_p\} \tag{4.8}$$

And:

$$\{\sigma_a^2\} = [S_{ij}^2]\{\sigma_p^2\} \tag{4.9}$$

Where:

$\{\mu_p\}$: mean vector of the sources of part variation $\{V\}$

$\{\sigma_p^2\}$: variance vector of the sources of part variation $\{V\}$

The standard deviation vector of the assembly $\{\sigma_p\}$ can be obtained by cacluating the squre root of Equation (4.9).

4.2 Modified Method of Influence Coefficients

In order to consider welding distortion at the same time, the welding distortion term should be included. Assuming the followings:

$\{F_d\}$: welding distortion force vector equivalent to welding distortion

$\{D\}$: welding distortion (displacement) vector

From Equation (4.1),

$$[K_w]\{U_w\} = [K_u]\{V_u\} \tag{4.10}$$

The left hand side is the clamping force after the parts are joined together without welding distortion and the right hand side is the clamping force before the parts are joined together. If we introduce the effect of welding distortion into this equation,

$$[K_w]\{U_w\} - \{F_d\} = [K_u]\{V_u\} \tag{4.11}$$

The new term, $\{F_d\}$, represent additional clamping force due only to welding distortion of the clamped parts. Since the clamping force of the welded structure, $[K_w]\{U_w\}$, has increased due to welding distortion by $\{F_d\}$, $\{F_d\}$ should be added to the right hand side and then solved to yield:

$$\{U_w\} = [K_w]^{-1}([K_u]\{V_u\} + \{F_d\}) = [K_w]^{-1}[K_u]\{V_u\} + [K_w]^{-1}\{F_d\} \tag{4.12}$$

or

$$\{U_w\} = [K_w]^{-1}[K_u]\{V_u\} + [K_w]^{-1}\{F_d\} = [S_{wu}]\{V_u\} + [K_w]^{-1}\{F_d\} \tag{4.13}$$

Since $\{F_d\}$ represents the force that is required to clamp the weld-distorted part to its original position and $[K_w]$ is the stiffness matrix, $[K_w]^{-1}\{F_d\}$ is the displacement vector due to welding distortion, $\{D\}$.

$$\{U_w\} = [S_{wu}]\{V_u\} + \{D\} \tag{4.14}$$

The above equation is the Modified Method of Influence Coefficients. It should be noted that $\{D\}$ is a displacement vector that explains the welding distortion of the non-nominal part. More precisely $\{D\}$ accounts only for the welding distortion of non-nominal parts that are clamped to their nominal positions. If we can predict how the clamping forces affect the welding distortion, the variational simulation considering welding distortion can be divided into two separate phases, which are variational simulation and welding distortion simulation, and the results can be linearly superimposed.

4.3 Three-bar Model Experiments for Part Variation Effect on Welding Distortion

Even though the clamping effect on welding distortion is a very complex problem that includes a three-dimensional constraint distribution in thermo-elasto-plastic analysis, a one-dimensional three-bar model is proposed for illustrative purposes. The welding distortion mechanism can be explained with this simple model and, in addition, the welding distortion simulation is also performed by the equivalent loading method based on the inherent strain method, which is fundamentally based on this one-dimensional model.

In order to consider the local clamping/fixturing effect, two different experiment settings are proposed. The first three-bar model is a clamped-clamped model that represents the region adjacent to the fixturing device and the other is a spring-clamped model that represents the region relatively far from the clamping devices. The spring-

clamped model is the more general case and the clamped-clamped model can be represented as a spring-clamped model with infinite spring stiffness. These models are shown in Figure 4.3. For both cases, analytic experiments were performed first and then a commercial FEM code (ABAQUS) was used to verify the analytic results. The material was assumed to be elastic-perfectly-plastic. For the numerical experiment, the following geometric properties were used.

- Mild steel (properties data from [Lee 1995])
- Nominal length of bars = 1.00 m
- Cross sectional area of center bar = 0.01 m^2
- Cross sectional area of side bars = 0.04 m^2 , each
- Maximum heating temperature = 500 °C

The result is expected to be as shown in Figure 4.4. When the center bar undergoes the heating and cooling process, the two side bars acts as elastic bodies that resist the deformation of the center bar. The clamping device confines any deformation in case of the clamped-clamped model. The center bar has the elastic deformation in relatively low temperature after being elastically deformed to its nominal position. It takes the compression, and the compression approaches the yielding stress as the temperature increases. The deformation is determined by the equilibrium, constitutive and compatibility equations. In the cooling phase, the center bar undergoes shrinkage and is subject to tension by the strength of sidebars or by clamping devices. After the temperature returns to its original condition, the system will "spring back" as the clamping device is removed. The degree of restraints in these experiments is:

$$\beta = \frac{K_{sides}}{K_{sides} + K_{center}} = \frac{0.8}{0.8 + 0.1} = 0.889.$$

The procedure assumed is as follows:

1. Part with initial variation. Variation is a dimensional discrepancy between the real part and the nominal part: STEP 1
2. Clamp the part to the nominal position: STEP 2 (path $\overline{OA}$ in Figure 4.4)
   a. For the clamped-clamped model, the part is clamped to its nominal position until released (displacement is confined and the external force to clamp the part changes)
   b. For the spring-clamped model, the part is forced to its nominal position by the spring until released (external force is confined and displacement changes). For this model, the positions of the supports are fixed until finally released.
3. Welding: STEP 3
   a. Elastic state during heating: STEP 3-1 (path $\overline{AB}$)
   b. Plastic state during heating: STEP 3-2 (path $\overline{BC}$)
   c. Elastic state during cooling: STEP 3-3 (path $\overline{CD}$)
   d. Plastic state during cooling: STEP 3-4 (path $\overline{DE}$)
4. Releasing and part springback: STEP 4 (path $\overline{EF}$)

The variables in the analytic experiments are the same as in Chapter III.

4.3.1 Thermal Stress Definition

Thermal stress is the stress due to thermal expansion of materials. Basically in this experiment, thermal stress is equivalent to the compressive stress that the rod undergoes when the thermally expanded rod is forced into its original length. For an infinitesimal temperature increase ΔT:

$$\delta\sigma^{th} = -\alpha(T)\delta T \cdot E(T) = -\varepsilon^{th} \cdot E(T) \tag{4.15}$$

Therefore,

$$\sigma^{th} = \int \delta\sigma^{th} = -\int \alpha(T) \cdot E(T) dT \tag{4.16}$$

Here, negative stress means compression and positive stress means tension. Since the thermal stress is a compressive stress when the thermally expanded rod (integral terms) is forced to its original length (elastic coefficient at T_2), the thermal stress at temperature T_2 is:

$$\sigma^{th} = -E(T_2) \int_{T_1}^{T_2} \alpha(T) dT \tag{4.17}$$

4.3.2 Clamped-Clamped Model Experiment

4.3.2.1 Step 1: Initial Variation

The initial length of the three-bar model is assumed to be $L + v$, and the analytic solutions for the residual stresses and strains are obtained for the initial variation v. The range of initial variation is then selected to be $-0.001 \leq v \leq 0.001$ m, for the numerical calculation. This range is determined by considering STEP 2, in which the initial variation should not cause plastic deformation while clamping to the nominal position.

4.3.2.2 Step 2: Calmping/Fixturing to the Nominal Position

In this step, the part with a initial variation is clamped to its nominal position. It's assumed that the initial variation is selected not to cause any plastic deformation during this step, since this step is a clamping process rather than forming process.

The equilibirium equation is:

$$2A_s\sigma_s + A_m\sigma_m - F_u = 0 \tag{4.18}$$

The constitutive equations are:

$$\begin{aligned}\sigma_s &= E_s\varepsilon_s \\ \sigma_m &= E_m\varepsilon_m\end{aligned} \tag{4.19}$$

The compatibility equation is:

$$\varepsilon_m = \varepsilon_s = \ln(\frac{L}{L+v}) \tag{4.20}$$

Substituting the constitutive equation into the equilibrium equation yields:

$$(2A_sE_s + A_mE_m)\ln(\frac{L}{L+v}) - F_u = 0$$

$$\therefore F_u = (2A_sE_s + A_mE_m)\ln(\frac{L}{L+v}) \tag{4.21}$$

Also we find:

$$\sigma_s = E_s \ln(\frac{L}{L+v}) \tag{4.22}$$

$$\sigma_m = E_m \ln(\frac{L}{L+v}) \tag{4.23}$$

4.3.2.3 Step 3: Welding/Joining

According to its mechnistric characteristics, this step is comprised of four sub steps. During these substeps, the material properties are considered as temperature dependent. The temperature dependent material properties are listed in Table 4.1 for the experiment; Figure 4.5 and 4.6 show the temperature dependent thermal expansion coefficient and yield stress, respectively.

4.3.2.3.1 Step 3-1: Elastic State during Heating

During this step, the center bar only experiences elastic deformation. The total strain is comprised of thermal strain and elastic strain.

The equilibrium equation is:

$$2A_s\sigma_s + A_m\sigma_m - F_1 = 0 \tag{4.24}$$

The constitutive equations are:

$$\begin{aligned} \sigma_s &= E_s\varepsilon_s \\ \sigma_m &= E_m(\varepsilon_m - \varepsilon_m^{th}) = E_m(\varepsilon_m - \int\alpha(T)dT) \end{aligned} \tag{4.25}$$

Substituting the constitutive equations into the equilibrium equation yields:

$$E_m(\varepsilon - \int\alpha(T)dT)A_m + 2E_s\varepsilon A_s = F_1 \tag{4.26}$$

Therefore:

$$F_1 = (E_mA_m + 2E_sA_s)\ln(\frac{L}{L+v}) - E_mA_m\int\alpha(T)dT \tag{4.27}$$

Also, from the compatibility equation (4.20) and the constitutive equations:

$$\begin{aligned} \sigma_s &= E_s\varepsilon_s = E_s\ln(\frac{L}{L+v}) \\ \sigma_m &= E_m\left(\ln(\frac{L}{L+v}) - \int\alpha(T)dT\right) \end{aligned} \tag{4.28}$$

4.3.2.3.2 Step 3-2: Plastic State during Heating

At a certain temperature, the internal stress in the central bar reaches its compressive yield stress. Then, the stress becomes $-\sigma_Y(T)$ and the elastic strain ε_m^e, becomes constant in terms of strain-stress relation. Because the limit of the elastic stress,

i.e., the yield strain constantly changes while temperature increases, the actual elastic strain also changes with time, i.e., $\varepsilon_m^e = -\sigma_Y(T)/E_m$. Also, since an elastic-perfectly plastic material is assumed, the following relation holds true during this step.

$$\sigma_m = -\sigma_Y(T) \tag{4.29}$$

The equilibrium equation is:

$$\sigma_m A_m + 2\sigma_s A_s = F_2 \tag{4.30}$$

The constitutive equation is:

$$\sigma_s = E_s \varepsilon_s \tag{4.31}$$

Applying the compatibility equation (4.20) yields:

$$\sigma_m = -\sigma_Y(T) \tag{4.32}$$

$$\sigma_s = E_s \ln(\frac{L}{L+v}) \tag{4.33}$$

4.3.2.3.3 Step 3-3: Elastic State during Cooling

The state of the central bar returns to the elastic region. Thus, the stress at the maximum temperature is set at the initial stress at the point C.

The equilibrium equation is:

$$\sigma_m A_m + 2\sigma_s A_s = F_3 \tag{4.34}$$

The constitutive equations are:

$$\varepsilon_m^{th} = \int \alpha(T) dT \tag{4.35}$$

$$\sigma_s = E_s \varepsilon_s \tag{4.36}$$

Therefore we find:

$$\sigma_m = \sigma_m(C) + E_m(\varepsilon_m^{th} - \varepsilon_m^{th}(C)) \tag{4.37}$$

where $\sigma_m(C)$ and $\varepsilon_m^{th}(C)$ are the stress and thermal strain of the center bar at point C, respectively.

4.3.2.3.4 Step 3-4: Plastic State during Cooling

The center bar undergoes the increase of tension induced by the cooling process. At point D, the tension reaches the plastic stress, i.e., the center bar has the plastic stress determined by the temperature.

$$\sigma_m = \sigma_Y(T) \tag{4.38}$$

The equilibrium equation is:

$$\sigma_m A_m + 2\sigma_s A_s = F_4 \tag{4.39}$$

The constitutive equation is:

$$\sigma_s = E_s \varepsilon_s \tag{4.40}$$

Therefore we find:

$$\sigma_m = \sigma_Y(T) \tag{4.41}$$

$$\sigma_s = E_s \ln(\frac{L}{L+v}) \tag{4.42}$$

4.3.2.3.5 Step 4: Releasing the Clamp/Fixturing

Springback of the welded structure is calculated. Basically the equations are the same as those of STEP 2. However, the initial stress and strain start with their conditions at point E.

The equilibrium equation is:

$$\sigma_m A_m + 2\sigma_s A_s = 0 \tag{4.43}$$

The constitutive equations are:

$$\varepsilon_m = \varepsilon_s = \varepsilon(E) - \Delta\varepsilon \tag{4.44}$$

$$\sigma_s = E_s \varepsilon_s \tag{4.45}$$

$$\sigma_m = E_m \varepsilon_m$$

Releasing the clamping devices can be interpreted as removing the confining force at point E. The removed force is equivalent to the strain that the welded structure undergoes without the clamping devices. Thus,

$$(2A_s E_s \varepsilon(E) + A_m \sigma_Y(E)) = (2A_s E_s + A_m E_m)\Delta\varepsilon \tag{4.46}$$

Therefore, the final strain will be:

$$\varepsilon = \varepsilon(E) - \frac{2A_s E_s \ln(\frac{L}{L+\nu}) + A_m \sigma_Y(E)}{2A_s E_s + A_m E_m} \tag{4.47}$$

$$\sigma_m = \sigma_m(E) + E_m(\varepsilon - \varepsilon(E)) \tag{4.48}$$

$$\sigma_s = E_s \varepsilon \tag{4.49}$$

If the residual stress σ_m is greater than the yielding stress:

$$\sigma_m = \sigma_Y(T) \tag{4.50}$$

$$\varepsilon = \varepsilon(E) - \frac{2A_s E_s \ln(\frac{L}{L+v}) + A_m \sigma_Y(E)}{2A_s E_s} \tag{4.51}$$

Since in this analysis, Cauchy stress and natural strain are considered, the cross sectional areas are the current area, not the initial areas. Assuming the bars have circular cross sections:

$$\ln r = \varepsilon_r + \ln r_0 \tag{4.52}$$

$$r = e^{\varepsilon_r} r_0 \tag{4.53}$$

Therefore:

$$A = \pi r_0^2 e^{2\varepsilon_r} = A_0 e^{2\varepsilon_r} \tag{4.54}$$

where:

A : current area

A_0 : initial area

ε_r : radial strain

The radial strain, ε_r, can be calculated as:

$$\varepsilon_r = -\mu\varepsilon \tag{4.55}$$

where μ is Poisson's ratio.

The analytical stress-temperature and strain-temperature relations are thus calculated and plotted using Matlab. The analytic results are plotted as stress in the center bar versus temperature, stress in the side bars versus temperature, and elastic strain/plastic strain/thermal strain versus temperature. Also, the stress and strain in the center bar, varying with the initial variation, is also calculated. Since the model is

clamped to its nominal length during the welding deformation phase, the total strains do not change while the temperature changes. However, due to the plastic strain and elastic strain generated during the welding phase, it springs back after release from the clamping devices.

Figures 4.7 through 4.9 show the stress histories in the middle bar and Figure 4.10 shows the thermal histories of the various strains in the middle bar. The initial variation does affect the residual stress by changing the starting point of the elastic-heating path in the welding process, which subsequently leads to different initial yieldings points. It should be noted that the welding paths including the stage changing points (point C, D, and E in Figure 4.4) except the elastic-heating path are identical. The different initial yielding points consequently cause the different residual strains by shifting the plastic-heating path of the plastic strain in the Figure 4.10.

Figure 4.11 shows residual stresses of the center bar with various initial variations. We can see that there is linearity between the residual stresses and the initial variations except where the springback causes plastic deformation in the center bar. The linear region is skewed with respect to the zero variation point. This is because of the specific combination of the areas of middle bar and side bars, i.e., the degree of restraints.

The initial variation does affect the residual stress and strain that causes the welding distortion, in this case, linearly. According to the result we can conclude that welding deformation is linearly dependent to the initial variation of the part as long as the initial variation is small enough so that the clamping would not cause the plastic deformation of the parts. This result also conforms to the nature of pre-tensioning, which is one of the mitigation techniques used to reduce the welding residual stress.

4.3.3 Spring-Clamped Model Experiment

4.3.3.1 Step 1: Initial Variation

The range of initial variation was assumed as same as the clamped-clamped model, i.e., $-0.001 \leq v \leq 0.001$ m. Zero value of K_C, the clamping spring stiffness, was not considered because that case cannot represent 'clamping parts into nominal postion'. Displacement Δx_1 is the required displacement of the clamping spring to set the part to its nominal length.

4.3.3.2 Step 2: Clamping/Fixturing to Nominal Position

The equilibrium equation is:

$$2A_s\sigma_s + A_m\sigma_m - F_u = 0 \tag{4.56}$$

The constitutive equations are:

$$\begin{aligned} \sigma_s &= E_s\varepsilon_s \\ \sigma_m &= E_m\varepsilon_m \end{aligned} \tag{4.57}$$

The compatibility equation is:

$$\varepsilon_m = \varepsilon_s = \ln(\frac{L}{L+v}) \tag{4.58}$$

Substituting the constutivie equations into the equilibrium equation yields:

$2A_sE_s\varepsilon_s + A_mE_m\varepsilon_m - F_u = 0$

Substituting the constutivie equations into the equilibrium equation yields:

or: $2A_sE_s\varepsilon_s + A_mE_m\varepsilon_m - F_u = 0$

$$(2A_sE_s + A_mE_m)\ln(\frac{L}{L+v}) - F_u = 0 \tag{4.59}$$

Thus:

$$F_u = (2A_sE_s + A_mE_m)\ln(\frac{L}{L+v})$$

Therefore:

$$\sigma_s = E_s \ln(\frac{L}{L+v}) \tag{4.60}$$

And:

$$\sigma_m = E_m \ln(\frac{L}{L+v}) \tag{4.61}$$

Also:

$$F_u = K_C \Delta x_1 = (2A_s E_s + A_m E_m) \ln(\frac{L}{L+v})$$

And thus:

$$\Delta x_1 = \frac{F_u}{K_C} = \frac{(2A_s E_s + A_m E_m)}{K_C} \ln(\frac{L}{L+v}) \tag{4.62}$$

where, K_C represents the stiffness coefficient that reflects the elastic constraining effect of the adjacent confined area.

4.3.3.3 Step 3: Welding/Joining

According to its mechanistic characteristics, this step is comprised of four sub steps. During the substeps, material properties are considered to be temperature dependent.

4.3.3.3.1 Step 3-1: Elastic State during Heating

The equilibrium equiation is:

$$2A_s\sigma_s + A_m\sigma_m - F_1 = 0$$

Thus:

$$F_1 = -K_C \cdot \Delta L + F_u = -K_C \cdot \Delta L + (2A_s E_s + E_m A_m) \ln(\frac{L}{L+v}) \tag{4.63}$$

The constitutive equations are:

$$\sigma_s = E_s \varepsilon_s$$
$$\sigma_m = E_m(\varepsilon_m - \varepsilon_m^{th}) = E_m(\varepsilon_m - \int \alpha(T)dT) \tag{4.64}$$

The compatibility equation is:

$$\varepsilon = \varepsilon_m = \varepsilon_s = \ln(\frac{L+\Delta L}{L+v}) \tag{4.65}$$

Substituting the constitutive equations into the equilibrium equation yields:

$$E_m(\varepsilon - \int \alpha(T)dT)A_m + 2E_s \varepsilon A_s = F_1 \tag{4.66}$$

Therefore:

$$F_1 = (E_m A_m + 2E_s A_s)\varepsilon - E_m A_m \int \alpha(T)dT \tag{4.67}$$

Also from the compatibility equation:

$$\Delta L = (L+v)e^{\varepsilon} - L \tag{4.68}$$

Therefore:

$$(E_m A_m + 2E_s A_s)\varepsilon + K_C(L+v)e^{\varepsilon}$$
$$-(E_m A_m + 2E_s A_s)\ln(\frac{L}{L+v}) - K_C L - E_m A_m \int \alpha(T)dT = 0 \tag{4.69}$$

or:

$$\varepsilon + Ae^{\varepsilon} - B = 0 \tag{4.70}$$

where:

$$A = \frac{K_C(L+v)}{(E_m A_m + 2E_s A_s)} \tag{4.71}$$

And:

$$B = \ln(\frac{L}{L+v}) + \frac{E_m A_m \int \alpha(T)dT + K_C L}{(E_m A_m + 2E_s A_s)} \tag{4.72}$$

The solution of the above equation is:

$$\varepsilon = B - W(Ae^{B}) \tag{4.73}$$

where the function $W(z)$ is Lambert W function that gives the solution for w in $z = we^{w}$ [Corless et al. 1996]. Otherwise we can use a Taylor expansion for the exponential term to make the equation easier to solve algebraically without using a mathematical function. Considering $\varepsilon = \ln(\frac{L+\Delta L}{L+\nu})$, where both ΔL and ν are relatively small compared to L and the value of the logarithm of their ratio also will be small and near zero, a Taylor expansion at the zero value can approximate the function very accurately. If we only use the first order term of the Taylor expansion, i.e., $e^{\varepsilon} \cong 1+\varepsilon$, the equation becomes

$$\varepsilon + A(1+\varepsilon) - B = 0 \tag{4.74}$$

The solution is:

$$\begin{aligned}
\varepsilon &= \frac{B-A}{1+A} \\
&= \frac{\ln(\frac{L}{L+\nu}) + \frac{E_m A_m \int \alpha(T)dT + K_C L - K_C(L+\nu)}{(E_m A_m + 2E_s A_s)}}{1 + \frac{K_C(L+\nu)}{(E_m A_m + 2E_s A_s)}} \\
&= \frac{(E_m A_m + 2E_s A_s)\ln(\frac{L}{L+\nu}) + E_m A_m \int \alpha(T)dT - K_C \nu}{(E_m A_m + 2E_s A_s) + K_C(L+\nu)}
\end{aligned} \tag{4.75}$$

Therefore:

$$\sigma_s = E_s \varepsilon_s = E_s \frac{(E_m A_m + 2E_s A_s)\ln(\frac{L}{L+\nu}) + E_m A_m \int \alpha(T)dT - K_C \nu}{(E_m A_m + 2E_s A_s) + K_C(L+\nu)} \tag{4.76}$$

$$\sigma_m = E_m(\varepsilon_m - \int\alpha(T)dT)$$
$$= E_m\left(\frac{(E_mA_m + 2E_sA_s)\ln(\frac{L}{L+v}) - (K_C(L+v) + 2E_sA_s)\int\alpha(T)dT - K_Cv}{(E_mA_m + 2E_sA_s) + K_C(L+v)}\right)$$

(4.77)

4.3.3.3.2 Step 3-2: Plastic State during Heating

At a certain temperature, the internal stress in the central bar reaches its compressive yield stress. From then, the stress, $\sigma_Y(T)$, and the elastic strain, ε_m^e became constant.

$$\sigma_m = -\sigma_Y(T) \tag{4.78}$$

The equilibrium equation is:

$$\sigma_mA_m + 2\sigma_sA_s = F_2$$

Thus:

$$F_2 = -K_C \cdot \Delta L + F_u = -K_C \cdot \Delta L + (2A_sE_s + A_mE_m)\ln(\frac{L}{L+v}) \tag{4.79}$$

The constitutive equation is:

$$\sigma_s = E_s\varepsilon_s \tag{4.80}$$

Substituting the compatibility equation (4.68) into the equilibrium equations, we obtain:

$$2A_sE_s\varepsilon + K_C(L+v)e^{\varepsilon} - \sigma_Y(T)A_m - K_CL - (2A_sE_s + A_mE_m)\ln(\frac{L}{L+v}) = 0 \tag{4.81}$$

or:

$$\varepsilon + Ae^{\varepsilon} - B = 0 \tag{4.82}$$

where:

$$A = \frac{K_C(L+\nu)}{2A_sE_s}$$
$$B = \frac{(2A_sE_s + A_mE_m)}{2A_sE_s}\ln(\frac{L}{L+\nu}) + \frac{\sigma_Y(T)A_m + K_CL}{2A_sE_s} \tag{4.83}$$

Using a first-order Talyor series expansion, we can get the following solution.

$$\varepsilon = \frac{B-A}{1+A}$$
$$= \frac{\frac{(2A_sE_s + A_mE_m)}{2A_sE_s}\ln(\frac{L}{L+\nu}) - \frac{K_C(L+\nu)}{2A_sE_s} + \frac{\sigma_Y(T)A_m + K_CL}{2A_sE_s}}{1+\frac{K_C(L+\nu)}{2A_sE_s}} \tag{4.84}$$
$$= \frac{(2A_sE_s + A_mE_m)\ln(\frac{L}{L+\nu}) + \sigma_Y(T)A_m - K_C\nu}{2A_sE_s + K_C(L+\nu)}$$

In this stage:

$$\sigma_m = -\sigma_Y(T) \tag{4.85}$$

$$\sigma_s = E_s\left(\frac{(2A_sE_s + A_mE_m)\ln(\frac{L}{L+\nu}) + \sigma_Y(T)A_m - K_C\nu}{2A_sE_s + K_C(L+\nu)}\right) \tag{4.86}$$

4.3.3.3.3 Step 3-3: Elastic State during Cooling

The state of the central bar returns to the elastic region. Thus, the stress at the maximum temperature is set as the initial stress at point C.

The equilibrium equation is:

$$\sigma_mA_m + 2\sigma_sA_s = F_3 \tag{4.87}$$

Thus:

$$
\begin{aligned}
F_3 &= -K_C \cdot \Delta L + F_u \\
&= -K_C \cdot \Delta L + (2A_s E_s + A_m E_m)\ln(\frac{L}{L+\nu})
\end{aligned}
\tag{4.88}
$$

The constitutive equation is:

$$\varepsilon_m^{th} = -\int \alpha(T)dT \tag{4.89}$$

Therefore:

$$\sigma_m = \sigma_m(C) + E_m(\varepsilon_m^e - \varepsilon_m(C) + \int \alpha(T)dT) \tag{4.90}$$

where $\sigma_m(C)$ and $\varepsilon_m(C)$ are the stress and strain of the center bar at point C, respectively.

$$
\begin{aligned}
&(2A_s E_s + A_m E_m)\varepsilon + K_C(L+\nu)e^{\varepsilon} \\
&- K_C L - (2A_s E_s + A_m E_m)\ln(\frac{L}{L+\nu}) + A_m\sigma_m(C) + A_m E_m(\int \alpha(T)dT - \varepsilon_m(C)) = 0
\end{aligned}
\tag{4.91}
$$

The above equation is obtained by substituting the comptibility equation and constitutive equation into the equilibrium equation. This equation can be expressed as Equation (4.82) where:

$$
\begin{aligned}
A &= \frac{K_C(L+\nu)}{(2A_s E_s + A_m E_m)} \\
B &= \ln(\frac{L}{L+\nu}) + \frac{K_C L - A_m E_m(\int \alpha(T)dT - \varepsilon_m(C)) - A_m\sigma_m(C)}{(2A_s E_s + A_m E_m)}
\end{aligned}
\tag{4.92}
$$

Using a first-order Taylor expansion for the exponentian term, we can get the following solution.

$$\varepsilon = \frac{B-A}{1+A}$$

$$= \frac{\ln(\frac{L}{L+v}) + \frac{K_C L - A_m E_m(\int \alpha(T)dT - \varepsilon_m(C)) - A_m \sigma_m(C)}{(2A_s E_s + A_m E_m)} - \frac{K_C(L+v)}{(2A_s E_s + A_m E_m)}}{1 + \frac{K_C(L+v)}{(2A_s E_s + A_m E_m)}}$$

$$= \frac{(2A_s E_s + A_m E_m)\ln(\frac{L}{L+v}) - K_C v - A_m E_m(\int \alpha(T)dT - \varepsilon_m(C)) - A_m \sigma_m(C)}{(2A_s E_s + A_m E_m) + K_C(L+v)} \tag{4.93}$$

Therefore:

$$\sigma_s = E_s \varepsilon$$

$$= E_s \left(\frac{(2A_s E_s + A_m E_m)\ln(\frac{L}{L+v}) - K_C v - A_m E_m(\int \alpha(T)dT - \varepsilon_m(C)) - A_m \sigma_m(C)}{(2A_s E_s + A_m E_m) + K_C(L+v)} \right) \tag{4.94}$$

And:

$$\sigma_m = \sigma_m(C) + E_m(\varepsilon - \varepsilon_m(C) + \int \alpha(T)dT) \tag{4.95}$$

4.3.3.3.4 Step 3-4: Plastic State during Cooling

The center bar undergoes an increase of tension induced by the cooling process. At point D, the tension reaches the plastic stress, i.e., the center bar has the plastic stress determined by the temperature.

$$\sigma_m = \sigma_Y(T) \tag{4.96}$$

The equilibrium equation is:

$$\sigma_m A_m + 2\sigma_s A_s = F_4 \tag{4.97}$$

Thus:

$$\begin{aligned} F_4 &= -K_C \cdot \Delta L + F_u \\ &= -K_C \cdot \Delta L + (2A_s E_s + A_m E_m)\ln(\frac{L}{L+v}) \end{aligned} \tag{4.98}$$

The constitutive equation is:

$$\sigma_s = E_s \varepsilon_s \tag{4.99}$$

The calculation of strain is similar to STEP3-2: plastic state during heating. The solution is:

$$\varepsilon = \frac{(2A_s E_s + A_m E_m)\ln(\frac{L}{L+v}) - \sigma_Y(T)A_m - K_C v}{2A_s E_s + K_C(L+v)} \tag{4.100}$$

Therefore:

$$\sigma_m = \sigma_Y(T) \tag{4.101}$$

$$\sigma_s = E_s \left(\frac{(2A_s E_s + A_m E_m)\ln(\frac{L}{L+v}) - \sigma_Y(T)A_m - K_C v}{2A_s E_s + K_C(L+v)} \right) \tag{4.102}$$

4.3.3.4 Step 4: Releasing the Clamp/Fixturing

Springback of welded structure is calculated. Basically the equations are same as those of STEP 2. However, the initial stress and strain start with the initial conditions at point E.

The equilibrium equation is:

$$\sigma_m A_m + 2\sigma_s A_s = 0 \tag{4.103}$$

The constitutive equations are:

$$\begin{aligned} \sigma_s &= E_s \varepsilon_s \\ \sigma_m &= E_m \varepsilon_m \end{aligned} \tag{4.104}$$

Releasing the clamping devices can be interpreted as removing the confining force at point E. The removed force is equivalent to the strain that the welded structure undergoes without clamping devices. The RHS terms explain equivalent clamping forces at the point E, and this should be equal to the total strain including the strain at the point E. Thus:

$$(2A_s E_s \varepsilon(E) + A_m \sigma_Y(E)) = (2A_s E_s + A_m E_m)\Delta\varepsilon \tag{4.105}$$

Therefore, the final strain will be:

$$\begin{aligned} \varepsilon &= \varepsilon(E) - \Delta\varepsilon \\ &= \varepsilon(E) - \frac{2A_s E_s \varepsilon(E) + A_m \sigma_Y(E)}{2A_s E_s + A_m E_m} \end{aligned} \tag{4.106}$$

And the stresses are:

$$\sigma_m = \sigma_m(E) + E_m(\varepsilon - \varepsilon(E)) \tag{4.107}$$

$$\sigma_s = E_s \varepsilon \tag{4.108}$$

The analytic stress-temperature and strain-temperature relations are calculated using Matlab. The results are shown in Figures 4.13 through 4.19. Figure 4.13, 4.14, and 4.15 show the stress-temperature relations with three different initial variations when K_c is 20 % of the material's Young's modulus. As dicussed in the clamped-clamped case,

the stress histories are identical except the elastic-heating paths. Thus the initial variation affects the residual stress and strain as it does in the clamped-clamped case, which is the shifting of the elastic-heating path of plastic strain shown in Figure 4.16. The patterns of elastic, plastic, and thermal strain of the center bar do not change with the initial variations, thus the total strains shown in Figure 4.17 are shifted in proportion to the various initial variations. As in the case of the clamped-clamped case, there are linear relations between the initial variations and the residual stress as well as the residual strains, which are shown in Figure 4.18 and Figure 4.19. However the slope is slightly different from that of the clamped-clamped case.

Compared to the result of the clamped-clamped model, the spring-clamped model has more springback which can be explained by having a smaller plastic strain component than the clamped-clamped model, with the same thermal strain component. This is because the spring elastically absorbs the elongation of the bars so that it consequently reduces the generation of plastic strains. Figures 4.20 through 4.32 shows the comparison of analytic results and finite element analysis result for verification purposes.

The initial variations linearly affect the residual stress and strain that account for the welding distortion as shown in Figure 4.33 and 4.34, while the clamping spring acts as if its strength is absorbed as the part of the degree of restraints. It should be noted that the difference in welding distortions, i.e, the residual strains, is about 10% of the initial variation difference. Considering that the welding distortion will be simulated by the equivalent loading method based on the inherent strain method, the initial variations in the plates to be welded should be translated into variations in the infinitesimal three-bars that are distributed longitudinally and transversally within the plates. If we consider the out-of-plane variations in the plates, it will become even more negligible because of the

differences in the initial variations in infinitesimal three-bars along the thickness direction.

4.4 Revised Mechanistic Variation Model

Through the study of the simplified one-dimensional schematic welding distortion model, the main governing mechanisms of welding distortion with intial part variations are reviewed and simulated. The following conclusions can be drawn:

1. Initial part variations affect the final residual strain and stress by changing the initial strain and stress of the part that are caused by clamping the part into its nominal position.
2. Compared to the magnitude of initial variation in terms of strain, the effect of initial variation in welding distortion is relatively small. The difference in welding distortion, i.e, the residual strain, is about 10% of initial variation difference.
3. Elastic clamping forces act as if their stength are absorbed as the part of the degree of restraints. However if a full plate assembly model is considered instead of infinitesimal three-bar model, it becomes negligible.
4. Some of the mitigation techniques to reduce welding deformation and residual stress, such as pre-tensioning and thermal tensioning, can be explained by changing the initial stress and strain, and reducing the temperature difference between the welded area and the adjacent area, which can be easily explained by the three-bar model.

Thus the mechanistic variation model considering welding distortion is:

$$\{U_w\} = [S_{wu}]\{V_u\} + [A]\{V_u\} + \{D\} \tag{4.109}$$

However, the variational effects on welding distortion term, $[A]\{V_u\}$, could be assumed to be negligible if the range of initial variation is relatively small compared to the total dimension of the non-nominal part and if we consider out-of-plane variations of the plate assemblies. Thus the Modified Method of Influence Coefficients is formulated as:

$$\{U_w\} = [S_{wu}]\{V_u\} + \{D\} \tag{4.110}$$

In the above equation, $\{D\}$ is a displacement vector and it means the welding distortion of nominal parts being clamped to its nominal position.

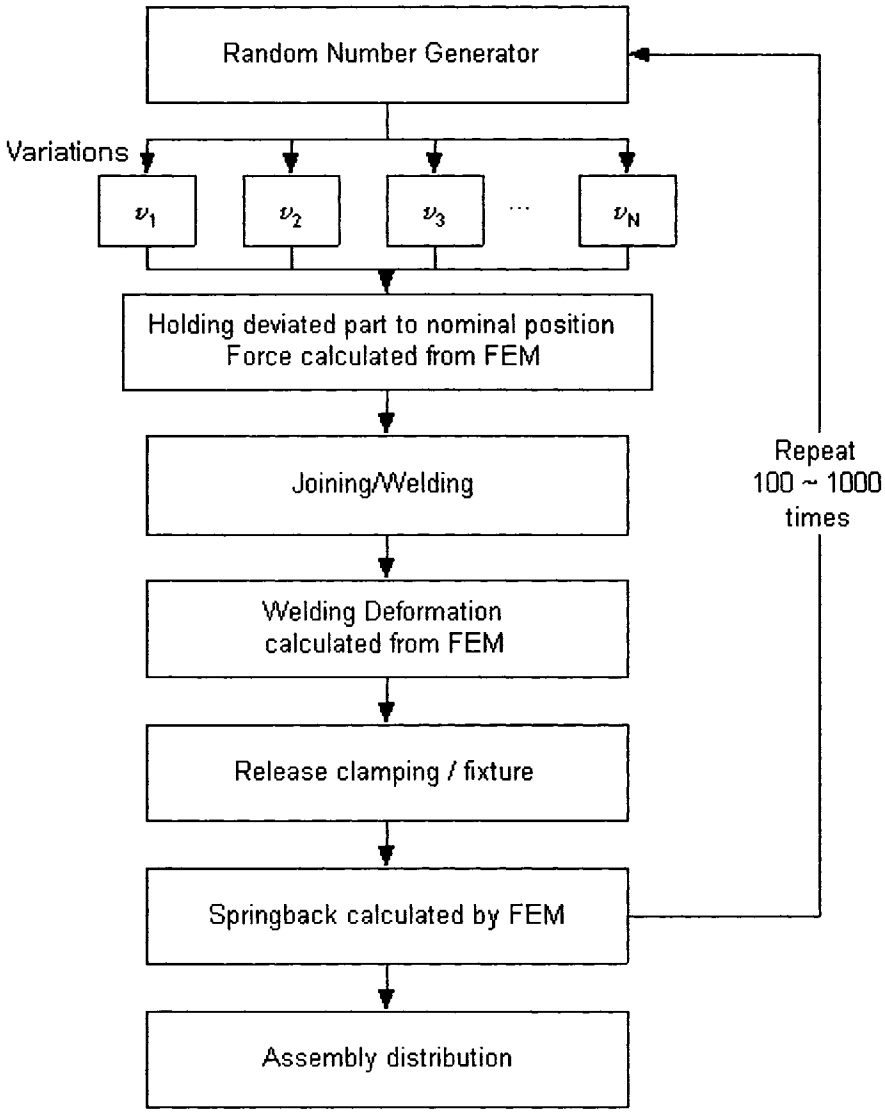

Figure 4. 1 Flow chart of Direct Monte Carlo simulation

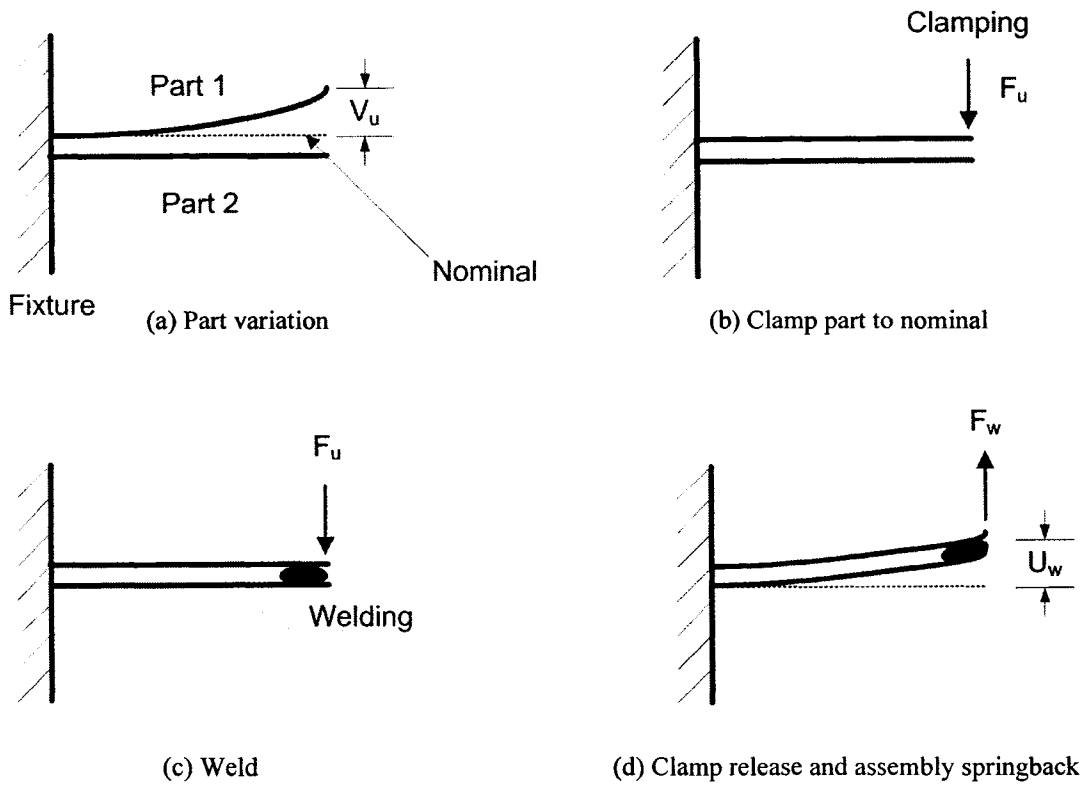

Figure 4. 2 Metal plate assembly process

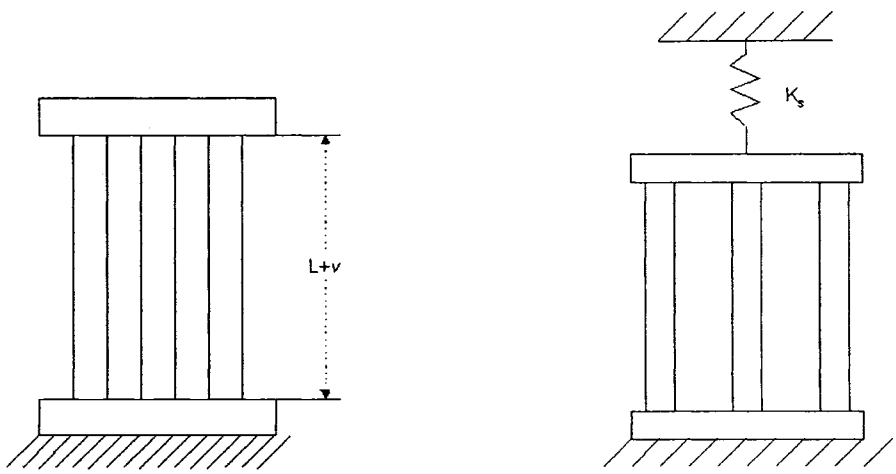

Figure 4. 3 Three-bar models

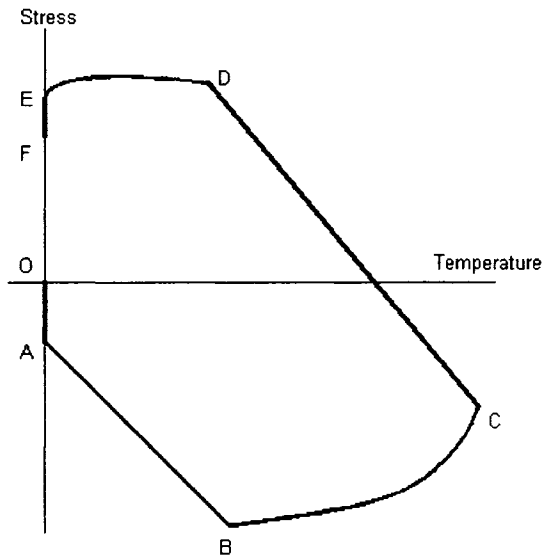

Figure 4. 4 Expected temperature-stress relation in the center bar of three-bar models

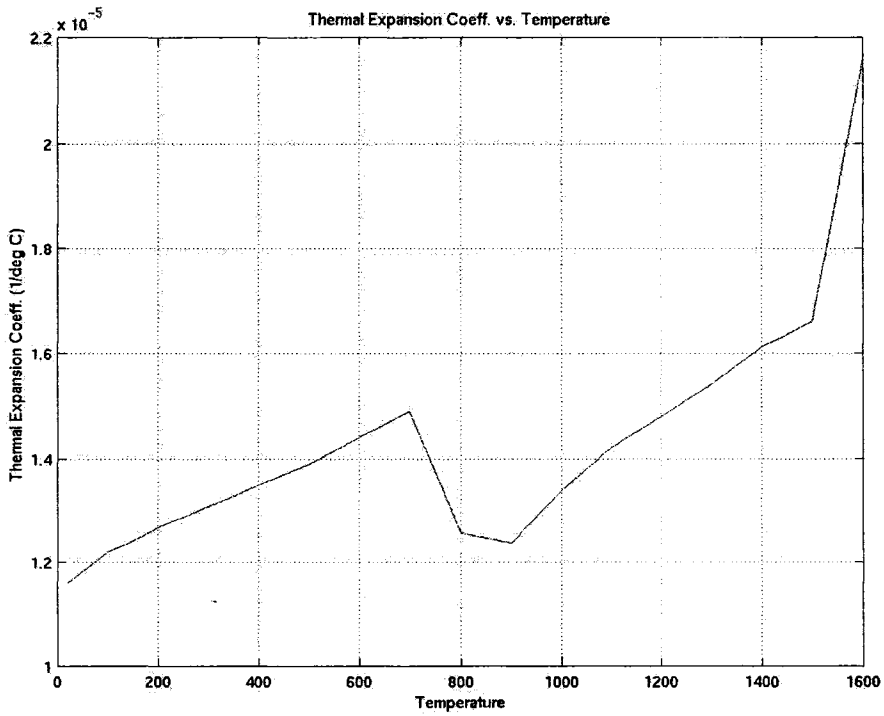

Figure 4. 5: Temperature dependent thermal expansion coefficient

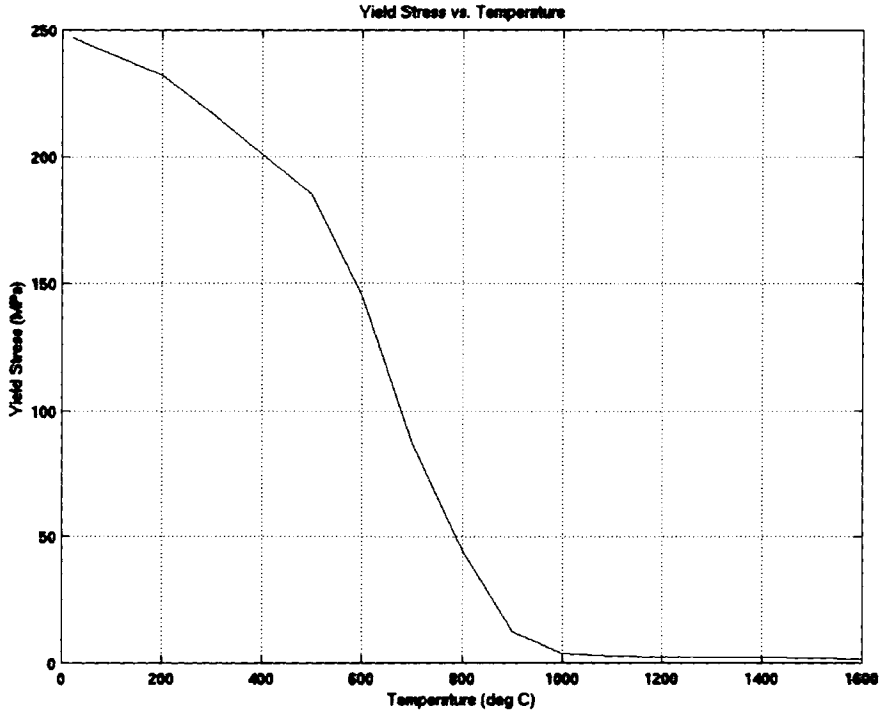

Figure 4. 6: Temperature dependent yield stress

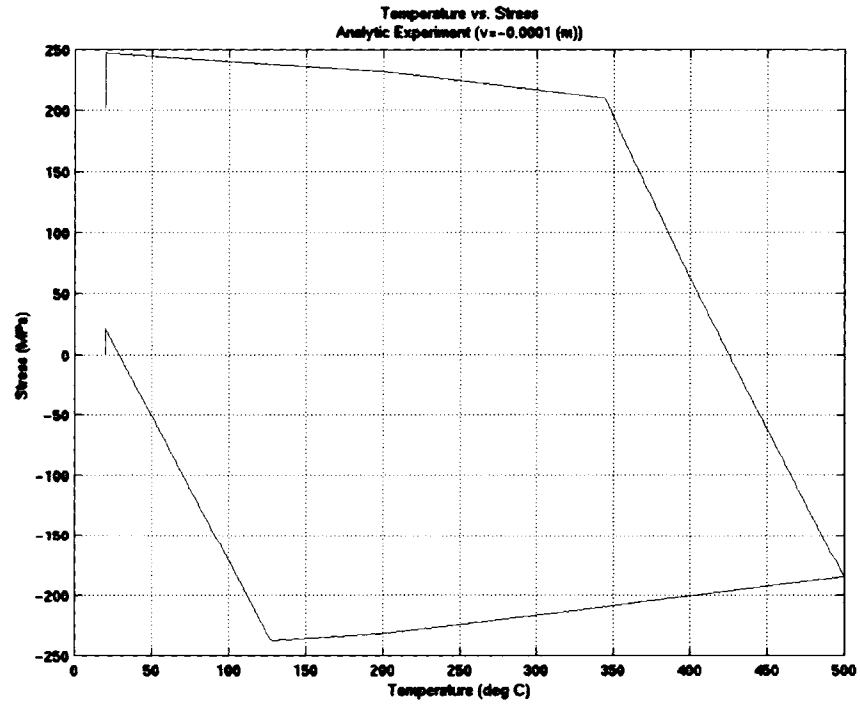

Figure 4. 7: Analytic result for clamped-clamped model with $v = -1.0e^{-4}\ m$

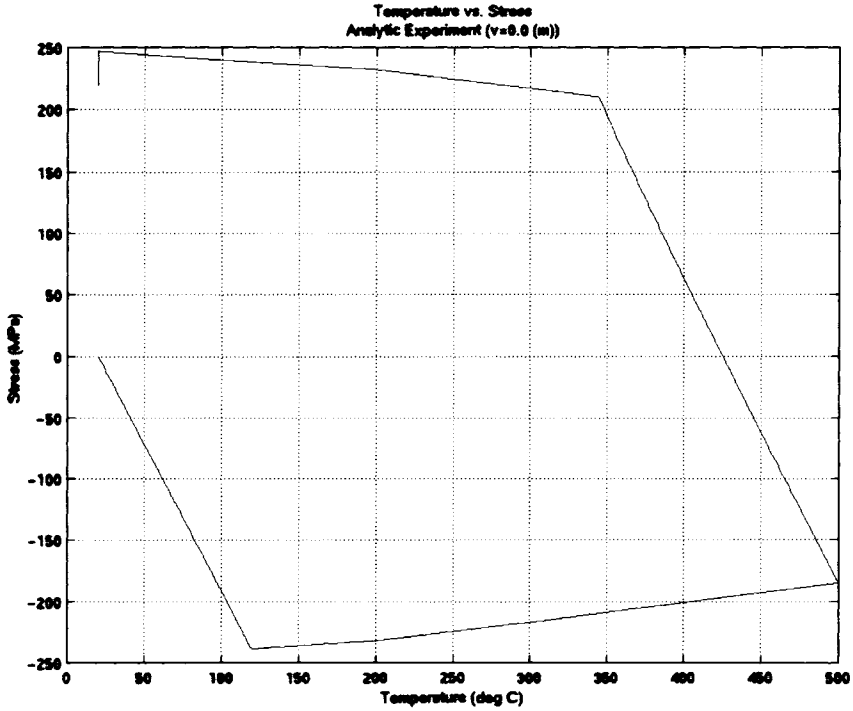

Figure 4. 8: Analytic result for clamped-clamped model with $v = 0.0\ m$

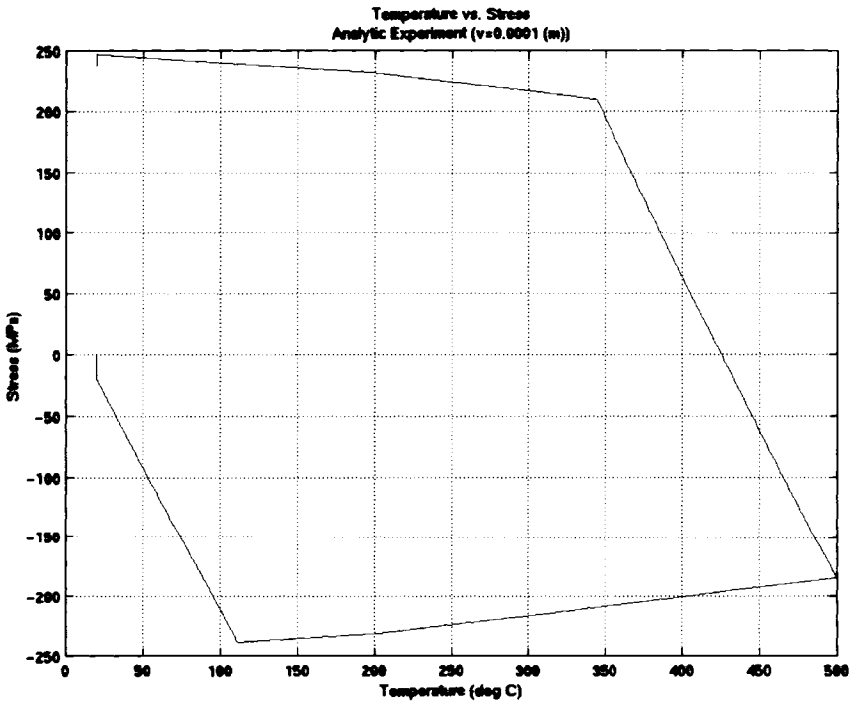

Figure 4. 9: Analytic result for clamped-clamped model with $v = 1.0e^{-4}\ m$

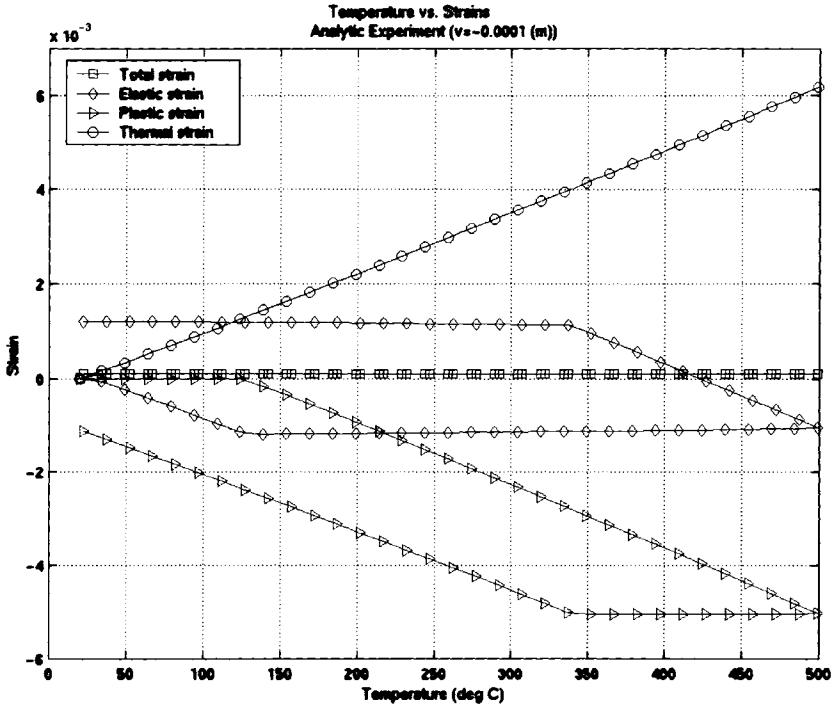

Figure 4. 10: Analytic result for strain-temperature relations with $v = -1.0e^{-4}\ m$

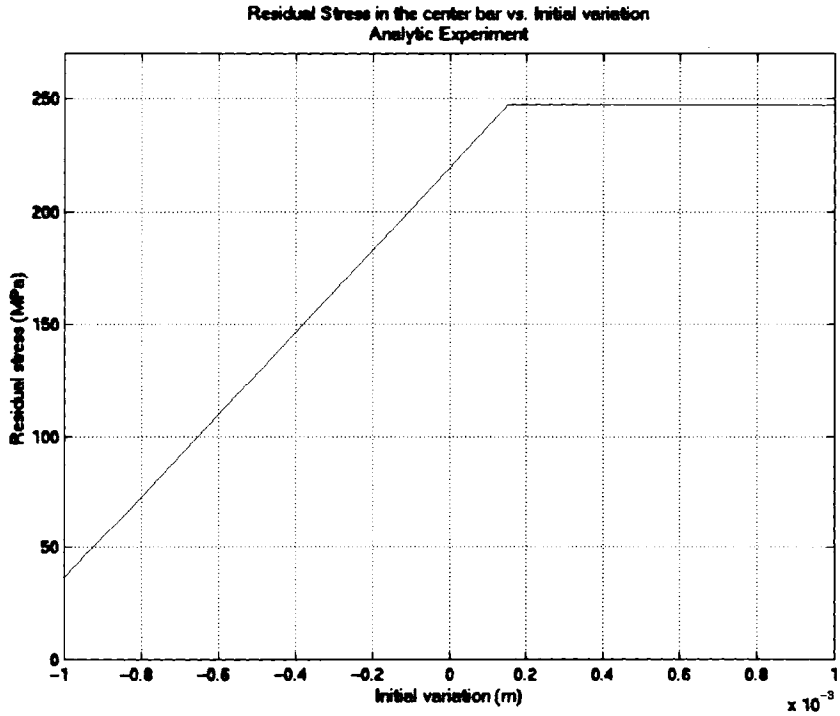

Figure 4. 11: Residual stress in the center bar with various initial variations

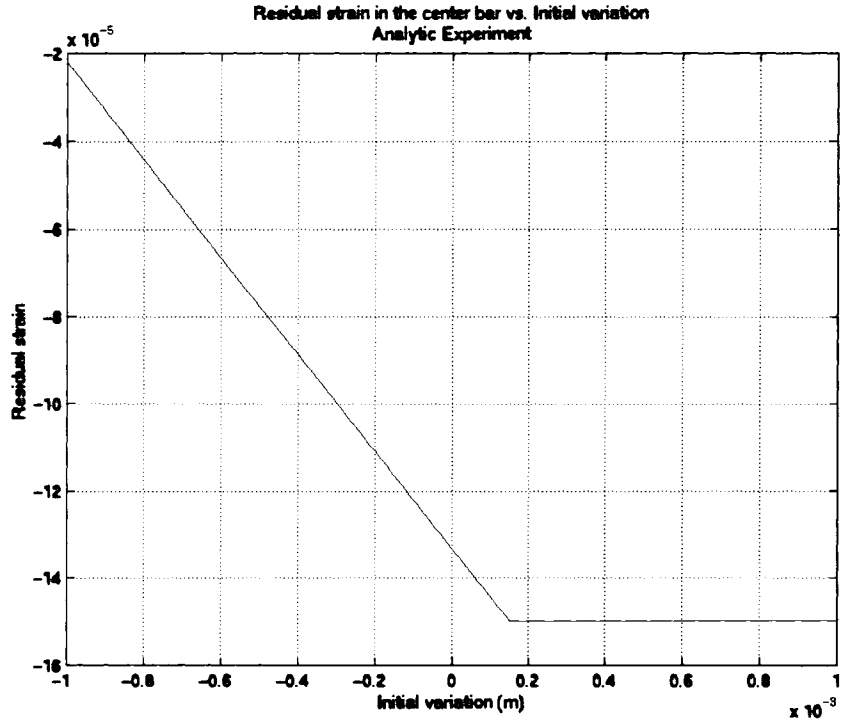

Figure 4. 12: Residual strain in the center bar with various initial variations

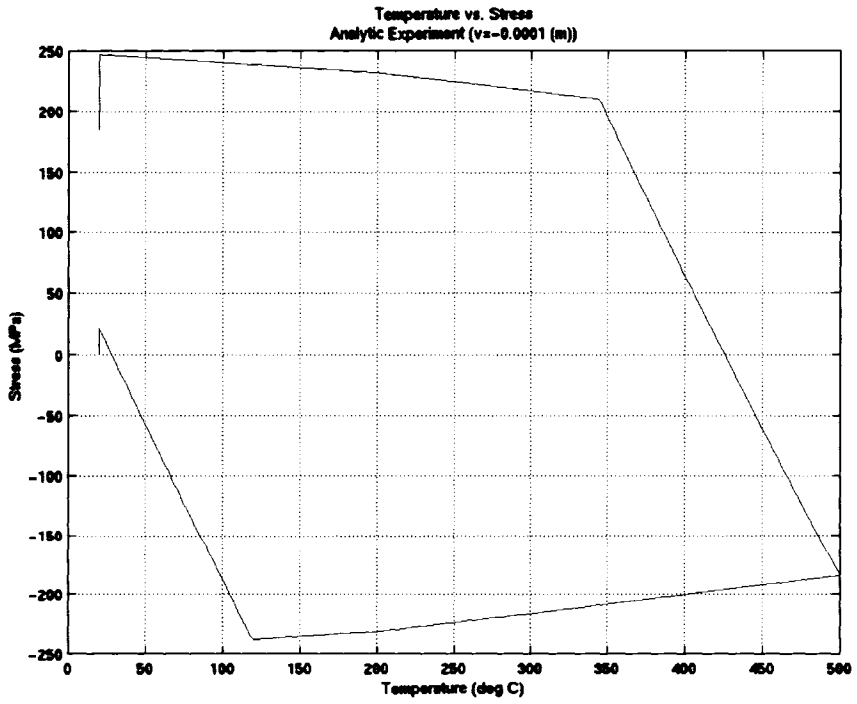

Figure 4. 13: Analytic result for spring-clamped model with $v = -1.0e^{-4}m$ and $K_c = 20\%$ of E

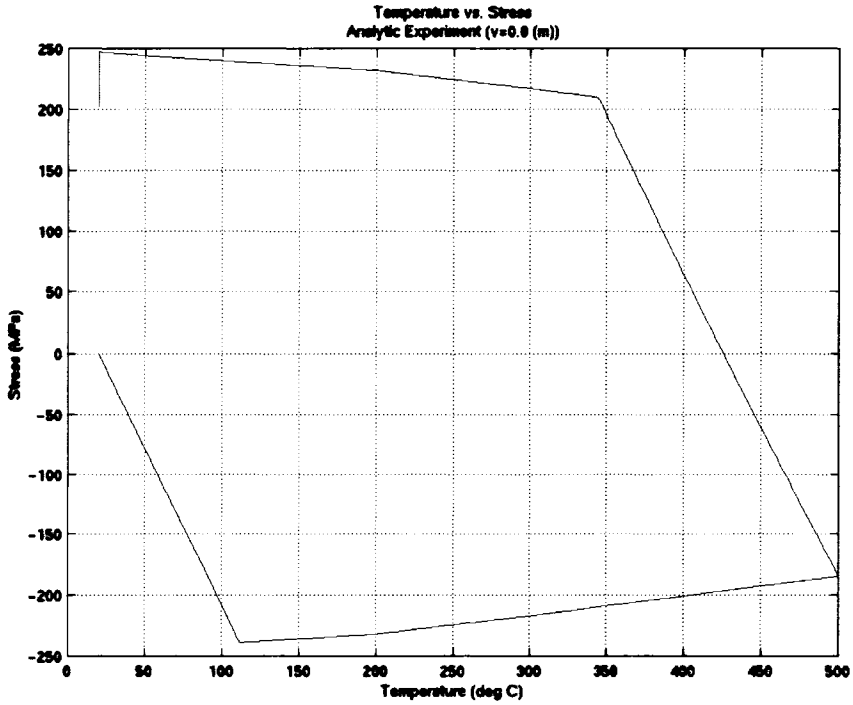

Figure 4. 14: Analytic result for spring-clamped model with $v = 0.0\,m$ and $K_c = 20\%$ of E

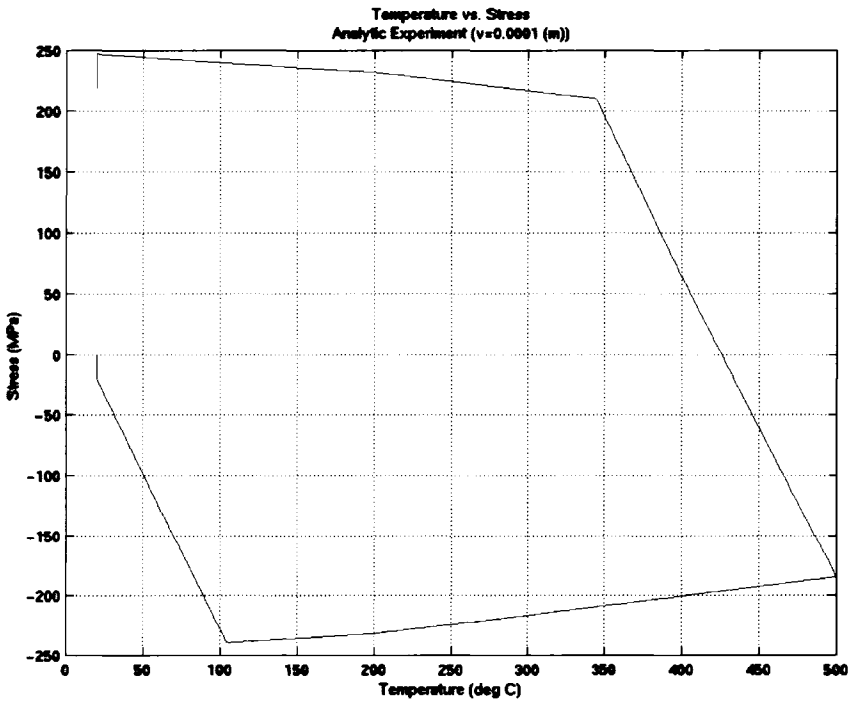

Figure 4. 15: Analytic result for spring-clamped model with $v = 1.0e^{-4}m$ and $K_c = 20\%$ of E

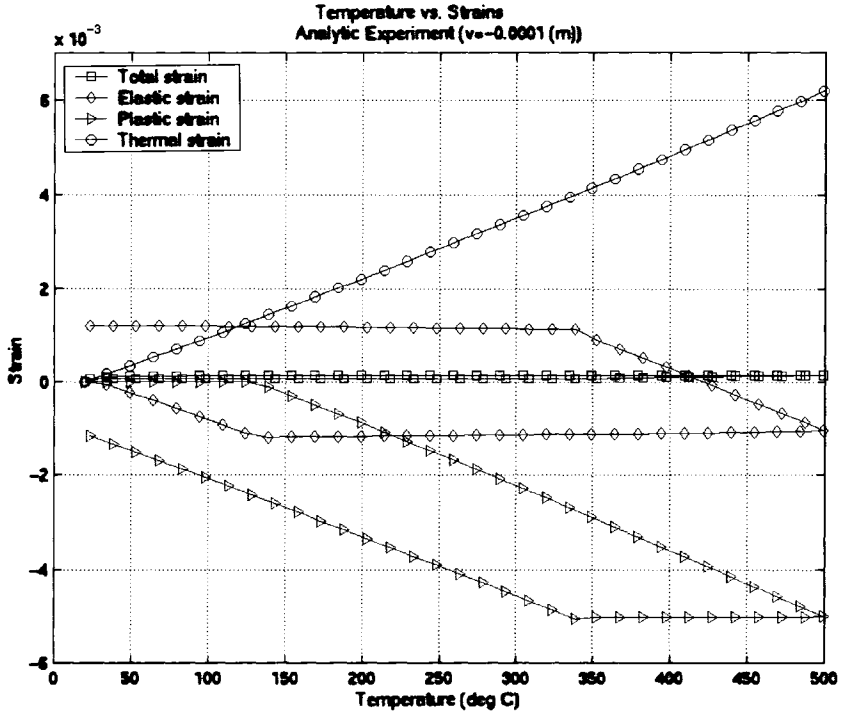

Figure 4. 16: Strains in the center bar with $v = -1.0e^{-4}m$ and $K_c = 20\%$ of E

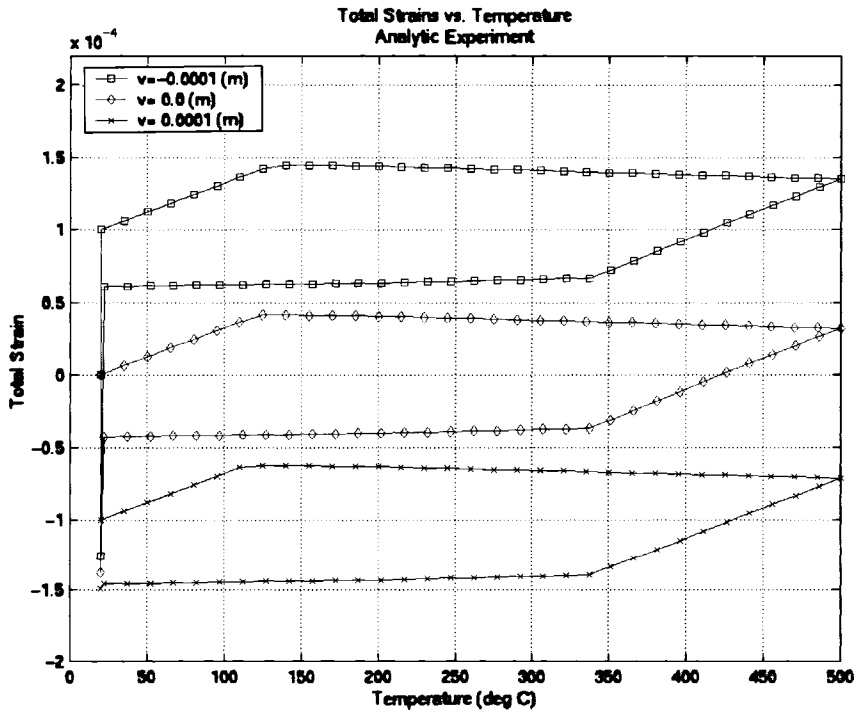

Figure 4. 17: Total strains in the center bar with various initial variations and $K_c = 20\%$ of E

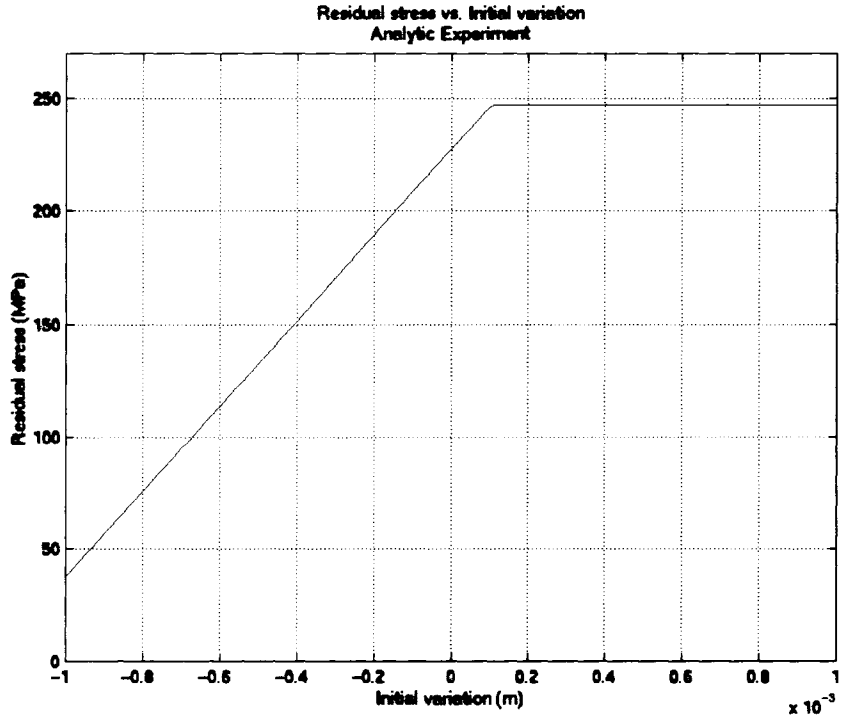

Figure 4. 18: Residual stress in the center bar with various initial variations and $K_c = 20\%$ of E

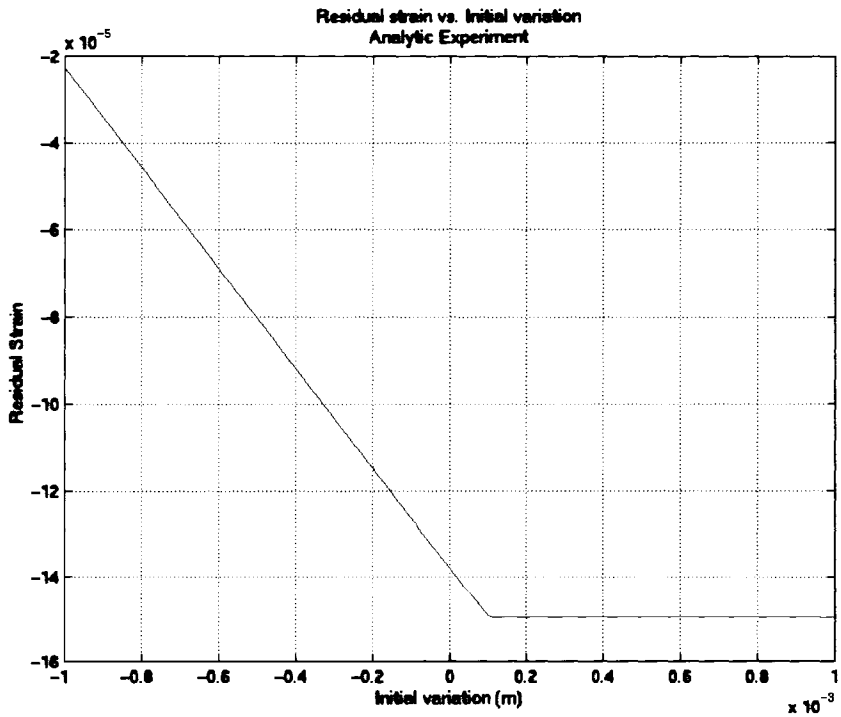

Figure 4. 19: Residual strain in the center bar with various initial variations and $K_c = 20\%$ of E

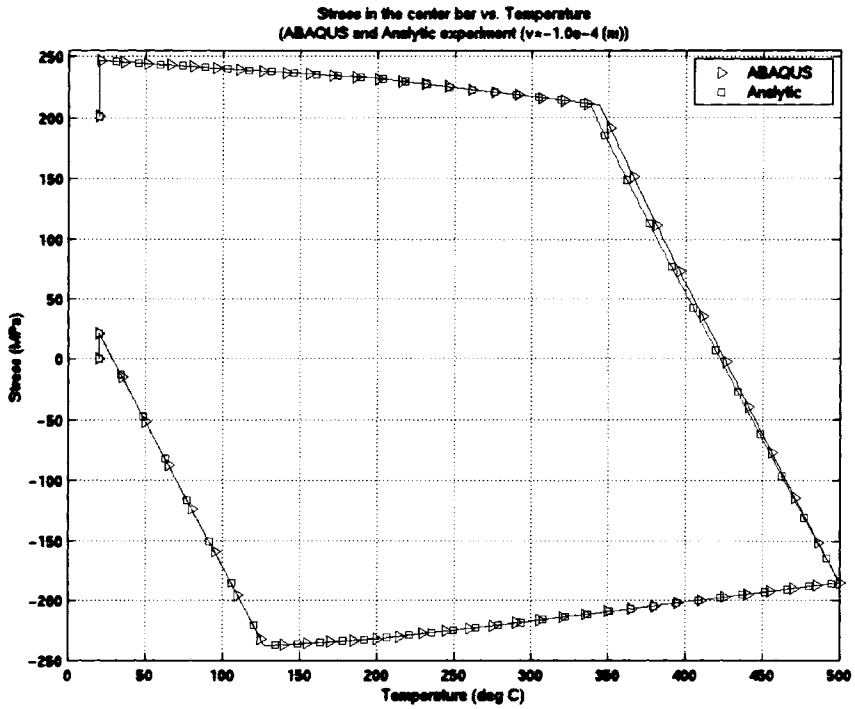

Figure 4. 20: Stress-temperature result comparison for clamped-clamped model

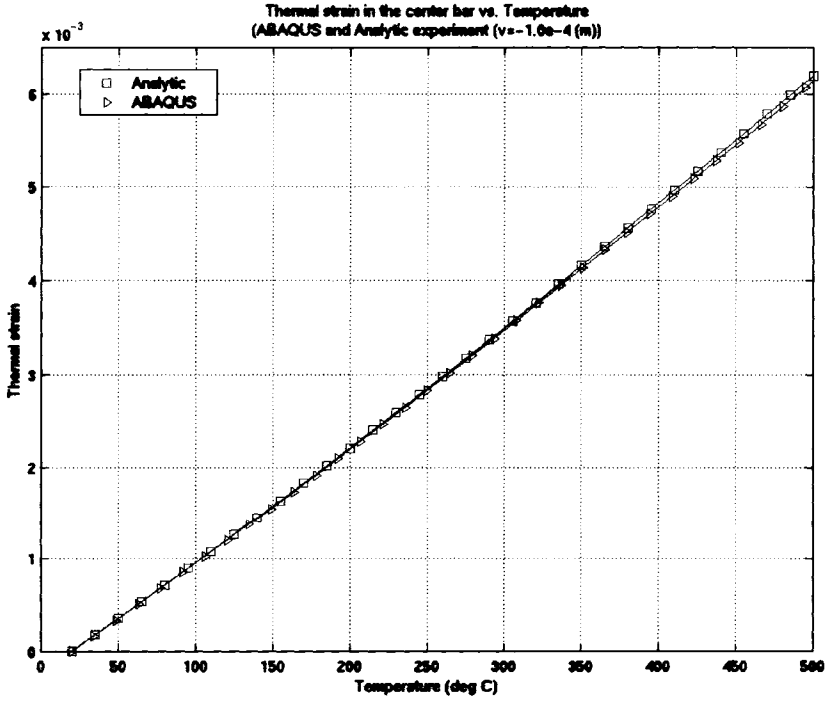

Figure 4. 21: Thermal strain comparison for clamped-clamped model

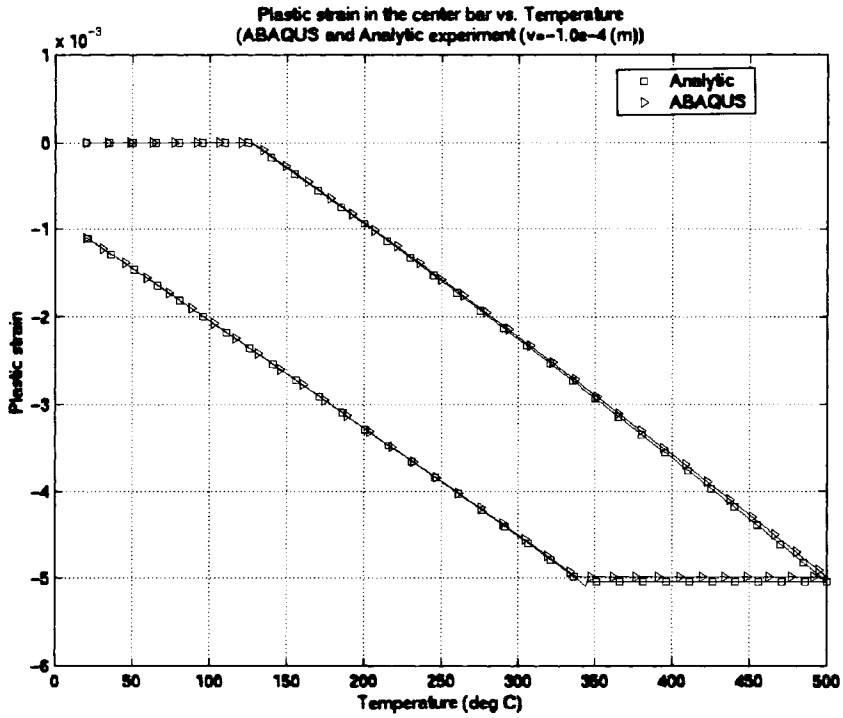

Figure 4. 22: Plastic strain comparison for clamped-clamped model

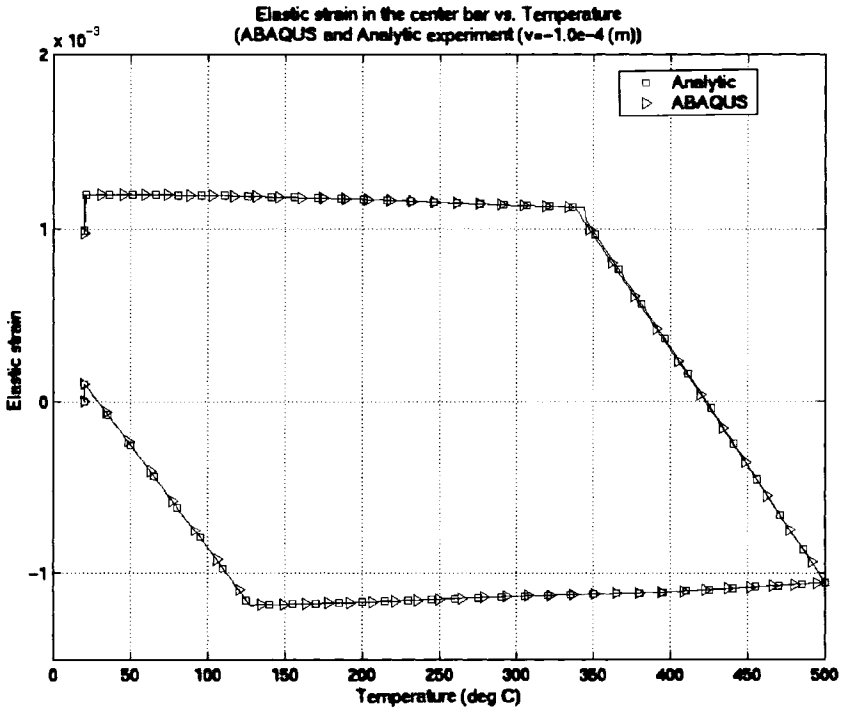

Figure 4. 23: Elastic strain comparison for clamped-clamped model

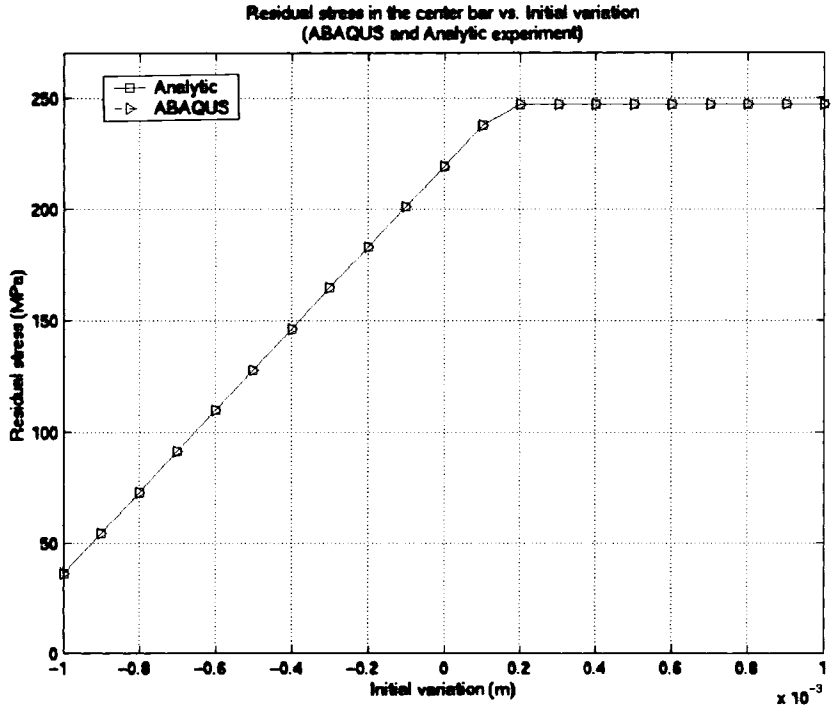

Figure 4. 24: Residual stress with various initial variations comparison for clamped-clamped model

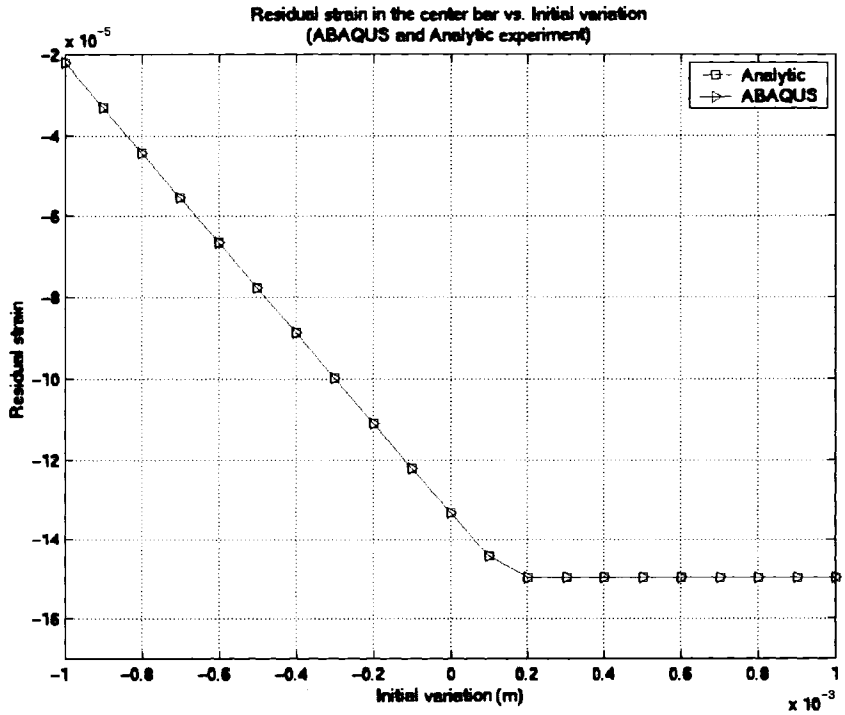

Figure 4. 25: Residual strain with various initial variations comparison for clamped-clamped model

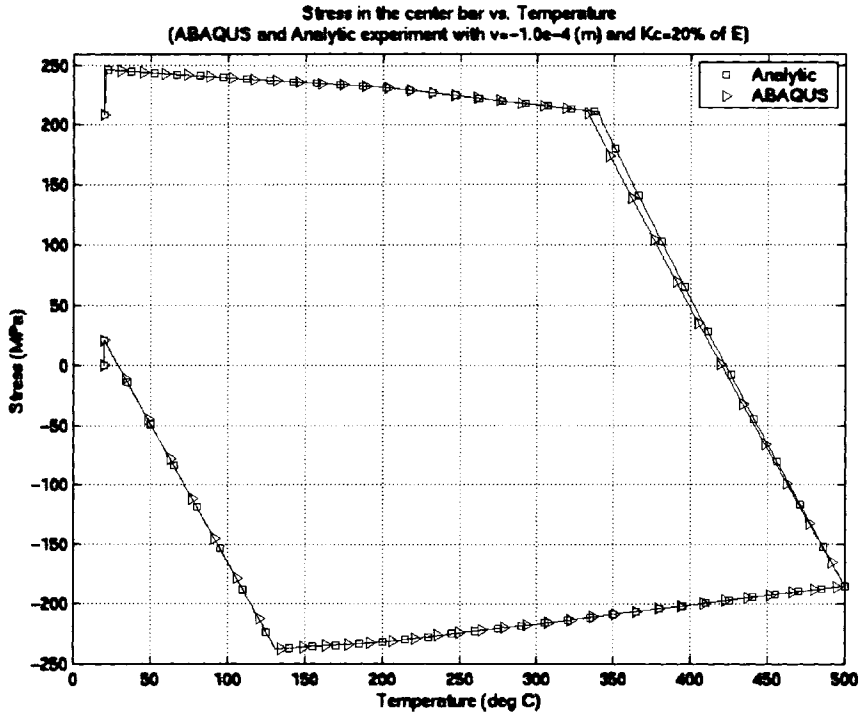

Figure 4. 26: Stress-temperature result comparison for spring-clamped model

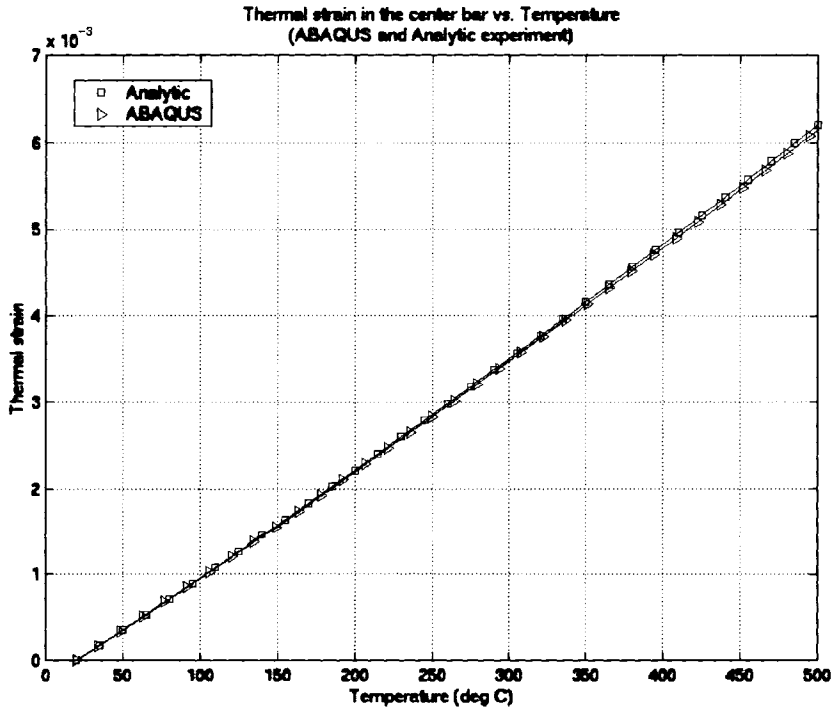

Figure 4. 27: Thermal strain comparison for spring-clamped model

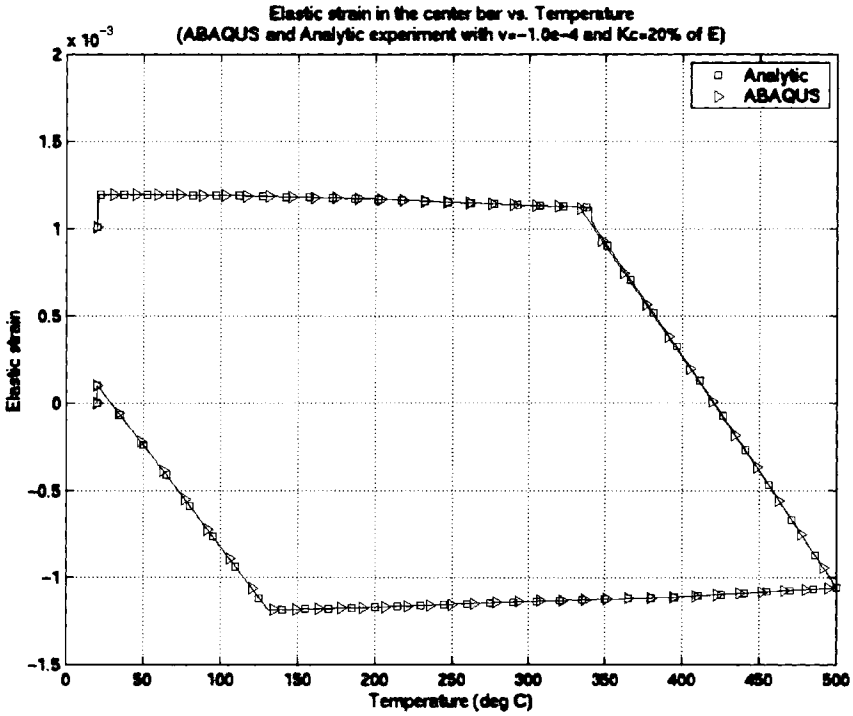

Figure 4. 28: Elastic strain comparison for spring-clamped model

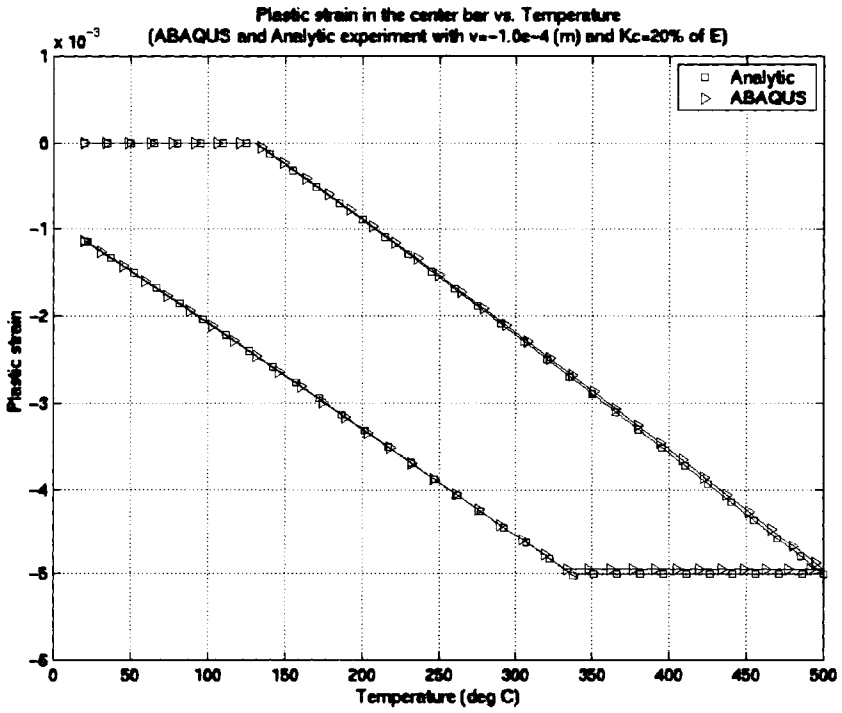

Figure 4. 29: Plastic strain comparison for spring-clamped model

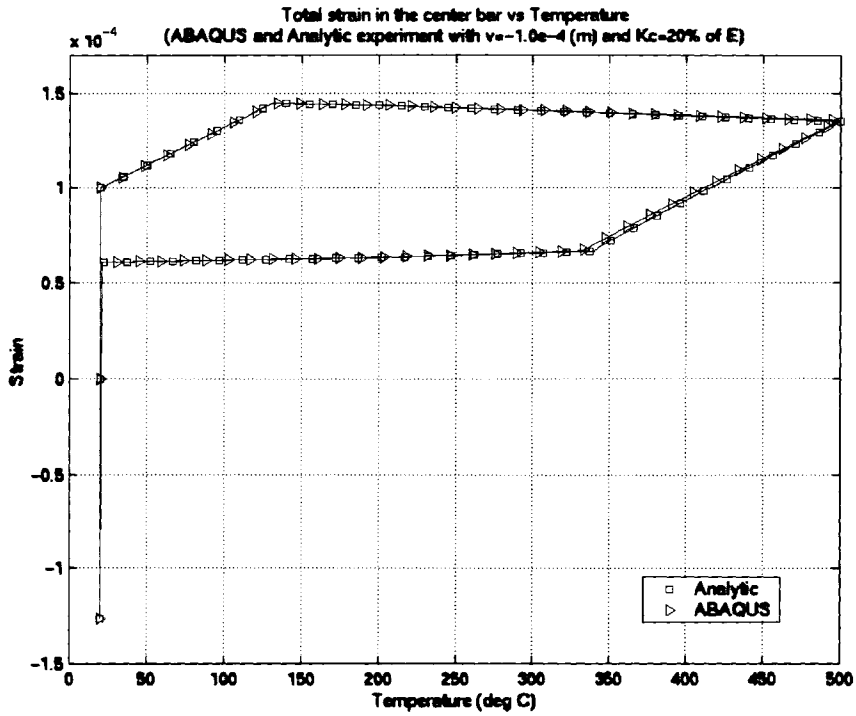

Figure 4. 30: Total strain comparison for spring-clamped model

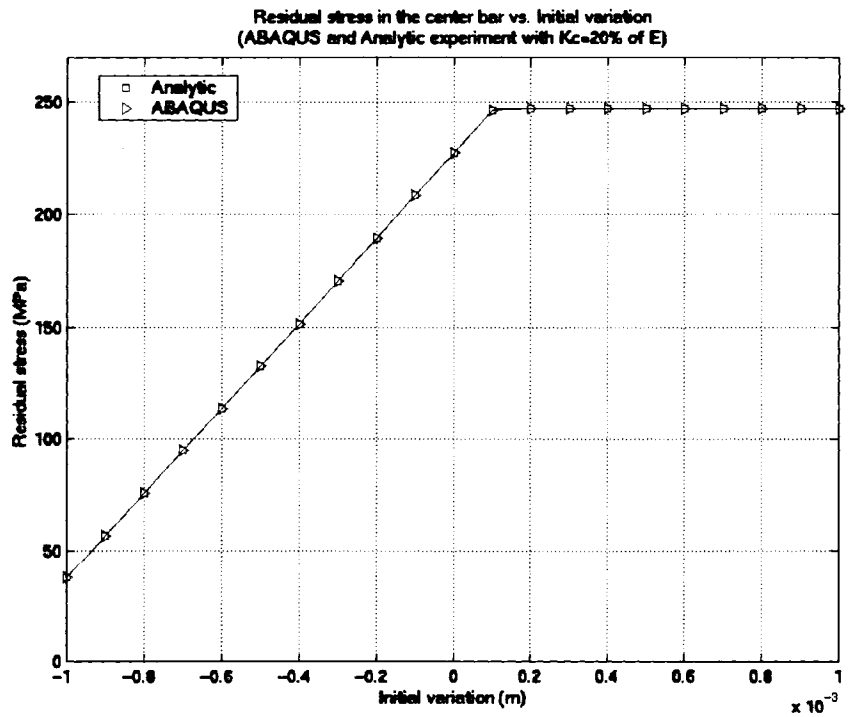

Figure 4. 31: Residual stress in the center bar with various initial variations comparison for spring-clamped model

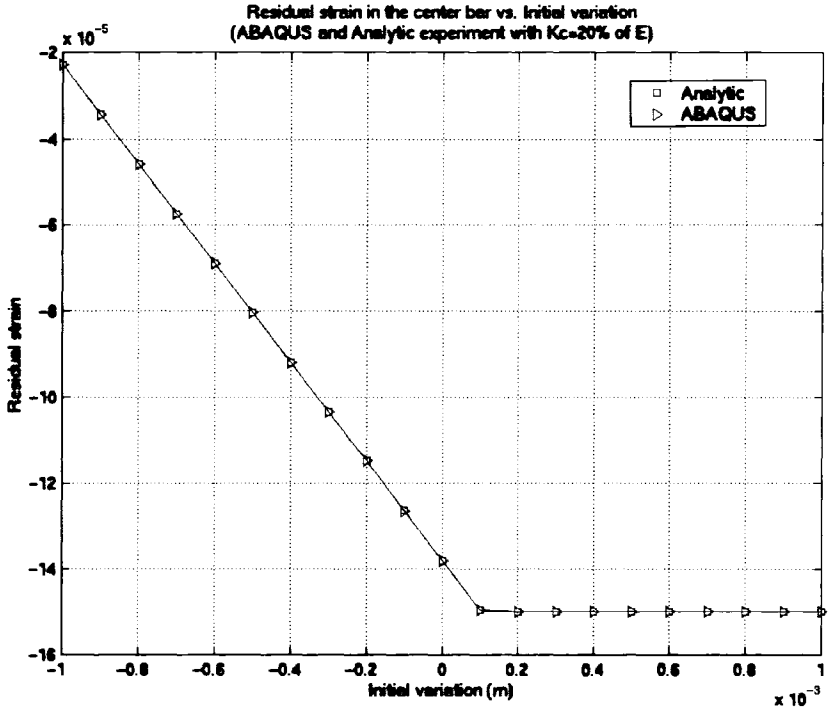

Figure 4. 32: Residual strain in the center bar with various initial variations comparison for spring-clamped model

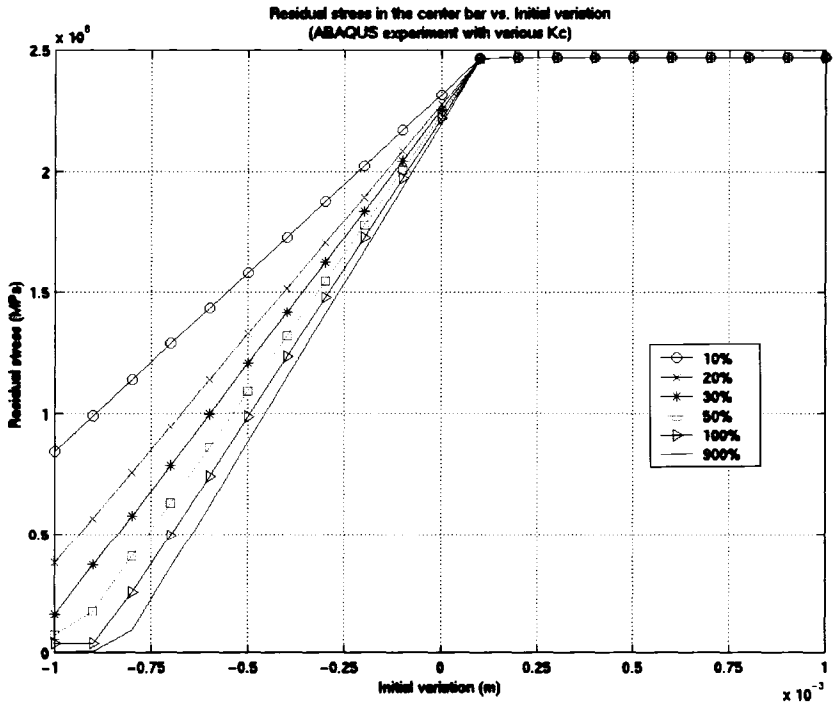

Figure 4. 33: Residual stress in the center bar with various K_c

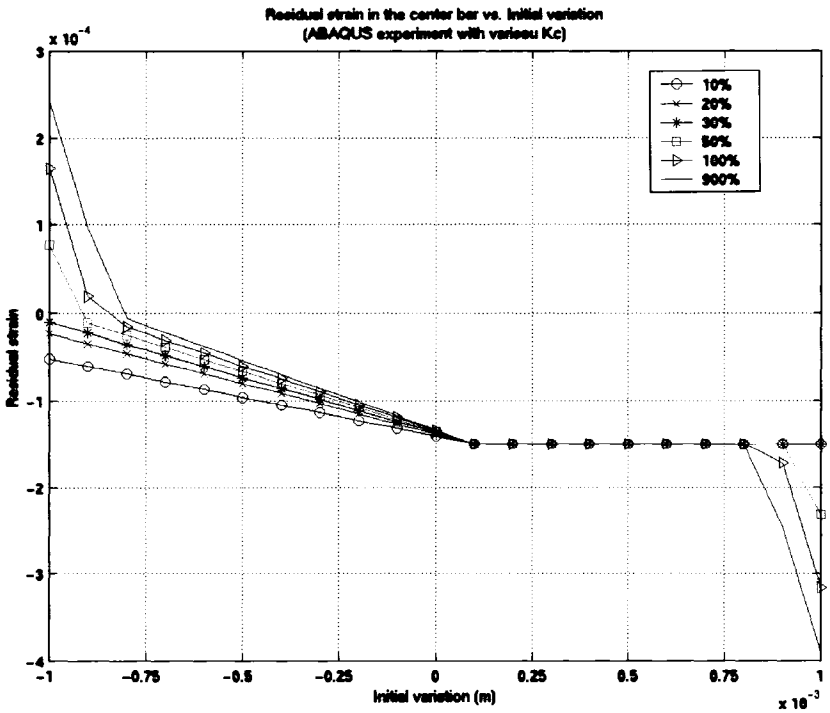

Figure 4. 34: Residual strain in the center bar with various K_c

CHAPTER V

VARIATION SIMULATION CONSIDERING WELDING DISTORTION

The main goal of the current dissertation is to investigate the Modified Method of Influence Coefficients that accounts for dimensional variations of a welded assembly. The numerical simulation for variational analysis is performed in this chapter. As an example, one-pass GMAW (Gas Metal Arc Welding) butt welding of 20 mm thick plates and 10 mm and 15 mm fillet welding of stiffeners and web frame were chosen. The structure used for the example is shown in Figure 5.1.

For the verification of the proposed method of variation simulation considering welding distortion, the butt welding for 20 mm thick plate example is considered.

5.1 Welding Distortion Simulation using Equivalent Loading Method

In this section, an example welding distortion analysis is performed using the equivalent loading method based on the inherent strain method. Butt welding of two identical rectangular plates with 20 mm thickness is analyzed, shown in Figure 5.2. Fillet welding cases are also analyzed. For the purpose of the distortion result comparison, the same welding distortion analysis is performed using the commercial FEM software ABAQUS. The detailed description of the welding process being analyzed can be found in three-dimensional FEM analysis section 5.2. The material of the plate is assumed to be mild steel and its temperature dependent material properties are summarized in Table 5.1.

T	E	σ_Y	ν	ρ	α	C	k	h_c
293	206.0	247.0	0.29	7830	1.16	435.83	52.7	0.50
373	201.0	240.0	0.31	7780	1.22	463.78	51.9	1.30
473	198.0	232.0	0.33	7740	1.27	491.74	51.1	1.50
573	191.0	217.0	0.35	7720	1.31	518.42	48.6	1.60
673	181.0	201.0	0.37	7710	1.35	557.81	44.4	1.70
773	175.0	185.0	0.39	7680	1.39	601.02	42.7	1.79
873	163.0	145.0	0.41	7650	1.44	667.09	39.4	1.86
973	121.0	87.7	0.43	7640	1.49	749.68	35.6	1.92
1073	80.3	44.5	0.44	7620	1.26	1108.0	31.8	1.98
1173	39.2	12.3	0.45	7600	1.24	817.03	26.0	2.04
1273	19.6	3.92	0.48	7580	1.34	626.43	26.4	2.09
1373	17.0	2.82	0.48	7550	1.42	622.62	27.2	2.14
1473	15.0	2.49	0.48	7540	1.48	622.62	28.5	2.18
1573	13.7	2.27	0.48	7500	1.54	637.86	29.7	2.22
1673	13.4	2.22	0.48	7200	1.61	645.49	30.5	2.26
1755	13.2	2.18	0.48	7200	1.66	645.49	105	2.29
2500	11.1	1.84	0.48	7200	2.16	645.49	105	2.32

T : Temperature $[K]$, E : Young's modulus $[GPa]$,

σ_Y : Yield stress $[MPa]$, ν : Poisson ratio

ρ : Density $[kg/m^3]$

α : Thermal expansion coefficient $[K^{-1}]$ $(\times 10^{-5})$

C : Specific heat $[J/kg \cdot K]$

k : Thermal conductivity coefficient $[Watt/m \cdot K]$

h_c : Heat convective coefficient $[Watt/m^2 \cdot K]$

Table 5. 1: Temperature dependent material properties of mild steel [Lee 1995]

5.1.1 Inherent Strain Chart

Based on the three-bar model in the previous chapters, the applicable inherent strain chart has been calculated and plotted in Figure 3.41. As mentioned before, the final plastic strain after the heating-and-cooling cycle is defined as the inherent strain. The chart presents this inherent strain for every β, from 0.02 to 0.98 as function of the highest temperature, from 200 to 2200 $^{\circ}C$. The FEM result for the inherent strain chart with the same range for β and same the highest temperature is shown in Figure 3.43. The inherent strain chart for the filler material that only experiences cooling cycle is also calculated and plotted and then compared with FEM results in Figure 3.42 and 3.44, respectively.

5.1.2 Determination of the Highest Temperatures

A two-dimensional heat transfer analysis was performed to determine the highest temperature distribution in the plate. The welding conditions and parameters for this analysis can be found in Table 5.2. For the case of complex structure welding, three-dimensional heat transfer analysis may be required since the heat dissipation through the adjacent stiffeners and web structures are not negligible. However in this case where two flat plates are welded together, a long welding line is assumed, which means that the temperature distribution can be regarded as the same longitudinally along the weld line. This assumption is quite valid throughout the welded plate except in small areas around the both ends of weld line. Figure 5.3 shows the highest temperature distribution in the half plate. The right upper area is where the filler material is applied. Figure 5.4 shows an enlarged view of highest temperature distribution near the weld line. The temperatures in the figures are given in Kelvin (K).

Based on the conclusion of the three-bar model result and the inherent strain chart, the 'inherent strain region' was determined by this temperature distribution. If the highest temperature is less than about $400\,°C$, which is equivalent to $673\,K$, no inherent strain is generated at all. For this example, the region within 30 mm distance from the weld line is taken as the inherent strain region to account for this effect.

Ambient temperature	$20\,°C = 293\,K$
Filler metal temperature	$2300\,K$
Solidus temperature	$1700\,K$
Liquidus temperature	$1755\,K$
Latent heat of fusion	$273790\,J/kg$
Density of base an filler metal	$7870\,kg/m^3$
Arc efficiency	40 %
Welding voltage	$28\,V$
Welding current	$220\,A$
Torch speed	$2\,mm/s$
Arc beam radius	$8\,mm$

Table 5. 2: Welding parameters for F.E. modeling of butt joint GMAW

5.1.3 Determination of Degree of Restraints

The best way to determine the degree of restraints would be the comparison with real plate welding experimental results. In this research, three-dimensional welding simulation results are taken as the standard of the comparison. The three-dimensional

FEM welding simulation results are explained in section 5.2. In order to determine the degree of restraints, the welding distortion simulations were performed several times for the butt and the fillet welding. And the degree of restraints for the basic welding configurations are calculated by the linear regression technique, Compared to the FEM results, the degree of restraints for the butt welding of flat 20mm thick plates are determined as follows:

$\beta_x = 0.310$ (transverse direction)

$\beta_y = 0.755$ (longitudinal direction)

It should be noted that the degree of restraints of a structure changes as the structure goes through the assembly processes. For example, the degree of restraints of a flat plates butt welding is different when several stiffeners are attached on the plates to be welded. To calculate this degree of restraints at a certain assembly stage, the unit load method is employed. The unit load method calculates the total stiffness ($K_w + K_s$) of the structure at a certain stage by applying a unit load along the edge of the heat affected zone and then calculate the total stiffness, $R = K_w + K_s$, based on the displacement.

$$R = K_w + K_s = \frac{P}{\delta} \tag{5.1}$$

$$K_w = (K_w + K_s) - K_s = R - K_s = (1-\beta)R \tag{5.2}$$

Where:

β : the degree of restraints

P : unit load applied at the edge of the inherent strain region

δ : displacement

The degree of restraints of the subsequent assembly stage is then calculated by applying the unit load method one more time to get $R_a = K_{wa} + K_{sa}$, where K_{sa} and K_{wa} are equvalent to K_s and K_w at a certain assembly stage, respectively. Then:

$$K_{wa} = K_w \tag{5.3}$$

$$\begin{aligned} K_{sa} &= (K_{sa} + K_{wa}) - K_{wa} = R_a - K_{wa} \\ &= R_a - K_w \end{aligned} \tag{5.4}$$

$$\beta_a = \frac{K_{sa}}{K_{sa} + K_{wa}} \tag{5.5}$$

Here we can assume that $K_{wa} = K_w$ since K_{wa} represents the stiffness of the heat affected zone, which does not vary due to the external structural configuration changes. Once K_{wa}, K_{sa} and R_a are obtained, the degree of restraints β_a at the stage is determined. The degrees of restraints of the subsequent assembly stages are calculated by re-applying Equations (5.3) through (5.5) repeatedly.

5.1.4 Inherent Strain Distribution and Equivalent Load Calculation

Figure 5.5 shows the transverse inherent strain distribution in the butt welded plate and Figure 5.6 shows the detailed distribution near the weld line. Once the inherent strain distributions are determined, the equivalent loads can be calculated by integrating the inherent strains as shown in Figure 5.7.

The transverse shrinkage force is:

$$f_y = \frac{1}{b_w} \int_{At} E\varepsilon_y^* dA = \frac{1}{b_w} \int_{-h}^{0} \int_{0}^{b_w} E\varepsilon_y^* dy dz \tag{5.6}$$

The transverse bending moment is:

$$m_y = \frac{1}{b_w}\int_{At} E\varepsilon_y^*(\frac{h}{2}+z)dA = \frac{1}{b_w}\int_{-h}^{0}\int_{0}^{b_w} E\varepsilon_y^*(\frac{h}{2}+z)dydz \tag{5.7}$$

The longitudinal shrinkage force is:

$$F_x = \int_{At} E\varepsilon_x^* dA = \int_{-h}^{0}\int_{0}^{b_w} E\varepsilon_x^* dydz \tag{5.8}$$

The longitudinal bending moment is:

$$M_x = \int_{At} E\varepsilon_x^*(\frac{h}{2}+z)dA = \int_{-h}^{0}\int_{0}^{b_w} E\varepsilon_x^*(\frac{h}{2}+z)dydz \tag{5.9}$$

After calculating the forces and moments, these forces and moments are applied as shown in Figure 3.5. The result of the inherent strain method is shown in Figure 5.8 and 5.9 shows the vertical displacement contour of the distortion.

5.2 Welding Distortion Simulation using Three-Dimensional FEM

5.2.1 Method and Procedure

The three-dimensional welding distortion and residual stress analysis was performed using the commercial FEM software, ABAQUS. The model used in this simulation was based on Lee's experimental work [Lee 1995]. Transient three-dimensional thermal analysis of welding was first performed to calculate the temperature distribution in the plates and then this result was applied as the input for subsequent thermo-elasto-plastic analysis. The result is compared with Lee's experimental results.

The welding method assumed in this research is single-pass GMAW (Gas Metal Arc Welding), which is widely used in the shipbuilding process. GMAW analysis consists of thermal modeling, where the highly non-uniform heat flux and temperature distribution are calculated, and mechanical modeling, where the thermo-elasto-plastic analysis is performed for the distortion simulation. Key considerations in these modelings are:

(1) Phase transition (solid/liquid) phenomenon in metal

(2) Temperature dependent material properties

(3) Convection boundary conditions for thermal analysis

(4) Modeling of filler metal by element birth-death technique

(5) Large deformation consideration

(6) Gaussian heat flux torch modeling

5.2.2 Thermal Analysis

For the analysis in this research, the following are assumed:

(1) Material behavior inside the welding pool such as buoyancy force, electro-magnetic force, and surface tension, are assumed to be negligible. Therefore, convective terms of liquidfied metal can be neglected in the thermal field analysis.

(2) During the welding process, the effect of distortion to the thermal field, i.e., shape deformation, plastic strain energy, and convective boundary condition changes, is much less than the heat flux from the torch and therefore can be neglected. Thus the thermal field analysis can be decoupled from the stress-strain field analysis and these analyses will be performed independently.

(3) The influx of filler metal is continuous and uniform.

(4) The vaporization of metal due to temperature increase is neglected.

(5) The heat flow at the clamping device is negligible.

(6) The crystallization effect of metal on thermal and stress-strain field can be neglected.

With these assumptions, the FEM mesh shown in Figure 5. 10 was generated. Since the welding is symmetric along the weld line, only a symmetric half plate was modeled.

5.2.3 Finite Element Mesh

The entire elements are 8-node isoparametirc three-dimensional elements and the model consists of 1656 elements and 2265 nodes. In order to accurately model incoming filler metal during the welding, the element birth-death technique is used. Since right under the torch the liquefied filler metal is pushed out by arc and shield gas, birth elements are modeled to newly generate right behind the torch, as shown in Figure 5.11.

5.2.3.1 Torch Modeling

The heat influx to the base metal consists of heat from the arc and the latent heat of the liquefied filler metal. The heat influx from the arc is modeled as a Gaussian distribution and can be expressed as [Lee 1995]:

$$q = q_0 e^{-3\left(\frac{r}{r_b}\right)^2} \tag{5.10}$$

$$q_0 = \frac{\eta_a VI}{\pi} \frac{3}{r_b^2} \tag{5.11}$$

where:

q : heat flux at (x, y)

$r^2 = (x - a)^2 + y^2$

r_b : arc beam radius

a : position of weld torch in x direction

η_a : arc efficiency

V, I: arc voltage and current

The above heat flux is applied to the relevant faces of elements as a heat flux surface force. For the latent heat influx of the liquefied filler metal, the initial temperature of the incoming filler metal determines the heat energy. In this research, the initial temperature is assumed to be 2300 K . Table 5.2 shows the weld parameters used in this FEM welding simulation.

5.2.3.2 Boundary Conditions Modeling

The boundary conditions for the thermal field analysis are comprised of convection and radiation conditions. In this research, the empirical boundary conditions accounting for convection and radiation at the same time are applied [Patel 1985].

$$q_n = h_{cr}(T - T_a)$$
$$h_{cr} = h_c + \sigma^r \varepsilon^r \cong 24.1 \times 10^{-4} \varepsilon^r T^{1.41} \quad (5.12)$$

where:

q_n : heat flux

h_c : convection heat transfer coefficient

σ^r : Stefan-Boltzman constant for radiation = $5.6703 \times 10^{-8}\ Watt/m^2K^4$

ε^r : hemispherical emissivity = 0.1

5.2.3.3 Material Properties Modeling

The most important material properties in thermal analysis are the heat capacity and thermal conductivity. Temperature dependent material properties for mild steel are shown in Table 5.1 and Figure 5.12.

5.2.3.4 Results and Discussions

Full transient heat transfer analysis was performed using ABAQUS. The analysis took 28130 seconds, i.e., 7 hours 48 minutes 50 seconds on a SUN BLADE-1500 system. The torch speed was set to 2 mm/sec. and the weld starts at time = 0. The torch begins to move at time = 2 second. Therefore, the total welding time is 42 seconds since the weld length is 80 mm. Total analysis time including cooling time is set to 4000 seconds. While the torch is moving, from 2 seconds to 42 seconds, the time step is set to $5/3$ second so that the torch is set to move one element length along z-axis. For the cooling process after 42 seconds, the time step is set to linearly increase until it reaches 500 seconds. The initial temperature of the filler metal is set to 2300 K and the filler metal is modeled using the element birth technique. Figure 5.13 shows the temperature contour around the weld line with continuously added filler metal. Figures 5.14 through 5.18 show the temperature history results at various points and their comparison with experimental data.

5.2.4 Thermo-Elasto-Plastic Analysis

The finite element mesh used in the thermal analysis is used again unchanged. The assumptions for this analysis are:

(1) Thermal field analysis is de-coupled from stress-strain field analysis.

(2) Since the time when the material experiences high temperature over melting point is very short relative to the whole mechanical behavior, viscosity effects can be neglected.

(3) Martensite effects can be neglected since the plate is not quenched but cooled by natural convection.

5.2.4.1 External Forces and Boundary Conditions

The external forces for the thermo-elasto-plastic analysis are the nodal temperatures, which are the result of thermal analysis. Symmetric boundary conditions are applied along the weld line and are transversally constrained at the opposite edge to the weld line.

5.2.4.2 Yield and Hardening Condition

Von Mises yielding condition and isotropic hardening are assumed for this analysis.

5.2.4.3 Results and Discussions

Full transient thermo-elasto-plastic analysis was performed using ABAQUS based on the result of the previous thermal analysis. The analysis took 64984 seconds, i.e., 18 hours 3 minutes 4 seconds on a SUN BLADE-1500 system. Total analysis time is the same as that of the thermal analysis, i.e., 4000 seconds. The initial stress and strain of the incoming filler metal is set to zero and the filler metal is modeled using the element birth technique once again. Figures 5.19 through 5.25 show the various residual stress distributions compared with experimental data and the final deformed shape.

5.3 Variational Simulation using the Modified Method of Influence Coefficients

In this section, the mechanistic variation simulation including welding distortion is analyzed for two metal plates joined by GMAW. For validation, the results of the simulation are compared with that of direct Monte Carlo simulation. The plate example used was an assembly of two plates joined by butt-joint GMAW, as shown in Figure 5.26 (a). The plate dimension is $250\,mm \times 500\,mm$ and the plate thickness is $20\,mm$. In the example, there are four sources of variation at the free corners of the two flat plate parts as marked by numbers in Figure 5.26. The numbers 1 and 3 represent the source of variation on the left plate and numbers 2 and 4 represent the variation on the right plate. The variations in the plates are assumed to be Z-direction only. The mean deviation (mm) at each source of variation assumed in this simulations are:

$$\{\mu_p\} = [10 \;\; 10 \;\; -5 \;\; -5]^T \tag{5.13}$$

and the standard deviation (mm) at each source of variation is also assumed as:

$$\{\sigma_p\} = [1 \;\; 1 \;\; 1 \;\; 1]^T \tag{5.14}$$

For simplicity, the sources of variation are assumed to be statistically independent.

5.3.1 Modified Method of Influence Coefficients

The Modified Method of Influence Coefficient (Chapter 3) is used to simulate the springback of the welded structure with initial deviation. The welding distortion terms are calculated by the equivalent loading method based on the inherent strain method and the

sensitivity matrix is derived by the Method of Influence Coefficient. The intermediate results, i.e., the matrix of influence coefficients, the stiffness matrix and the sensitivity matrix are given in the following.

5.3.1.1 Matrix of Influence Coefficients

Since there are four sources of variation, matrix $[C]$ will be a 4×4 matrix derived from Equation (4.4):

$$[C]=\begin{bmatrix} 1.54\times10^{-4} & 0 & 1.14\times10^{-5} & 0 \\ 0 & 1.57\times10^{-4} & 0 & 1.14\times10^{-5} \\ 1.14\times10^{-5} & 0 & 1.57\times10^{-4} & 0 \\ 0 & 1.14\times10^{-5} & 0 & 1.54\times10^{-4} \end{bmatrix} \tag{5.15}$$

The interpretation of the first column can be stated as: unit force at the first source of variation will result in the displacements of 0.154, 0, 0.0114, and 0 *mm* at the four sources of variation, respectively. The other columns of the matrix can be interpreted similarly.

5.3.1.2 The Stiffness Matrix

The stiffness matrix $[K]$ is the inverse of $[C]$:

$$[K]=\begin{bmatrix} 6528.6 & 0 & -474.1 & 0 \\ 0 & 6403.8 & 0 & -474.1 \\ -474.1 & 0 & 6403.8 & 0 \\ 0 & -474.1 & 0 & 6528.6 \end{bmatrix} \tag{5.16}$$

The interpretation of the first column can be stated as: unit displacement at the first source of variation will need forces in the magnitude of 6528.6, 0 –474.1, and 0 *N* from the clamp, respectively.

5.3.1.3 The Sensitivity Matrix

The sensitivity matrix calculated from Equation (4.7) is shown in Table 5.3. The interpretation of the first column can be stated as: unit deviation at the first source of variation will affect the displacements in each node in the assembled model in the magnitude of the numbers in the corresponding rows.

Node(i)	S_{i1}	S_{i2}	S_{i3}	S_{i4}
1	.0000	.0000	.0000	.0000
2	.1240	.1145	-.0119	-.0112
3	.2500	.2397	-.0237	-.0233
4	.2480	.2401	-.0237	-.0234
5	.2440	.2390	-.0235	-.0234
6	.1140	.1190	-.0124	-.0130
7	.0000	.0000	.0000	.0000
8	.0000	.0000	.0000	.0000
9	.0506	.0478	-.0022	-.0019
10	.0983	.0955	-.0048	-.0044
11	.0985	.0959	-.0049	-.0045
12	.0982	.0958	-.0049	-.0046
13	.0509	.0518	-.0037	-.0038
14	.0000	.0000	.0000	.0000
15	.0000	.0000	.0000	.0000
16	.0113	.0109	.0137	.0138
17	.0254	.0244	.0246	.0255
18	.0255	.0246	.0246	.0255
19	.0255	.0246	.0244	.0254
20	.0138	.0137	.0109	.0113
21	.0000	.0000	.0000	.0000
22	.0000	.0000	.0000	.0000
23	-.0038	-.0037	.0518	.0509
24	-.0046	-.0049	.0958	.0982
25	-.0045	-.0048	.0959	.0986
26	-.0044	-.0047	.0955	.0983
27	-.0019	-.0022	.0478	.0506
28	.0000	.0000	.0000	.0000
29	.0000	.0000	.0000	.0000
30	-.0130	-.0124	.1190	.1141
31	-.0233	-.0234	.2391	.2444
32	-.0233	-.0236	.2401	.2477
33	-.0232	-.0237	.2397	.2496
34	-.0112	-.0118	.1145	.1244
35	.0000	.0000	.0000	.0000

Table 5. 3: Sensitivity matrix for mechanistic variation simulation

5.3.1.4 Results and Discussion

From the sensitivity matrix, the contours of the mean and variance of the assembly variation can be calculated based on Equations (4.8) and (4.9). Since we assumed that the welding distortion can be linearly superposed onto the mechanistic variation simulation, the results are obtained by superposing the welding distortion with the variational simulation results, which are shown in Figure 5.27, Figure 5.28, Figure 5.29, and Figure 5.30. The results of direct Monte Carlo simulation are shown in Figure 5.31 and Figure 5.32. The patterns of mean deviation and standard deviation are almost same but the values are little different.

Method	Direct Monte Carlo	Modified Method of Influence Coefficient
Average maximum distortion	0.003398	0.003746
Standard deviation of distortion (m)	0.0007	0.0004
No. of FEM runs	1000	3
Real CPU time (sec)	12082	25

Table 5. 4: Comparison of the two methods

Since the equivalent loading method is not suitable for exact prediction of welding distortion of the edge area, another butt-weld with initial variation in the middle of the weld line case was examined, as shown in Figure 5.26 (b). In this case, the left plate has same initial variation as the previous case but the right plate has only one source of variation in the middle of the weld line. Figure 5.33 and 5.34 shows the results of Modified Method of Influence Coefficients and Figure 5.35 and Figure 5.36 show the

results of direct Monte Carlo Simulation. As the figures show, the differences resulting from the direct Monte Carlo simulation and the Modified Method of Influence Coefficients are small. However, there is a tremendous difference in the computational time between these two methods. Table 5.4 shows the comparison of the results from the direct Monte Carlo simulation and the Modified Method of Influence Coefficients.

5.3.2 Assembly Example

In order to validate that the Modified Method of Influence Coefficient can be easily applied to more complex structure case, an assembly example is analyzed in this section. The construction steps of the assembly are:

(1) Two identical base plates ($1.6\,m \times 3\,m \times 20\,mm$) are first joined together by butt-welding (Figure 5.37)

(2) The welded base plates are clamped for stiffener attachment (Figure 5.38)

(3) Stiffeners ($3\,m \times 300\,mm \times 10\,mm$) are attached and then fillet welded (Figure 5.39)

(4) The subassembly is clamped for web frame ($3.2\,m \times 700\,mm \times 15\,mm$) attachment and then the web frame is fillet welded (Figure 5.40)

(5) All the clamps are released to show the final shape (Figure 5.41)

For the welding distortion simulation, the equivalent loading method based on the inherent strain method is utilized. The welding distortion simulation result for the base plate is shown in Figure 5.42. The mechanistic variation simulation is also performed. The results are shown in Figure 5.43 and Figure 5.44. Table 5.5 shows the comparison of the two methods in terms of the average maximum out-of-plane deviations in the base plates of the assembly. The average maximum deviations are located at the centers of the ten contour packets in Figure 5.42 and Figure 5.43. Since the assembly is symmetric, the

average maximum deviations of the upper five packets are compared. The first row of the Table 5.5 represents the locations of the average maximum deviations, given in m. As shown in Table 5.5 the deviation values are very similar quantitatively. The contour patterns are also comparable qualitatively, as shown in Figure 5.42 and Figure 5.43.

	Left edge	Mid. left	Middle	Mid. right	Right edge
ANSYS	0.0022	0.0013665	0.0014263	0.00135	0.0019
Modified Method of Influence Coefficients	0.0028	0.001312	0.0014762	0.001312	0.0028

Table 5. 5: Comparison of the two methods in terms of the average maximum deviations

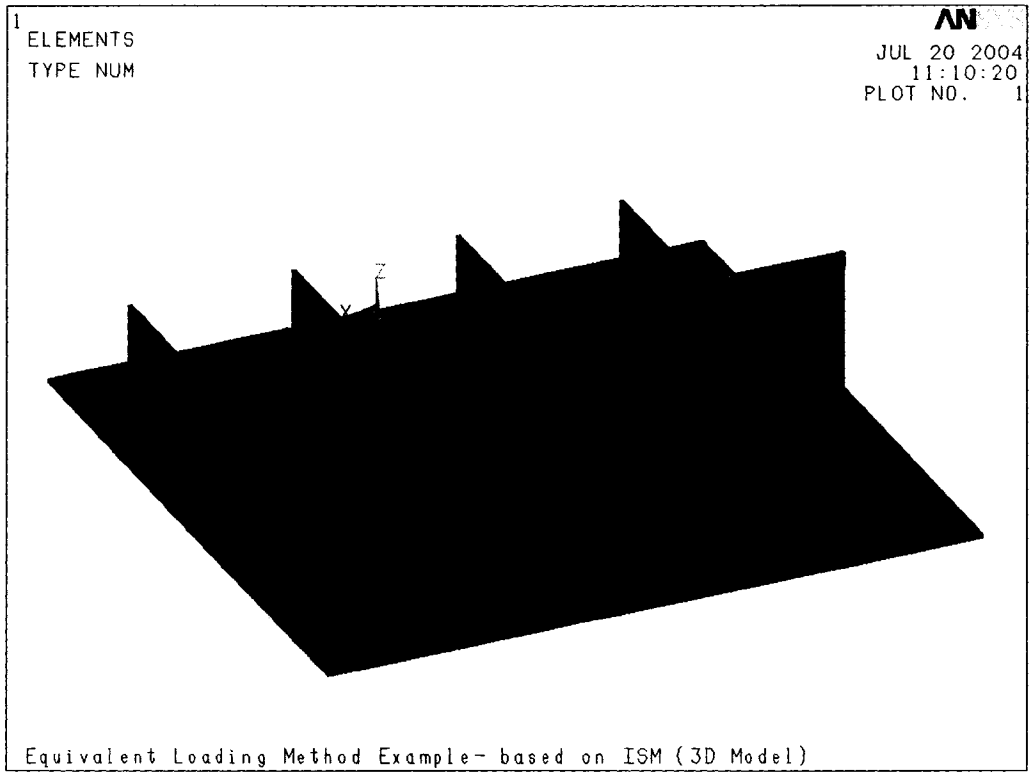

Figure 5. 1: Assembly example of equivalent loading method

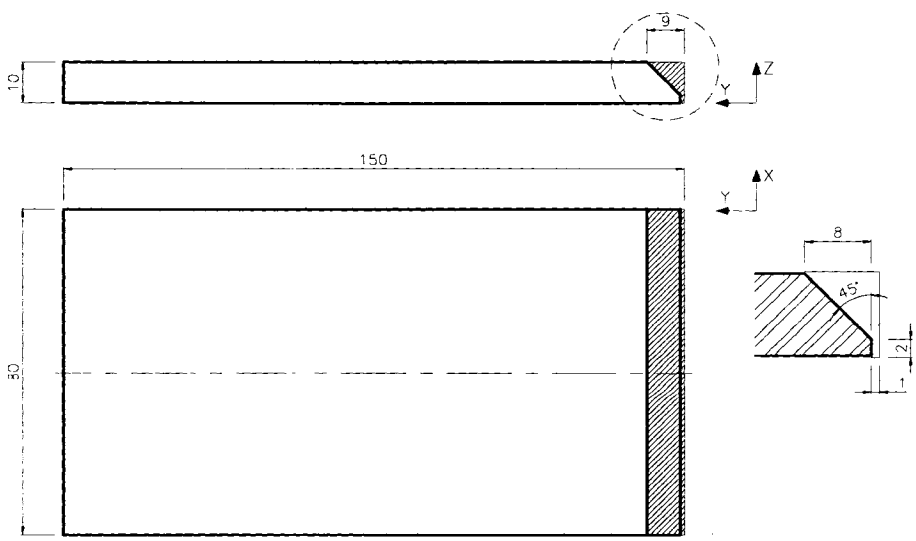

Figure 5. 2 : Butt-joint weld specimen with V-groove [Lee 1995]

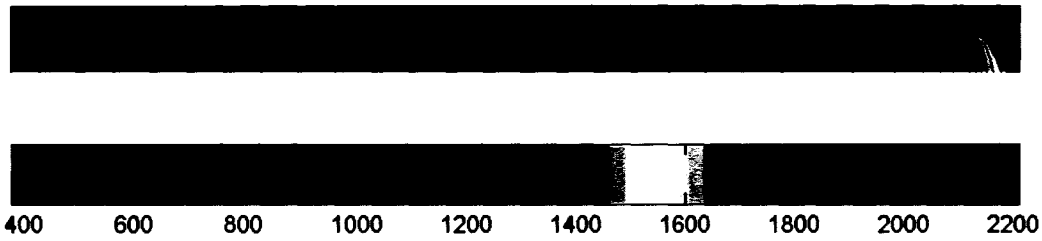

Figure 5. 3 : Highest temperature distribution in the half plate ($^{\circ}K$)

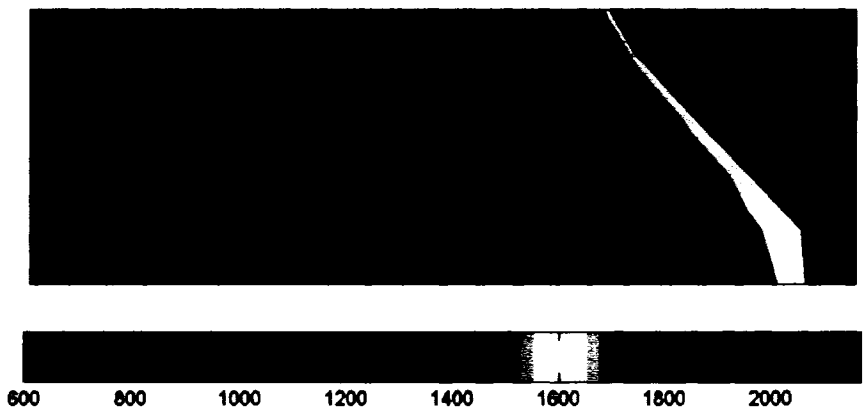

Figure 5. 4 : Highest temperature distribution near the weld line ($^{\circ}K$)

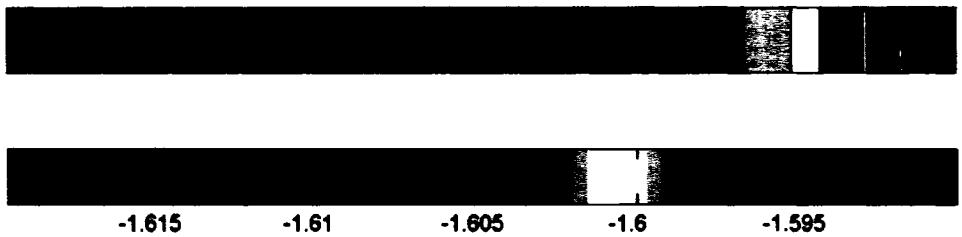

Figure 5. 5 : Inherent strain distribution in transverse direction

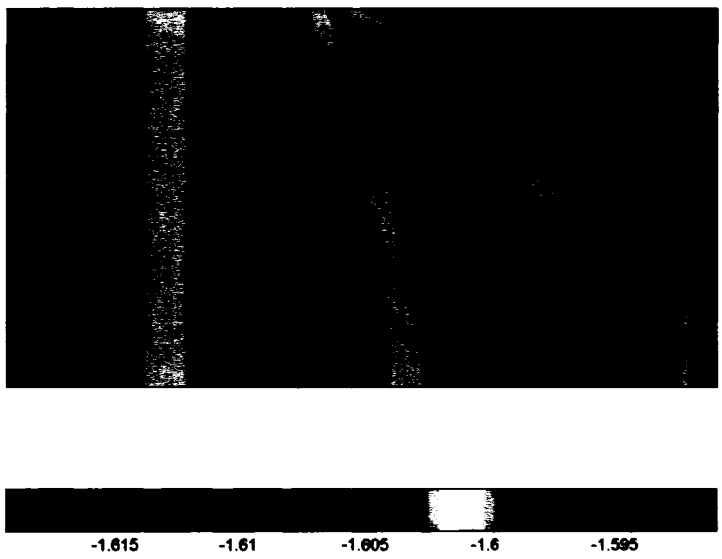

Figure 5. 6 : Inherent strain distribution near weld line

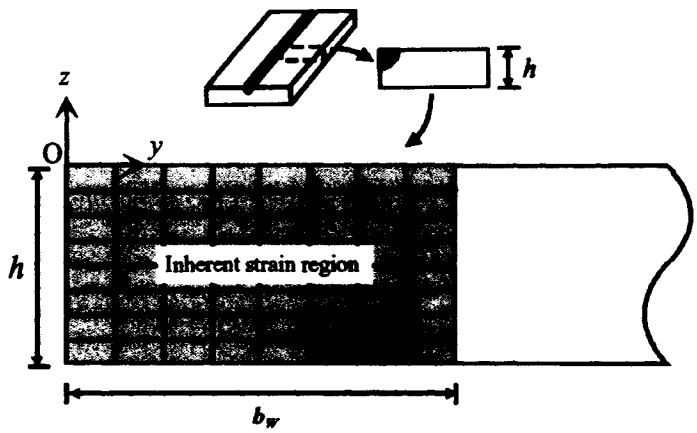

Figure 5. 7 : Equivalent load calculation based on inherent strain distribution [Lee 2002]

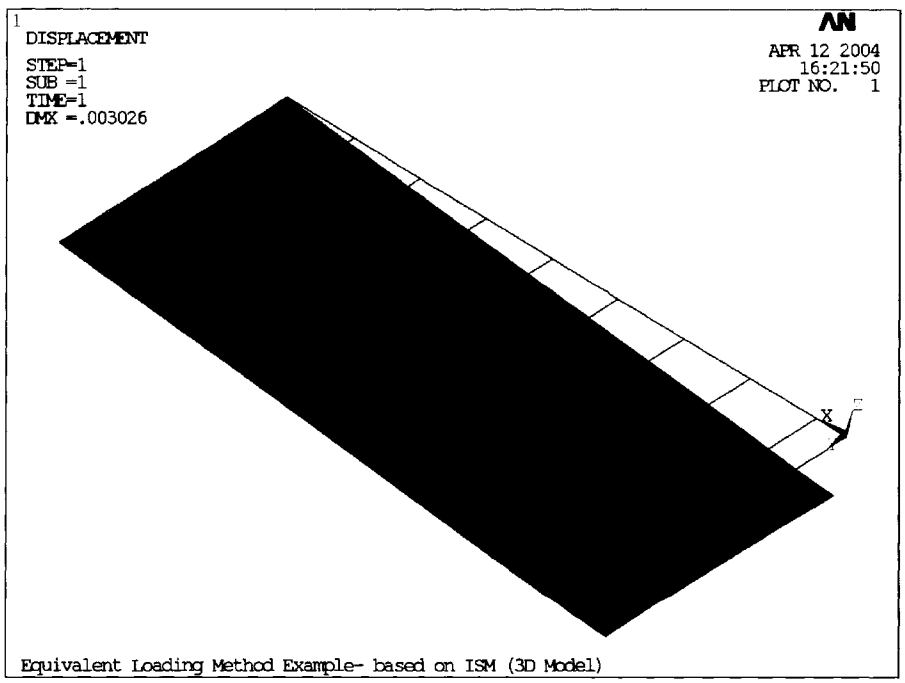

Figure 5. 8 : Welding deformation calculated by inherent strain method (half plate)

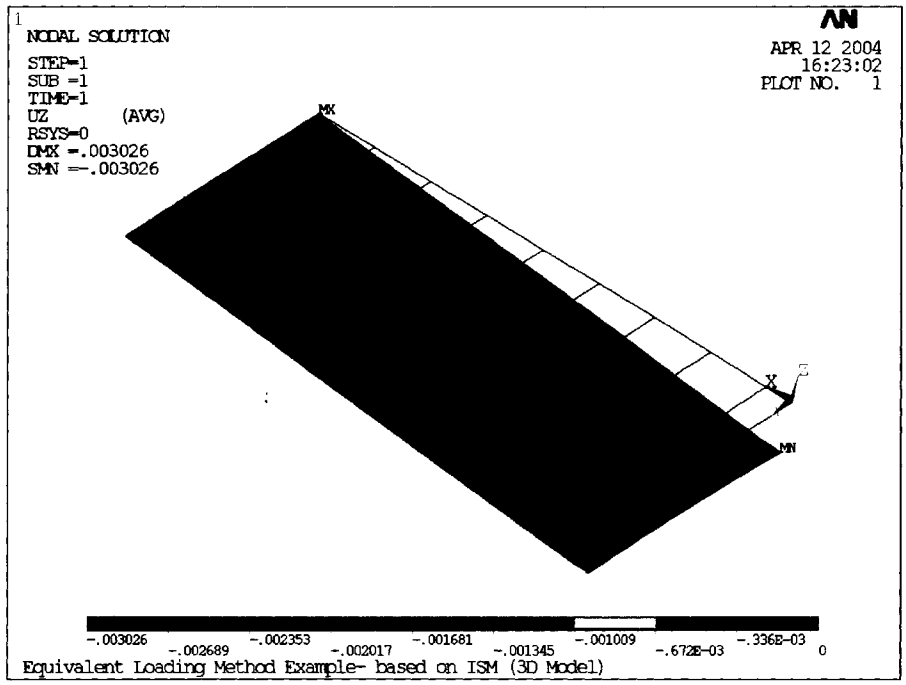

Figure 5. 9 : Vertical displacement contour of welding distortion

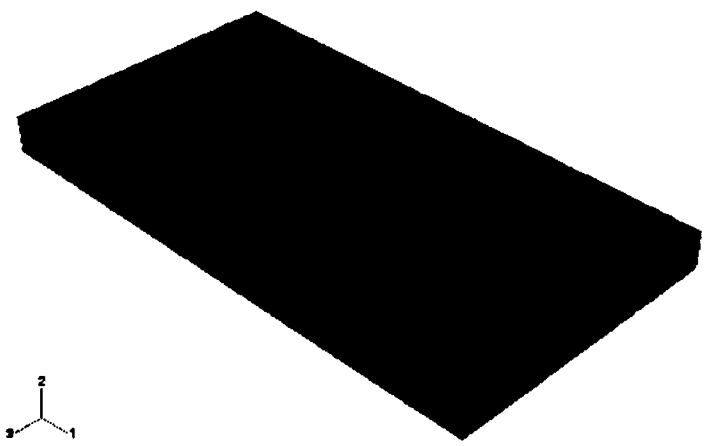

Figure 5. 10 : Finite element mesh for butt-joint GMAW

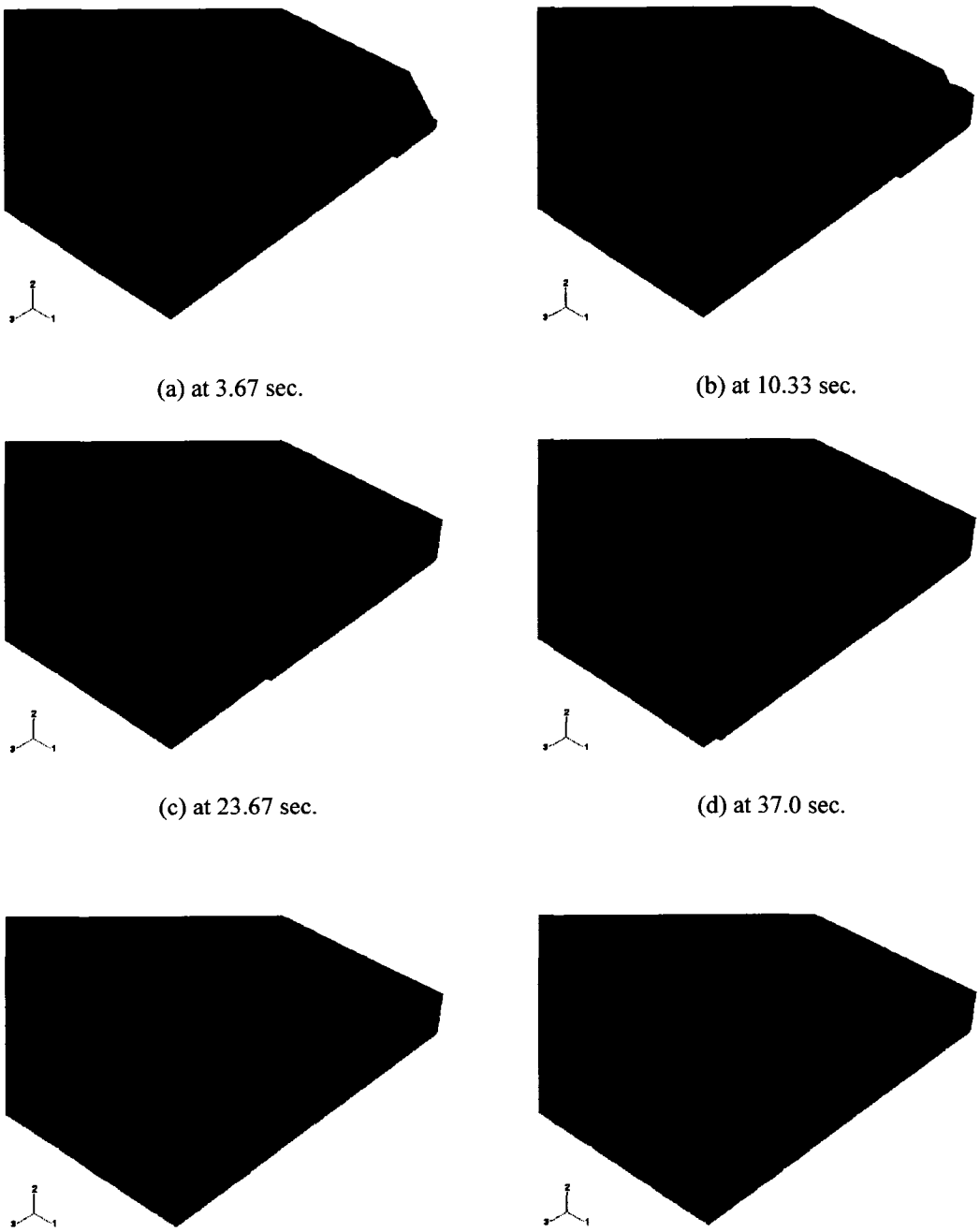

(a) at 3.67 sec.

(b) at 10.33 sec.

(c) at 23.67 sec.

(d) at 37.0 sec.

(e) at 40.33 sec.

(f) at 42.0 sec.

Figure 5. 11 : Element birth technique to simulate weld filler metal

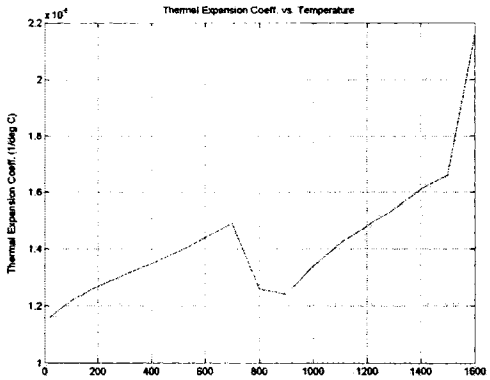

(a) Thermal expansion

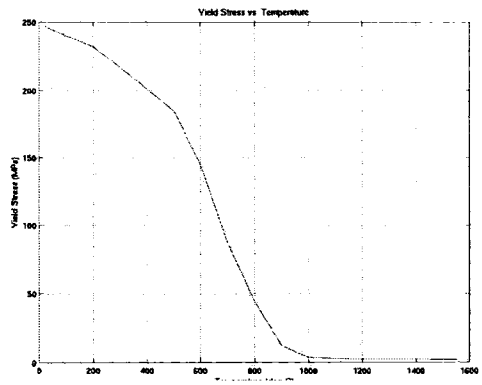

(b) Yield stress

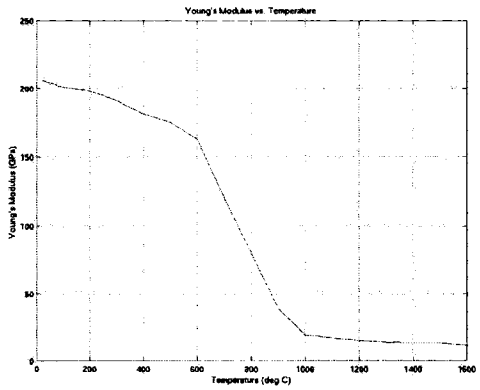

(c) Young's modulus

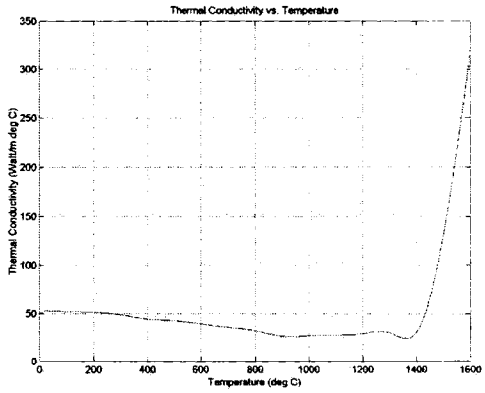

(d) Thermal conductivity

Figure 5. 12 : Temperature dependent material properties for mild steel

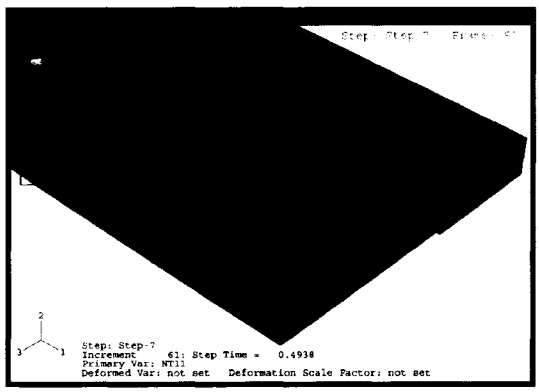

(a) at 12.5 sec.

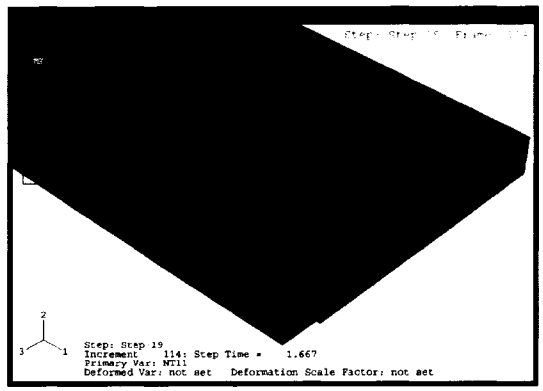

(b) at 33.67 sec.

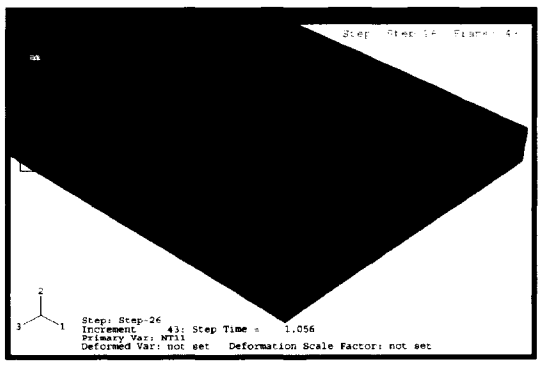

(c) at 43.056 sec.

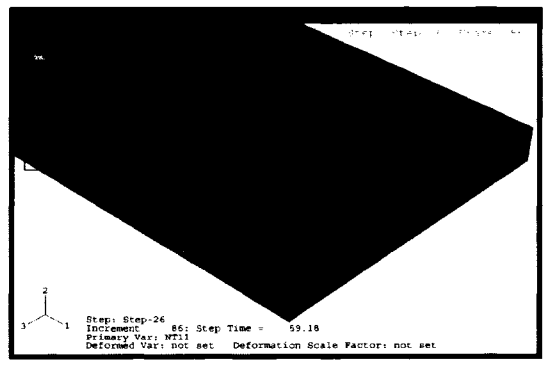

(d) at 101.18 sec.

Figure 5. 13 : Temperature distributions at various times

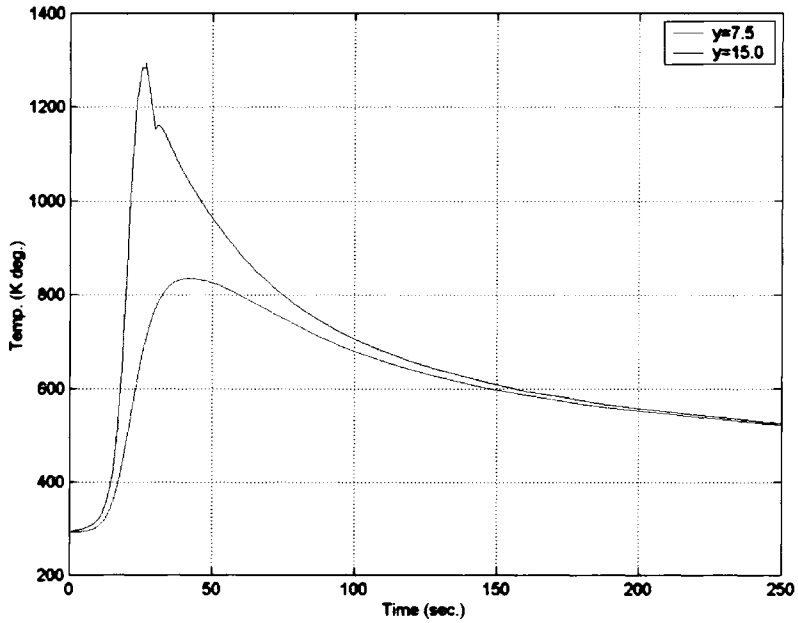

Figure 5. 14 : Temperature histories at various points on plate surface ($y = 7.5mm, 15mm$)

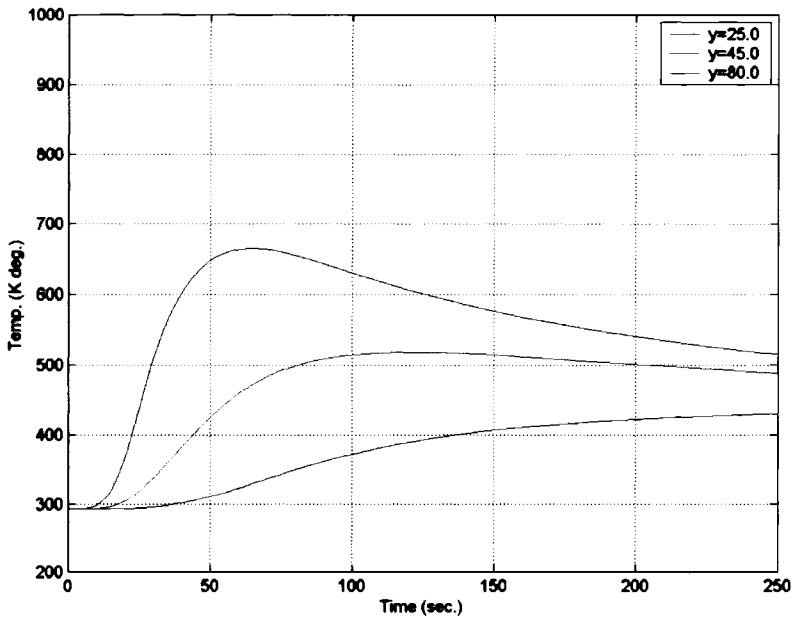

Figure 5. 15 : Temperature histories at various points on plate surface ($y = 25mm, 45mm, 80mm$)

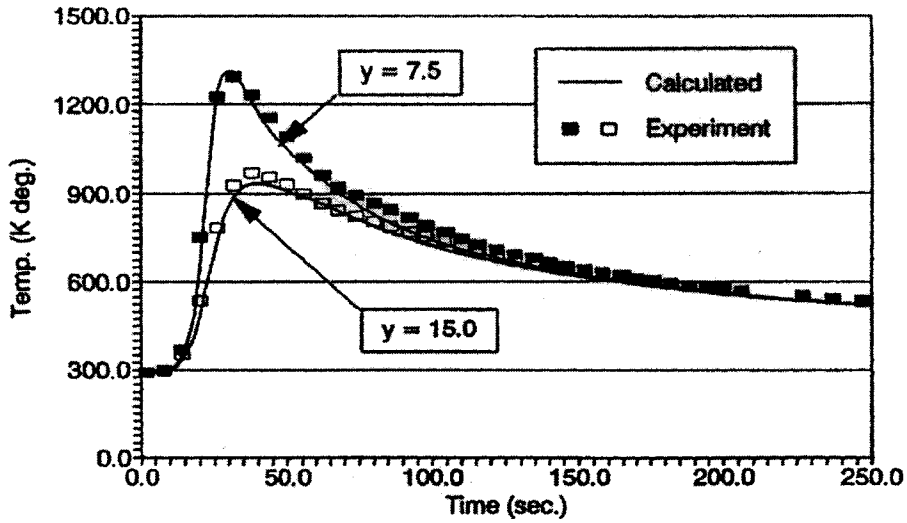

(a) at (x,y,z) = (-40., 7.5, 0.) and (-40., 15., 0.)

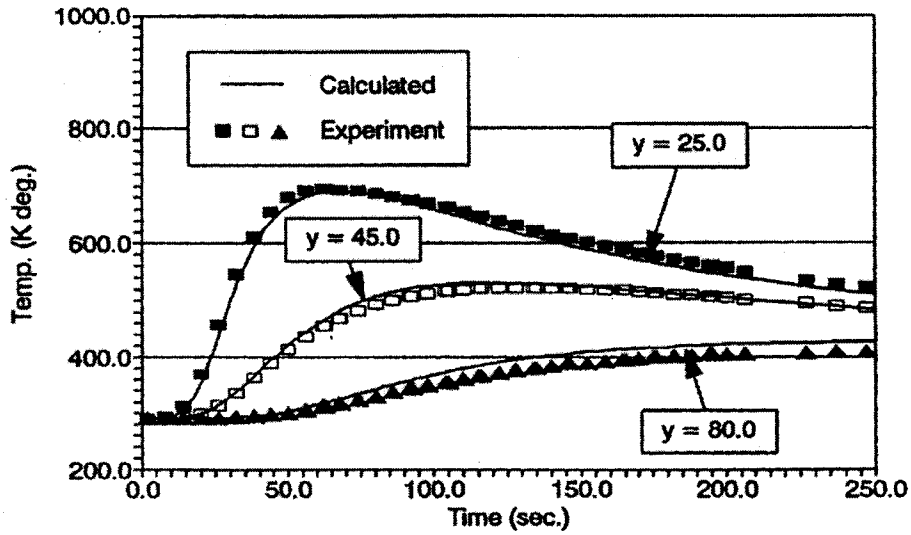

(b) at (x,y,z) = (-40, 25, 0.), (-40., 45., 0.), and (-40., 80., 0.)

Figure 5. 16 : Comparison of temperature histories between the calculated and the experimental data [Lee 1995]

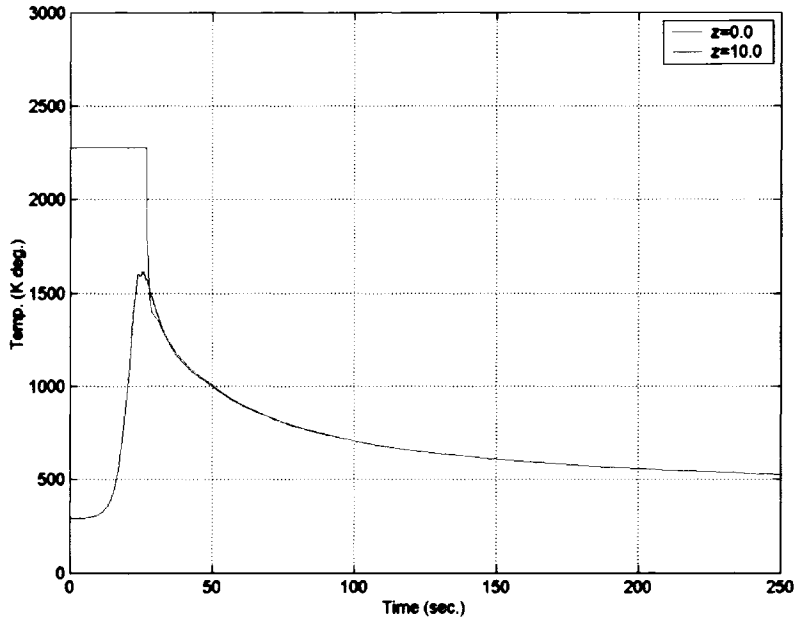

Figure 5. 17 : Temperature histories at various points along the plate thickness

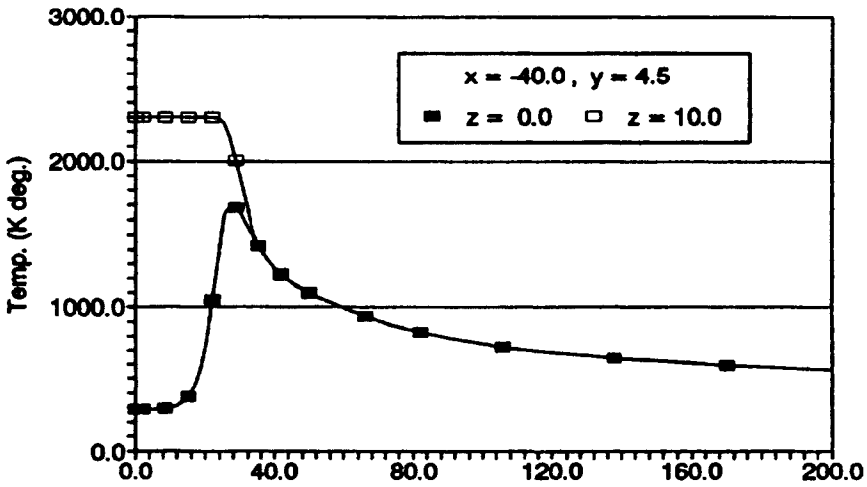

Figure 5. 18 : Comparison of temperature histories between calculated and the experimental data [Lee 1995]

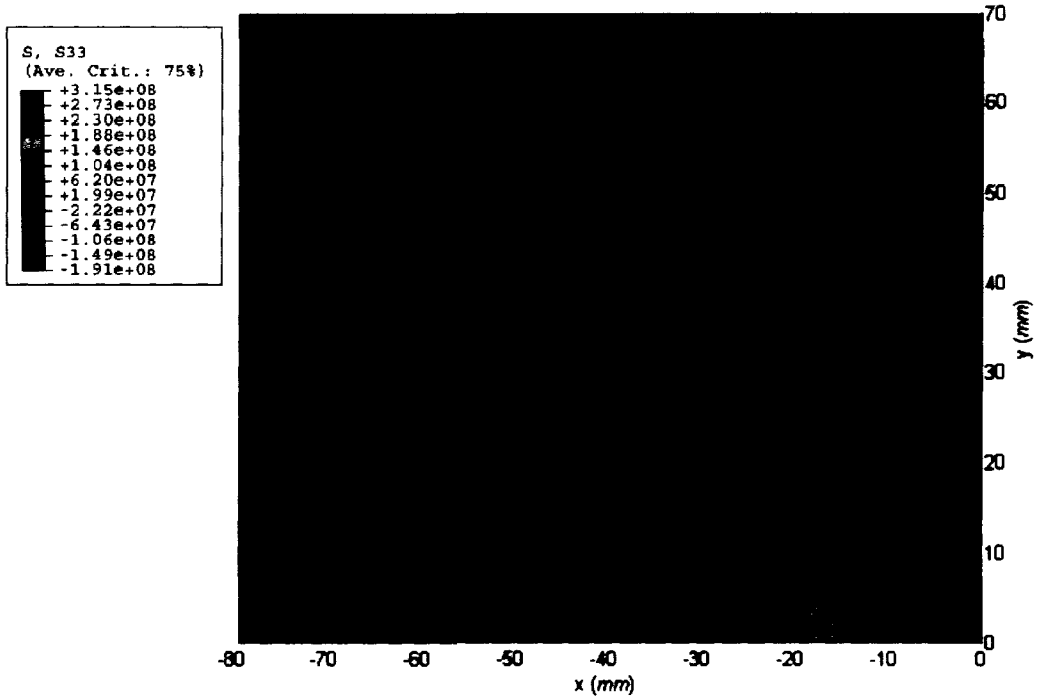

Figure 5. 19 : Residual stress (σ_{xx}) distribution on top surface (Pa)

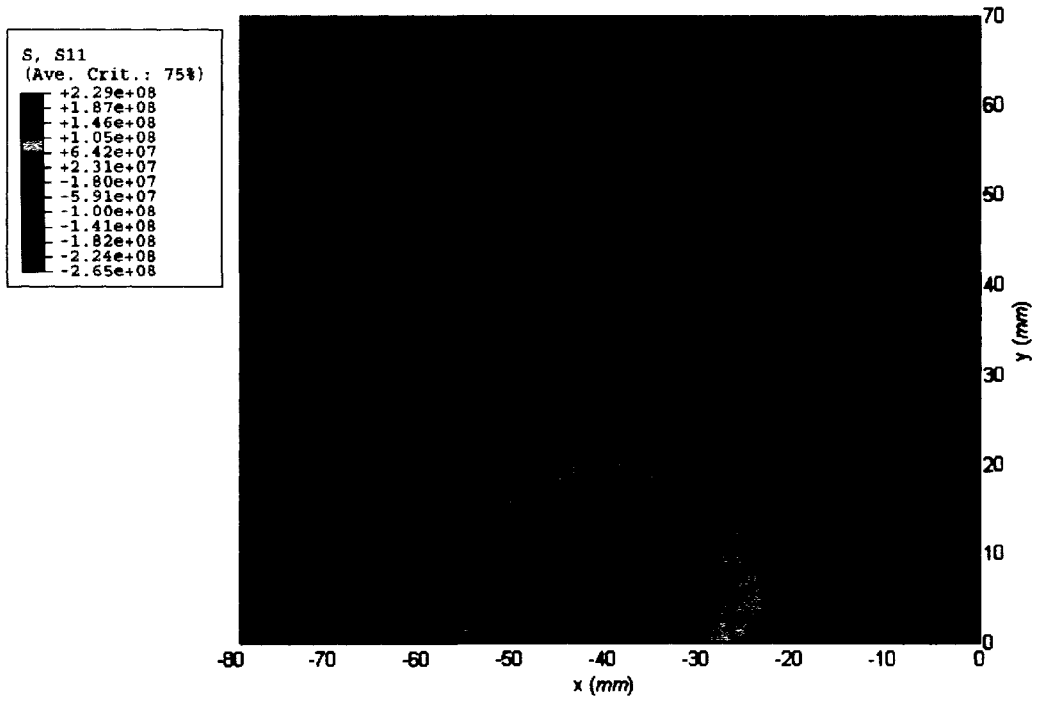

Figure 5. 20 : Residual stress (σ_{yy}) distribution on top surface (Pa)

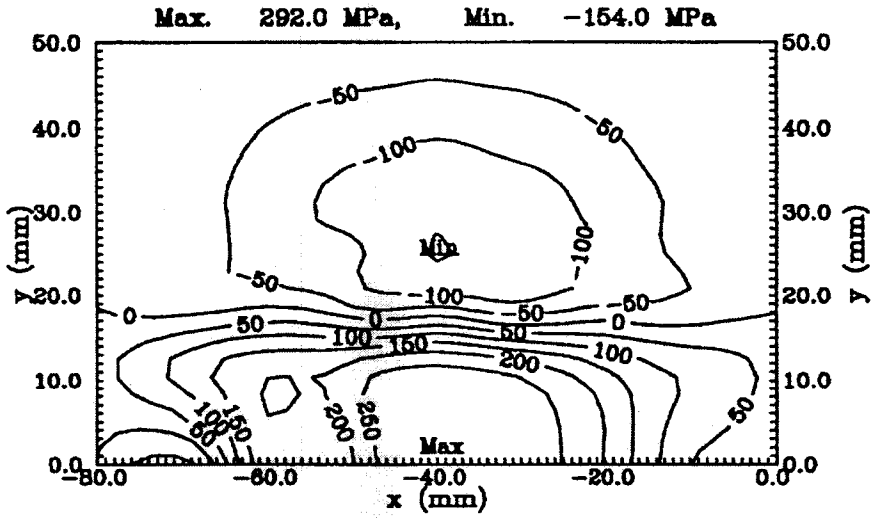

(a) Residual stress σ_{xx} on the top surface

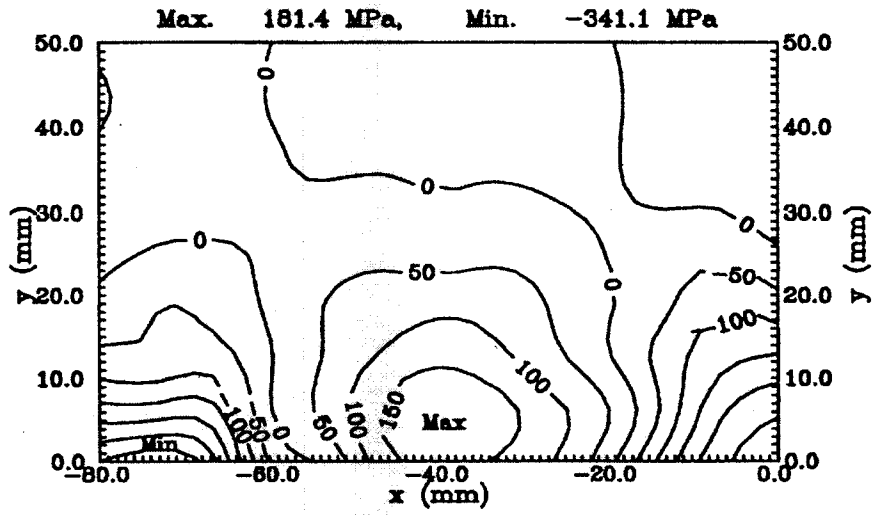

(b) Residual stress σ_{yy} on the top surface

Figure 5. 21 : Experimental result of residual stress on top surface [Lee 1995]

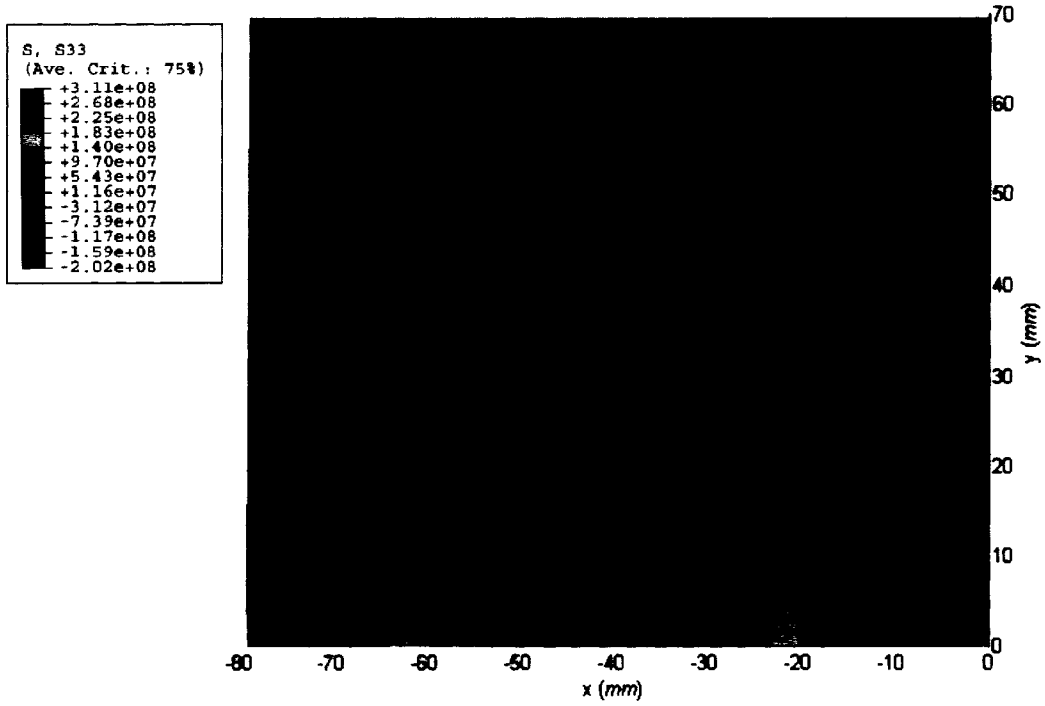

Figure 5. 22 : Residual stress (σ_{xx}) distribution on bottom surface (Pa)

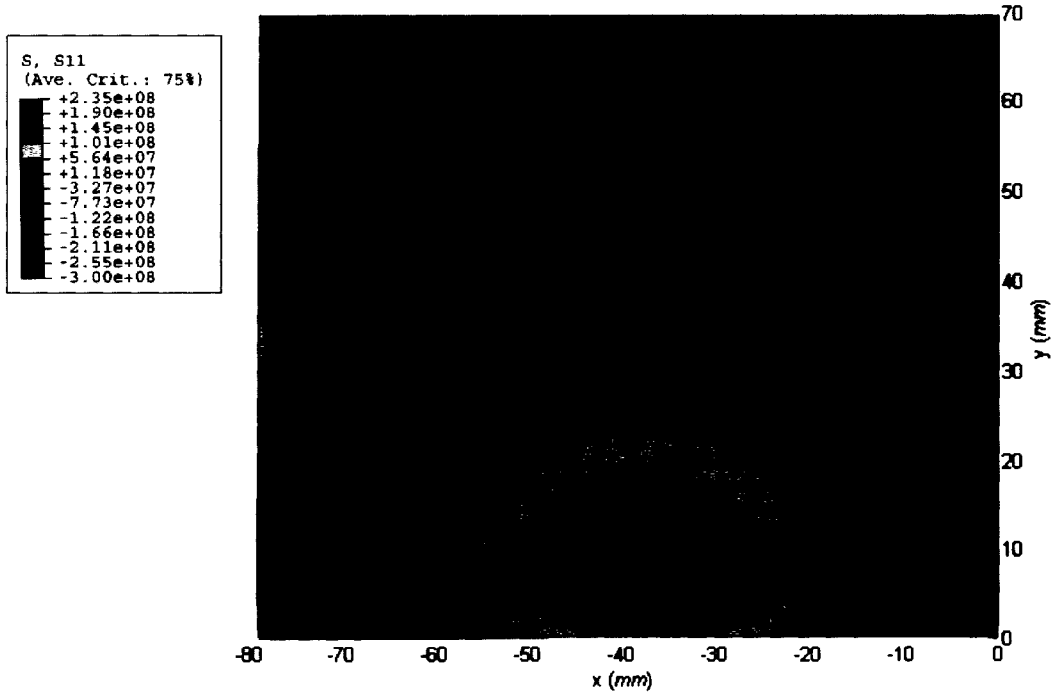

Figure 5. 23 : Residual stress (σ_{yy}) distribution on bottom surface (Pa)

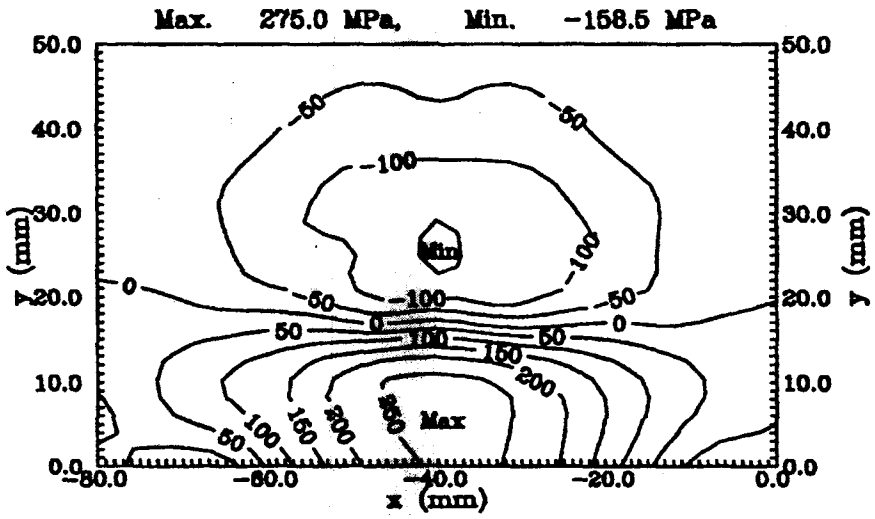

(a) Residual stress σ_{xx} on the bottom surface

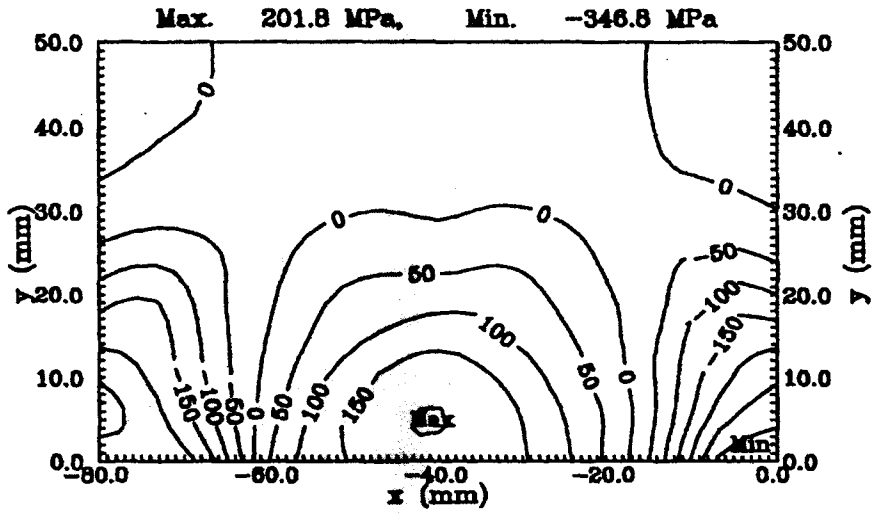

(b) Residual stress σ_{yy} on the bottom surface

Figure 5. 24 : Experimental result of residual stress on bottom surface [Lee 1995]

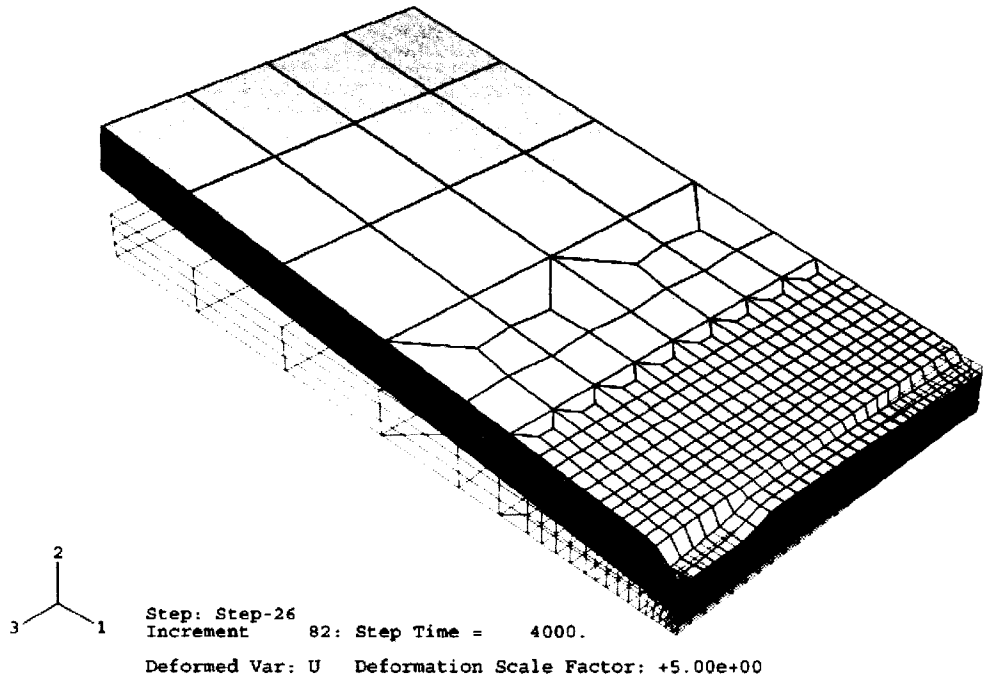

Figure 5. 25: Welding distortion simulation by FEM

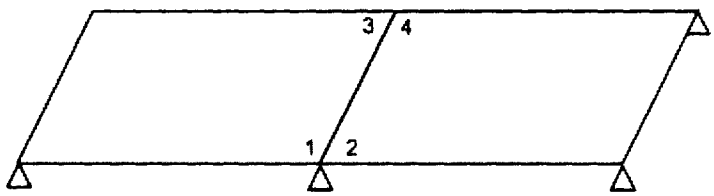

(a) Four sources of variation case

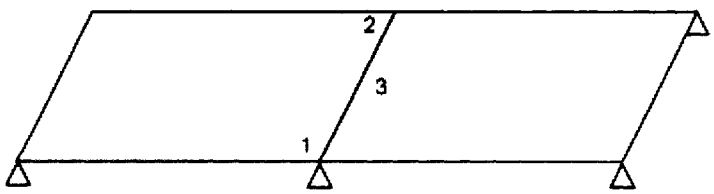

(b) Three sources of variation case

Figure 5. 26: Two example cases of butt welding of non-nominal plate assembly

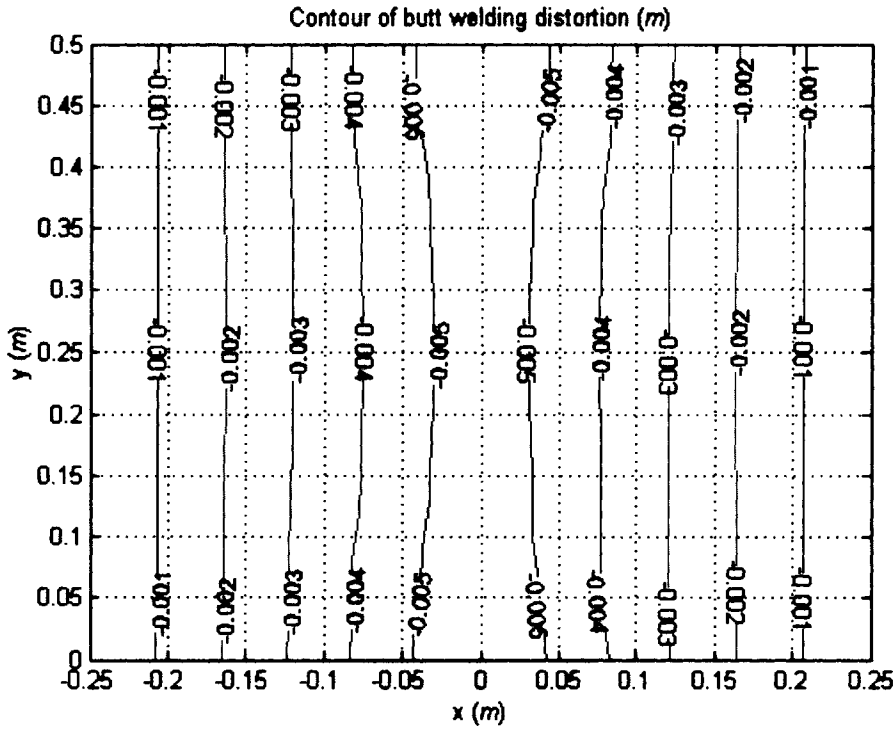

Figure 5. 27: Contour of welding distortion

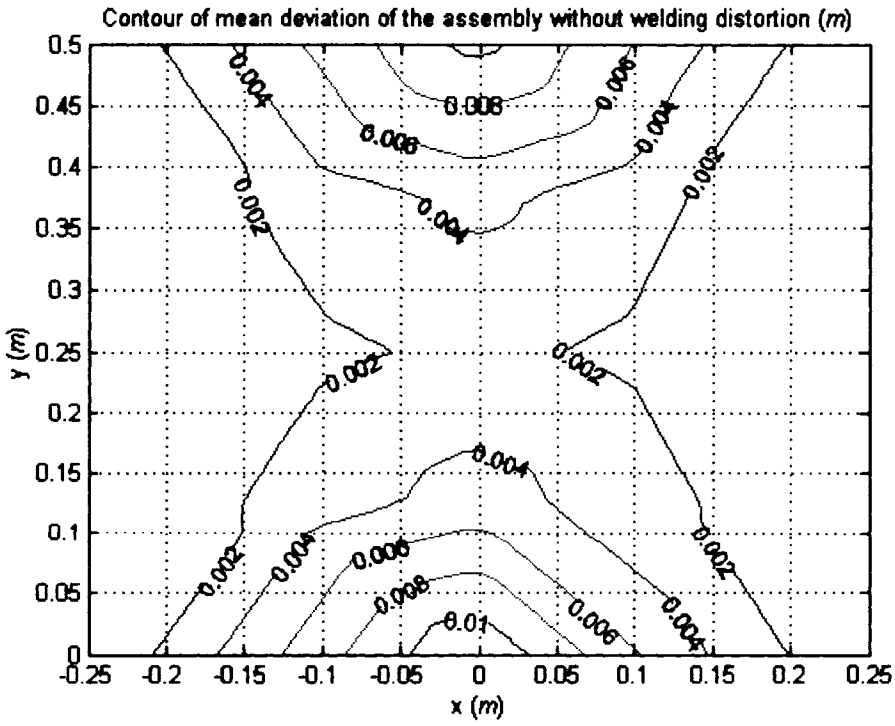

Figure 5. 28: Contour of mean deviation without welding distortion

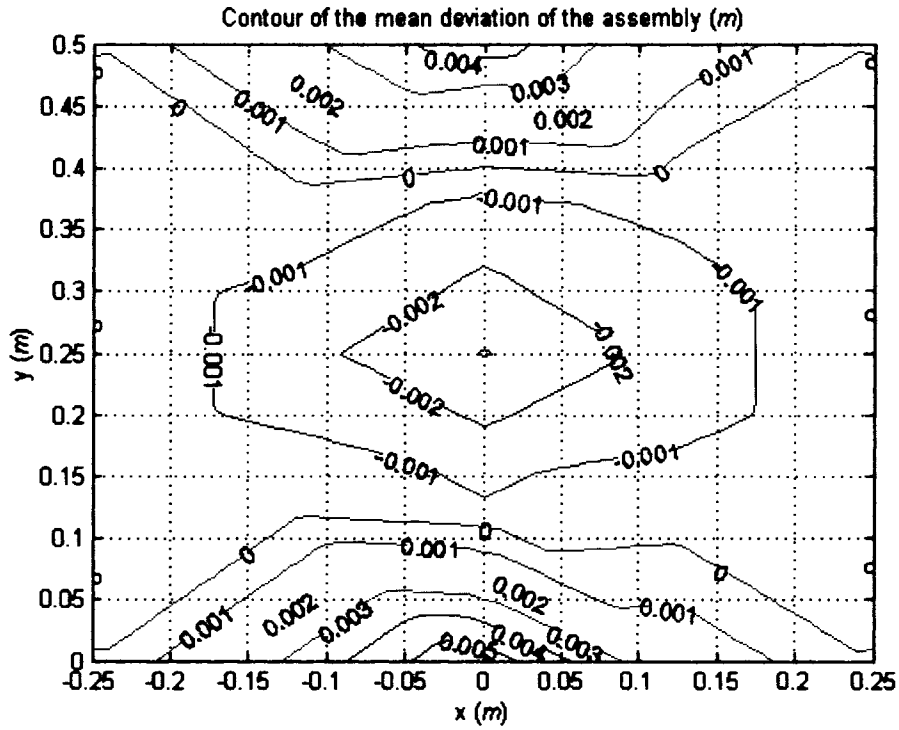

Figure 5. 29: Contour of mean deviation of the assembly

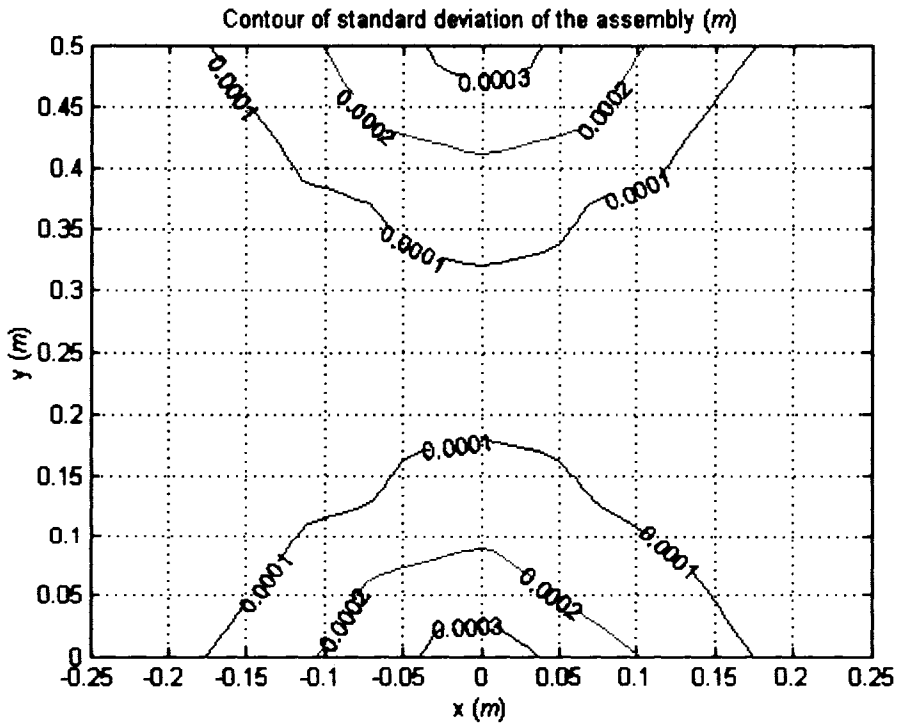

Figure 5. 30: Contour of standard deviation of the assembly

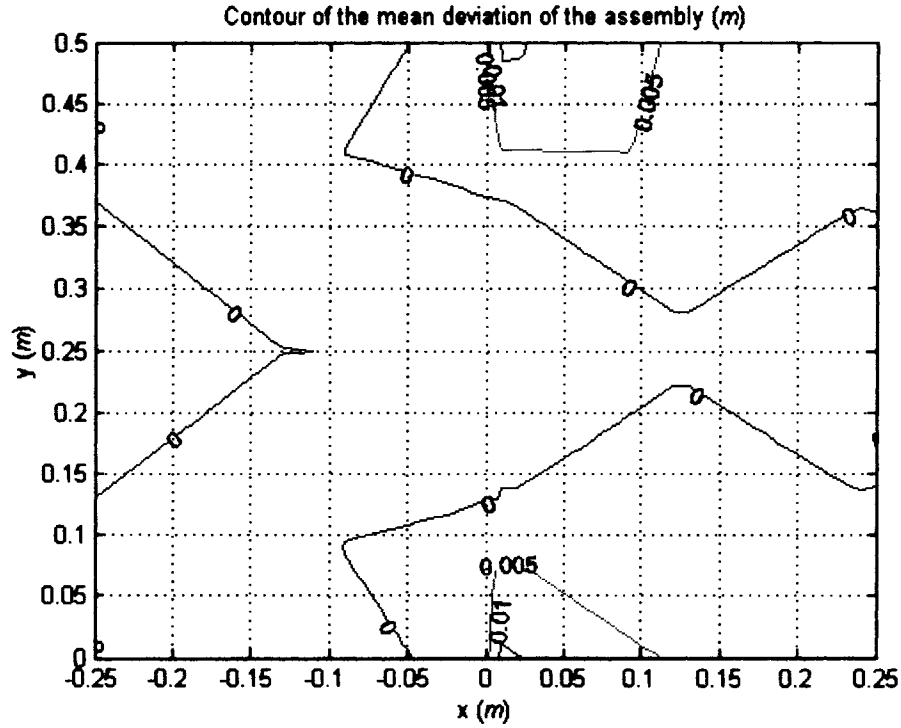

Figure 5. 31: Contour of mean deviation (Direct Monte Carlo Simulation)

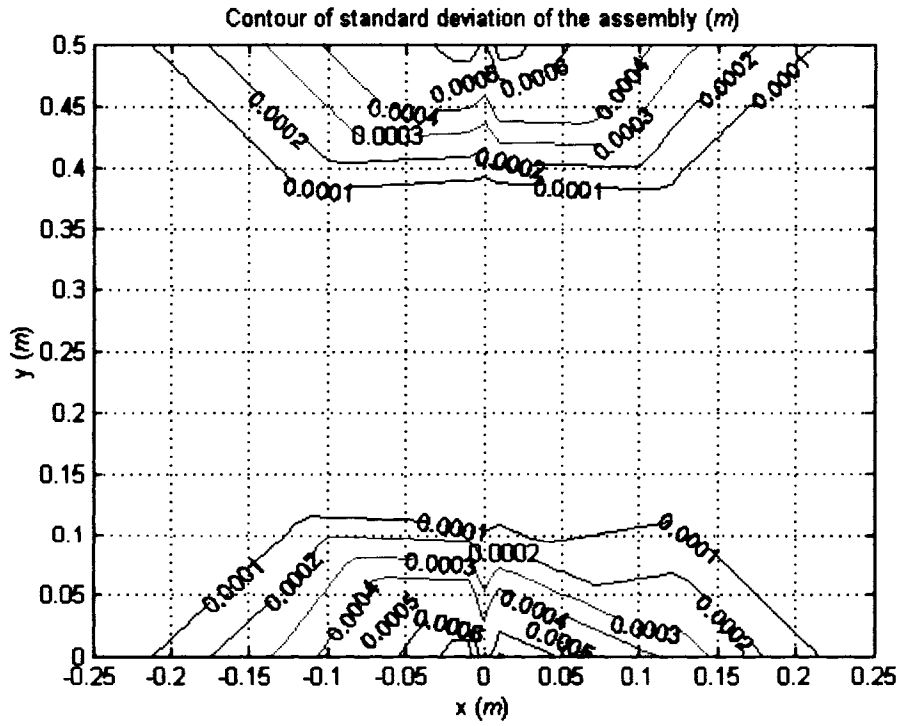

Figure 5. 32: Contour of standard deviation (Direct Monte Carlo Simulation)

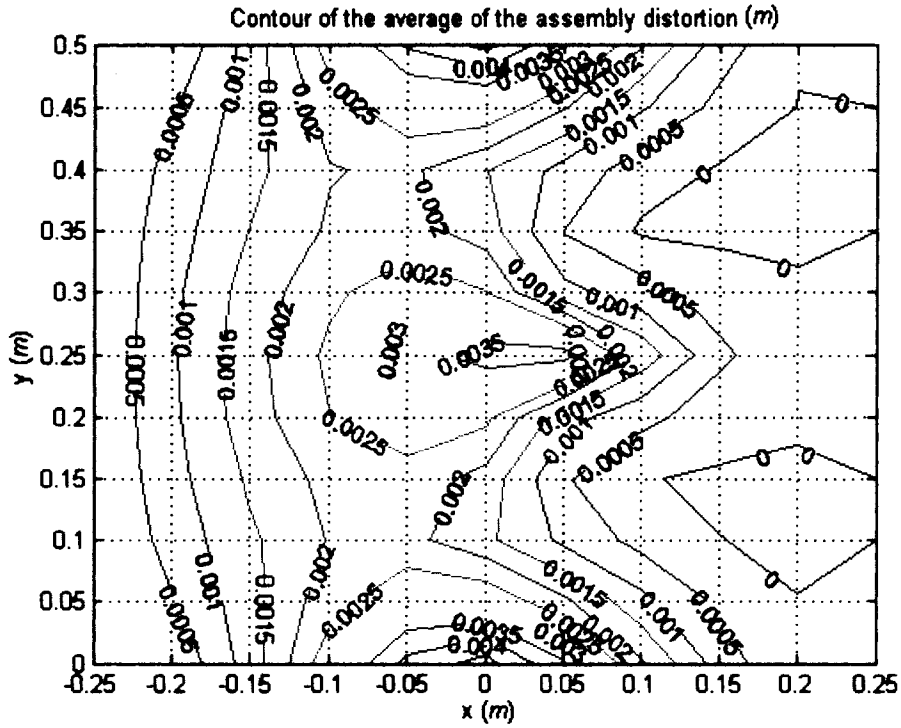

Figure 5. 33: Contour of average of the assembly deviation

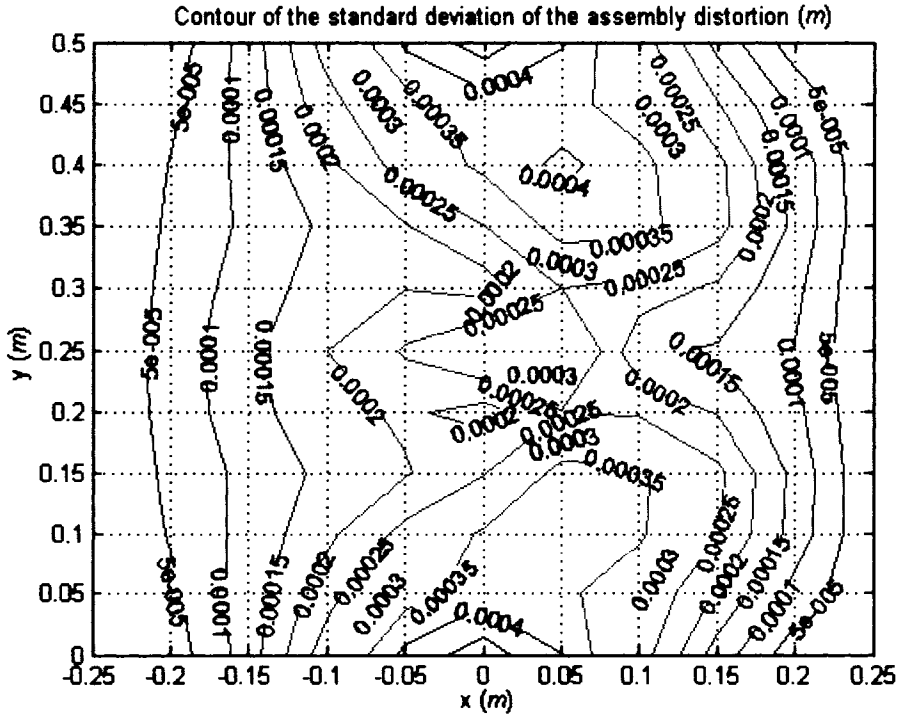

Figure 5. 34: Contour of standard deviation of the assembly deviation

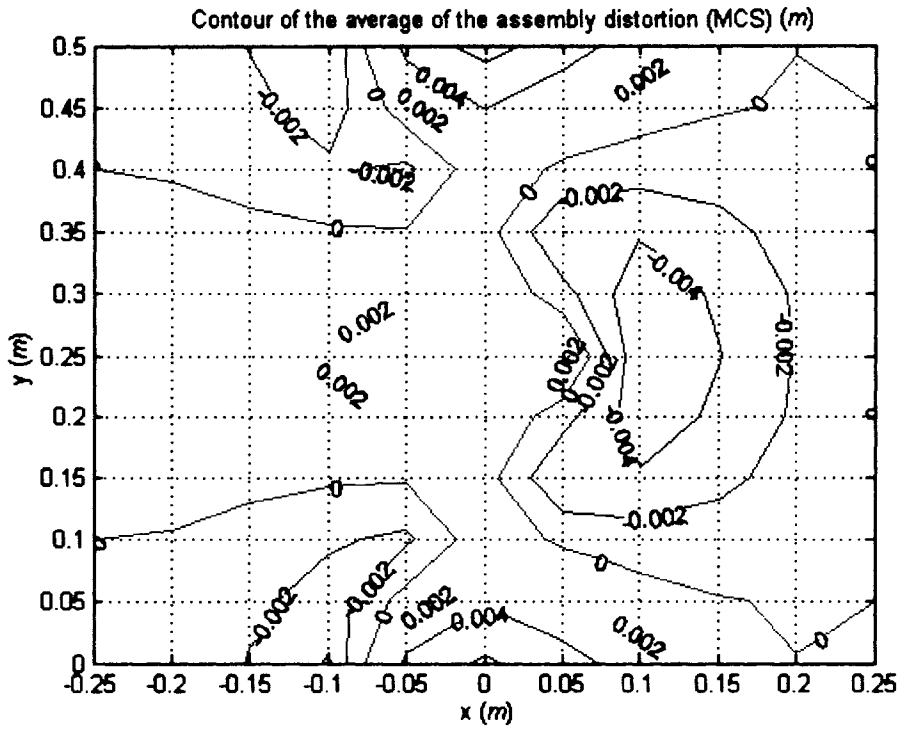

Figure 5. 35: Contour of average of the assembly deviation (MCS)

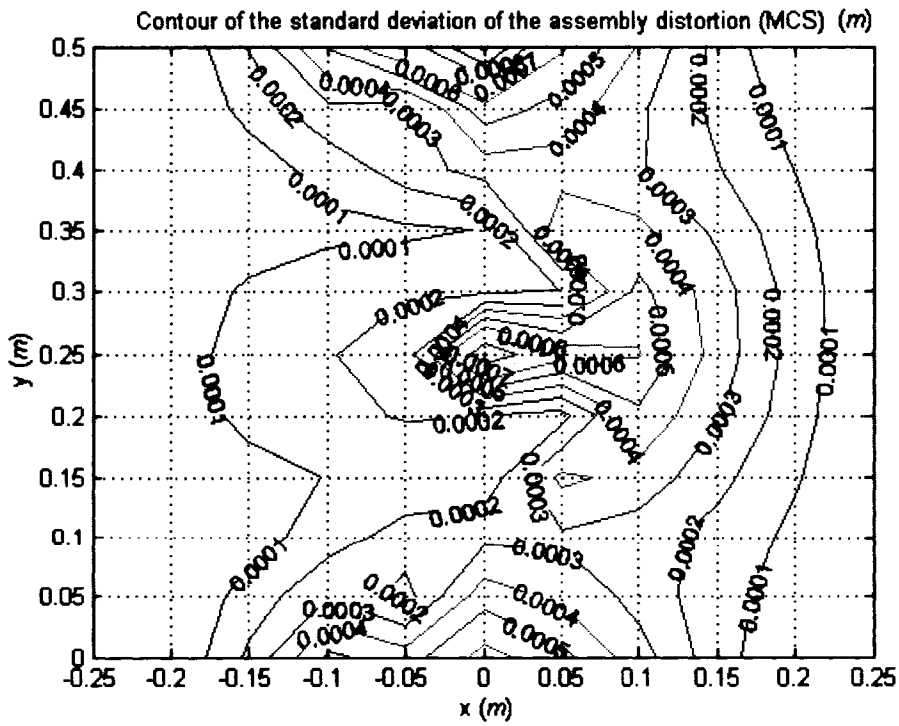

Figure 5. 36: Contour of standard deviation of the assembly deviation (MCS)

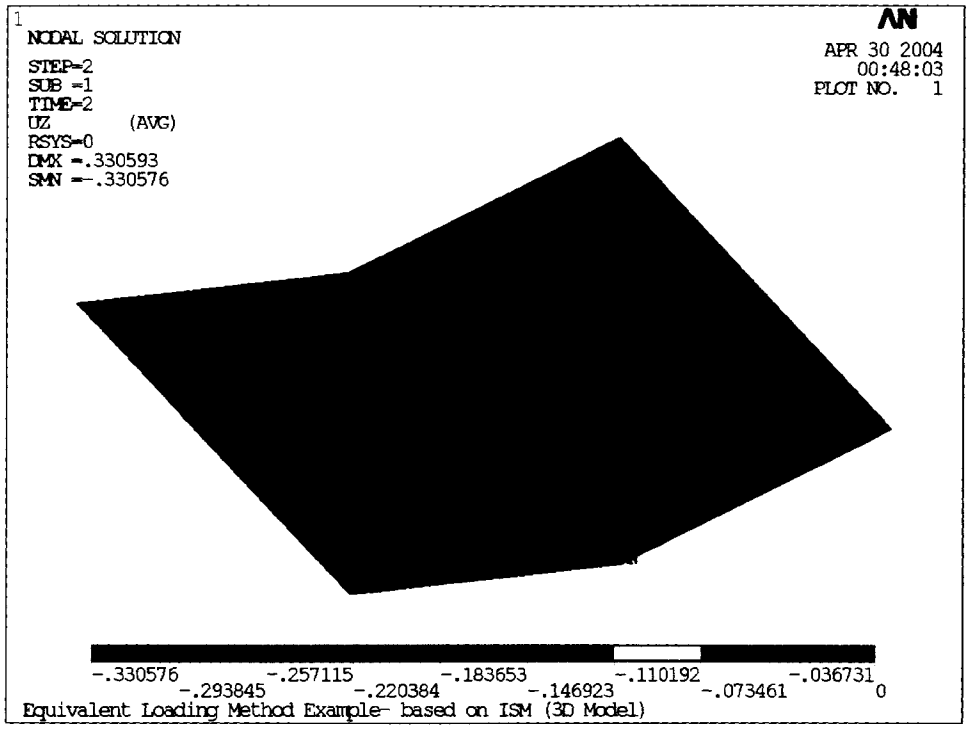

Figure 5. 37: Butt welding of two plates (displacement unit: *m*)

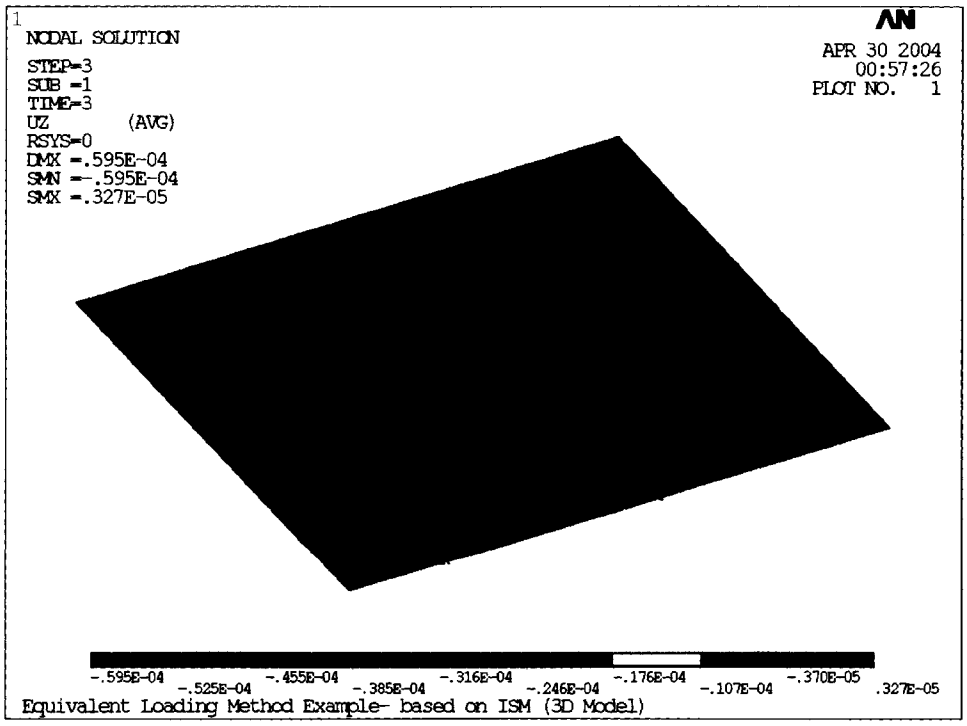

Figure 5. 38: Clamping for stiffener attachment (displacement unit: *m*)

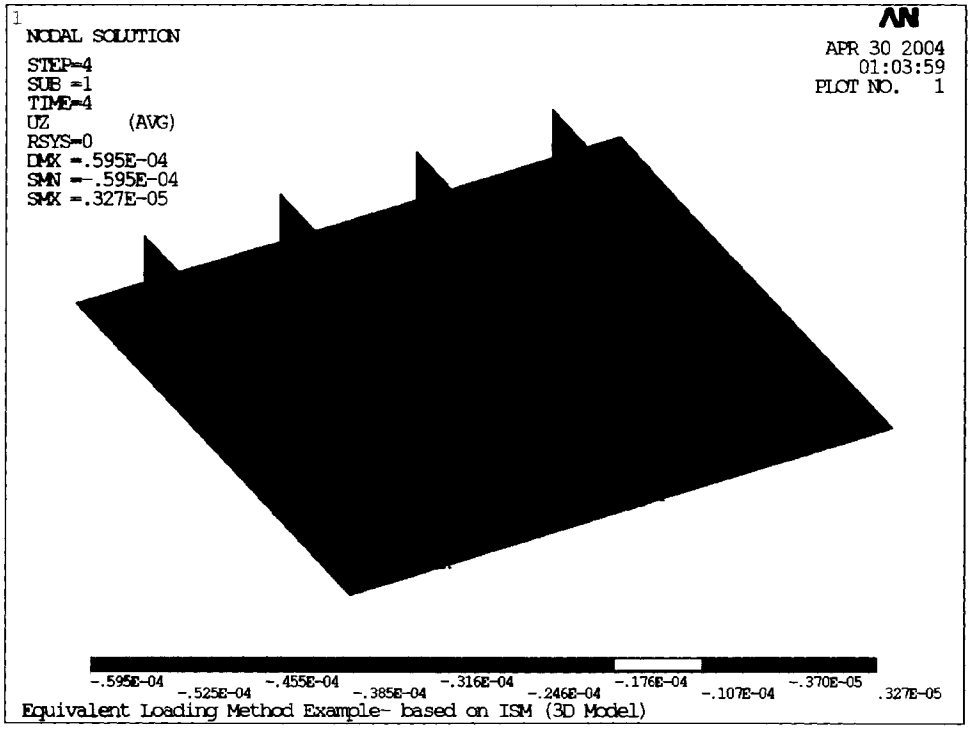

Figure 5. 39: Stiffeners are welded (displacement unit: m)

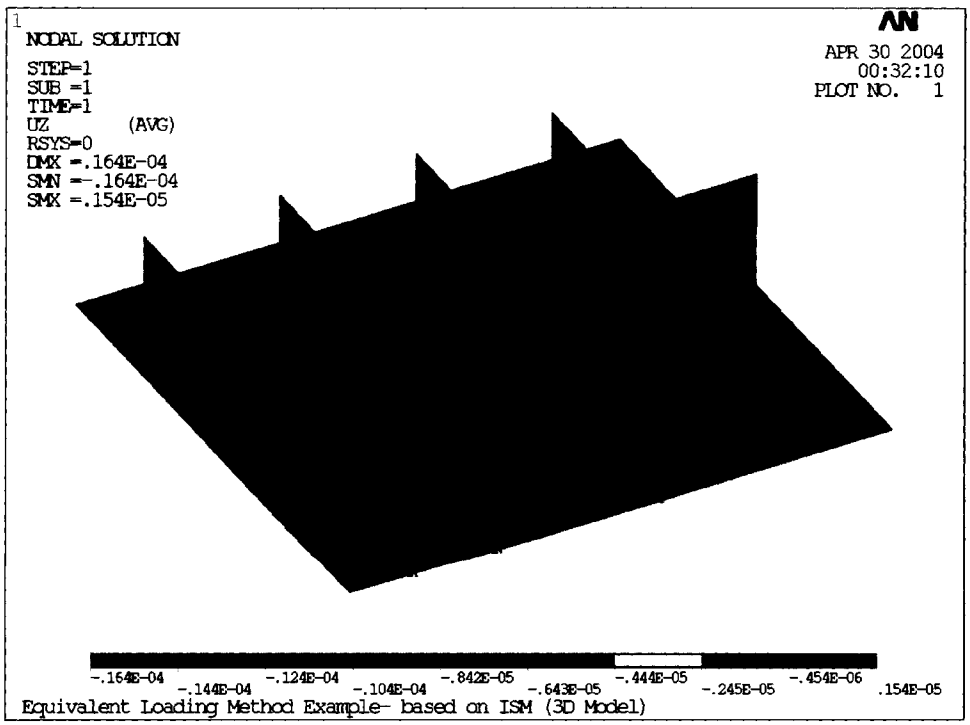

Figure 5. 40: Web frame is attached (displacement unit: m)

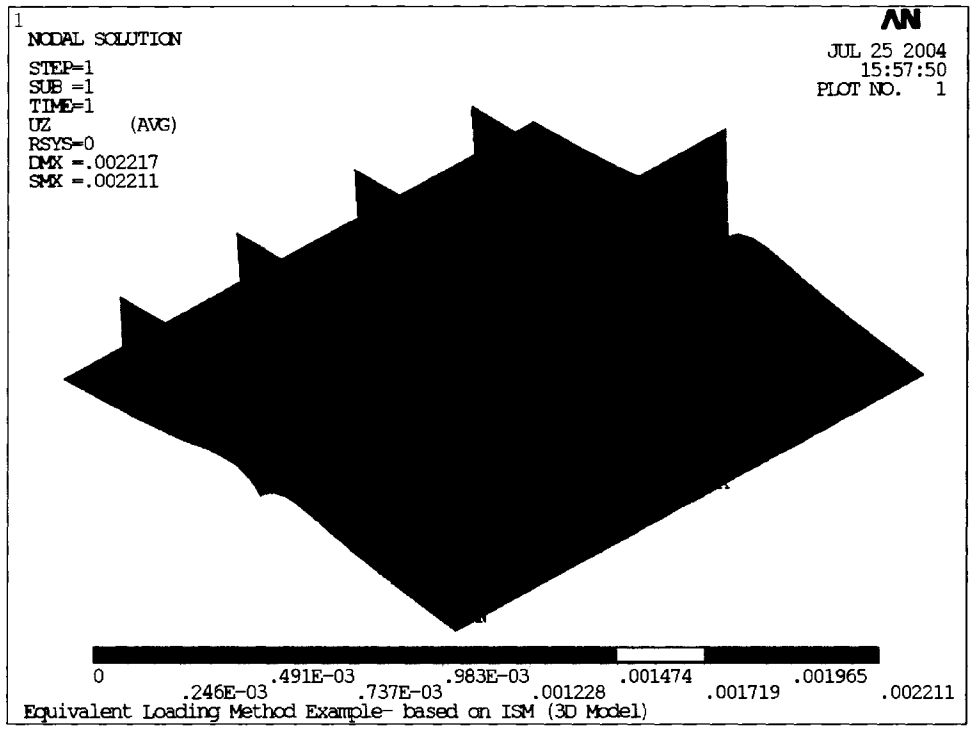

Figure 5. 41: Final shape of the assembly (displacement unit: m)

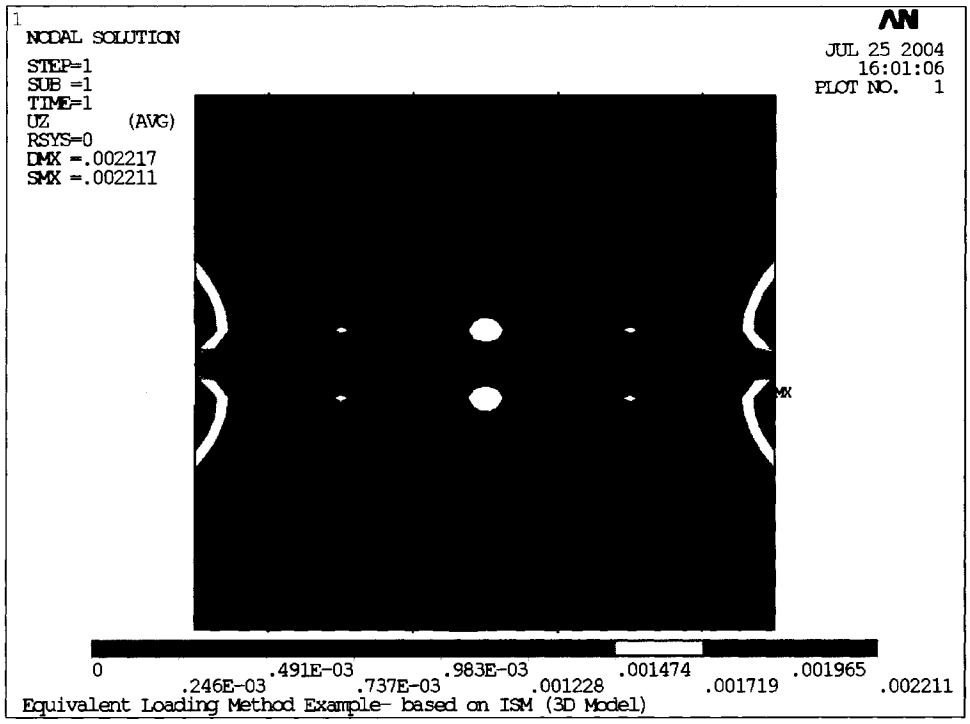

Figure 5. 42: Contour of base plate welding distortion (displacement unit: m)

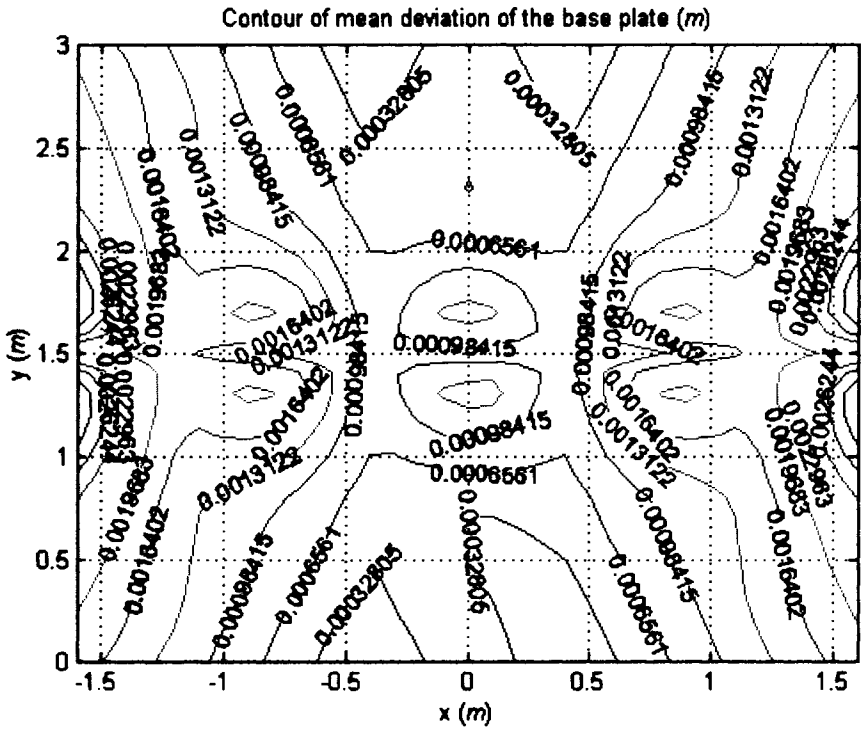

Figure 5. 43: Contour of the mean deviation (Modified Method of Influence Coefficients)

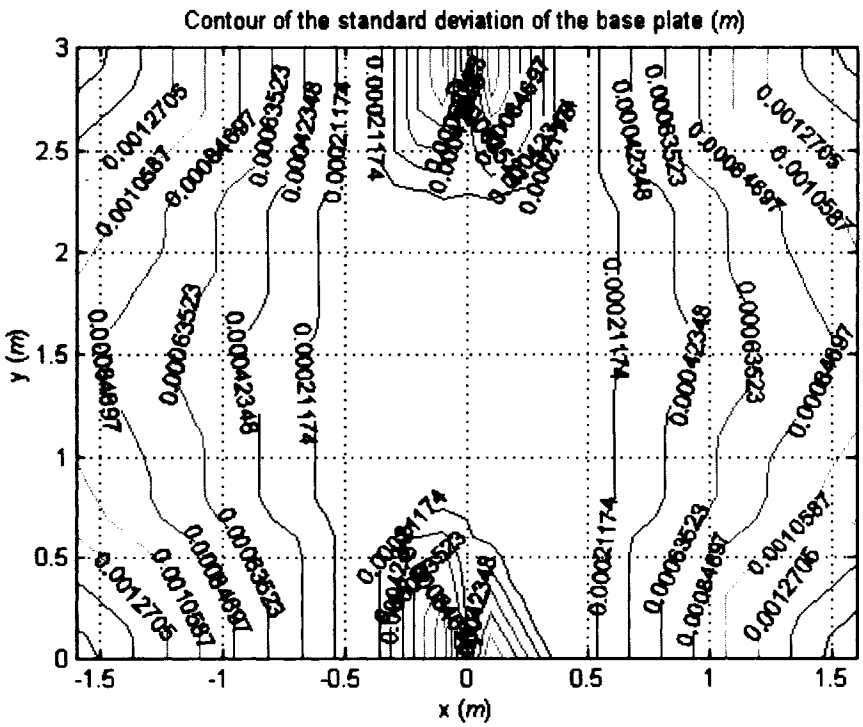

Figure 5. 44: Contour of the standard deviation (Modified Method of Influence Coefficients)

CHAPTER VI

CONCLUSION AND RECOMMENDATIONS FOR FUTURE WORK

A numerical investigation of the part variation problem in ship block assembly was conducted in this research. The investigation focuses on simplified methods to alleviate heavy computation requirements that are needed in the Finite Element Method used for variational simulation and welding distortion simulation.

First, the characteristics of GMAW (Gas Metal Arc Welding) that is commonly used in ship block construction were investigated to validate the numerical scheme and modeling of the inherent strain method and the equivalent loading method based on the inherent strain method for welding distortion prediction with much less computation time and resources. Second, the characteristics and effects of various clamping strength cases were investigated to research the main thesis of this research, the linear superposition of welding distortion and variation of assembled parts. A simple flat plate case was investigated to validate the thesis and a more complex assembly case was also investigated in order to validate that the new Modified Method of Influence Coefficient can be applied to predict the final variations in assembled structure considering welding distortion.

6.1 Conclusion

In the first part of this research the welding distortion phenomenon is investigated using a simple three-bar model. In this research, the numerical simulation and the

analytical experiment of a one-dimensional three-bar model show that the highly non-uniform temperature distribution in the welded parts causes welding distortion. The side bars (adjacent region) experience plastic deformations due to the thermal expansion of middle bar (heated region). The magnitude and distribution of the distortion depend on the non-uniformity of temperature distribution and temperature dependent material properties as well.

The inherent strain concept is well suited to the prediction of welding distortion since it captures the core mechanism of welding distortion generation. From the three-bar model example, residual stress, i.e., inherent strain that accounts for welding distortion, is determined by the highest temperature distribution during the welding process and the Degree of Restraints (DOR) at each point in the welded structure. This is well explained by the one-dimensional three-bar model. The degree of restraints consists of both the internal restraint and external restraint. The internal restraint accounts for the effect of regional generations of inherent strain caused by non-uniform temperature distribution while the external restraint accounts for the external constraint forces such as clamping and fixturing that confine the movement of the welded part. The one-dimensional three-bar model with initial variation and clamping force can explain that the welding distortion is dependent upon the ratio of internal and external restraints, not their absolute magnitudes.

The equivalent loading method based on inherent strain can be used to derive welding distortion results comparable to the fully nonlinear three-dimensional thermo-elasto-plastic finite element simulation, which takes much more computation time. However, since it employs a 'long weld assumption', the welding distortions in the middle of weld line are best predicted. At the beginning and ending end of the weld line, the result might be inaccurate. However, by employing three-dimensional heat transfer

analysis for the determination of highest temperature it should result in more exact results.

The internal restraint can account for most welding configurations, such as plate thickness, welding type (e.g., butt-weld or fillet weld), torch shape, torch strength and material properties. Thus typical welding configurations for primitive members can be defined without considering actual part size, shape, and clamping conditions. Thus the results of the primitive welding members can be used as the 'basis' of welding distortion simulation.

There exists a range of initial variations in the three-bar model that does not affect the final length of springback. The analytic simulation shows that this phenomenon happens when the initial variation and the clamping forces are working for the generation of the plastic deformation of middle bar during the heating process and thus preventing the plastic deformation of side bars during the cooling process. When the initial variation and clamping force are working for the generations of plastic deformation in the side bars, the magnitude of initial variation and clamping force have a linear relation with the residual stress and strain generated. This can be explained as the initial variation and clamping forces are working for the thermal expansion of the middle bar thus causing more plastic deformation in side bars during the cooling process.

Among many welding distortion mitigation techniques, the mechanical stretching method, i.e., application of tension along the welding line direction in order to reduce longitudinal welding distortion, can be explained as the application of tension to the three-bar model, which will result in much less residual stress. The thermal tensioning method, i.e., application of heating pad alongside the welding line to reduce temperature difference between the heated area and the adjacent area, causes a reduction of the non-uniformity of temperature distribution between the middle bar and the side bars.

Since the angular distortion of the butt welded plates depends on the non-uniformity of the temperature field in the through-thickness direction, the thermal tensioning method for angular distortion, i.e., two-sided welding or the application of heating pad on the other side of plate being welded, can be also explained by the three-bar model. The clamping that restrains the angular distortion is interpreted as the application of tension to the three-bar model.

Based on these conclusions the Modified Method of Influence Coefficients was proposed and various cases were examined to validate the proposed method. The numerical experiments showed that the Modified Method of Influence Coefficients can predict the metal plate assembly variation considering welding distortion with much less computation time. A total of three runs of a linear elastic finite element analysis are sufficient for deriving the sensitivity matrix needed for the variation simulation and predicting the welding distortion of the assembly. In addition once the welding distortion of the nominal part assembly and the sensitivity matrix are obtained, the plate assembly variation stack up can be performed for any values of the mean deviation and standard deviation, without any additional finite element runs, whereas the Direct Monte Carlo simulation requires a new set of finite element analysis runs for each new set of mean deviation and standard deviation.

Since the Modified Method of Influence Coefficient employs the linear superposition of welding distortion terms and variation simulation terms, the magnitude of part variation should lie in the 'elastic range' of welding deformation, which means that the clamping of the part with initial variation into its nominal position does not generate any plastic deformation of the parts being joined. Preferably, for the more exact simulation, the magnitudes of initial part variation should be less than that of the welding distortion of the nominal parts assembly.

Since the plate part variation and the welding distortion are assumed to be independent to each other and the equivalent loading method is employed to predict welding distortion, the method predicts the variation stack up in the assembly more accurately when the magnitudes of variations are smaller, the plates are thinner, the plates are larger, and the welding line is longer.

Plate part variation is somewhat absorbable, considering the fact that the assembly variation could be less that the variation of the parts. Stiffener parts contribute more variation to the assembly than the plate parts do. For the perpendicular variations in the base plate where stiffeners are being attached, the variations in the base plate are eliminated to follow the shape of the stiffeners since the difference in the stiffness of plate and the stiffeners or web frames is very large. The methodology proposed in this research is equally valid for the assembly variation simulation considering welding distortion for any other three-dimensional free-form surfaces.

6.2 Recommendations for Future Work

In order to simulate the variation stack up in complex metal plate assemblies joined by welding process, it is necessary to develop a more sophisticated representation of variation distribution in plate parts. Current research assumes that the plate variation is only in the perpendicular direction and the in-plane dimensions are to the nominal since the in-plane dimensional accuracy problems are usually taken care of by allowing some margins along the edge in many shipyards. However the effects of in-plane weld shrinkage and its associated variation together with in-plane part variation should be integrated for the more complete application. For the deformable metal plate assembly

with more complex shape, such as joining of two free-form surface plates, the variation in surface can hardly be represented in one direction as in the case of flat plate assembly.

In this research, a one-dimensional model is used for the transverse and the longitudinal directions and they are assumed to be independent to each other in the process of residual strain generation. However, in reality the plastic strains are inter-related by the three-dimensional volume constraints and this should be further investigated. For more robust and complete analysis, a more general explanation of the interaction among the plate variations and welding distortion should be included in the analysis. In order to include the interaction effects, the inherent strain method should be first refined to account for the general statistical distribution of external degree of restraints through the assembly sequence.

In addition, the optimal block assembly sequence can be determined based on the proposed Modified Method of Influence Coefficients. In order to determine the optimal assembly sequence that minimizes the dimensional errors in the final assembly without any additional mitigation techniques, a discrete optimization algorithm that can generate possible assembly sequence candidates purely based on the geometrical interferences of parts is needed. Also during the optimization process, the cost function that will grade the quality of an alternative needs to be evaluated as much as the number of possible alternatives. The cost function should be able to evaluate the quality, which are the magnitude of variations and/or the residual stresses in the assembly, in fast and efficient manner since the performance of optimization process heavily depends on that of the cost function. Current research provides the Modified Method of Influence Coefficients as a fast and efficient tool for the assembly variation simulation considering welding distortion, but it also can be used as a cost function of the optimization process, which is left as a future research topic.

BIBLIOGRAPHY

BIBLIOGRAPHY

American Society of Mechanical Engineers, *Weld Residual Stresses and Plastic Deformation*, ASME, New York, 1989.

Anderson, C., "General System for Least Cost Tolerance Allocation in Mechanical Assemblies", Master's Thesis, Brigham Young University, Provo, Utah, 1990.

Aoyama, K., Nomoto, T., and Takechi, S., "Basic Studies on Accuracy Management System for Shipbuilding", *International Conference on Computer Applications in Shipbuilding*, pp. 323-338, October, 1997.

Artem, P., "Computer Simulation of Residual Stress and Distortion of Thick Plates in Multi-electode Submerged Arc Welding. Their Mitigation Techniques", Ph.D. Thesis, Dept. of Machine Design and Material Technology, Norwegian University of Science and Technology, Trondheim, Norway, July, 2001.

Bathe, K. J., *Finite Element Procedures*, Prentice-Hall International, London, UK, 1996.

Bjorke, O., *Computer-Aided Tolerancing*, Tapir Publishers, Norway, 1978.

Brown, S. and Song, H., "Finite Element Simulation of Welding of Large Structures", *ASME Journal of Engineering for Industry*, Vol. 144, pp. 441-451, 1992.

Chang, M., and Gossard, D. C., "Modeling the Assembly of Compliant, Non-ideal Parts", *Computer Aided Design*, Vol. 29, No. 10, pp. 701-708, 1997.

Chase, K., and Greenwood, W., "Design Issues in Mechanical Tolerance Analysis", *Manufacturing Review*, Vol. 1, No. 1, pp. 50-59, March, 1988.

Chase, K., Greenwood, W., Loosli, B., and Hauglund, L., "Least Cost Tolerance Allocation for Mechanical Assemblies with Automated Process Selection", *Manufacturing Review*, Vol. 3, No. 1, pp. 49–59, March, 1990.

Chase, K., and Parkinson, A. R., "A Survey of Research in the Application of Tolerance Anaysis to the Design of Mechanical Assemblies", *Research in Engineering Design*, No. 3, pp. 23-37, 1991.

Chirillo, L., Storch, R. L., and Chirillo, R., "Process Analysis Via Accuracy Control", *NSRP publication*, Maritime Administration, with Todd Pacific Shipyard Corp., 1982.

Chirillo, L., Storch, R. L., and Chirillo, R., "Process Analysis Via Accuracy Control", *National Shipbuilding Research Program (NSRP) Report 0143*, Maritime Administration, with Todd Pacific Shipyard Corp., 1982.

Chirillo, L., Storch, R. L., and Chirillo, R., "Process Analysis Via Accuracy Control - Revised", *National Shipbuilding Research Program (NSRP) Report 0214*, Maritime Administration, with Todd Pacific Shipyard Corp., 1985.

Corless, R. M., Gonnet, G. H., Hare, D. E. G., Jeffrey, D. J., and Knuth, D. E., "On the Lambert W Functions", *Advances in Computational Mathematics*, Vol. 5, No. 1, pp. 329-359, 1996.

Chris, C., and Randy, D., "Control of Distortion in Thin Ship Panels", *Journal of Ship Production*, Vol. 13, No. 2, pp. 83-92, 1997.

Chung, H., and Karr, D. G., "Use of B-Spline Surface Geometry for predicting Clamping Forces and Stresses during plate Assembly", *The Ninth International Symposium on Practical Design of Ships and Other Floating Structures*, Lübeck-Travemünde, Germany, September 12-17, 2004.

Craig, M., "Managing Tolerance by Design using Simulation Methods", *Failure prevention and reliability*, ASME publication, DE-Vol 16, pp.153-163, 1989.

DeVor, R. E., Chang, T., and Sutherland, J. W., *Statistical Quality Design and Control*, Macmillan Publishing Company, New York, 1992.

Fang, Y., and Liou, F., "Geometric Modeling and Simulation of Mechanical Assmblies with Elastic Components", *Advances in Design Automation – 20th ASME Design Automation Conference Proceedings*, Minneapolis, September 11-14, 1994.

Friedman, E., "Thermomechanical Analysis of the Welding Process Using the Finite Element Method", *ASME Journal of Pressure Vessel Technology*, Vol. 97, No. 3, pp. 206-213, 1975.

Fujimoto, T., "A Method for Analysis of Residual Welding Stresses and Deformations Based on the Inherent Strain", *Journal of Japan Welding Society*, Vol. 39, No. 4, pp. 236-252, 1970. (in Japanese)

Gao, J., "Nonlinear Tolerance Analysis of Mechanical Assemblies", Ph.D. Thesis, Dept. of Mechanical Engineering, Brigham Young University, Provo, Utah, 1993.

Gordis, J., and Flannelly, W., "Analysis of Stress due to Fastener Tolerance in Assembled Components", *AIAA (American Institute of Aeronautics and Astronautics) Journal*, Vol. 32, No. 12, pp 2440-2446, December, 1994.

Greenwood, W., and Chase, K., "A New Tolerance Analysis Method for Designers and Manufacturers", *Journal of Engineering for Industry*, Vol. 109, pp. 112-116, 1987.

Greenwood, W., and Chase, K., "Worst Case Tolerance Analysis with Nonlinear Problems", *Journal of Engineering for Industry*, Vol. 110, pp. 232-235, 1988.

Greenwood, W., and Chase, K., "Root Sum Squares Tolerance Analysis with Nonlinear Problems", *Journal of Engineering for Industry*, Vol. 112, pp. 232-235, 1990.

Haugland, L., "Combining Manufacturing Process Selection and Optimum Tolerance Allocation in Design Automation", Master's Thesis, Dept. of Mechanical Engineering, Brigham Young University, Provo, Utah, 1987.

He, P., Zhang, J. H., Terasaki, T., and Akiyama, T., "Distribution of Inherent Strains and Residual Stresses in Medium Thickness Plate Weldment", *Journal of Material Science and Technology*, Vol. 17, No. 2, pp 252-256, March, 2001a.

He, P., Zhang, J. H., Terasaki, T., and Akiyama, T., "Distribution of Longitudinal Inherent Strains in Multiple-Passes Welding", *Journal of Material Science and Technology*, Vol. 17, No. SUPPL., pp S151-S154, October, 2001b.

Henzold, G., *Handbook of Geometircal Tolerancing: Design, Manufacturing, and Inspection*, John Wiley & Sons, New York, 1995.

Hsieh, C. C., and Oh, K. P., "A Framework for Modeling Variation in Vehicle Assembly Process", *International Journal of Vehicle Design*, Vol. 18, No. 5, pp. 466-473, 1997.

International Institute of Welding, *The Physics of Welding*, Pergamon, Oxford, 1986.

Jang, C. D. and Lee, C. H., "A Study on the Prediction and Control of Welding Deformations of Ship Hull Blocks", *Journal of the Soceity of Naval Architects of Korea*, Vol. 37, No. 2, pp. 127-136, 2000. (in Korean)

Jang, C. D. and Seo, S. I., "A Simplified Method to Estimate Longitudinal Deformations of Built-up Beams Due to Welding and Heating", *Journal of Ship Research*, Vol. 39, No. 2, pp. 176-183, 1995.

Jang, C. D., Seo, S. I., and Ko, D. E., "A Study on the Prediction of Deformations of Plates Due to Line Heating using a Simplified Thermal Elastio-Plastic Analysis", *Journal of Ship Production*, Vol. 13, No. 1, pp. 22-27, 1997

Jang, C. D., Ha, Y. S., Ko, D. E., and Moon, S. C., "Determination of Inherent Strain Regions to Estimate Plate Deformation by Line Heating", *Journal of the Society of Naval Architects of Korea*, Vol. 39, No. 1, pp. 82-89, 2002. (in Korean)

Jang, C. D., Ha, Y. S., and Ko, D. E., "An Improved Inherent Strain Analysis for the Prediction of Plate Deformation Induced by Line Heating Considering Phase Transformation of Steel", *Proceedings of the International Offshore and Polar Engineering Conference – ISOPE 2003,* pp 2397-2402, 2003.

Jang, C. D., Ryu, H. S., and Lee, C. H., "Prediction and Control of Welding Deformations in Stiffened Hull Blocks Using Inherent Strain Approach", *Proceedings of the International Offshore and Polar Engineering Conference – ISOPE 2004*, pp 159-165, 2004.

Karlsson, L., *Mechanical Effects of Welding*, Springer-Verlag, New York, 1992.

Kim, S. I., Cho, Y. K., Lee, H. W., and Lee, J. S., "Prediction of Welding Deformation of Panel Block Using Simplified Analysis Method", *Proceedings of the Annual Spring Meeting, Soceity of Naval Architects of Korea*, pp. 271-276, 1996. (in Korean)

Larsen, D., "An Efficient Method for Iterative Tolerance Design using Monte-Carlo Simulation", Master's Thesis, Dept. of Mechanical Engineering, Brigham Young University, Provo, Utah, 1989.

Lee, C. H., "Prediction of Welding Deformations of Ship Hull Panel Blocks using Equivalent Loading Method based on Inherent Strain", Ph.D. Thesis, Dept. of Naval Architecture and Ocean Engineering, Seoul National University, Seoul, Korea, 2002. (in Korean)

Lee, D. W., "Thermo-Elasto-Plastic Modeling of GMAW using the Finite Element Method", Ph.D. Thesis, Dept. of Mechanical Design and Production Engineering, Seoul National University, Seoul, Korea, 1995. (in Korean)

Lee, W. J., and Woo, T. C., "Optimum Selection of Discrete Tolerances", *Journal of Mechnisms, Transmissions and Automation in Design*, Vol. 111, 1989.

Lee, W. J., and Woo, T. C., "Tolerances: Their Analysis and Synthesis", *ASME Journal of Engineering for Industry*, Vol. 112, pp. 113-121, 1990.

Leung, A. Y. T., and Au, F. T. K., "Spline Finite Elements for Beam and Plate", *Computers and Structures*, Vol. 37, No. 5, pp 717-729, 1990

Liu, S. C., "Variation Simulation for Deformable Sheet Metal Assembly", Ph.D. Thesis, Dept. of Mechanical Engineering, University of Michigan, Ann Arbor, Michigan, 1995.

Liu, S. C., and Hu, S. J., "An Offset Finite Element Model and Its Applications in Predicting Sheet Metal Assembly Variation", *International Journal of Machine Tool and Manufacture*, Vol. 35, No. 11, pp. 1545-1557, 1995.

Liu, S. C., and Hu, S. J., "A Parametric Study of Joint Performance in Sheet Metal Assembly", *International Journal of Machine Tools and Manufacture*, Vol. 37, No. 6, pp. 873-884, 1997a.

Liu, S. C., and Hu, S. J., "Variation Simulation for Deformable Sheet Metal Assemblies using Finite Element Methods", *ASME Journal of Manufacturing Science and Engineering*, Vol. 119, pp. 368-374, 1997b.

Liu, S. C., Hu, S. J., and Woo, T. C., "Tolerance Analysis for Sheet Metal Assemblies", *ASME Journal of Mechanical Design*, Vol. 118, No. 1, pp. 62-67, 1996.

Loosli, B., "Manufacturing Tolerance Cost Minimization using Discrete Optimization for Alternate Process Selection", Master's Thesis, Dept. of Mechanical Engineering, Brigham Young University, Provo, Utah, 1987.

Masubuchi, K. and Ich, N. T., "Computer Analysis of Degree of Constraint of Practical Butt Joints", *Welding Journal*, Vol. 49, No. 4, pp. 166-176, 1970.

Masubuchi, K., *Analysis of Welded Structures: Residual Stresses, Distortion, and Their Consequences*, Pergamon Press, Oxford, 1980.

Merkley, K., "Tolerance Analysis of Compliant Assemblies", Ph.D. Thesis, Dept. of Mechanical Engineering, Brigham Young University, Provo, Utah, 1998.

Merkley, K., Chase, K., and Perry, E., "An Introduction to Tolerance Analysis of Flexible Assemblies", *Proceedings of the 1996 MSC World Users Conference*, MacNeal-Schwendler Corp., Newport Beach, California, June, 1996.

Michael, W., and Siddall, J. N., "The Optimal Tolerance Assignment with Less Than Full Acceptance", *Journal of Mechanical Design, Transactions of the ASME*, Vol. 104, No. 4, pp. 855-860, 1982.

Mochizuki, K., Hayashi, M., and Hattori, T., "Residual Stress Analysis by Simplified Inherent Strain at Welded Pipe Junctures in a Pressure Vessel", *Journal of Pressure Vessel Technology, Transactions of the ASME*, Vol. 121, No. 4, pp 353-357 November, 1999.

Mura, T., *Micromechanics of Defects in Solids*, Martinus Nijhoff Publishers, Hague, Netherland, 1982.

Murakawa, H., Luo, Y., and Ueda, Y., "Prediction of Welding Deformation and Residual Stress by Elastic FEM Based on Inherent Strain (1st Report)", Journal of the Society of Naval Architects of Japan, Vol. 180, pp. 739-751, 1996. (in Japanese)

Nomoto, T., Takeshi, S., and Aoyama, K., "Basic Studies on Accuracy Management System Based on Estimation of Welding Deformations", *Journal of the Society of Naval Architects of Japan*, Vol. 181, pp. 249-290, 1997. (in Japanese)

Okumoto, Y. and Matsuzaki, S., "Approach to Accurate Production of Hull Structures", *Journal of Ship Production*, Vol. 13, No. 3, pp. 207-214, August, 1997

Park, J. U., Lee, H. W., and Bang, H. S., "Effects of Mechanical Constraints on Angular Distortion of Welding Joints", *Science and Technology of Welding and Joining*, Vol. 7, No. 4, pp. 232-239, August, 2002.

Parkinson, D. B., "Assessment and Optimization of Dimensional Tolerances", *Computer Aided Design*, Vol. 17, No. 4, pp 191-199, 1985.

Patel, B., "Thermo-Elasto-Plastic Finite Element Formulation for Deformation and Residual Stresses Due to Welds", Ph.D. Thesis, Dept. of Mechanical Engineering, Carleton University, Ottawa, Ontario, Canada, 1985.

Roh, J. K., and Shin, J. K., "An Assembly Simulation of a Plane Block with Gravity and Welding Deformations", *Journal of Society of Naval Architects of Korea*, Vol. 36, No. 3, pp. 123-134, 1998.

Rosenthal, D., and Nortom, J. T., "A Method of Measuring Triaxial Residual Stresses in Plates", *Welding Journal*, Vol. 24, pp. 295s-307s, 1945.

Roy, U., Liu, C., and Woo, T., "Review of Dimensioning and Tolerancing: Representation and Processing", *Computer Aided Design*, Vol. 23, No. 7, pp. 466-483, 1991.

Seo, S. I., and Jang, C. D., "A Study on the Prediction of Deformation of Welded Structures", *Journal of Korean Welding Society*, Vol. 15, No. 5, pp. 438-447, 1997. (in Korean)

Seo, S. I., and Jang, C. D., "A Study on the Prediction of Deformation of Welded Ship Structures", *Journal of Ship Production*, Vol. 15, No. 2, pp. 73-81, 1999.

Soman, N., "A Model of the Assembly of Compliant Parts", Ph.D. Thesis, Dept. of Mechanical Engineering, Massachusetts Institute of Technology, Cambridege, Massachusetts, 1996.

Spicknall, M. H. and Kumar, R., "A Dimensional Engineering Process for Shipbuilding", *Journal of Ship Production*, Vol. 18, No. 2, pp 105-115, May, 2002.

Spicknall, M. H., and Kumar, R., "Development of Demensional Variation Simulation and Analysis Tool for the Shipbuilding Industry", *Journal of Ship Production*, Vol. 19, No. 4, pp207-216, November, 2003.

Storch, R. L., "Accuracy Control Variation-Merging Equations: A Case Study of Their Application in U.S. Shipyards", *Journal of Ship Production*, Vol. 1, No. 2, 1985.

Storch, R. L., and Giesy, P. J., "The Use of Computer Simulation of Merged Variation to Predict Rework Levels on Ship's Hull Blocks", *Journal of Ship Production*, Vol. 4, No. 3, 1988.

Takeda, Y., "Prediction of Butt Welding Deformation of Curved Shell Plates by Inherent Strain Method", *Journal of Ship Production*, Vol. 18, No. 2, 2002.

Takezawa, N., "An Improved Method for Establishing the Process-wise Quality Standard", *Reports of Statistical Application Research, Union of Japanese Scientists and Engineers*, Vol. 27, No. 3, pp 1-13, 1980.

Tekriwal, P., "Three-Dimensional Transient Thermo-Elasto-Plastic Modeling of Gas Metal Arc Welding using the Finite Element Method", Ph.D. Thesis, Dept. of Mechanical and Industrial Engineering, University of Illinois at Urbana-Champaign, Urbana, Illinois, 1989.

Tekriwal, P., and Mazumder, J., "Transient and Residual Thermal Strain-Stress Analysis of GMAW", *ASME Journal of Engineering Material Technology*, Vol. 113, pp. 336-343, July, 1991.

Terasaki, T., and Akiyama, T., "Mechanical Behavior of Joints in FSW: Residual Stress, Inherent Strain and Heat Input Generated by Friction Stir Welding", *Welding in the World*, Vol. 47, No. 11-12, pp 24-31, November/December, 2003.

Timoshenko, S. P., and Goodier, J. N., *Theory of Elasticity*, McGraw-Hill, New York, 1970.

Ueda, Y., Fukuda, K., Nakacho., K, and Endo, S., "A New Measuring Method of Residual Stresses with the Aid of Finite Element Method and Reliability of Estimated Values", *Transactions of JWRI (Joining and Welding Research Institute of Osaka University)*, Vol. 4, No. 2, pp 123-131, 1975.

Ueda, Y., Kim, Y. C., and Umekuni, A., "Measuring Theory of Three-dimensional Residual Stresses Using a Thinly Sliced Plate Perpendicular to Welded Line", *Transactions of JWRI*, Vol. 14, No. 2, pp 151-157, 1985.

Ueda, Y. and Nakacho, K., "Distributions of Welding Residual Stresses in Various Welded Joints of Thick Plates", *Transactions of JWRI*, Vol. 15, No. 1, pp. 113-124, 1986a.

Ueda, Y., Nakacho, K., and Moriyama, S., "Compressive Ultimate Strength of Rectangular Plate with Initial Imperfections due to Welding (4th Report)", *Journal of the Society of Naval Architects of Japan*, Vol. 159, pp. 282-294, 1986b. (in Japanese)

Ueda, Y., and Fukuda, K., "New Measuring Method of Three-Dimensional Residual Stresses in Long Welded Joints using Inherent Strains as Parameters-Lz Method", *Journal of Engineering Materials and Technology Transactions of the ASME*, Vol. 111, No. 1, pp. 1-8, 1989.

Ueda, Y., Nakacho., K., and Yuan, M., "Application of FEM to Theoretical Analysis, Measurement and Prediction of Welding Residual Stresses", *Transactions of JWRI*, Vol. 20, No. 1, pp. 97-107, 1991.

Ueda, Y., and Ma, M. X., "Measuring Method of Three-Dimensional Residual Stress with Aid of Distribution Function of Inherent Strain (Report III)", *Transactions of JWRI*, Vol. 24, No. 2, pp. 123-130, 1995.

Watanabe., M., and Satoh, K., "Effect of Welding Conditions on the Shrinkage Distortion in Welded Structures", *Welding Journal*, Vol. 40, pp. 377-384, August, 1961.

Yuan, M. G. and Ueda, Y., "Prediction of Residual Stresses in Welded T- and I-Joints using Inherent Strains", *Journal of Engineering Materials and Technology*, Vol. 118, No. 2, pp. 229-234, April, 1996.